4 RESULTS AND DISCUSSION

The finding of the current study entitled "**Inhibitive performance of selected biomass- *Passiflora vitifolia, Pyrostegia venusta* and marine algae-*Sargassum polycystum, Padina boergesenii* on acid and alkali corrosion of mild steel and aluminium alloy – Experimental and Theoretical approach"** is discussed under the following headings.

Phase I: Characterization of selected plant parts and seaweed extracts

Phase II: Methods adopted-Electrochemical & Mass loss measurements

Phase III: Surface Analytical Techniques

Phase IV: Theoretical calculation using Mopac software.

Phase I

4. 1. Characterization of selected Biomass extracts

The following techniques were performed to characterise the selected plant parts and seaweed extracts- ***Passiflora vitifolia* (PAVL), *Pyrostegia venusta* (PVL) and marine algae-*Sargassum polycystum* (SP), *Padina boergesenii* (PB)**

4.1.1 Phytochemical screening

4.1.2 UV-Visible spectroscopic analysis

4.1.3 FT-IR spectroscopic analysis

4.1.4 GC-MS analysis

4.1.5 HPTLC analysis

Phase II

Methods adopted - Electrochemical & Mass loss measurements

4.2. Electrochemical measurements

4.2.1 Potentiodynamic polarisation studies for MS (Mild Steel)/ PAVL/PVL/ SP/ PB/1M HCl

4.2.2 Electrochemical impedance measurements for MS/ PAVL/ PVL/ SP/ PB/1M HCl

4.2.3 Potentiodynamic polarisation studies for AA (Aluminium Alloy)/PAVL/ PVL/ SP/ PB/1M HCl

4.2.4 Electrochemical impedance measurements for AA PAVL/ PVL/ SP/ PB/1M HCl

4.2.5 Potentiodynamic polarisation studies for AA/PAVL/PVL/ SP/ PB/1M NaOH

4.2.6 Electrochemical impedance measurements for AA/ PAVL/ PVL/ SP/ PB/1M NaOH

4.3. Mass loss Measurements

4.3.1. Effect of concentration of selected inhibitors for MS/PAVL/PVL/SP/PB/1M HCl

4.3.2. Impact of temperature on MS/PAVL/PVL/SP/PB/1M HCl

4.3.3. Effect of concentration of selected inhibitors for AA/PAVL/PVL/SP/PB/1M HCl

4.3.4. Impact of temperature on AA/PAVL/PVL/SP/PB/1M HCl

4.3.5. Effect of concentration of selected inhibitors for AA/PAVL/PVL/SP/PB/1M NaOH

4.3.6. Impact of temperature on AA/PAVL/PVL/SP/PB/1M NaOH

4.3.7 Adsorption isotherm

Statistical Analysis using SPSS package was performed to examine whether the inhibitor system is statistically significant or not.

4.3.8 Activation Parameters for the inhibition process

4.3.9 Thermodynamic adsorption parameters

Phase III

4.4. Surface Analytical Techniques

The following surface analytical techniques were used to study the surface of mild steel and aluminium in the absence and presence of selected biomass extracts.

4.4.1. UV Visible spectrophotometric Analysis

4.4.2 FT-IR spectral studies

4.4.3 Scanning Electron Microscopic studies

4.4.4 Energy dispersive X-ray analysis

4.4.5 X-ray diffraction Analysis

4.4.6 3D optical profilometry

Phase IV

4. 5. Theoretical calculation using Mopac software

Quantum chemical calculations were carried out to supplement the experimental results with theoretical calculations

4.1. Characterization of PAVL, PVL, SP and PB extracts

4.1.1. Phytochemical screening of selected biomass extracts

A preliminary phytochemical screening test was used for detection and identification of active phytochemical compounds present in leaves and seaweed extracts of PAVL, PVL, SP and PB extracts. Preliminary phytochemical analysis for alkaloids, cardiac glycosides, flavonoids, glycosides, phenols, resins, saponins, steroids, tannins, terpenoids and triterpenoids were examined by the standard procedures given in **Harborne, 1973**.

Table. 4.1 Preliminary phytochemical screening of the crude extracts of PAVL/PVL/SP/PB

Phytochemical constituents	Leaves extract		Seaweed extract	
	PAVL	PVL	SP	PB
Flavonoids	+	+	+	+
Alkaloids	+	+	+	+
Terpenoids	+	+	-	+
Saponins	+	+	+	+
Steroids	+	+	+	+
Tannins	-	+	+	-
Reducing sugar	-	-	-	-
Cholesterol	+	-	-	
Carbohydrates	-	+	-	+
Coumarins	-	+	-	+
Glycoside	+	+	-	-
Polyphenols	+	-	-	-
Anthroquinones	-	+	-	-
Sterol	-	-	+	+
Cardiac glycoside	-	-	+	-
Phenolic groups	-	-	+	-

(+) present; (-), Absent

The results revealed the presence of flavonoids, alkaloids, saponins, steroids and other secondary metabolites in PAVL, PVL, SP and PB extracts (Table 4.1). The results revealed that N and O rich compounds were present in the investigated inhibitors. The presence of these compounds reflect the ability of the plant extracts to inhibit corrosion.

4.1.2 UV analysis

UV-Visible spectroscopy is important in determining the nature of phytochemical constituents present in PAVL/PVL/SP/PB crude extracts. Plants/seaweeds were found to have plenty of organic constituents and it was not easy to isolate every compound present in the extract. Figure 4.1 showed the absorption spectrum of PAVL/PVL/SP/PB extracts and these were transparent in the wavelength region of 200-800 nm. The obtained absorption bands for PAVL/PVL/SP/PB plant extracts are displayed in Table 4.2.

4.1.2.1 UV spectroscopic study of PAVL extract

Due to the sharpness of the peaks and proper baseline, the UV-Vis spectrum of the PAVLextract was observed at 200 to 800 nm wavelength region. The UV spectra of PAVL crude extract is shown in Figure 4.1 and listed in Table 4.2. Figure 4.1 revealed a major peak at 232 nm and 250 nm. The UV spectrum displayed maxima at 270 nm, 308 nm and 322 nm characteristic of a flavone nucleus for PAVL plant extract. Due to electron transition of $n \rightarrow \sigma^*$ in N and O atoms were present in the PAVL extract, a strong peak is noticed at 232 nm **(Sachdev *et al*, 1986)**. The result revealed that PAVL extract had flavonoids and some other compounds containing N or O atoms.

4.1.2.2 UV spectroscopic study of PVL extract

UV spectra of PVL extract are shown in Figure 4.1(Table 4.2).Two characteristic absorption peaks have appeared for flavonoid compound in the range of at 300-400 nm and 240-280 nm. In UV spectra, the absorption peaks were obtained at 409 nm, 380 nm, 225 nm, 200 nm respectively. This was due to the presence of alkaloids, steroids aromatic ring and other compounds containing N and O atoms **(Ji *et al*, 2013, Mesmer *et al,* 1997)**.

4.1.2.3 UV spectral discussion of SP extract

UV spectrum of SP extract is depicted in the Figure 4.1(Table 4.2). The figure showed two major peaks were observed at 219 nm and 340 nm which was identified that the compound possessed flavonoids and additional compounds containing N or O atoms. In general UV spectrum of flavonoids were found to display one peak in the range at 300-400 nm (band I) and another peak in the range at 240-280 nm (band II **(Li *et al,* 2012b)**. The spectral data revealed that SP extract was found to have flavonoids and other compounds which were contained N or O atoms in it **(Kamal *et al*, 2012)**.

4.1.2.4 UV spectroscopic study of PB extract

UV spectra of PB extract is depicted in Figure 4.1(Table 4.2). The spectral values revealed that two major peaks were observed in the range of 200 nm and 230 nm

(Ojha *et al*, 2017, Kalaichelvi *et al,* 2017). Due to π→π* transition, the absorption band was obtained at 200 nm. Chromophores, amino group and carbonyl groups were present in the PB extract which was shown in the UV-Visible region. Thus the PB extract may consist of flavonoid type compound.

Characterization of the studied inhibitors by HPTLC, GC-MS, FT-IR and UV-Vis spectral studies were proved that the investigated inhibitors possessed flavonoids, alkaloids and steroids and other phytochemical constituents. .

Table: 4.2. UV spectral data of crude PAVL/PVL/SP/PB extracts

Inhibitor	Absorption bands (nm)	Transitions
PAVL	322, 308, 270, 250, 232, 200	n → π* π → π* n → σ*
PVL	409, 380, 225, 200	
SP	404, 380, 377, 340, 219, 200	
PB	401, 380, 379, 340, 230, 200	

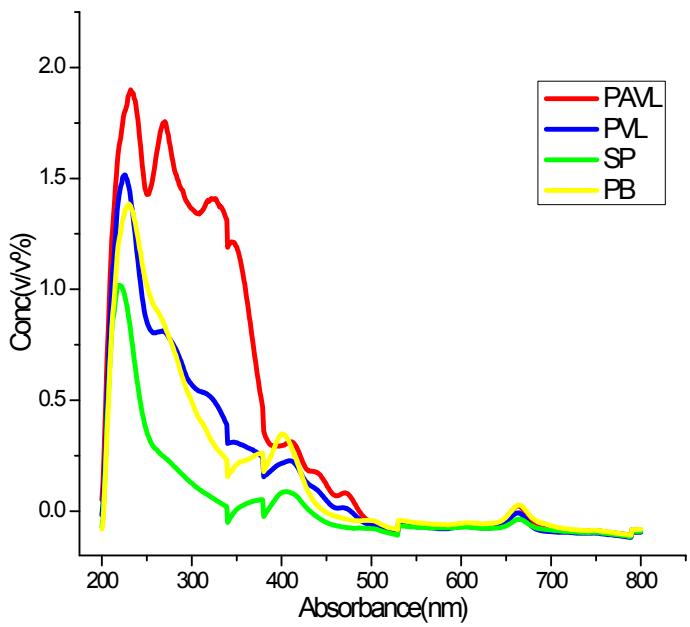

Figure 4.1. UV spectra for (a) PAVL (b) PVL (c) SP (d) PB extracts

4.1.3 FT-IR Analysis

Fourier Transform Infra-Red (FTIR) tests have been carried out to gain some information about the functional groups present in the PAVL, PVL, SP and PB extracts. The frequencies of the FT-IR bands of the investigated inhibitors PAVL, PVL, SP and PB are presented in Table 4.3.

Table 4.3. FT-IR spectral results of the crude PAVL/PVL/SP/PB extracts

Observed IR Frequency, (cm^{-1})				Assignment
PAVL	**PVL**	**SP**	**PB**	
3977 3699 3318	3360 3348	3988 3981 3344	3788 3332	O-H stretch H-bonded N-H stretch
2924	2920	2924	2924	C-H stretch
2855	2851	2850	2866	C=O stretch
-	2322	2376	2318	-C≡N stretch
1605	1628	1627	1643	C=O stretch
1512	1527	1516	-	C-C in ring
1489	1446	1408	1435	C-O stretch
1396 1366	1381 1350	1381 1303	-	C-O-C stretch
1242	1222	1226	1234	C-O stretch
1045	1049	-	1060	C-O stretch
829	898	883	-	O-H bend
768	717	-	-	O-H bend
633	632	-	617	C-H “bend”

4.1.3.1 FT-IR Spectroscopic study of PAVL extract

The FT-IR spectra of PAVL indicated a strong band at 3318 cm^{-1}pertaining to N-H/OH stretching vibration. The band corresponding to $–CH_2$ stretching was indicated at 2924 cm^{-1}. The absorption band at 1605 cm^{-1} related to C=O stretching vibration. Two peaks at 1512 cm^{-1}, 1045 cm^{-1} were noticed for C=C/ C-O stretching vibration in the aromatic system. One peak at 633 cm^{-1} reflected that the bending vibration of C=C present in the aromatic ring system. The FT-IR spectral values revealed that the O and N atoms containing compounds present in PAVL extract **(Oliveira *et al,* 2016)** (Figure 4.2 and Table 4.3).

4.1.3.2 FT-IR Spectral analysis of PVL extract

The FTIR Spectral values of PVL extract is presented in Table 4.3 and Figure 4.2. An intense band was detected at 3360 cm^{-1} attributed to N-H or O-H frequencies. A band at 2920 cm^{-1} was observed suitable for C-H stretching vibration. The absorption peak at 1628 cm^{-1} may be ascribed to C=C/C=N stretching or N-H bending mode of vibration. One peak at 1446 cm^{-1} reflected to C-O stretching vibration. The aliphatic and aromatic C-H functional groups were shown at 1000 cm^{-1} frequency. The FT-IR spectral values of PVL extract supported that the extract possessed alkaloids, flavonoids and steroids in it **(Visveshwari *et al*, 2017)**.

4.1.3.3 FT-IR Spectral results of SP extract

Figure 4.2 and Table 4.3 explained the FT-IR spectrum of SP extract. One peak appeared at 2924 cm^{-1} corresponding to aliphatic and aromatic C-H stretching frequency. The peak at 1627 cm^{-1} was observed for the stretching modes of carbonyl groups in ester (R-CO-O-R) or aldehyde (R-CO-H) and ketones (R-CO-R) or organic acids (RCOOH). One intense peak for C-O stretching mode was detected at 1408 cm^{-1}. Peaks at 1381cm^{-1}/1303 cm^{-1} was related to C-O-C stretching and the peak ascribed to C-O stretching frequency was indicated at 1226 cm^{-1}. The FT-IR spectral values of SP extract supported that the extract contained flavonoid and other compounds present in it **(Kannan, 2014)**.

4.1.3.4 FT-IR Spectral discussion of PB extract

The FT-IR spectrum of the PB extract and their spectral values are listed in Table. A intense broadband at 3332 cm^{-1} ascribed for O-H stretching. A band at 2924 cm^{-1} was correlated to C-H stretching vibration, and a band at 1643 cm^{-1} correspond to C=O stretching vibration. The band at 1435 cm^{-1} was assigned for C-O stretching vibration. A peak at 1234 cm^{-1} was attributed to C-O stretching vibration. One band at 1060cm^{-1} indicated the stretching vibration of C-O. Thus, PB extract was found to have oxygen, nitrogen-containing functional groups (O-H, N-H, C=O, C-N, C-O, C=C) and aromatic ring in it (**Rajiv *et al*, 2017)** (Table 4.3 and Figure 4.2).

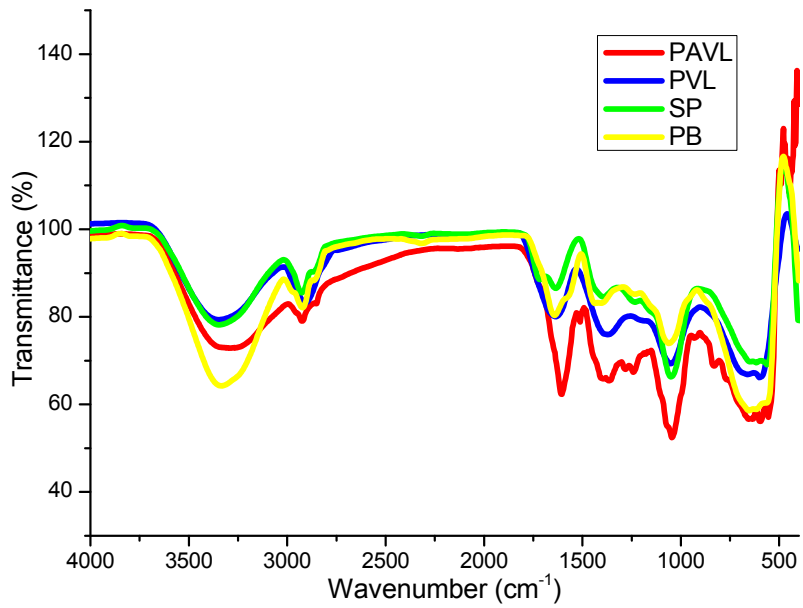

Figure 4.2 FT-IR spectrum of (a) PAVL (b) PVL (c) SP (d) PB extracts

4.1.4. GC-MS Spectral study

Figures (4.3, 4.4, 4.5, 4.6) show the Gas chromatography-Mass spectroscopy of methanolic extract of PAVL, PVL, SP and PB. The peaks with suitable retention time, the molecular formula of the compound, molecular ion peak, base peaks, fragmentation peaks and concentrations of major phytochemicals observed from reliable spectral values are presented in Table 4.4. Fragmentation pattern of the phytochemicals present in the investigated inhibitors are given in Appendix II. The spectral values proved that the investigated inhibitors contained some phytochemicals which had hetero atoms or π electrons in their aromatic or long carbon chain. This may have facilitated the transfer of electrons from the inhibitors molecule to the charged surface of the metal, hence retarded the corrosion reaction of the metal.

Table 4.4. GC-MS analysis of PAVL/PVL/SP/PB extracts

Components	Structure	RT	PAVL	PVL	SP	PB
Phytol		18.03	+	+	–	–
Cyclo hexane 1,2,3,trimethoxy	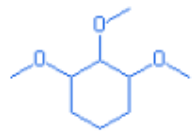	7.83	+	–	–	–
Cyclopentanone, 2-cyclopentylidene	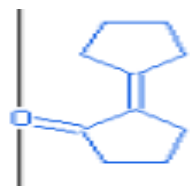	11.02	+	–	–	–
Flavone	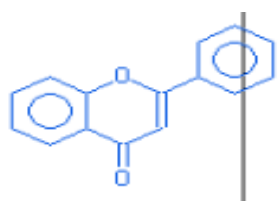	13.83	+	–	–	–
Geranylisovalerate	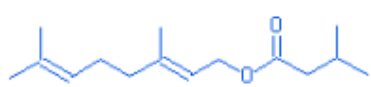	15.65	+	–	–	—
4H-1-Benzopyran-4-one,5,7-dihydroxy-2-(4-hydroxyphenyl)-	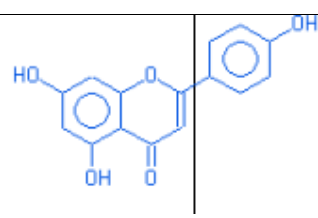	16.22	+	–	–	–
Estra -1,3,5(10)trienl-17 a -ol	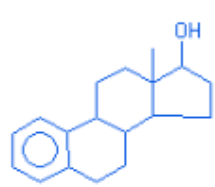	17.1	+	–	–	–

Components	Structure	RT	PAVL	PVL	SP	PB
Dasycarpidan-1-methanol,acetate (ester)	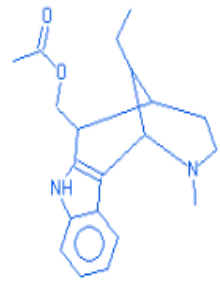	18.95	+	+	–	–
18, 19-Secoyohimban-19-Oic acid, 16,17,20,21,-tetra dehydro-16-(hydroxymethyl)-methyl ester, (15a,16 E)	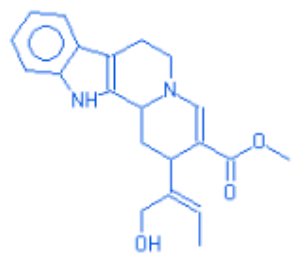	22.82	+	+	–	–
1,2-bis(1-methyl-3,6-diazahomoadamantantylidene-9)hydrazine	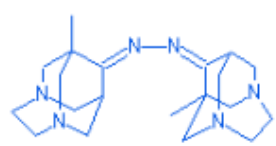	30.53	+	+	–	–
Palmitic acid		17.8	–	+	–	+
(-)-spathulenon	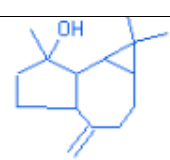	13.33	–	+	–	–
9,12-octadecadienoic acid (ZZ)-,octyl ester		33.7	–	+	–	–
3,5-heptadienal,2-ethylidene-6-methyl-	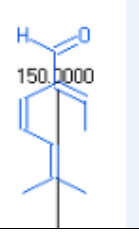	11.33	–	+	–	–

Components	Structure	RT	PAVL	PVL	SP	PB
seychellene	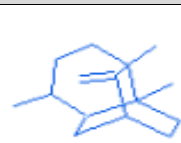	12.03	–	+	–	–
Aromadendrene oxyl-(1)	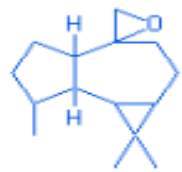	14.12	–	+	–	–
isoaromadendre neepoxide	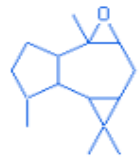	14.68	–	+	–	–
5-cyclohexadecan-1-one		16.1	–	+	–	–
Methyl-11 tetradecenoate		17.05	–	+	–	–
Oleicacid		19.52	–	+	+	+
(1,1^{-} - bicycle propyl)-2-octanoicacid, 2^{-} - hexyl-,methyl ester		19.98	–	+	–	–
Indole,N-methyl-5-(4-nitrostyryl)-	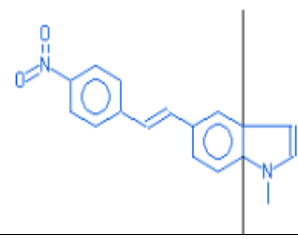	22.75	–	+	–	–

Components	Structure	RT	PAVL	PVL	SP	PB
9,12-octadecadienoic acid (ZZ)-,2-hrdroxy-1-(hydroxymethyl) methylester	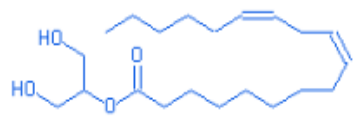	23.78	–	+	–	—
Naphthalene-2-yl-acidic acid,6-hydroxy-6-methyl-cyclodecyl ester	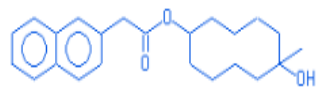	30.38	–	+	–	–
n-hexadecoic acid		17.78	–	–	+	–
9-octadecenoic acid(Z) -, methyl ester	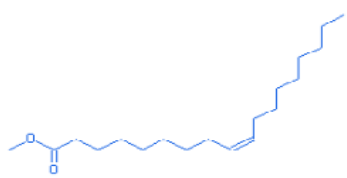	18.8	–	–	+	–
4-piperidinol, 4-ethynyl-2,2,6,6-tetra methyl -		23.12	–	–	+	–
Cis-9-hexadecenal	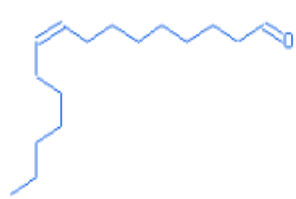	16.55	–	–	+	–
Docosanoic acid, methyl ester		30.43	–	–	+	–
11-oxatetra cyclo (4,2,1,1 (2,5),1(7,10)und ec-3ene,9-methoxy-9-methyl-	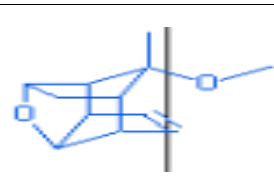	13.97	–	–	+	–

Components	Structure	RT	PAVL	PVL	SP	PB
1-acetyl-2,7-napthalene diol	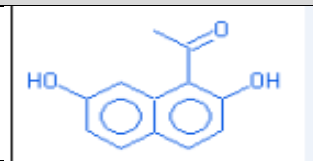	14.53	–	–	+	–
E-2-tetradecen-1-ol		16.1	–	–	+	+
Methyl tetradecanoate		17.05	–	–	+	–
13-hexyioxacyclotridec-10-en-2-one	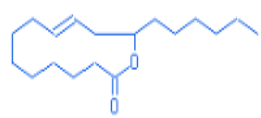	18.5	–	–	+	–
13,16-octadecadienoic acid, methyl ester		20.68	–	–	+	–
Z-(13,14-epoxy) tetradec-11-en-1-ol acetate		21.28	–	–	+	–
Ethanol,2-(9-octadecenyloxy)-, (Z)-	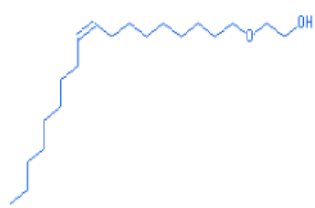	24.5	–	–	+	–
8,11,14-Eicosatrienoic acid,(ZZZ)-		20.28	–	–	–	+
Tricycle(4,2,0,0(2,4))octan-5-one,(1a,2a,4a,6a)-	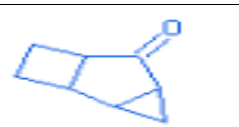	14.12	–	—	–	+

Components	Structure	RT	PAVL	PVL	SP	PB
3-heptanone,2,6-dimethyl-	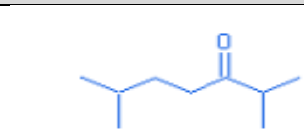	15	–	–	–	+
Tridecanedial		16.55	—	–	–	+
Dodecanoic acid, 10-methyl- ,methyl ester		17.05	–	–	–	+
Cis-9-hexadecenal	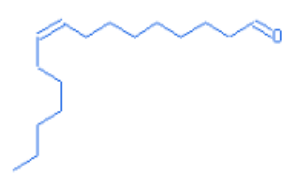	18.52	–	—	–	+
9-octadecenoic acid (Z)-, methyl ester	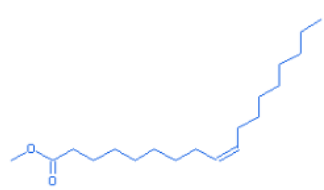	18.78	–	–	–	+
Hexadecenoic acid, Z-11-	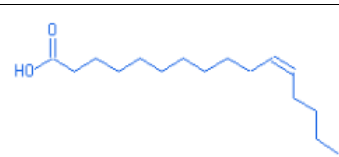	20.7	–	–	–	+
Elaidic acid, isopropyl ester		21.55	–	–	–	+

Components	Structure	RT	PAVL	PVL	SP	PB
Ricinoleic acid	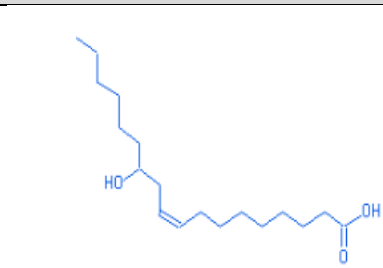	22.73	–	–	–	+
2H-naphtalen-1-one,3,4-dihydro-6-methoxy-2-(4-methoxybenzylideno)-	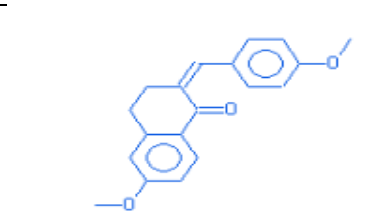	23.78	–	–	–	+
9,12-octadecadienoic acid (ZZ)-,2,3-dihydroxypropyl ester	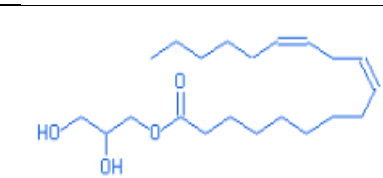	26.17	–	–	–	+

4.1.4.1. GC-MS result of PVL extract

The GC spectra of PVL extract exhibited seven peaks at various retention time 17.8, 13.33, 14.12, 16.1, 17.05, 18.98 and 19.52 (Figure 4.3). NIST data analysis indicated that the mass spectrum and fragmentation pattern of GC- peaks at retention time 17.8 matched with palmitic acid; retention time 13.33 corresponded to (-)- Spathulenol ; retention time 14.12 Aromadendrene oxide-[1] , retention time 16.1 5-cyclohexadecen-1-one;17.05 retention time, Methyl z-11-tetradecenoate. , retention time 18.97 phytol , retention time 19.52, oleic acid.

4.1.4.2 GC-MS Analysis of SP extract

Figure 4.4 represented the GC-MS and peak fragmentation spectra of SP extract. The SP extract spectrum reflected seven peaks at retention time 17.78, 18.8, 16.1, 17.05, 18.5 and 20.63. NIST data analysis inferred that the mass spectrum and fragmentation pattern of GC- peaks at retention time 17.78 matched with n-hexadecoic acid; retention time 18.8 ,16.1, 17.05, 18.5, 20.63 matched with 9-Octadecenoic acid[z]-methyl ester, E-2-Tetradecen-1-ol, methyl tetra decanoate, 13-hexyloxacyclotridec-10-en-2-one, Oleic acid.

4.1.4.3 GC-MS Spectral results of PB extract

Mass spectra of PB (Figure 4.5) exhibited that the plant extract contains seven different compounds. GC-MS spectrum profile of PB recorded seven peaks at 16.1, 16.55, 17.05, 17.75, 18.52, 18.78 and 22.73 retention time. NIST data analysis reflected the probable phytochemicals: at 16.1 retention time E-2-tetradecen-1-ol; 16.55 RT indicated Tridecanedial. 17.05 retention time reflected Dodecanoic acid 10-methyl-methyl ester;at retention time 17.75 palmitic acid; at the retention time of 18.52 cis-9-Hexadecenal; at 18.78 retention time, 9-Octadecenoic acid[z]-methyl ester; at 22.73 retention time revealed the presence of ricinoleic acid.

4.1.4.4 GC-MS Analysis of PAVL extract

Mass spectrum and its peak fragmentation for PAVL extract is depicted in Figure 4.6. GC spectrum of PAVL extract exhibited five peaks at 18.03, 16.22, 17.1, 18.95 and 30.53 retention time. NIST data analyses matched the observed retention time with the following chemical components : at 18.03 retention time, the spectrum matched with phytol.; at 16.22 retention time 4H-1-Benzopyran-4-one, 5, 7-dihydroxy-2(-4-hydroxyphenyl). at 17.1 retention time Estra-1,3,5(10)trien-17a-ol; at 18.95 retention time, Dasycarpidan-1-methanol, acetate (ester) and at retention time 30.53 1, 2-Bis[1-methyl-3,6-diazahomoadamantantylidene-9) hydrazine.

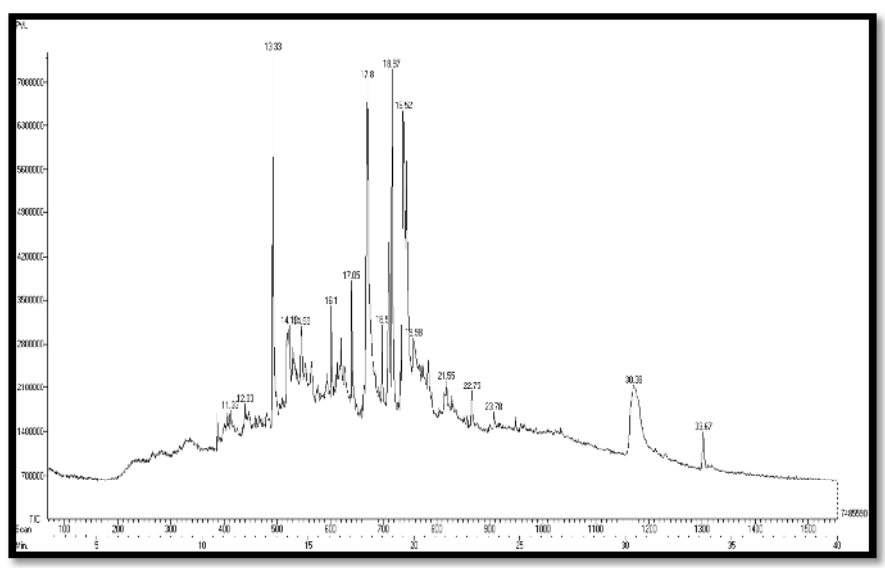

Figure 4.3 GC-MS picture for PVL extract

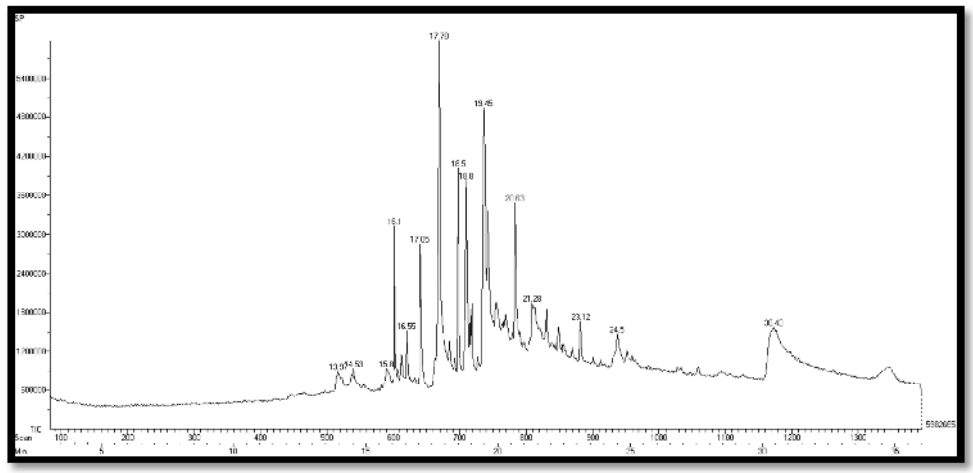

Figure 4.4. GC-MS picture for SP extract

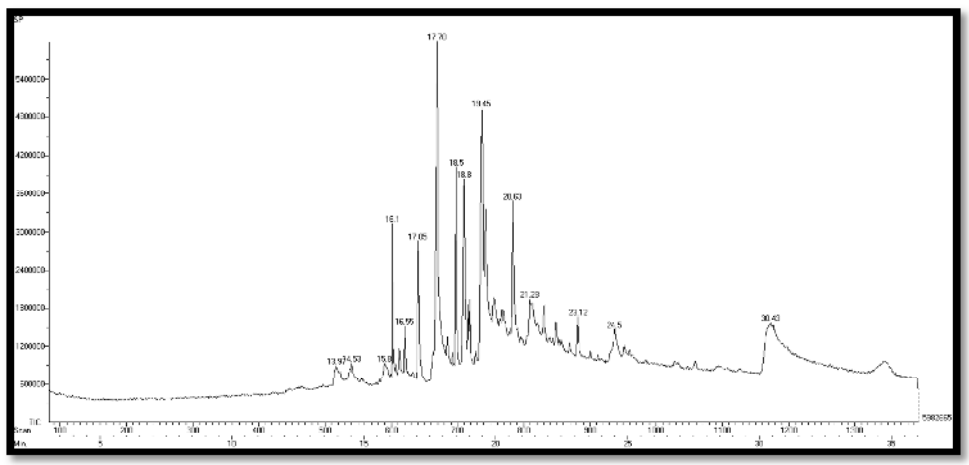

Figure 4.5. GC-MS picture for PB extract

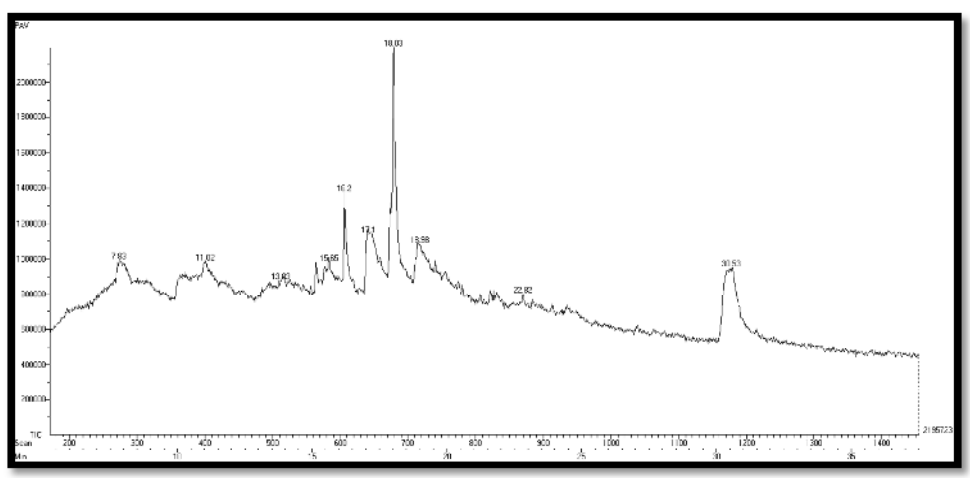

Figure 4. 6. GC-MS picture for PAVL extract

4.1.5 HPTLC analysis of PAVL, PVL, SP and PB extracts

HPTLC is an analytical technique to identify the presence of alkaloid, flavonoid and steroid present in the plant and seaweed extracts. HPTLC technique is performed for methanolic leaves extracts of PAVL, PVL and seaweed extracts of SP and PB.

To find out the presence of alkaloid, flavonoid and steroid present in the methanolic extract of PAVL, PVL, SP and PB, different compositions of the mobile phase of HPTLC analysis were tested to obtain high resolutions and reproducible peaks. The desired solvent system for alkaloid, flavonoid and steroid namely Ethyl acetate-Methanol-Water (10 : 1.35 : 1), Toluene-Acetone-Formic acid (4.5 : 4.5 : 1), Toluene-Acetone (9 : 1) were used.

4.1.5.1 Alkaloid profile of PAVL, PVL, SP and PB extract

The HPTLC analysis of methanoic extract of the plant PAVL and PVL reflected the presence of twenty three different types of alkaloids with R_f values 0.02, 0.07, 0.17, 0.29, 0.34, 0.42, 0.45, 0.53, 0.87, 0.93, 0.03, 0.08, 0.12, 0.15, 0.18, 0.21, 0.28, 0.36, 0.40, 0.52, 0.58, 0.86 and 0.92 (Table 4.5*)*. The seaweed extract of SP and PB reflected the presence of twelve different types of alkaloids with R_f values 0.02, 0.13, 0.18, 0.43, 0.49, 0.55, 0.80, 0.92, 0.02, 0.12, 0.16 and 0.38 (Table 4.6*)*. Blue, Violet coloured zone appeared from the chromatogram after derivatization, which proved that alkaloids were present in the inhibitors (Figure 4.7 and 4.8).

Table 4.5. Alkaloid profile *of* PAVL and PVLextract

Track	Peak	R_f	Height	Area	Assigned substance
Sample PAVL	1	0.02	87.2	730.4	Unknown
Sample PAVL	2	0.07	138.9	3420.1	Unknown
Sample PAVL	3	0.17	373.2	14636.0	Unknown
Sample PAVL	4	0.29	164.1	4636.8	Unknown
Sample PAVL	5	0.34	48.6	979.5	Unknown
Sample PAVL	6	0.42	83.8	1817.4	Alkaloid 1
Sample PAVL	7	0.45	179.9	4426.3	Alkaloid 2
Sample PAVL	8	0.53	374.9	10253.0	Alkaloid 3
Sample PAVL	9	0.87	108.1	5300.4	Unknown
Sample PAVL	10	0.93	330.1	18681.4	Unknown
COL	1	0.41	757.6	22608.5	Colchicine standard
Sample PVL	1	0.03	15.1	76.3	Unknown
Sample PVL	2	0.08	17.8	375.1	Unknown
Sample PVL	3	0.12	18.7	233.6	Unknown
Sample PVL	4	0.15	26.2	488.4	Unknown
Sample PVL	5	0.18	19.0	300.3	Unknown
Sample PVL	6	0.21	26.6	485.3	Unknown
Sample PVL	7	0.28	18.8	426.6	Alkaloid 1
Sample PVL	8	0.36	26.7	713.8	Alkaloid 2
Sample PVL	9	0.40	13.1	266.9	Unknown
Sample PVL	10	0.52	32.7	1741.9	Unknown
Sample PVL	11	0.58	41.2	1406.7	Unknown
Sample PVL	12	0.86	81.8	2004.5	Unknown
Sample PVL	13	0.92	410.1	25464.0	Unknown

Table.4.6 Alkaloid profile of SP and PB Extract

Track	Peak	R_f	Height	Area	Assigned substance
Sample SP	1	0.02	116.1	1266.3	Unknown
Sample SP	2	0.13	19.2	689.4	Alkaloid 1
Sample SP	3	0.18	64.1	1092.5	Alkaloid 2
Sample SP	4	0.43	38.8	1937.9	Unknown
Sample SP	5	0.49	31.6	982.0	Unknown
Sample SP	6	0.55	19.1	510.3	Unknown
Sample SP	7	0.80	30.7	906.0	Unknown
Sample SP	8	0.92	400.3	26093.8	Unknown
COL	1	0.41	751.0	23899.9	Colchicine standard
Sample PB	1	0.02	97.5	1260.8	Unknown
Sample PB	2	0.12	12.6	239.6	Unknown
Sample PB	3	0.16	57.6	1410.7	Alkaloid 1
Sample PB	4	0.38	24.5	621.7	Unknown
Sample PB	5	0.54	33.5	1290.3	Alkaloid 2
Sample PB	6	0.91	418.9	34991.2	Unknown

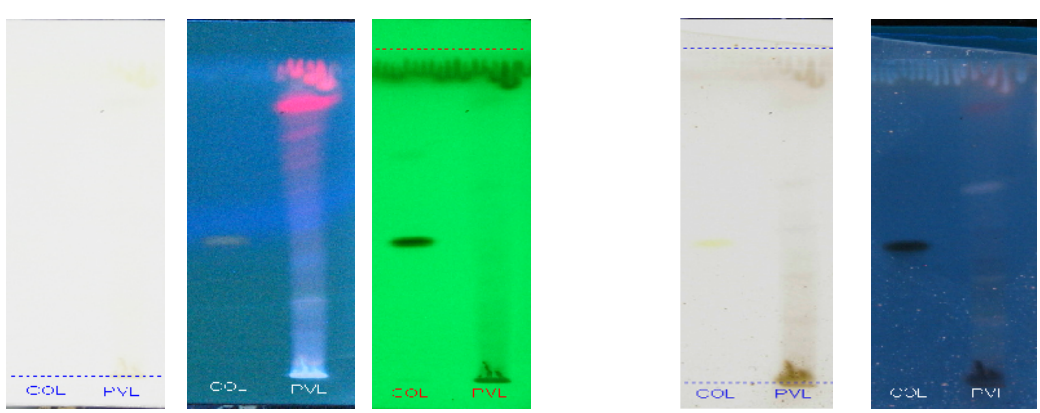

Before derivatization **After derivatization**

Figure 4.7 Alkaloid chromatogram of PVL extract before and after derivatization

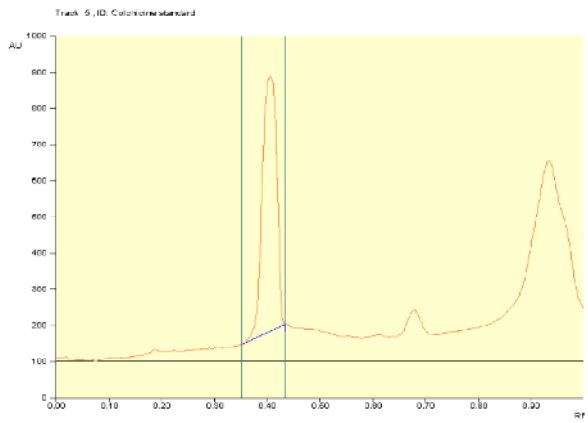

Alkaloid standard Baseline display (Scanned at UV 254nm)

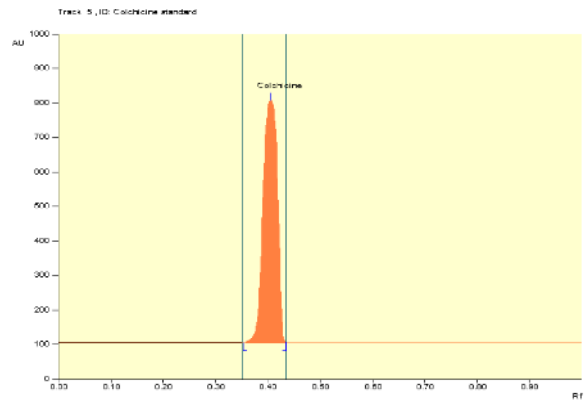

Alkaloid standard Peak densitogram display (Scanned at UV 254nm)

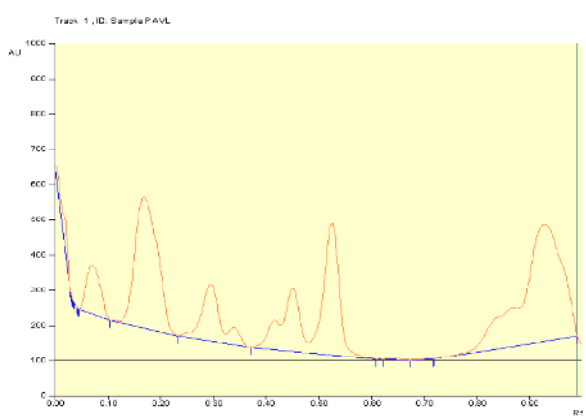

PAVL –Baseline display (Scanned at UV 254nm)

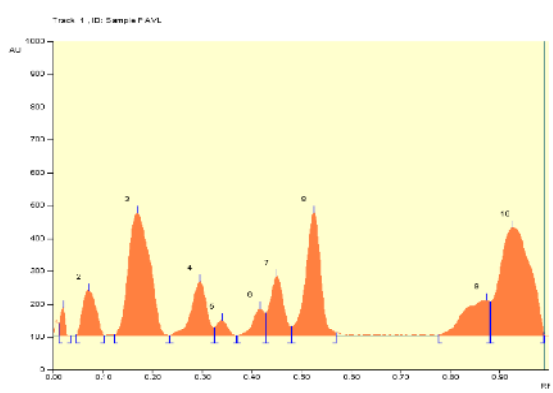

PAVL –Peak densitogram display (Scanned at UV 254nm)

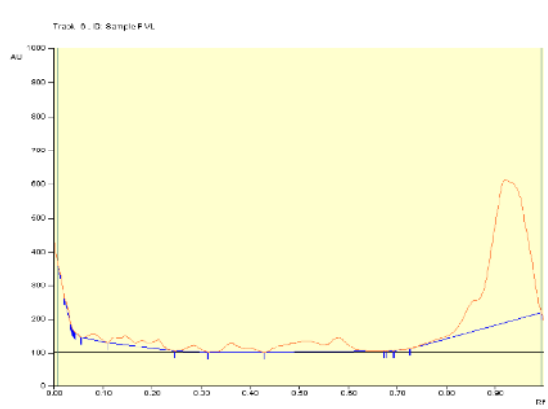

PVL –Baseline display (Scanned at UV 254nm)

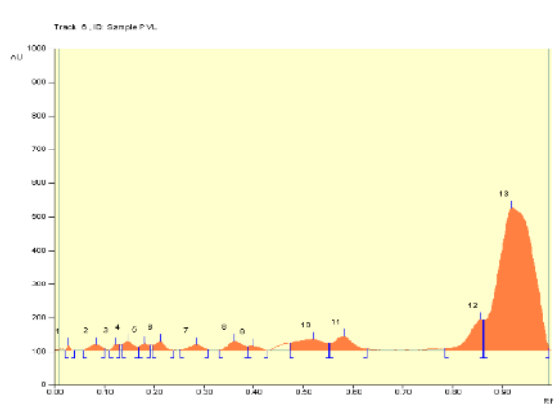

PVL –Peak densitogram display (Scanned at UV 254nm)

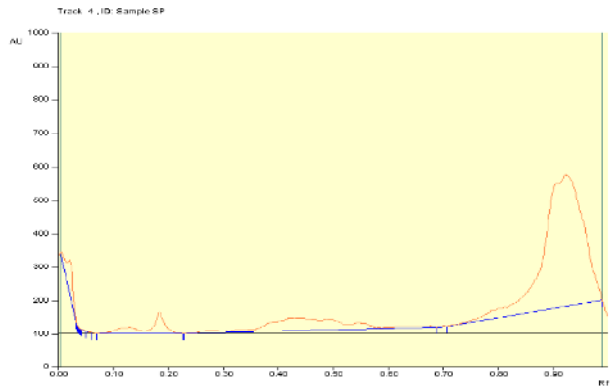

SP –Baseline display
(Scanned at UV 254nm)

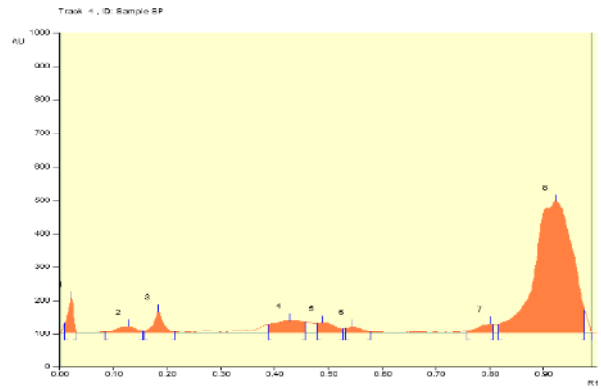

SP –Peak densitogram display
(Scanned at UV 254nm)

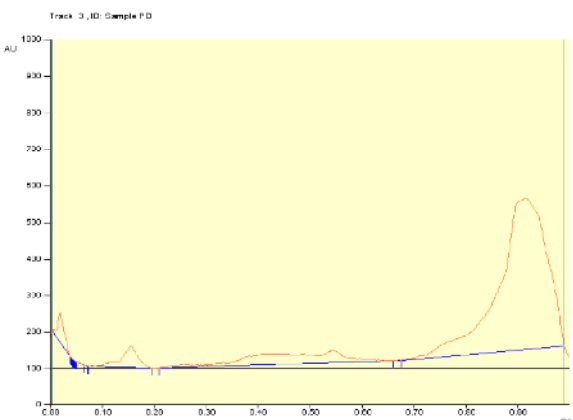

PB –Peak densitogram display
(Scanned at UV 254nm)

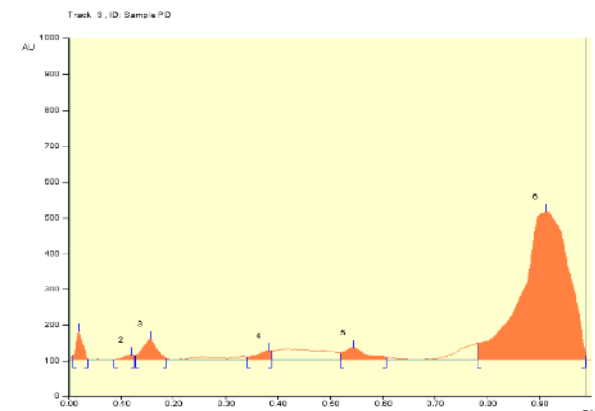

PB –Baseline display
(Scanned at UV 254nm)

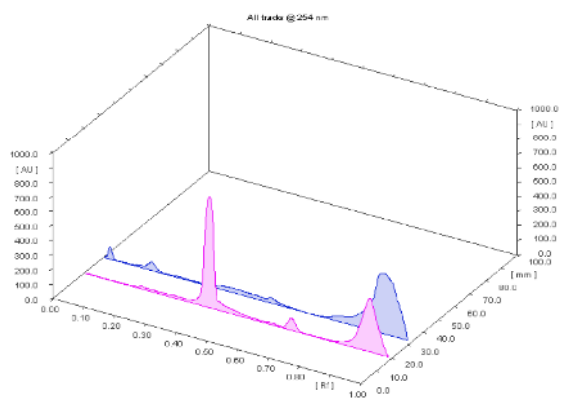

3D Display of all Tracks

Figure 4.8. Baseline and peak densitogram display of the investigated inhibitors and 3D display of all tracks for alkaloid profile

4.1.5.2 Flavonoid profile of PAVL, PVL, SP and PB extracts

The methanoic extract of the plant PAVL and PVL reflected the presence of seventeen various types of flavonoids with R_f values 0.06, 0.16, 0.29, 0.39, 0.56, 0.83, 0.91, 0.96, 0.98 and 0.02, 0.11, 0.22, 0.47, 0.81, 0.92, 0.95, 0.98 (Table 4.7*)*. The seaweed extract of SP and PB reflected the presence of eight different types of flavonoids with R_f values 0.02, 0.06, 0.08, 0.79, 0.95 and 0.09, 0.80, 0.95 (Table 4.8*)*. Reddish blue coloured zone indicated that the flavonoid type of compounds were present in the inhibitors(Figures 4.9 and 4.10).

Table 4.7. Flavonoid profile of PAVL and PVL Extract

Track	Peak	R_f	Height	Area	Assigned substance
Sample PAVL	1	0.06	385.7	11568.9	Flavonoid 1
Sample PAVL	2	0.16	214.9	7942.0	Flavonoid 2
Sample PAVL	3	0.29	219.8	10649.3	Flavonoid 3
Sample PAVL	4	0.39	370.8	18389.8	Flavonoid 4
Sample PAVL	5	0.56	18.0	715.7	Flavonoid 5
Sample PAVL	6	0.83	287.9	15207.4	Unknown
Sample PAVL	7	0.91	24.1	702.5	Unknown
Sample PAVL	8	0.96	75.1	878.8	Unknown
Sample PAVL	9	0.98	51.5	564.6	Unknown
QUE	1	0.80	755.1	45091.2	Quercetin standard
Sample PVL	1	0.02	19.8	233.3	Unknown
Sample PVL	2	0.11	98.0	2333.1	Flavonoid 1
Sample PVL	3	0.22	19.4	327.6	Flavonoid 2
Sample PVL	4	0.47	61.4	2708.2	Flavonoid 3
Sample PVL	5	0.81	265.4	14247.0	Unknown
Sample PVL	6	0.92	20.3	320.5	Unknown
Sample PVL	7	0.95	38.0	382.1	Unknown
Sample PVL	8	0.98	16.1	149.3	Unknown

Table 4.8. Flavonoid Profile of SP and PB Extract

Track	Peak	R_f	Height	Area	Assigned substance
Sample SP	1	0.02	19.8	233.3	Unknown
Sample SP	2	0.06	15.8	220.6	Flavonoid 1
Sample SP	3	0.08	14.8	456.4	Flavonoid 2
Sample SP	4	0.79	193.2	11147.6	Unknown
Sample SP	5	0.95	53.5	1517.1	Unknown
QUE	1	0.80	738.1	40589.0	Quercetin standard
Sample PB	1	0.09	36.9	1420.3	Unknown
Sample PB	2	0.80	262.8	17287.1	Unknown
Sample PB	3	0.95	77.8	3040.1	Unknown

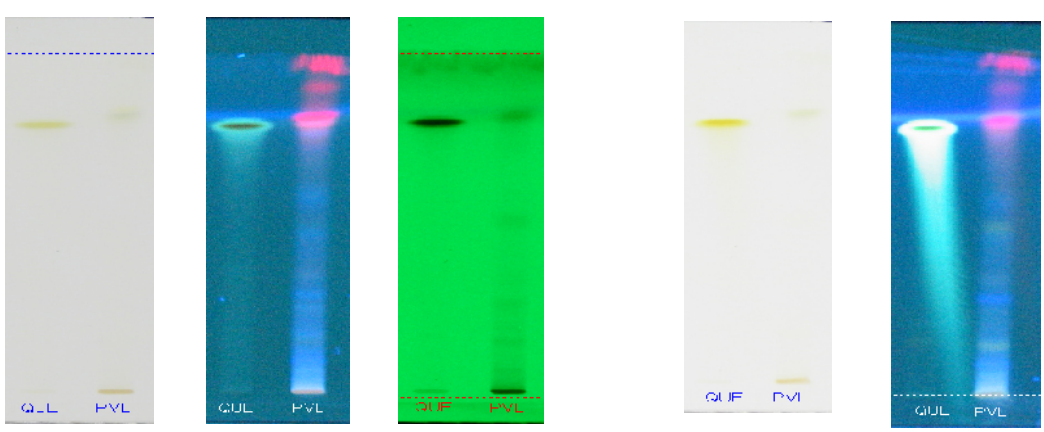

Before derivatization **After derivatization**

Figure 4.9. Flavonoid chromatogram of PVL extract before and after derivatization

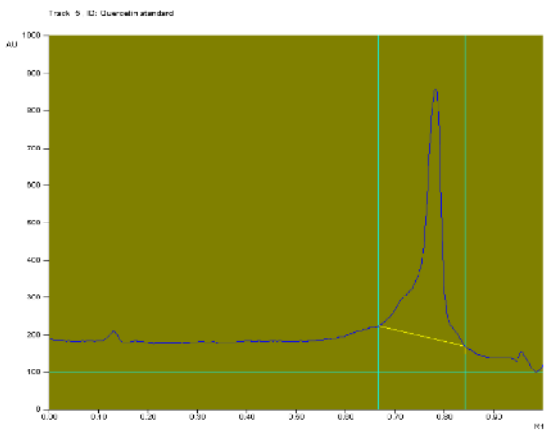

Flavonoid – Quercetin standard
Baseline display
(Scanned at UV 366nm)

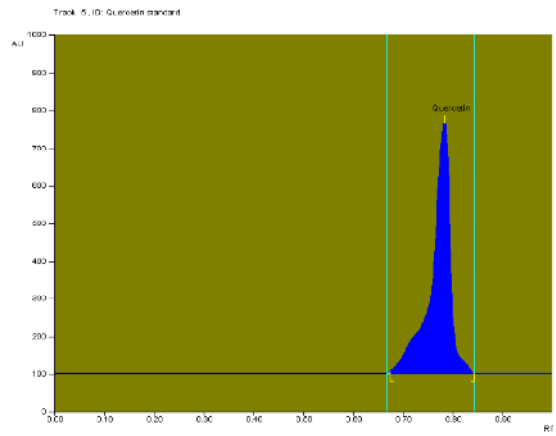

Flavonoid – Quercetin standard
Peak densitogram display
(Scanned at UV 366nm)

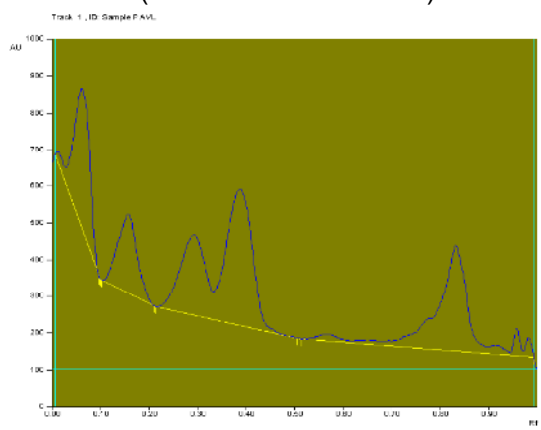

PAVL –Baseline display
(Scanned at UV 366nm)

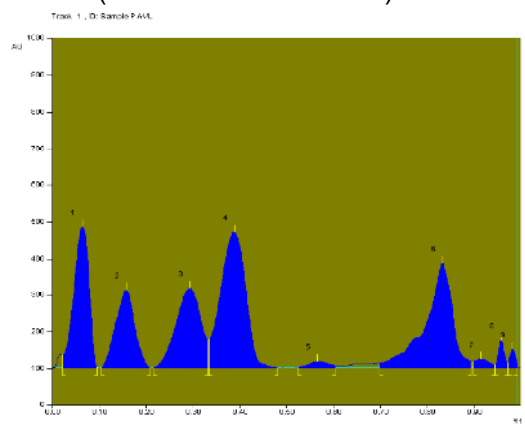

PAVL –Peak densitogram display
(Scanned at UV 366nm)

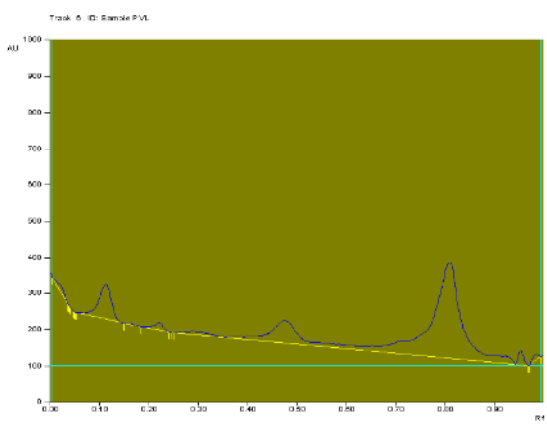

PVL –Baseline display
(Scanned at UV 366nm)

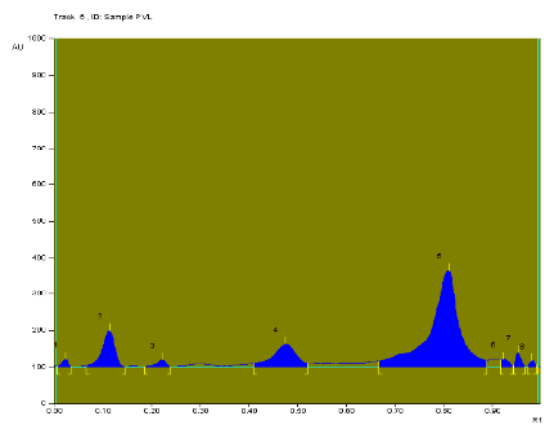

PVL –Peak densitogram display
(Scanned at UV 366nm)

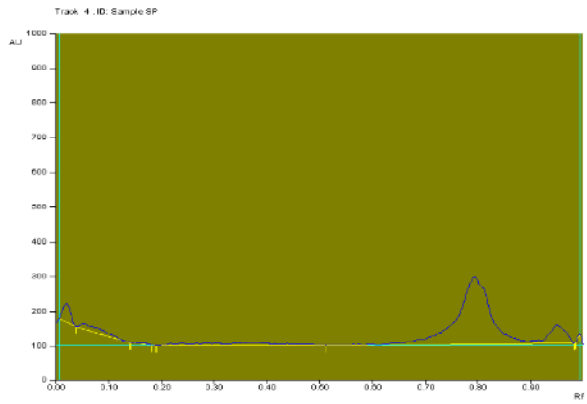

SP –Baseline display
(Scanned at UV 366nm)

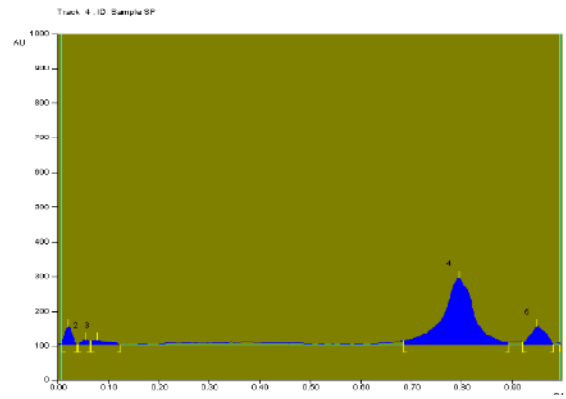

SP–Peak densitogram display
(Scanned at UV 366nm)

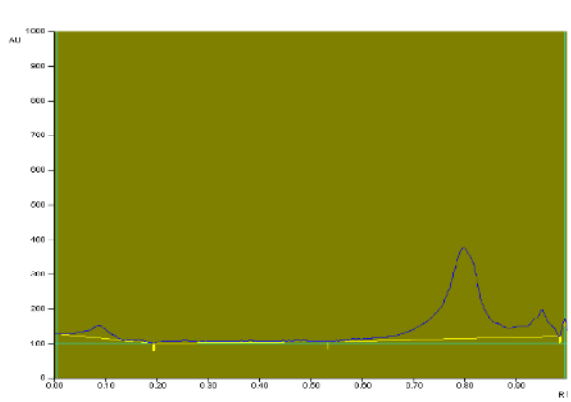

PB –Baseline display
(Scanned at UV 366nm)

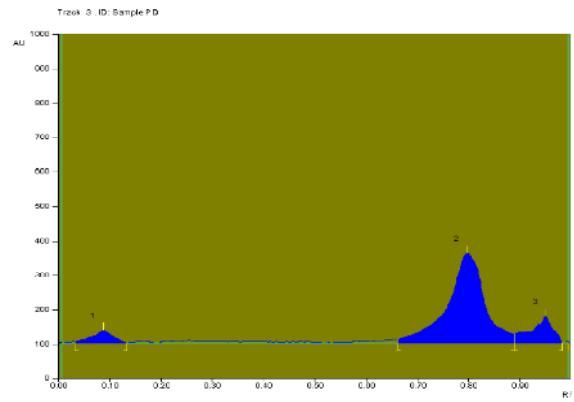

PB–Peak densitogram display
(Scanned at UV 366nm)

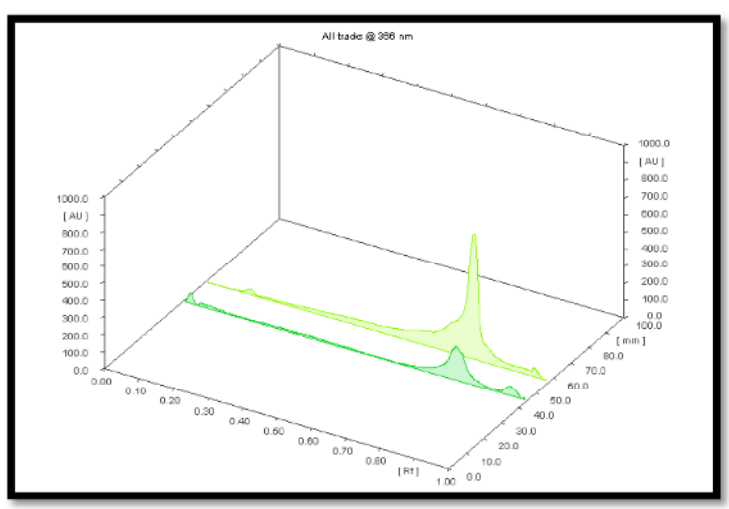

3D Display of all Tracks

Figure 4.10. Baseline and peak densitogram display of the investigated inhibitors and 3D display of all tracks for flavonoid profile

4.1.5.3 Steriod profile of PAVL, PVL, SP and PB extract

HPTLC analysis of methanolic extract of the plant PAVL and PVL indicated the presence of twenty one different types of steroids with R_f values 0.09, 0.17, 0.30, 0.42, 0.70, 0.88, 0.94, 0.98, 0.05, 0.26, 0.28, 0.38, 0.41, 0.73, 0.76, 0.79, 0.81, 0.86, 0.90, 0.94 and 0.96 (Table 4.9). The seaweed extract of SP and PB reflected the presence of twelve different types of steroids with R_f values 0.33, 0.41, 0.48, 0.68, 0.89, 0.94, 0.97, 0.34, 0.41, 0.76, 0.91 and 0.98 (Table 4.10*)*.Reddish pale blue coloured zone prove that steroids compounds were present in the extracts (Figures 4.11 and 4.12).

Table 4.9. Steriod profile of PAVLand PVL Extract

Track	Peak	R_f	Height	Area	Assigned substance
Sample PAVL	1	0.09	25.2	384.2	Steroid 1
Sample PAVL	2	0.17	24.5	410.6	Steroid 2
Sample PAVL	3	0.30	30.9	1436.6	Steroid 3
Sample PAVL	4	0.42	78.1	2967.3	Steroid 4
Sample PAVL	5	0.70	56.0	1618.2	Unknown
Sample PAVL	6	0.88	35.8	1483.0	Unknown
Sample PAVL	7	0.94	29.0	386.3	Unknown
Sample PAVL	8	0.98	11.4	116.7	Unknown
SGL	1	0.41	73.4	2987.2	Stigmasterol standard
Sample PVL	1	0.05	16.2	122.8	Unknown
Sample PVL	2	0.26	29.8	521.4	Unknown
Sample PVL	3	0.28	31.2	797.6	Steroid 1
Sample PVL	4	0.38	25.1	484.7	Unknown
Sample PVL	5	0.41	53.5	1748.2	Steroid 2
Sample PVL	6	0.73	41.0	1294.9	Unknown
Sample PVL	7	0.76	41.9	498.8	Unknown
Sample PVL	8	0.79	49.3	1028.0	Unknown
Sample PVL	9	0.81	37.7	618.2	Unknown
Sample PVL	10	0.86	58.4	1581.3	Unknown
Sample PVL	11	0.90	50.1	1037.5	Unknown
Sample PVL	12	0.94	49.1	633.2	Unknown
Sample PVL	13	0.96	74.6	1265.3	Unknown

Table 4.10. Steroid Profile of SP and PB Extract

Track	Peak	R_f	Height	Area	Assigned substance
Sample SP	1	0.33	63.6	2155.6	Steroid 1
Sample SP	2	0.41	34.5	1013.5	Steroid 2
Sample SP	3	0.48	17.0	430.3	Unknown
Sample SP	4	0.68	10.3	203.2	Unknown
Sample SP	5	0.89	31.2	820.0	Unknown
Sample SP	6	0.94	14.3	246.2	Unknown
Sample SP	7	0.97	33.4	460.6	Unknown
SGL	1	0.41	67.3	2509.1	Stigmasterol standard
Sample PB	1	0.34	18.9	585.6	Steroid 1
Sample PB	2	0.41	61.0	1598.5	Steroid 2
Sample PB	3	0.76	11.0	128.1	Unknown
Sample PB	4	0.91	27.3	607.7	Unknown
Sample PB	5	0.98	22.0	233.5	Unknown

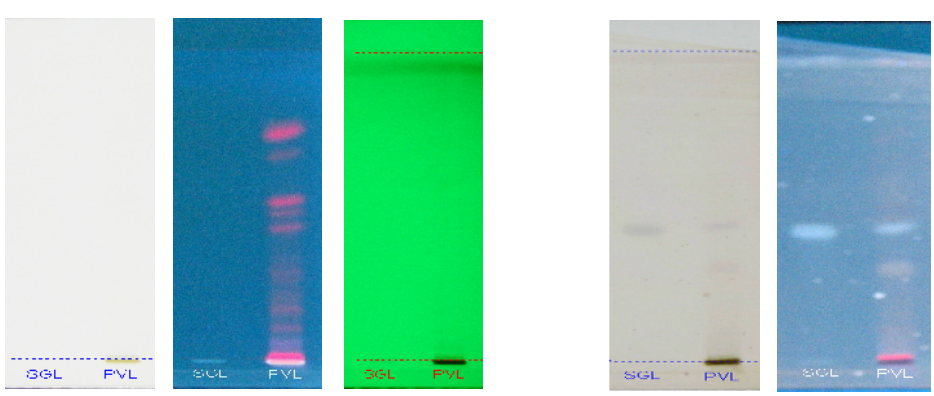

Before derivatization

After derivatization

Figure 4.11 Steroid chromatogram of PVL extract before and after derivatization

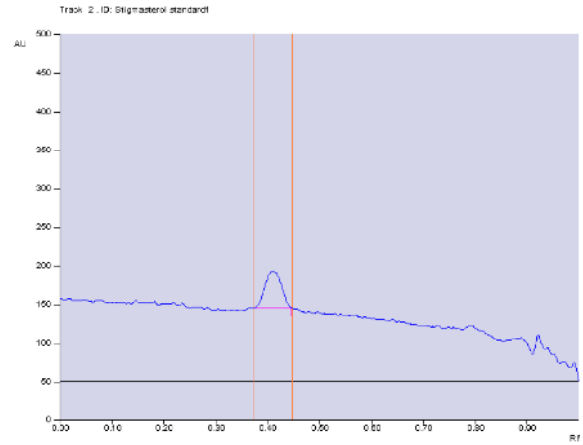

Steroid – Stigamasterol standard display
(Scanned at UV 366nm)

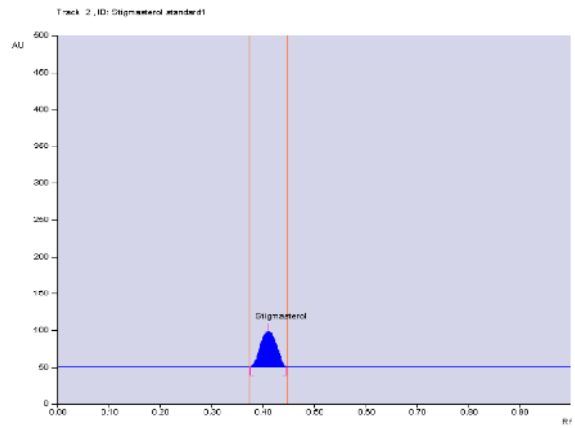

Steroid – Stigamasterol standard Peak densitogram display (Scanned at UV 366nm)

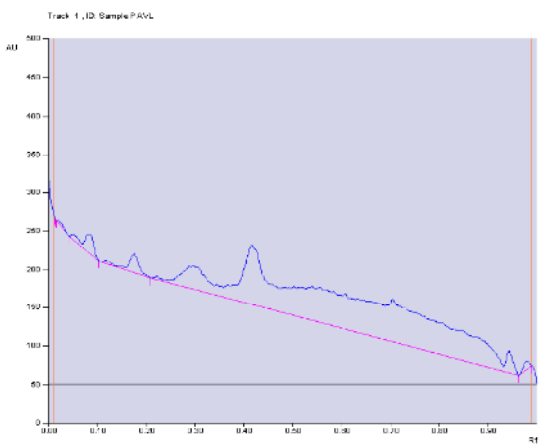

PAVL –Baseline display
(Scanned at UV 366nm)

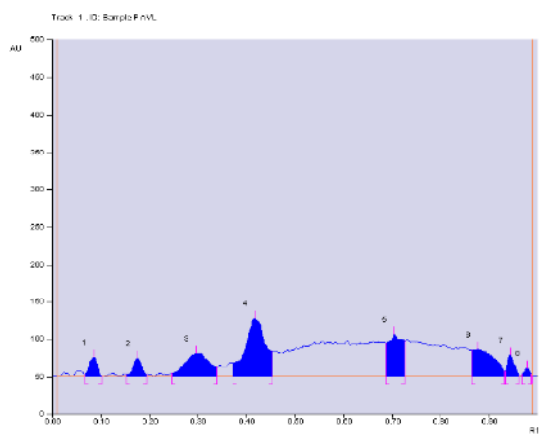

PAVL –Peak densitogram display
(Scanned at UV 366nm)

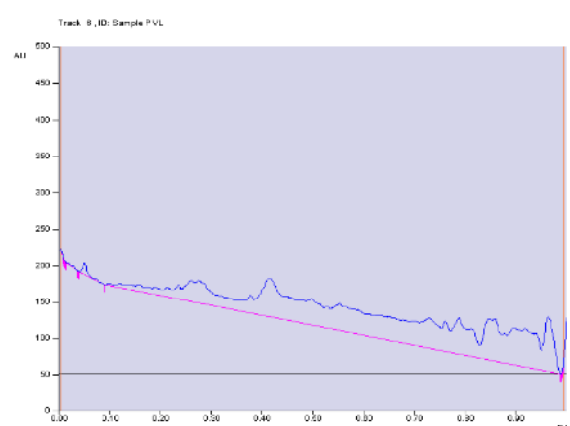

PVL –Baseline display
(Scanned at UV 366nm)

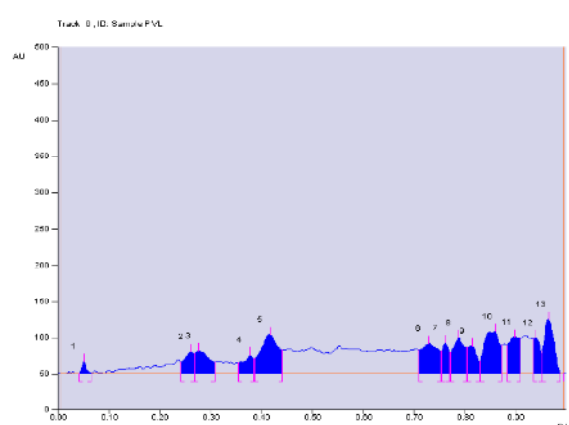

PVL –Peak densitogram display
(Scanned at UV 366nm)

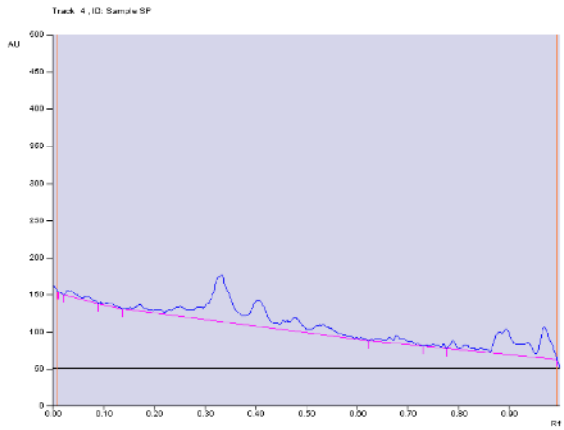

SP –Baseline display
(Scanned at UV 366nm)

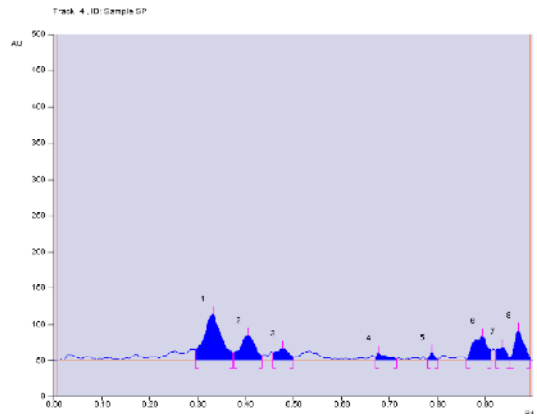

SP –Peak densitogram display
(Scanned at UV 366nm)

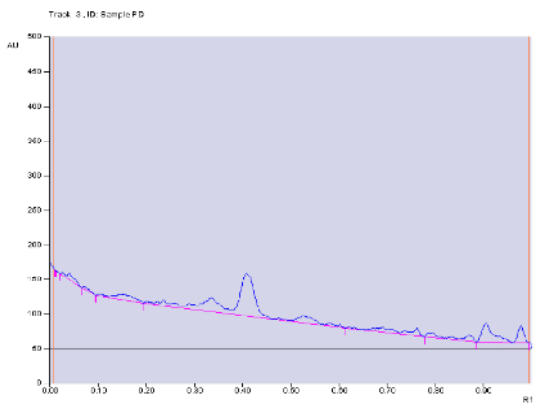

PB –Baseline display
(Scanned at UV 366nm)

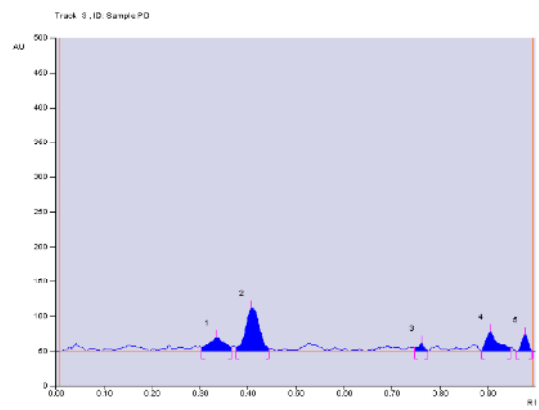

PB –Peak densitogram display
(Scanned at UV 366nm)

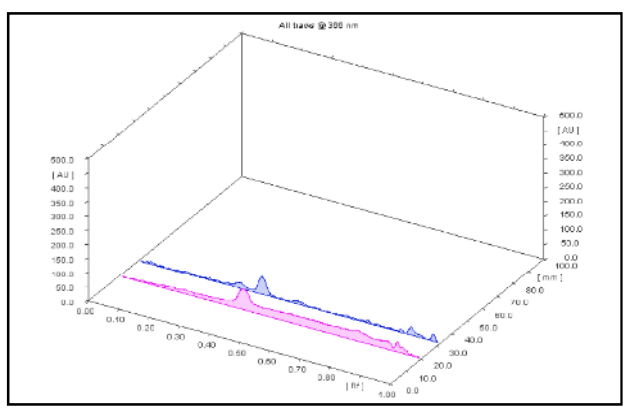

3D Display of all Tracks

Figure 4.12. Baseline and peak densitogram display of the investigated inhibitors and 3D display of all tracks for steroid profile

4.2 Electrochemical measurements

Potentiodynamic polarization studies were performed to know the effect of leaves and seaweed extracts of PAVL, PVL, SP and PB extract on the kinetic of the anodic and cathodic reactions. The polarization curves were helped to understand the inhibitive performance of the studied inhibitors. The changes observed from the polarization curves after the addition of the inhibitor are usually used as the criteria to classify inhibitors as cathodic, anodic or mixed. The data observed from polarization curves by tafel extrapolations for all the investigated inhibitors are discussed below. Electrochemical impedance spectrospopy (EIS) is widely used in investigating corrosion inhibition processes as it provid more information on both the resistive and capacitive behavior at metal/ solution interface. Impedance measurements provide an insight into the kinetics of interfacial mass transfer process **(Bentiss *et al*, 1999).** In the current study, the electrochemical measurements were performed to obtain information about the kinetics of metal corrosion in corrosive media at the metal/solution interface in presence of leaves and seaweed extract of PAVL, PVL, SP and PB. The obtained results are discussed below.

4.2.1 Potentiodynamic polarisation technique - MS/PAVL/PVL/SP/PB/1M HCl

Electrochemical studies are used to predict the nature of the inhibitor and to determine the suitable mechanism for the inhibition process. The extrapolation of Tafel straight line allowed to find out the corrosion current density (i_{corr}). The values of i_{corr}, the corrosion potential (E_{corr}) , cathodic and anodic Tafel slopes (b_a and b_c) and inhibition efficiency (%IE) are given in Tables 4.11-4.14 and Figures 4.13(a-d). There was a small change in the anodic (b_a) and cathodic (b_c) curves with and without addition of PAVL extract (Figure 4.13 (a) and Table 4.11). This was the indicative of the control of cathodic and anodic reaction.From the intersection of cathodic and anodic tafel lines, corrosion current density was calculated. The results revealed that I_{corr} values decreased with increase in the concentration of PAVL extract. Inspection of the values showed that I_{corr} values decreased from 212 µA/cm^2 to 22 µA/cm^2. It indicated that the inhibitor was able to minimize corrosion of MS in the investigated acid medium **(Doner *et al*, 2011, Singh *et al*, 2011)**. A maximum of 89.8 percentage of inhibition was obtained at 0.7% concentration of PAVL extract. No significant shifts in the E_{corr} values were noticed in the presence of the inhibitor. In the current study, the E_{corr} values were lower than 85 mV than the blank value, indicating that all the investigated inhibitors were mixed type of the inhibitors **(Singh *et al*, 2010)**. R_p values were found to vary from 159 Ohm/cm^2 for the

acidic solution to 710 Ohm/cm^2 at 0.7% concentration of PAVL solution. The inhibitor afforded an efficiency of 77.6 percentage. This might be due to the adsorption of active compounds present in PAVL extract onto the metal surface.

In the case of PVL extract when the concentration increased, the IE(%) also increased and their corresponding R_p values were increased (Figure 4.13(b) and Table 4.12). The highest inhibition efficiency 91.1% was obtained by adding 0.7% PVL extract. I_{corr} value decreased from 212 µA/cm^2 to 18.9 µA/cm^2. R_P value increased from 159 Ohm/cm^2 to 767Ohm/cm^2.

In the case of SP extract a maximum inhibition efficiency of 91.8% was achieved in 0.7% concentration of the SP extract. The IE was increased from 65.4 % to 91.8 % in 1M HCl solution (Figure 4.13(c) and Table 4.13). The results show that R_p values increased from 159 Ohm/cm^2 to 866 Ohm/cm^2. The increased in R_p values with increase in inhibitor concentration suggested that the process of adsorption of SP extract on MS surface. I_{corr} value decreased from 212 µA/cm^2 to 22.5 µA/cm^2.

In the case of PB extract the maximum IE (%) efficiency of PB extract was 89.5 percentage (Figure 4.13 (d) and Table 4.14). The main reason was that the adsorption ofthe compounds present in the PB extract onto the metal surface. I_{corr} value decreased from 212 µA/cm^2 to 22.2 µA/cm^2. R_p value increased from 159 Ohm/cm^2 to 1176 Ohm/cm^2.

For all the investigated inhibitors there were no significant changes in the E_{corr} values. There was a small change in the anodic (b_a) and cathodic (b_c) curves with and without addition of the investigated inhibitors.

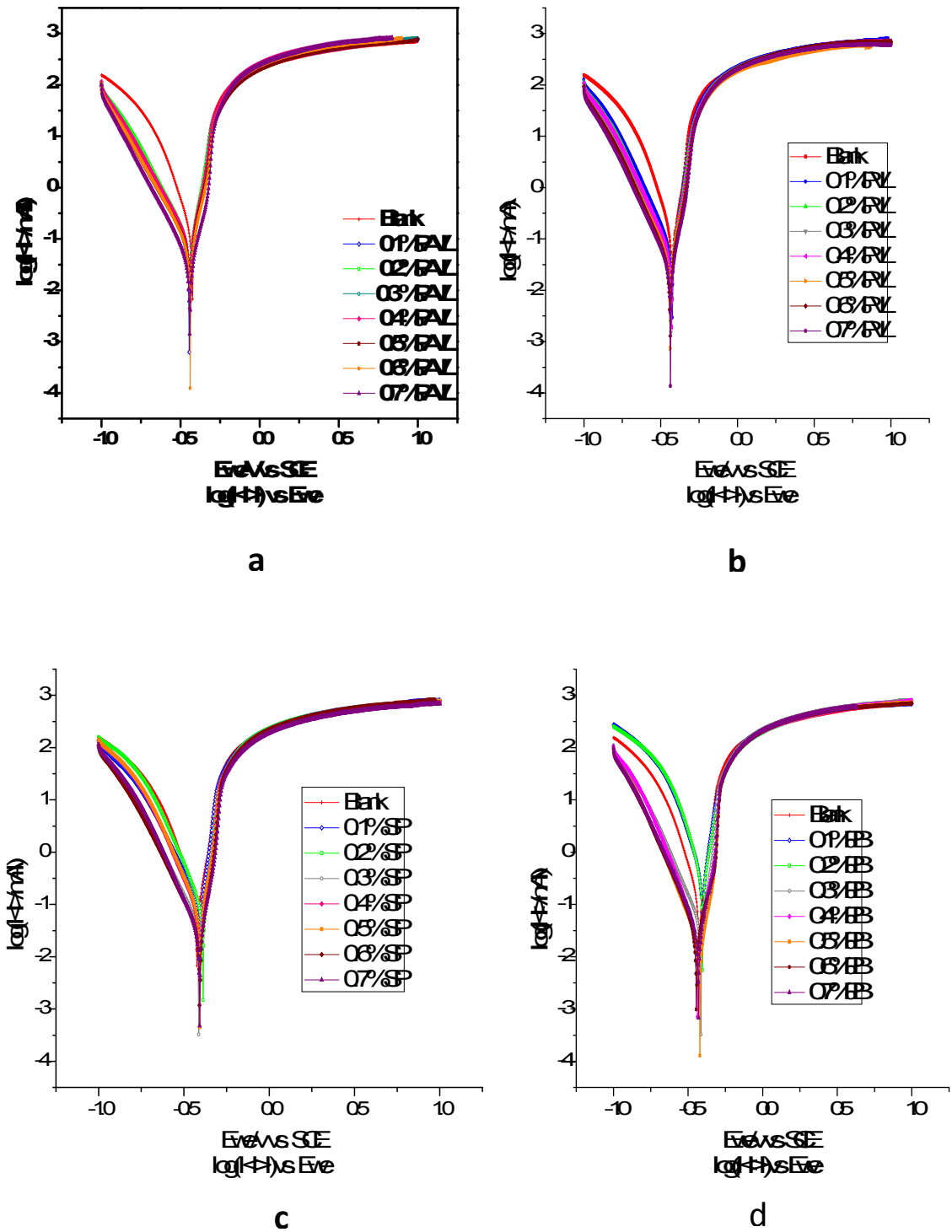

Figure 4.13. Potentiodynamic polarisation curves for MS in 1M HCl in the absence and presence of (a) PAVL (b) PVL (c) SP (d) PB

Table 4.11: Electrochemical polarisation parameters for MS/PAVL/1M HCl

S. No.	Conc (%v/v)	E_{corr} (mV/ SCE)	I_{corr} ($\mu A/cm^2$)	b_a (mV/dec)	b_c (mV/dec)	IE %	R_p Ω/cm^2	IE (%)
1	Blank	-444	212	78.8	115.9	-	159	-
2	0.1	-438	101	61.1	160.0	52.4	267	40.4
3	0.2	-447	79	70.8	171.4	62.7	276	42.4
4	0.3	-434	70	61.9	172.5	67.0	329	51.7
5	0.4	-430	64	61.5	178.7	69.8	335	52.5
6	0.5	-426	61	60.9	184.1	71.2	350	54.6
7	0.6	-418	49	55.4	174.8	77.0	379	58.0
8	0.7	-401	22	43.7	167.6	89.8	710	77.6

Table 4.12. Potentiodynamic polarisation parameters for MS/PVL/1M HCl

S. NO	Conc	E_{corr} (mV/ SCE)	I_{corr} ($\mu A/cm^2$)	b_a (mV/dec)	b_c (mV/dec)	IE %	R_p Ω/cm^2	IE (%)
1	Blank	-444	212	78.8	116	-	159	-
2	0.1	-448	93.5	74.3	149	55.9	298	46.6
3	0.2	-435	50.9	63.9	150	76.0	381	58.3
4	0.3	-440	48.7	63.4	142	77.0	405	60.7
5	0.4	-430	37.6	59.3	147	82.3	456	65.1
6	0.5	-422	31.0	55.4	159	85.4	512	68.9
7	0.6	-422	24.4	53.1	150	88.5	652	75.6
8	0.7	-414	18.9	49.3	154	91.1	767	79.3

Table 4.13. Potentiodynamic polarisation parameters for MS/SP/1M HCl

S. NO	Conc	E_{corr} (mV/ SCE)	I_{corr} ($\mu A/cm^2$)	b_a (mV/dec)	b_c (mV/dec)	IE %	R_p Ω/cm^2	IE (%)
1	Blank	-444	212	79	116	-	159	-
2	0.1	-472	98.2	98	152	65.4	457	56.3
3	0.2	-482	85.5	94	133	76.5	501	70.8
4	0.3	-435	75.7	85	128	79.1	585	75.5
5	0.4	-428	68.7	78	131	82.5	653	79.9
6	0.5	-427	59.6	70	131	84.1	717	83.4
7	0.6	-413	43.1	64	124	88.4	855	85.0
8	0.7	-401	22.5	59	113	91.8	866	89.0

Table 4.14. Potentiodynamic polarisation parameters for MS/PB/1M HCl

S. NO	Conc	E_{corr} (mV/ SCE)	I_{corr} (μA/cm^2)	b_a (mV/dec)	b_c (mV/dec)	IE %	R_p Ω/cm^2	IE (%)
1	Blank	-444	212	78.8	115.9	-	159	-
2	0.1	-443	81.5	118	124	61.6	534	70.2
3	0.2	-424	62.6	104	122	70.5	615	74.1
4	0.3	-408	55.5	220	187	73.8	788	79.8
5	0.4	-431	36.7	41.5	145	82.7	712	77.7
6	0.5	-436	36.3	42.4	130	82.9	718	77.9
7	0.6	-446	32.8	39.3	147	84.5	795	80.0
8	0.7	-422	22.2	39.4	138	89.5	1176	86.5

4.2.2 Electrochemical Impedance Measurements– MS/PAVL/PVL/SP/PB/1M HCl

The observed impedance spectra exhibited a single depressed semicircle whose diameter was increased with increase in concentration of the inhibitor implied a charge transfer process for the corrosion inhibition process **(Lebrini *et al,* 2011c).** From The impedance parameters suggested an increase in charge transfer resistance (R_{ct}) values by increasing in the inhibitor concentrations. Nyquist plot of single capacitive semicircle was related to single time constant which was representated in Bode plot **(Oguzie *et al*, 2014)**. Nyquist plot for the investigated inhibitors are depicted in Figures 4.14(a, b) and 4.15 (c, d). Nyquist plot was analysed by a simple circuit model as depicted in Figure.4.16 which included solution resistance (R_s), charge transfer element (R_{ct}), constant phase element (CPE) and surface inhomogeneity (n) and the values are listed in (Tables 4.15-4.18). The plots showed an increase in impedance response on MS on addition of the investigated inhibitors by increased a diameter which was related to charge transfer resistance (R_{ct}) values **(Rodriguez-Torres *et al,* 2018).** The R_{ct} value increased from 19.7 Ωcm^2 to 144.4 Ωcm^2 and C_{dl} value decreased from 89.4 μF/cm^2 to 44.1 μF/cm^2 with increase in concentration of PAVL extract. The decreased in C_{dl} values were noticed with increase in PAVL extract concentration. The increased in IE reflected the increase in the surface coverage which was due to the presence of PAVL molecules of plant extract. 86.4 percentage IE was observed at 0.7% concentration of PAVL (Table 4.15 and Figure 4.14 (a)).

In case of PVL extract, R_{ct} value increased from 19.7 Ωcm^2 to 375.4Ωcm^2 and C_{dl} value decreased from 89.4 $\mu F/cm^2$ to 29.4 $\mu F/cm^2$ with increase in concentration of PVL extract. The reduced C_{dl} values could be attributed to the adsorption of the chemical constituents of PVL extract at the metal surface. It has been reported that the adsorption process on the metal surface was characterized by a decrease in C_{dl} value. A maximum inhibition efficiency of 94.8 percentage achieved for 0.7% concentration for PVL extract.This proved that the higher shielding effect of inhibitors molecules on metal surface by the adsorption of the PVL compounds over metal surface (Table 4.16 and Figure 4.14 (b)).

In the case of SP extract, the inhibition efficiency (% IE) calculated from R_{ct} values were found to provide a maximum efficiency of 94.7 percentage at 0.7% SP concentration in 1M HC1 solution.The R_{ct} value increased from 19.7 Ωcm^2 to 368.1Ωcm^2 and C_{dl} value decreased from 89.4 $\mu F/cm^2$ to 44.3 $\mu F/cm^2$ with increase in concentration of SP extract. The value of C_{dl} decreased with increase in the inhibitor concentration **(Arul zavier stango *et al*, 2018)** (Table 4.17 and Figure 4.15 (c)). The reason was that decreased in local dielectric constant with an increase thickness of the electrical double layer capacitance **(Singh *et al*, 2014).** This is indicative that the inhibition reaction took place on MS surface due to the adsorption of SP extract molecules.

In the case of PB extract, greater inhibition efficiency (%IE) of 97.1 percentage was achieved at 0.7% concentration of PB extract. The R_{ct} value increased from 19.7 Ω/cm^2 to 685.3 Ω/cm^2 and C_{dl} value decreased from 89.4 $\mu F/cm^2$ to 36.2 $\mu F/cm^2$ with increase in concentration of PB extract. Assessment of Table 4.18 and Figure 4.15 (d) revealed that the C_{dl} values reduced while R_{ct} values enhanced with enhancing the inhibitor solution than the blank solution. The decreased C_{dl} for the inhibited systems with decrease in local dielectric constant signify that the inhibitor molecules function by adsorption at the metal/electrolyte interface **(Singh *et al,* 2012a).**

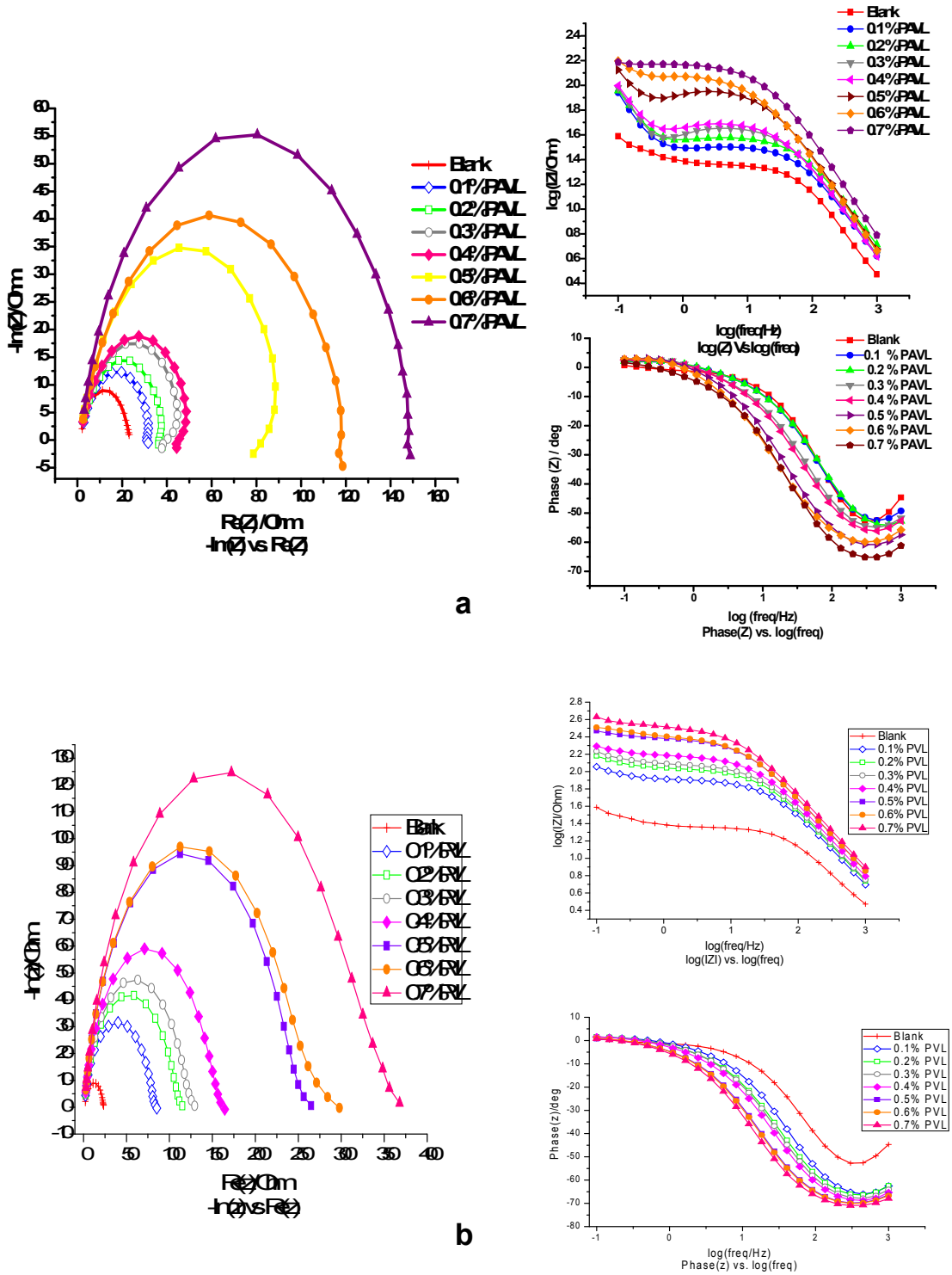

Figure 4.14. Nyquist and Bode diagrams for MS in 1M HCl in the absence and presence of (a) PAVL (b) PVL

Table 4.15. Electrochemical Impedance parameters for MS/PAVL/1M HCl

Conc (%)	PAVL								
	R_S (Ωcm^2)	Y_0 ($\mu F/cm^2$)	n	R_{ct} (Ωcm^2)	IE (%)	f_{max} (Hz)	C_{dl} ($\mu F/cm^2$) $X10^{-6}$	θ	τ (S^n)
Blank	2.1	8083	0.78	19.7	-	90.4	89.4	-	0.0018
0.1	2.8	5769	0.80	27.6	28.6	92.0	62.7	0.30	0.0017
0.2	3.2	4870	0.80	32.7	39.8	97.4	50.0	0.44	0.0016
0.3	2.9	4179	0.84	38.1	48.3	68.9	60.7	0.32	0.0023
0.4	2.9	3773	0.85	42.2	53.3	59.5	63.4	0.29	0.0027
0.5	3.1	2060	0.90	77.3	74.5	37.9	54.3	0.39	0.0042
0.6	3.1	1369	0.95	116.3	83.1	23.3	58.8	0.34	0.0068
0.7	3.6	1102	0.93	144.4	86.4	25.0	44.1	0.51	0.0064

Table 4.16. Electrochemical Impedance parameters for MS/PVL/1M HCl

Conc (%)	PVL								
	R_S (Ωcm^2)	Y_0 ($\mu F/cm^2$)	n	R_{ct} (Ωcm^2)	IE (%)	f_{max} (Hz)	C_{dl} ($\mu F/cm^2$) $X10^{-6}$	θ	τ (S^n)
Blank	2.1	8083	0.78	19.7	-	90.4	89.4	-	0.0018
0.1	2.2	1841	0.93	86.5	77.2	30.0	61.4	0.31	0.0053
0.2	2.9	1271	0.95	125.3	84.3	23.1	55.1	0.38	0.0069
0.3	3.6	1142	0.94	139.4	85.9	24.5	46.6	0.48	0.0065
0.4	3.1	962	0.94	165.5	88.1	22.4	42.9	0.52	0.0071
0.5	1.9	611	0.96	260.5	92.4	15.6	39.3	0.56	0.0102
0.6	2.8	539	0.95	295.5	93.3	15.7	34.3	0.62	0.0101
0.7	5.0	424	0.94	375.4	94.8	14.4	29.4	0.67	0.0110

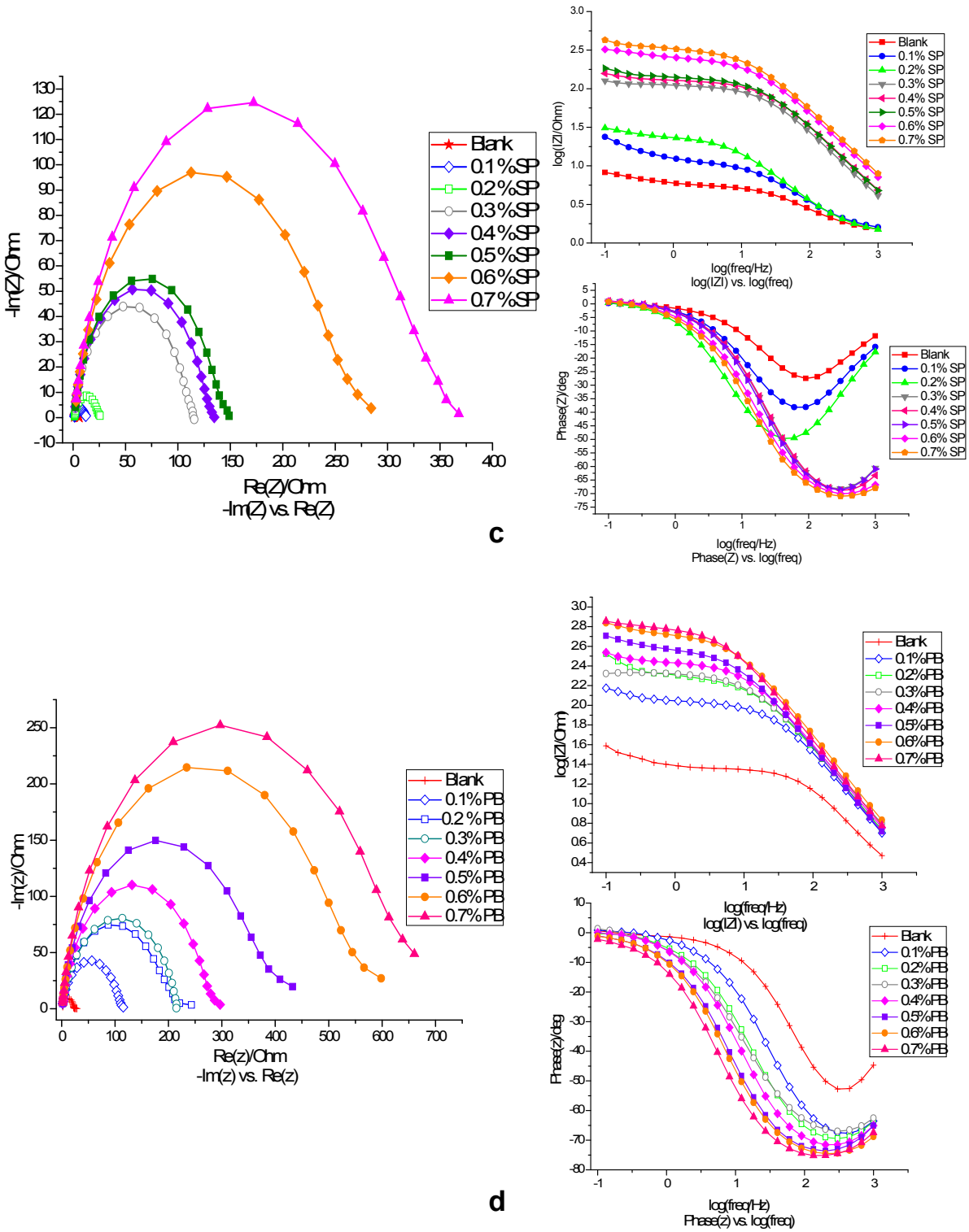

Figure 4.15. Nyquist and Bode diagrams for MS in 1M HCl in the absence and presence of (c) SP (d) PB

Table 4.17. Electrochemical Impedance parameters for MS/SP/1M HCl

Conc (%)	SP								
	R_S (Ωcm^2)	Y_0 ($\mu F/cm^2$)	n	R_{ct} (Ωcm^2)	IE (%)	f_{max} (Hz)	C_{dl} ($\mu F/cm^2$) X10^{-6}	θ	τ (S^n)
Blank	2.1	8083	0.78	19.7	-	90.4	89.4	-	0.0018
0.1	3.5	6553	0.81	24.3	18.9	73.7	88.9	0.01	0.0022
0.2	2.1	6196	0.81	25.7	23.4	79.5	77.9	0.13	0.0020
0.3	3.4	1377	0.95	115.6	83.0	23.2	59.4	0.34	0.0069
0.4	2.8	1182	0.97	134.7	85.4	20.1	58.9	0.34	0.0079
0.5	1.0	1067	0.96	149.3	86.8	20.8	51.2	0.43	0.0076
0.6	1.4	560	0.99	284.2	93.1	12.6	44.4	0.50	0.0126
0.7	3.6	433	1.00	368.1	94.7	9.8	44.3	0.50	0.0163

Table 4.18. Electrochemical Impedance parameters for MS/PB/1M HCl

Conc (%)	PB								
	R_S (Ωcm^2)	Y_0 ($\mu F/cm^2$)	n	R_{ct} (Ωcm^2)	IE (%)	f_{max} (Hz)	C_{dl} ($\mu F/cm^2$) X10^{-6}	θ	τ (S^n)
Blank	2.1	8083	0.78	19.7	-	90.4	89.4	-	0.0018
0.1	2.2	1271	0.95	125.3	84.3	23.0	55.3	0.38	0.0069
0.2	4.9	757	0.97	210.4	90.6	16.7	45.3	0.49	0.0095
0.3	2.6	629	0.98	253.2	92.2	14.0	45.0	0.50	0.0114
0.4	3.1	515	0.99	309.4	93.6	11.4	45.0	0.50	0.0139
0.5	1.9	354	1.02	450.1	95.6	7.9	44.7	0.50	0.0201
0.6	2.5	262	1.01	608.5	96.8	7.0	37.4	0.58	0.0228
0.7	1.9	232	1.01	685.3	97.1	6.4	36.2	0.60	0.0248

4.2.2.1 Analysis of Impedance spectral data for MS/PAVL/PVL/SP/PB/1M HCl

The Nyquist impedance plots for MS exposed in 1M HCl in the absence and presence of the investigated inhibitors are shown in Figures 4.14(a, b) and Figure 4.15 (c, d) and Tables 4.15 – 4.18 . Impedance diagrams were found to have semicircles shape and presence of the inhibitors did not change their profile. It was reflected that the charge transfer process generally retarded the dissolution of MS in 1M HCl. While increasing the concentration of the investigated inhibitors, the diameter of the semicircle also increased which was indicated that the formation of a strong inhibitive film over the surface of the metal. The proposed equivalent circuit model is depicted in Figure 4.16.

When the concentration of inhibitors increased, it increased the polarisation resistance (R_{ct}) and decreased the double layer capacitance (C_{dl}).The obtained results related the reduction in local dielectric constant and increased in the thickness of the electrical double layer suggested that the inhibitor molecules were adsorbed on the mild steel-solution interface **(Lorenz et al, 1981).**

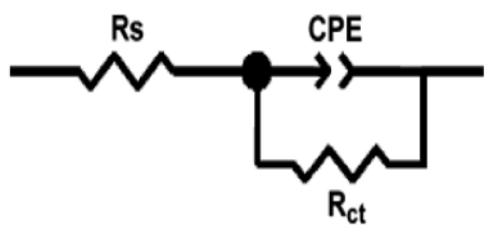

Figure 4.16. Equivalent circuit model for MS/1M HCl

Good fit with this model was observed for all experimental data. The impedance of a constant phase element was described by the expression **(Macdonald, *et al*, 1987)**

$$Z_{CPE}=Y_o^{-1}(j\omega)^{-n} \quad (4.1)$$

Where Y_o is a proportional factor, n is a phase shift. The value of double layer capacitance (C_{dl}) obtained from the following equation

$$C_{dl} = Y_o(\omega)^{n-1} \quad (4.2)$$

Where w is the frequency at which the imaginary part of the impedance has a maximum.

It was apparent from Tables 4.15- 4.18 that the values of C_{dl} decreased and the IE increased with increasing the concentration of the inhibitor solution. The decreased in the C_{dl} with decrease in local dielectric constant which increased in the thickness of the electrical double layer.It was suggested that PAVL, PVL, SP and PB extracts functioned

by the adsorption of the inhibitors molecules at the metal/solution interface and replacement of water molecules by the investigated inhibitors **(Li *et al*, 2007).**

Bode plot in Figures 4.14(a, b) and Figure 4.15 (c, d) displayed a single time constant behaviour, and the values of phase angle and impedance magnitude(IZI) increased with increasing PAVL, PVL, SP and PB extract concentration, which indicated better protection occurred by the studied inhibitors with higher concentration **(Hassan, 2007).**

4.2.3 Potentiodynamic polarisation study- AA/PAVL/PVL/SP/PB/1M HCl

Tafel studies were carried out in order to investigate the effect of the investigated inhibitors on cathodic and anodic reaction of aluminum alloy. Figures.4.17 (a-d) and Tables 4.19-4.22 represented the potentiodynamic polarisation curves without and with different concentrations of investigated inhibitors.The various parameters obtained from polarisation curves are placed in Table 4.19-4.22. The shape of Tafel plots of the unprotected system and protected system remains the same which indicated that, the addition of different amounts of the investigated extracts effectively hindered the corrosion current density values. The decreased in I_{corr} values with improve in the investigated inhibitors concentration was due to enhance the blocked portion on the surface of the aluminum metal by studied inhibitors. Hence, the protection efficiency increased, whereas the corrosion rate decreased with an increased in the amount of investigated extract constituents.

In the case of PAVL extract, a maximum IE (%) of 85.3 percentage was obtained at 0.7% concentration of PAVL extract. From the Table 4.19 and Figure 4.17 (a) it is observed that, the I_{corr} value decreased from 34377 μA/cm^2 to 5055 μA/cm^2 by the adsorption of PAVL molecule on AA surface. From Table 4.19, it was observed that, the I_{corr} values gradually decreased from 34377 μA/cm^2 to 5055 μA/cm^2 and inhibition efficiency increased with increase in the concentration of the PAVL extract. R_p value increased from 1.13 Ω/cm^2 to 4.43 Ω/cm^2. These results again highlight the effectiveness of PAVL for protecting aluminium alloy specimen against acid attack. The largest displacement in E_{corr} value was observed at 0.7% concentration of PAVL extract which was much less than 85 mV. This was suggested that PAVL functioned as mixed-type inhibitor

While considering the PVL extract, with increasing concentration of PVL extract, the R_p value increased from 2.3 Ω/cm^2 to 41.6 Ω/cm^2 and IE also increased from 42.8

percentage to 97.9 percentage. In general, an inhibitor is anodic or a cathodic if the variation of E_{corr} against the blank is higher or above than 85 mV. I_{corr} value decreaed from 14249 μA/cm^2 to 294 μA/cm^2. The results of the present study suggested that the PVL could be considered as a mixed type inhibitor (Table 4.20 and Figure 4.17 (b)).

In the case the SP extract, a maximum %IE of 84.7 percentage was obtained at 0.7% concentration of SP extract. I_{corr} value decreased from 17950 μA/cm^2 to 4201 μA/cm^2 and R_p value increased from 1.13 Ω/cm^2 to 7.4 Ω/cm^2 by increased in the concentration of SP extract (Table 4.21 and Figure 4.17 (c)). There was no much difference in the corrosion potential (E_{corr}) values **(Pavithra *et al*, 2013).**

In the case of PB extract, while increasing the PB extract concentration I_{corr} values decreased from 14249 μA/cm^2 to 1185 μA/cm^2 (Table 4.22 and Figure 4.17 (d)), which is indicative of the adsorption of inhibitor molecules on the AA surface. When the concentration of PB extract increased, the R_p value increased from 2.3 Ω/cm^2 to 22.6 Ω/cm^2. The maximum inhibition efficiency (%IE) 91.7 percentage was obtained at 0.7% concentration of PB extract. In addition, the values of E_{corr} are not shift beyond ±85mV which was suggested that PB acted as a mixed-type in presence of PB extract **(Ansari *et al*, 2015, Maayta *et al,* 2004).**

The anodic (b_a) and cathodic (b_c) tafel constants were not shifted towards any particular side were evidence of mixed corrosion inhibition property for al the investigated inhibitors.

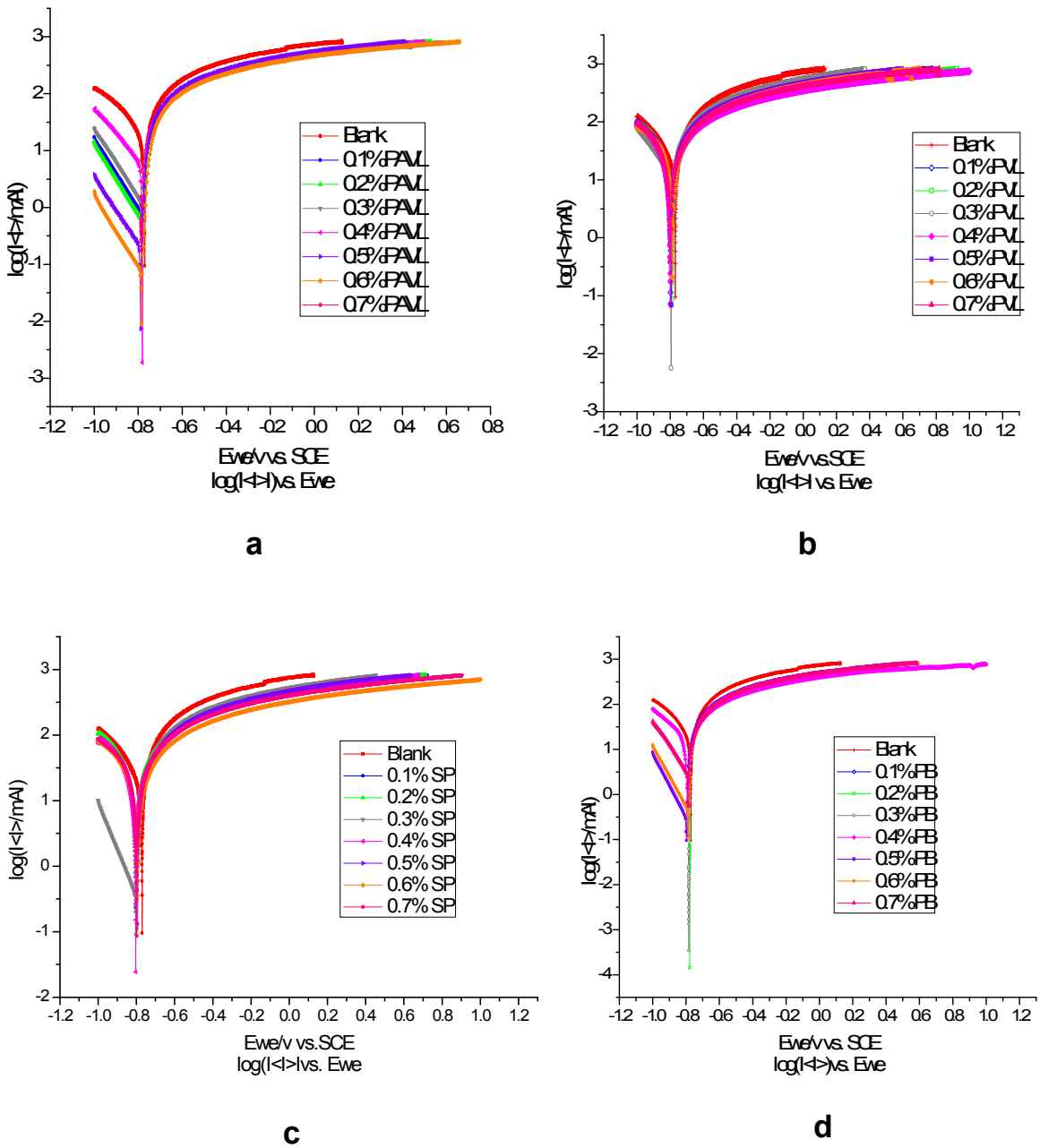

Figure 4.17. Potentiodynamic polarisation plots for AA in 1M HCl in the absence and presence of (a) PAVL (b) PVL (c) SP (d) PB

Table 4.19. Polarisation parameters for AA/PAVL/1M HCl

S. No.	Conc (%v/v)	$-E_{corr}$ (mV/ SCE)	I_{corr} ($\mu A/cm^2$)	b_a (mV/dec)	b_c (mV/dec)	IE %	R_p Ω/cm^2	IE (%)
1	Blank	817	34377	308	295	-	1.13	-
2	0.1	798	23887	313	338	30.5	2.05	44.9
3	0.2	795	21856	307	305	36.4	2.15	47.4
4	0.3	827	17379	300	331	49.4	2.29	50.7
5	0.4	822	17324	307	308	49.6	2.34	51.7
6	0.5	871	13972	298	236	59.4	2.46	54.1
7	0.6	867	13601	301	239	60.4	2.51	55.0
8	0.7	791	5055	217	287	85.3	4.43	74.5

Table 4.20.Potentiodynamic polarisation data and Inhibition efficiency (I.E.) of AA/PVL/1M HCl

S. No	Conc	$-E_{corr}$ (mV/ SCE)	I_{corr} ($\mu A/cm^2$)	b_a (mV/dec)	b_c (mV/dec)	IE %	R_p Ω/cm_2	IE (%)
1	Blank	866	14249	279	221	-	2.3	-
2	0.1	779	8145	83	145	42.8	3.17	27.4
3	0.2	782	5034	60	190	64.7	4.52	49.1
4	0.3	855	2146	113	163	84.9	5.81	60.4
5	0.4	862	1849	113	160	87.0	7.41	69.0
6	0.5	807	1710	57	167	88.0	10.1	77.2
7	0.6	887	747	101	169	94.8	16.9	86.4
8	0.7	884	294	87	157	97.9	41.6	94.5

Table 4.21.Tafel plots values for corrosion inhibition of AA/SP/1M HCl

S. NO	Conc	$-E_{corr}$ (mV/ SCE)	I_{corr} ($\mu A/cm^2$)	b_a (mV/dec)	b_c (mV/dec)	IE %	R_p Ω/cm^2	IE (%)
1	Blank	767	17950	103	226	-	1.13	-
2	0.1	866	14249	279	221	20.6	2.26	50.0
3	0.2	800	12599	173	259	29.8	2.33	51.5
4	0.3	795	7278	81	98	59.5	2.35	51.9
5	0.4	927	7271	268	160	59.5	2.54	55.5
6	0.5	787	7107	95	120	60.4	3.36	66.4
7	0.6	796	6555	73	85	63.5	5.92	80.9
8	0.7	898	4201	130	141	76.6	7.4	84.7

Table 4.22. Potentiodynamic polarisation parameters for AA/PB/1M HCl

S. NO	Conc	$-E_{corr}$ (mV/ SCE)	I_{corr} (μA/cm^2)	b_a (mV/dec)	b_c (mV/dec)	IE %	R_p Ω/cm^2	IE (%)
1	Blank	866	14249	279	221	-	2.3	-
2	0.1	787	10117	120	157	29.0	2.22	26.0
3	0.2	848	4369	134	171	69.3	3.25	29.2
4	0.3	812	3857	95	166	72.9	3.63	36.6
5	0.4	813	2714	79	175	81.0	5.67	59.4
6	0.5	884	1992	128	147	86.0	16.9	86.4
7	0.6	887	1301	108	144	90.9	18.7	87.7
8	0.7	849	1185	85	151	91.7	22.6	89.8

4.2.4 Electrochemical impedance spectroscopy (EIS) measurements- AA/PAVL/PVL/SP/PB/1M HCl

The corrosion behaviour of aluminium alloy in 1 M HCl solution in the absence and presence of different concentrations for all the investigated inhibitors by the EIS method. The fact that impedance diagram was an approximately semi-circular appearance shown that the corrosion of AA in 1M HCl was controlled by a charge transfer resistance process. Small distortion was observed in some diagrams, this distortion may be attributed to frequency dispersion **(Bessone *et al*, 1983)** as a result of surface roughness, impurities, dislocations, and grain boundaries, adsorption of inhibitor and formation of porous layers and inhomogeneity of the electrode surface. The model consisted of the solution resistance (R_s), the charge-transfer resistance of the interfacial corrosion reaction (R_{ct}), and the double layer capacitance (C_{dl}).

In the case of PAVL extract, the C_{dl} values decreased and the R_{ct} values increased with increase of the inhibitor concentrations. The R_{ct} value increased from 5.8 Ω/cm^2 to 146.7 Ω/cm^2 (Table 4.23 and Figure 4.18 (a)). The reason was that the gradual replacement of water molecules by the adsorption of the inhibitor molecules on the metal surface thereby reducing the dissolution reaction of AA in presence of 1M HCl solution. The C_{dl} value decreased from 34.6 μF/cm^2 to 11.5 μF/cm^2. The decreased in the C_{dl} with decrease of the local dielectric constant and/or from the increased the thickness of the electrical double layer **(Bosch *et al*, 2001)** suggested that PAVL molecules were adsorbed at the metal/solution interface. The maximum %IE of 96.1 percentage was obtained at 0.7% concentration of PAVL extract.

In PVL extract the maximum inhibitor efficiency is 96.5 percentage for 1 M HCl at 0.7% of PVL extract (Table 4.24 and Figure 4.18 (b)). The results revealed that R_{ct} significantly increased (5.8 Ω/cm^2 to 164.7 Ω/cm^2) with increase in concentration of inhibitor and C_{dl} tends to decrease. The C_{dl} value decreased from 34.6 µF/cm^2 to 17.5 µF/cm^2. This decreased in C_{dl} value may possibly due to decrease in local dielectric constant with an increase in the thickness of a protective layer at electrode surface, which enhanced the corrosion resistance of AA. The increased in R_{ct} values were ascribed to the formation of protective film at the metal-solution interface **(Fouda *et al*, 2013, Xionga *et al,* 2017).** These observations suggested that adsorption occurred over the surface of AA through PVL extract thereby causing decreased C_{dl} values and increased in R_{ct} values **(Abd El Rehim *et al*, 2002, Unnisa *et al,* 2018)**.

In case of SP extract, the addition of the inhibitor increase R_{ct} value from 5.8 Ω/cm^2 to 445.4 Ω/cm^2, at the same time it decreased the C_{dl} values from 34.6 µF/cm^2 to 17.8 µF/cm^2 by the adsorption of inhibitor on AA surface. A maximum inhibition efficacy (%IE) of 98.7 percentage was achieved for SP extract (Table 4.25 and Figure 4.19 (c)). The results revealed that formed protective layer in the metal surface reduced the charge transfer reaction and thus retarded the corrosion process, leading to increase in R_{ct} values **(Abd El Rehim *et al,* 2001)**. Besides, the adsorbed SP molecules reduced the electrical double layer capacitance of the electrode/solution interface thus decreased the value of C_{dl}.

In case of PB extract (Table 4.26 and Figure 4.19 (d)) reflected that the R_{ct} values were enhanced and the C_{dl} values were reduced in the presence of PB extract, which might be due to the adsorption of PB onto the metal/solution interface. The R_{ct} value increased from 9.8Ω/cm^2 to 221.4 Ω/cm^2 and C_{dl} value decreased from 61.9 µF/cm^2 to 13.1 µF/cm^2 with increase in concentration of PB extract. The size of capacitive loops in Figure 4.19 (d) increased with the addition of PB extract. The decreased C_{dl} value with decrease in the dielectric constant and increased in the thickness of the electrical double layer indicated the formation of a protective film on the AA surface and preventing corrosion **(Bedair *et al*, 2017)**. The maximum value of the inhibition efficiency was 95.6%.

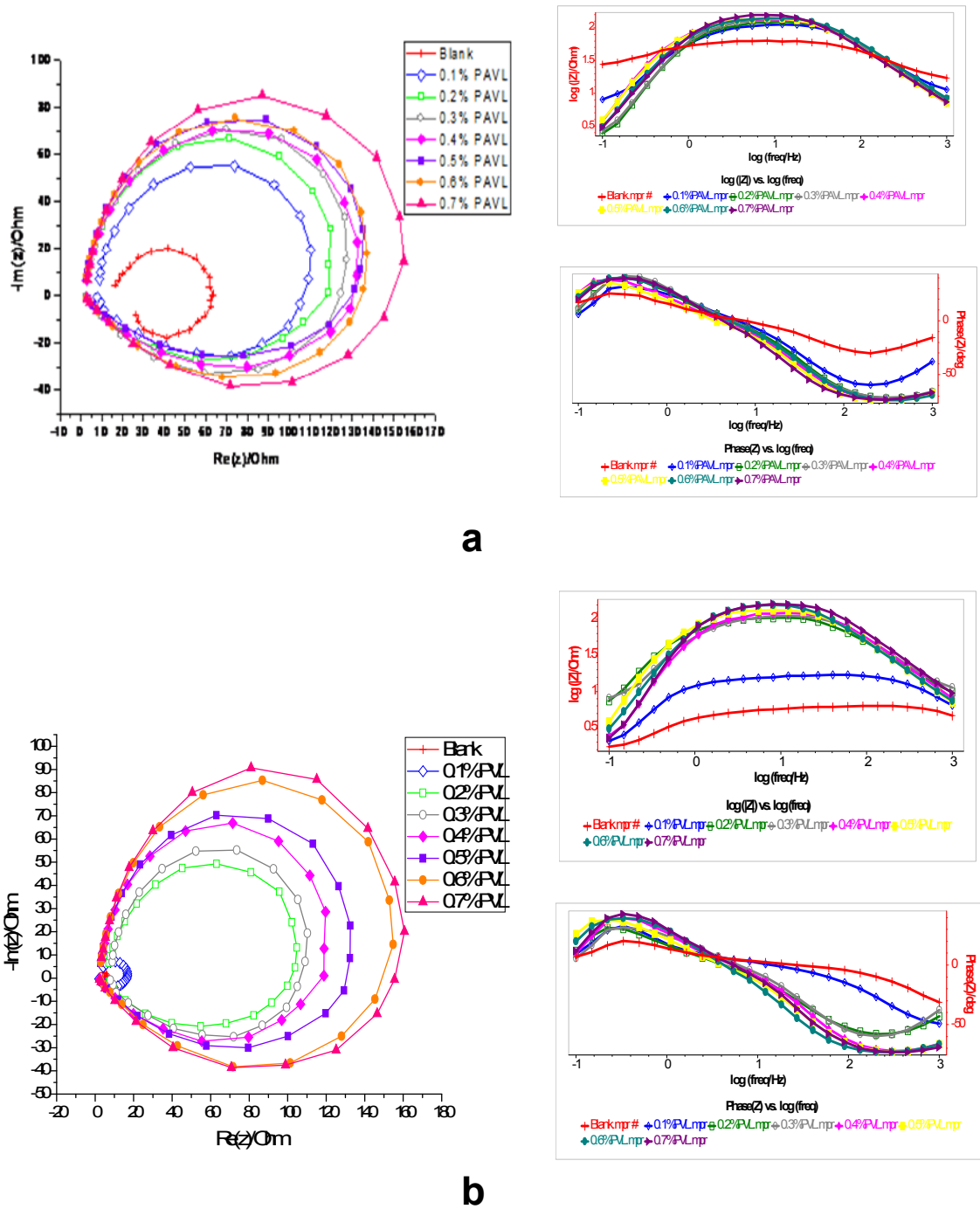

Figure 4.18. Impedance response of AA electrode in the absence and presence of (a) PAVL (b) PVL in Nyquist and Bode formate

Table 4.23. Electrochemical Impedance parameters for AA/PAVL/1M HCl

Conc (%)	PAVL								
	R_S (Ωcm^2)	Y_0 ($\mu F/cm^2$)	n	R_{ct} (Ωcm^2)	IE (%)	f_{max} (Hz)	C_{dl} ($\mu F/cm^2$) $X10^{-6}$	θ	τ (S^n)
Blank	3.5	27454	0.51	5.8	-	793.5	34.6	-	0.0002
0.1	3.3	1567	0.86	101.6	94.3	48.5	32.3	0.07	0.0033
0.2	3.2	1368	0.87	116.4	95.0	42.9	31.9	0.08	0.0037
0.3	3.3	1341	0.87	118.7	95.1	42.9	31.3	0.10	0.0037
0.4	6.2	1278	0.87	124.6	95.4	41.1	31.1	0.10	0.0039
0.5	7.5	1244	0.83	128.0	95.5	51.8	24.0	0.31	0.0031
0.6	4.7	1233	0.75	129.1	95.5	84.5	14.6	0.58	0.0019
0.7	4.4	1085	0.71	146.7	96.1	94.4	11.5	0.67	0.0017

Table 4.24. Electrochemical Impedance values for AA/PVL/1M HCl

Conc (%)	PVL								
	R_S (Ωcm^2)	Y_0 ($\mu F/cm^2$)	n	R_{ct} (Ωcm^2)	IE (%)	f_{max} (Hz)	C_{dl} ($\mu F/cm^2$) $X10^{-6}$	θ	τ (S^n)
Blank	3.4	27454	0.51	5.8	-	794	34.6	-	0.0002
0.1	4.3	3424	0.80	46.5	87.5	103	33.4	0.03	0.0016
0.2	8.7	1619	0.83	98.3	94.1	62	26.1	0.25	0.0026
0.3	1.5	1555	0.81	102.4	94.3	67	23.2	0.33	0.0024
0.4	3.6	1527	0.80	104.3	94.4	72	21.1	0.39	0.0022
0.5	6.2	1347	0.81	118.2	95.1	65	20.8	0.40	0.0025
0.6	5.2	1198	0.79	132.9	95.6	67	17.9	0.48	0.0024
0.7	3.1	967	0.80	164.7	96.5	55	17.5	0.49	0.0029

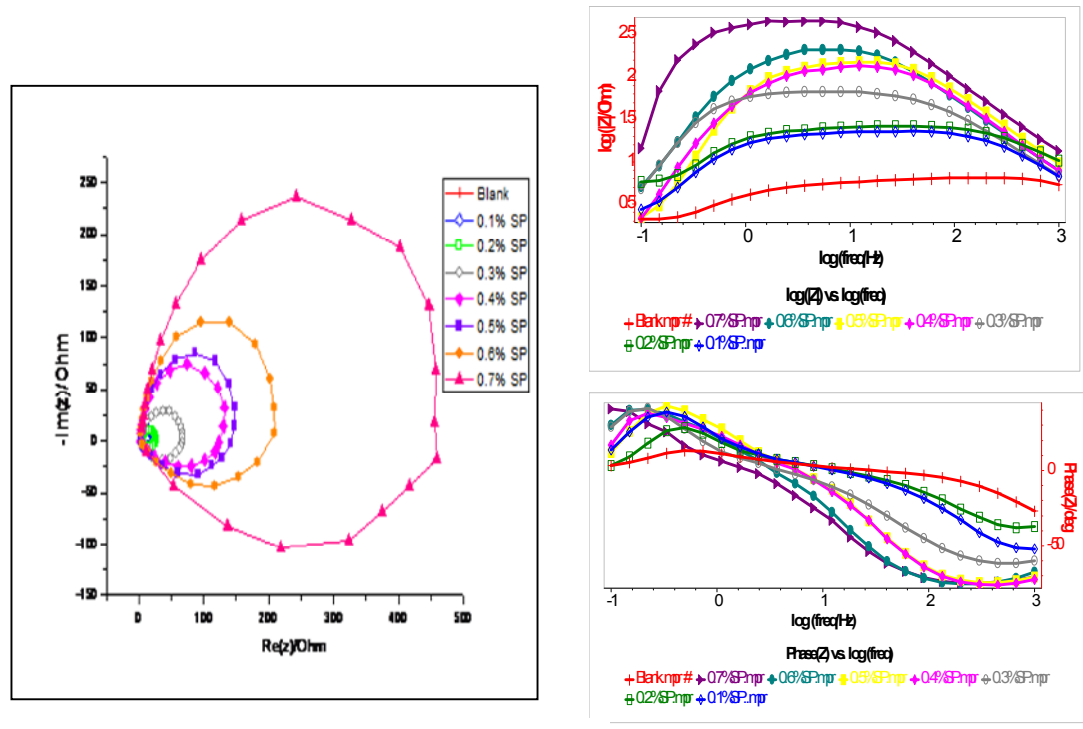

c

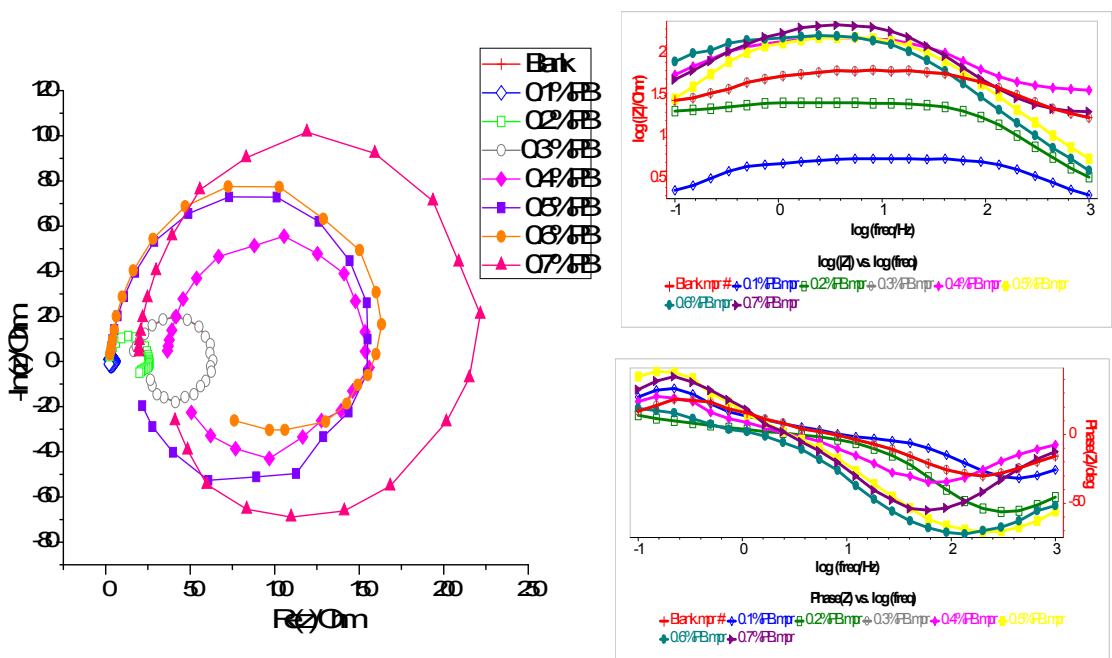

d

Figure 4.19. Nyquist and Bode plots of AA in 1M HCl in the absence and presence of (c) SP (d) PB extract

Table 4.25. Electrochemical Impedance parameters for AA/SP/1M HCl

Conc (%)	SP								
	R_S (Ωcm^2)	Y_0 ($\mu F/cm^2$)	n	R_{ct} (Ωcm^2)	IE (%)	f_{max} (Hz)	C_{dl} ($\mu F/cm^2$) $X10^{-6}$	θ	τ (S^n)
Blank	3.4	27454	0.51	5.8	-	794	34.6	-	0.0002
0.1	3.2	7077	0.70	22.5	74.2	256	27.6	0.20	0.0006
0.2	7.9	6663	0.70	23.9	75.7	248	26.9	0.22	0.0006
0.3	3.6	2818	0.77	56.5	89.7	115	24.5	0.29	0.0014
0.4	2.8	1218	0.81	130.7	95.6	59	20.7	0.40	0.0027
0.5	3.4	1195	0.80	133.3	95.7	61	19.5	0.44	0.0026
0.6	6.6	809	0.83	196.8	97.1	42	19.5	0.44	0.0038
0.7	2.4	358	0.85	445.4	98.7	20	17.8	0.49	0.0079

Table 4.26. Impedance values for AA/PB/1M HCl

Conc (%)	PB								
	R_S (Ωcm^2)	Y_0 ($\mu F/cm^2$)	n	R_{ct} (Ωcm^2)	IE (%)	f_{max} (Hz)	C_{dl} ($\mu F/cm^2$)	θ	τ (S^n)
Blank	1.2	16249	0.64	9.8	-	262.5	61.9	-	0.0006
0.1	3.1	10340	0.71	15.4	36.4	184.6	56.0	0.10	0.0009
0.2	3.7	6269	0.78	25.4	61.4	115.7	54.2	0.12	0.0014
0.3	3.1	3381	0.81	47.1	79.2	89.9	37.6	0.39	0.0018
0.4	4.9	1041	0.91	153.0	93.6	27.9	37.3	0.40	0.0057
0.5	2.4	955	0.84	166.8	94.1	42.6	22.4	0.64	0.0037
0.6	1.3	965	0.81	165.0	94.1	50.0	19.3	0.69	0.0032
0.7	4.6	719	0.76	221.4	95.6	54.9	13.1	0.79	0.0029

4.2.4.1 Analysis of Impedance Spectral data for AA/ PAVL/PVL/SP/PB/1M HCl

The impedance spectra of aluminium alloy (AA) corrosion in 1MHCl solution in the absence and presence of the investigated inhibitors (PAVL, PVL, SP and PB) were found to have an approximate elliptic shape. Similar study was reported on AA in 1M HCl medium **(Li *et al*, 2011a, Garrigues et al, 1996, Ge *et al,* 2008).**

The capacitive loop at high frequency in acid solution could be assigned to the formation of oxide layer on AA. The electrode surface was covered with an oxide layer because of the ex situ pre-treatment of the electrode.In fact, it was very difficult to produce an oxide free AA surface. Even if producing such a surface, it was oxidized very fast by O_2 **(Burstein *et al*, 1992)**. In addition, the capacitive loop was related to the interfacial reactions, mainly the reaction of aluminium oxidation at the metal/oxide/electrolyte interface **(Brett *et al*, 1992)**. Noticeably, the capacitive arc at HF was only some ohms of impedance, which specify that the dissolution rate was high. The dissolution process mainly included the formation of Al^{+} ions at the metal/oxide interface, and their migration through the oxide/solutioninterface where they were further oxidized to $Al^{3+.}$ In the presence of the investigated inhibitors, the complex of (metal–oxide–hydroxide–inhibitor)$_{ads}$ could also be formed **(Metlkos-Hukovic *et al*, 1998)**. It was suggested that all these processes were represented by only one loop which was related either to the overlapping of the loops of processes, or to the assumption that one pronounced when the intermediates were strongly adsorbed. The relaxations of adsorbed species include H_{ads}^{+}, acid anions, O^{2-} ion, or inhibitor species on the electrode surface. In 1M HCl solution, the inductive loop was attributed to the re-dissolution of the oxide layer surface or AA-dissolution at low frequencies.

The EIS results in HCl solution was simulated by the equivalent circuits shown in Figure 25. R_s, R_{Ct} and R_L are the solution resistance, charge transfer resistance and inductive resistance, respectively. CPE is constant phase element. L is the inductance, which was intimately associated with the inductiveloop. When the equivalent circuit Figure 4.20 is used, the polarization resistance (R_p) could calculated from the following equation **(Noor, 2009b).**

$$R_p = R_{Ct}xR_L/R_{Ct}+R_L \qquad (4.3)$$

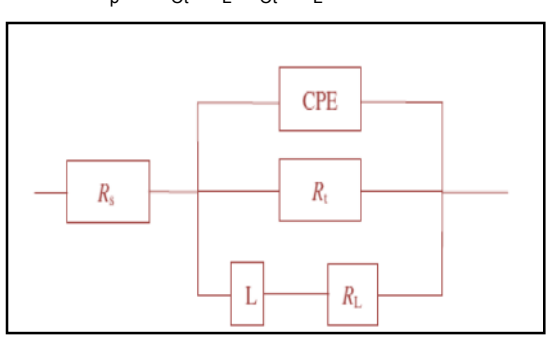

Figure 4.20. Equivalent circuit model for AA/Inhibitors/1M HCl (Li *et al*., 2012b)

The %IE obtained from EIS measurements were close to those deduced from the polarisation method. The inhibition efficiency obtained from the EIS measurements were above 95% for PAVL, PVL SP and PB inhibitors.

The shape of the Bode plots were related to the thickness and the dielectric properties of the film formed on the AA electrode. In the high-frequency region the phase angle approaches 0° while in the middle frequency region the capacitive behaviour of the system was evident for all concentrations, determined by the dielectric properties of the formed film. Also, depression of phase angle at relaxation frequency occurred at lower concentration of the investigated inhibitors resulting in decrease of capacitive response with the decrease of inhibitor concentration. Such a phenomenon could be attributed to higher corrosion activity at low concentrations of inhibitors. The increase of absolute impedance at low frequencies in Bode plot confirmed the higher protection with increasing the concentration of inhibitors, which was related to adsorption of inhibitors on the AA surface **(Mahdavian *et al*, 2006).**

4.2.5 Potentiodynamic Polarisation measurements-AA/PAVL/PVL/SP/PB/1M NaOH

Figures 4.21 (a-d) show the potentiodynamic polarisation curves recorded for aluminium alloy in 1 M NaOH solution in the absence and presence of various doses of investigated inhibitors. The polarisations curves remain almost the same with and without addition of the extract, but in the presence of extract both b_a and b_c shifted to the lower values of corrosion current densities compared to the blank solution. This shift was enhanced with enhancing the extract doses. The electrochemical parameters derived from the polarisation curves in Figures 4.21 (a-d) are given in Tables 4.27-4.30.

In case of PAVL extract, it is noted from this Table 4.27 and Figure 4.21 (a), that I_{corr} values decreased from 5997 μA/cm^2 to1532 μA/cm^2 with improvement of extract doses, due to the increase in the blocked fraction of the AA surface by adsorption of extract components. When the concentration of PAVL extract increased, it can increase the R_p value form 1.9 Ω/cm^2 to 12.9 Ω/cm^2. A maximum IE (%) of 85.3 percentage was achieved at 0.7% concentration of PAVL extract. The Tafel slopes do not change remarkably upon addition of PAVL extract, which indicated that both anodic and cathodic reactions are controlled. There was no changes in the b_a and b_c values after addition of PAVL extract. Generally, an inhibitor can be classified as cathodic or anodic type if the shift of corrosion potential in the presence of the inhibitorwas more than 85 mV with respect to that in the absence of the inhibitor **(Tao *et al*, 2009)**. In the present study, the results revealed that PAVL extract can be arranged as mixed-type inhibitor.

In the case of PVL extract, the observed results suggest that the plant extract consisted the various phytochemical compounds such as alkaloids; flavonoids etc., all of which might be acted through specific mechanism and the overall effect may be a mixed mode of inhibition **(Ashassi-Sorkhabi *et al*, 2006)**. When the concentration of the PVL extract extract increased, the I_{corr} vaue decreaed and R_p value increased. I_{corr} value decreased from 5997 μA/cm^2 to 1763 μA/cm^2 and R_p value increased from 1.9 Ω/cm^2 to 11.9 Ω/cm^2.The IE values were found to increase with increase in the concentration of the extract. The highest inhibition efficiency at an optimum concentration at 0.7% of PVL extract in 1M NaOH was found to be 84 percentage. In the present study, there were no changes in the b_a and b_c values after addition of PVL extract (Table 4.28 and Figure 4.21(b).

In case of SP extract, I_{corr} values decreased from 5997 μA/cm^2 to 1205 μA/cm^2. A maximum of 79.9 percentage was obtained at 0.7% concentration of SP extract. Table 4.29 and Figure 4.21(c) also provided the polarisation resistance (R_p) values at all concentration of all the inhibitors. R_p values were calculated from the slope of electrode potential and current density relationship. R_p value increased from 1.9 Ω/cm^2 to 8.08 Ω/cm^2 if the concentration of SP extract increased. According to the literature report, if the shift in E_{corr} value for inhibited system is more than ±85 mV with respect to uninhibited system then the inhibitor can be regarded as anodic or cathodic type **(Yadav *et al*, 2013)**. Any noticeable shifts were not observed in E_{corr} values for SP with respect to the uninhibited system indicated mixed mode of corrosion inhibition. There was no change in the b_a and b_c vaues after addition of SP extract.

In case of PB extract, it was noticed that if the displacement of E_{corr} is > 85 mV, an inhibitor can be classified as cathodic or anodic. From Table 4.30 and Figure 4.21 (d) results indicated that the mixed type inhibitor can be attributed to PB extract **(Satapathy *et al*, 2009, Ahamad *et al*, 2010)**. As illustrated in the same Table 4.30, it was clear that I_{corr} values decreased and R_p values were increased (1.9 Ω/cm^2 to 7.67 Ω/cm^2) with increasing concentration of PB extract. The decreased I_{corr} values from 5997 μA/cm^2 to 1433 μA/cm^2 were observed with enhancing concentration of PB extract. On the other hand, no change in b_a and b_c values were observed after the addition of PB extract. A maximum IE (%) of 76.1 percentage was achieved in PB extract.

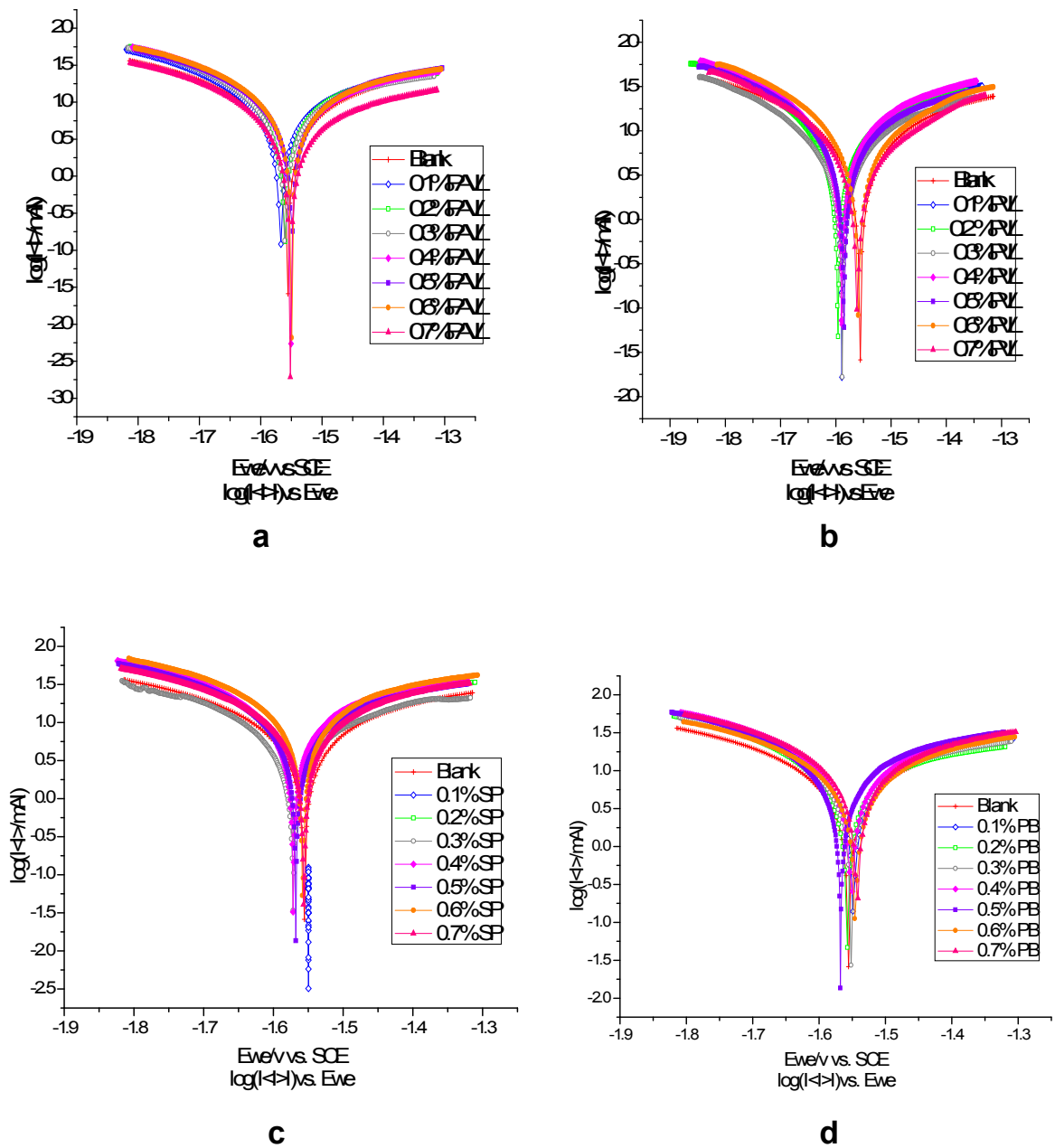

Figure 4.21.Potentiodynamic polarisation curves of AA in 1M NaOH in the absence and presence of (a) PAVL (b) PVL (c) SP (d) PB

Table 4.27.Potentiodynamic polarisation parameters of AA/PAVL/1M NaOH

S. No.	Conc (%v/v)	$-E_{corr}$ (mV/ SCE)	I_{corr} ($\mu A/cm^2$)	b_a (mV/dec)	b_c (mV/dec)	IE %	R_p Ω/cm^2	IE (%)
1	Blank	1556	5997	342	285	-	1.9	-
2	0.1	1538	4801	195	180	19.9	6.16	69.2
3	0.2	1537	4742	131	202	20.9	6.17	69.2
4	0.3	1556	3856	169	145	35.7	6.18	69.3
5	0.4	1550	3344	147	121	44.2	6.25	69.6
6	0.5	1546	3090	121	122	48.5	6.29	69.8
7	0.6	1544	2895	105	115	51.7	6.41	70.4
8	0.7	1545	1532	142	128	74.5	12.9	85.3

Table 4.28. Potentiodynamic Polarisation parameters for AA/PVL/1M NaOH

S. No.	Conc (%v/v)	$-E_{corr}$ (mV/SCE)	I_{corr} ($\mu A/cm^2$)	b_a (mV/dec)	b_c (mV/dec)	IE %	R_p Ω/cm^2	IE (%)
1	Blank	1556	5997	342	285	-	1.9	-
2	0.1	1592	4139	137	129	31.0	5.29	64.1
3	0.2	1593	3809	144	137	36.5	5.39	64.7
4	0.3	1561	2813	113	190	53.1	5.56	65.8
5	0.4	1584	2682	78	98	55.3	6.31	69.9
6	0.5	1586	2540	102	90	57.6	6.79	72.0
7	0.6	1555	2442	101	101	59.3	8.1	76.5
8	0.7	1555	1763	103	109	70.6	11.9	84.0

Table 4.29. Potentiodynamic polarisation parameters for AA/SP/1M NaOH

S. No.	Conc (%v/v)	$-E_{corr}$ (mV/ SCE)	I_{corr} ($\mu A/cm^2$)	b_a (mV/dec)	b_c (mV/dec)	IE %	R_p Ω/cm^2	IE (%)
1	Blank	1556	5997	342	285	-	1.9	-
2	0.1	1548	4530	212	170	24.5	4.51	57.9
3	0.2	1559	4298	124	150	28.3	4.69	59.5
4	0.3	1554	3149	115	185	47.5	5.44	65.1
5	0.4	1567	3038	84	93	49.3	5.45	65.1
6	0.5	1559	2970	87	110	50.5	5.68	66.5
7	0.6	1557	2827	78	78	52.9	5.79	67.2
8	0.7	1554	1205	93	101	79.9	8.08	76.5

Table 4.30. Potentiodynamic polarisation parameters for AA/PB/1M NaOH

S. No.	Conc (%v/v)	$-E_{corr}$ (mV/SCE)	I_{corr} ($\mu A/cm^2$)	b_a (mV/dec)	b_c (mV/dec)	IE %	R_p Ω/cm^2	IE (%)
1	Blank	1556	5997	342	285	-	1.9	-
2	0.1	1543	4718	193	186	21.3	5.42	64.9
3	0.2	1556	3599	179	138	40.0	5.51	65.5
4	0.3	1555	3230	151	116	46.1	6.44	70.5
5	0.4	1548	3118	101	104	48.0	6.6	71.2
6	0.5	1581	2980	168	105	50.3	6.7	71.6
7	0.6	1545	2658	114	108	55.7	6.87	72.3
8	0.7	1540	1433	87	88	76.1	7.67	75.2

4.2.6 Electrochemical impedance measurement-AA/PAVL/PVL/SP/PB/1M NaOH

The EIS of AA in 1M NaOH with and without various concentrations of investigated inhibitors are summarized as Bode and Nyquist plots in Figure 4.22 (a-b) and 4.23 (c-d) respectively. The Bode plot clearly show that the addition of an increasing amount of the investigated inhibitors led to an increase in the electrode impedance. The Nyquist plots (Figure 4.22 (a-b) and 4.23 (c-d)) showed three parts: the capacitive loop in the high-frequency region, the inductive loop in the middle-frequency region, and the capacitive loop in the low-frequency region. The high-frequency capacitive loop may be related to the charge transfer resistance (R_{ct}). The inductive loop may cause by the adsorbed intermediate. The low-frequency capacitive loop influenced the growth and dissolution of the surface film **(Shao *et al*, 2001)**. An equivalent circuit model of Figure 4.24 and Tables 4.31-4.34 was suggested for the corrosion behaviour of the AA electrode in 1M NaOH with and without the addition of the studied inhibitors. Values of R_{ct}, C_{dl} and IE% for inhibited and uninhibited systems were estimated and are listed in Table 4.31-4.34 and Figure 4.22 (a-b) and 4.23 (c-d). A complete inspection of Table 4.31-4.34 reveal that R_{ct} values increased with increasing inhibitor concentration. Whereas the values of C_{dl} decreased with an increase in the concentration of the studied inhibitor.

In the case of PAVL extract, a maximum of 78.8 percentage inhibition efficiency was obtained at 0.7% concentration of PAVL extract. The R_{ct} values increased from 0.6541 Ω/cm^2 to 3.091 Ω/cm^2 and Cdl value decreased from 84.1 μFcm^{-2} to 22.3 μFcm^{-2} with increase in PAVL extract concentration (Table 4.31 and Figure 4.22 (a)).

In the case of PVL extract, a maximum R_{ct} value of 6.747Ω/cm^2 and minimum C_{dl} value of 0.0421 μFcm^{-2} and a maximum inhibition efficiency of 90.3 percentage was obtained at the best concentration (0.7%) of PVL extract(Table 4.32 and Figure 4.22 (b)).

In the case of SP extract, a maximum of 95.4 percentage of inhibition efficiency obtained at 0.7% concentration of SP extract. The R_{ct} values increased from 0.6541 Ω/cm^2 to 4.268 Ω/cm^2 and C_{dl} value decreased from 6.122 μFcm^{-2} to 0.0522 μFcm^{-2} with increases in SP extract concentration (Table 4.33 and Figure 4.23 (c)).

While considering PB extract, a maximum of 82.7 percentage inhibition efficiency was obtained at 0.7% concentration of PB extract. The R_{ct} values increased from 0.6541Ω/ cm^2 to 3.769 Ω/cm^2 and C_{dl} value decreased from 6.1220 μFcm^{-2} to 0.0723 μFcm^{-2} with increases in PB extract concentration (Table 4.34 and Figure 4.23 (d)). The results revealed that increased in surface coverage with increase in the inhibitor concentration, which was reflected in an increase in IE%. The thickness of the protective layer, δ, was related to C_{dl} by the following equation:

$$\delta = \varepsilon_o \varepsilon_r / c_{dl} \qquad (4.4)$$

where ε_o is the vacuum dielectric constant and ε_r is the relative dielectric constant. So, the decreased in the C_{dl} value, which can result from a decreased in the local dielectric constant and/or an increase in the thickness of electrode double layer, suggested that the inhibitor species function by adsorption at the metal/solution interface **(Mccafferty *et al,* 1972, Bentiss *et al,* 2002)**.

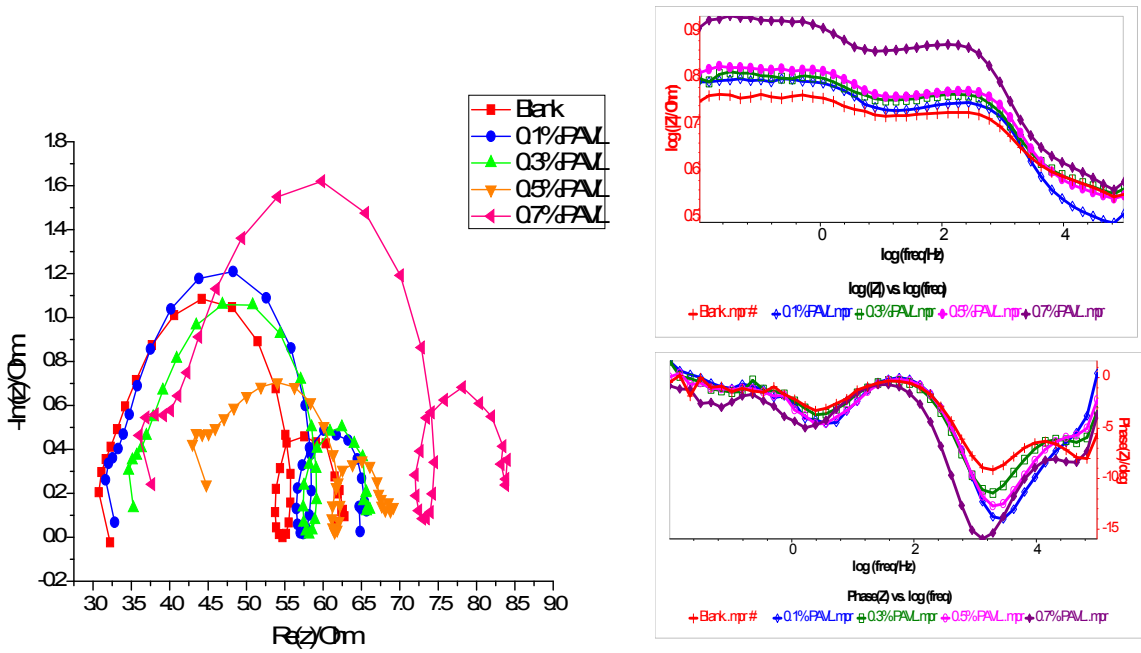

a

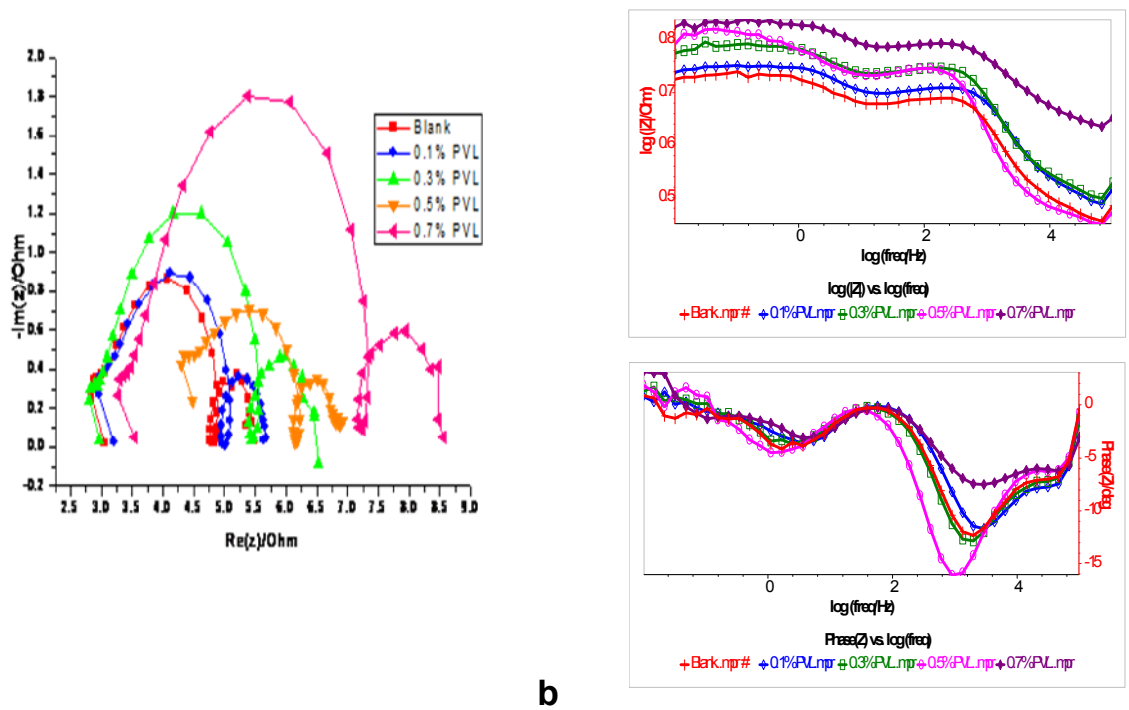

b

Figure 4.22. Nyquist plots and Bode plots for AA in 1M NaOH in the absence and presence of (a) PAVL (b) PVL

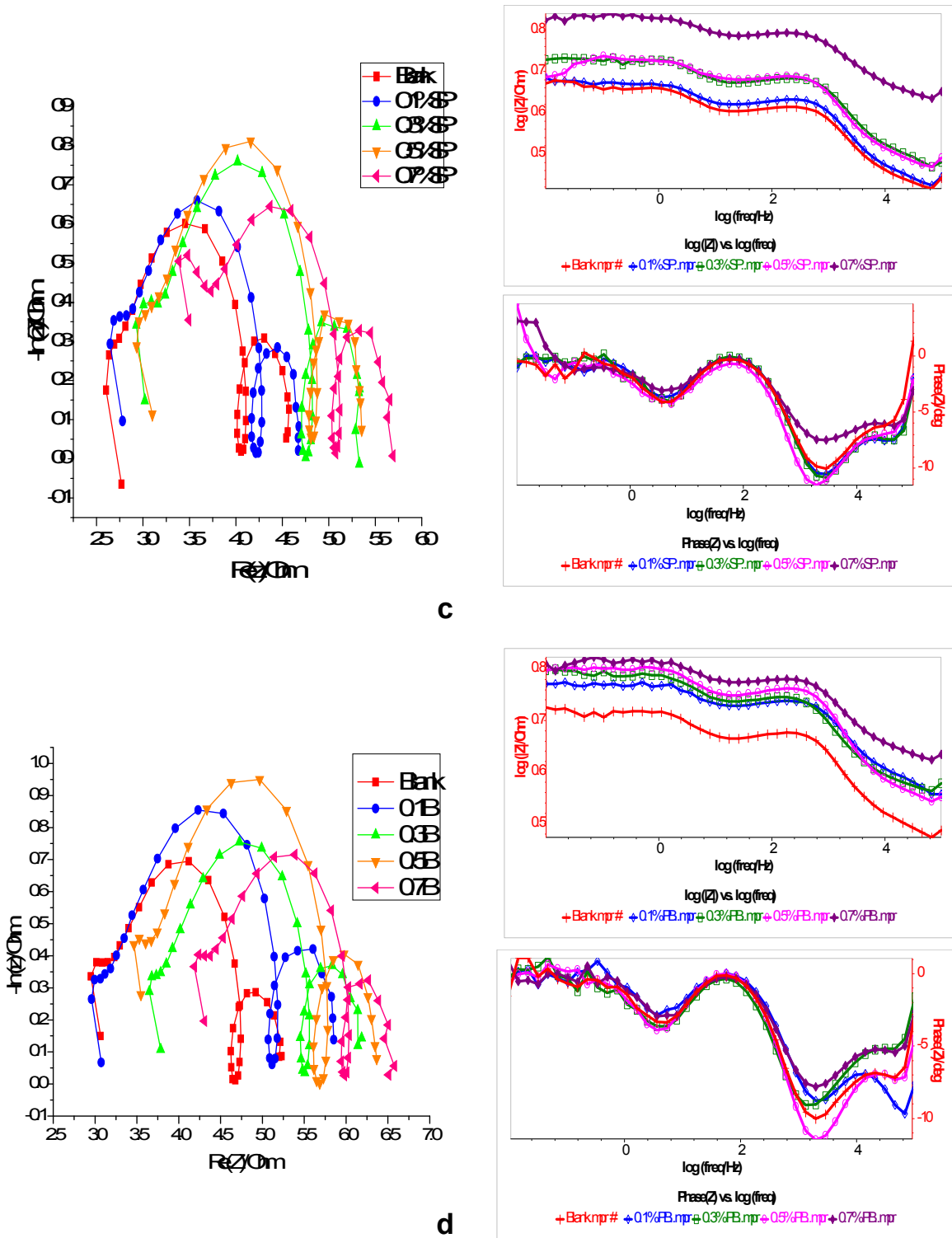

Figure 4.23. Nyquist plots and Bode plots for AA in 1M NaOH in the absence and presence of (c) SP (d) PB

Table 4.31. Electrochemical impedance parameters for AA/PAVL/1M NaOH

Inhibitor	R_s (Ω)	n_1	$(R_{ct})_1$ (Ωcm^2)	L ($H\ cm^2$)	R_L ($\Omega\ cm^2$)	n_2	$(R_{ct})_2$ ($\Omega\ cm^2$)	$(C_{dl})_1$ ($\mu F\ cm^{-2}$) mx10^{-6}	IE (%)	IE (%)	$(C_{dl})_2$ ($\mu F\ cm^{-2}$)
Blank	2.3	0.20	0.6541	0.6177	1.7860	0.66	0.4387	84.13	-	-	6.1220
0.1	2.2	0.08	0.8322	0.1532	0.8550	0.18	0.5859	47.20	21.4	25.1	0.1930
0.3	2.4	0.18	1.5830	0.0492	2.5110	0.13	0.7132	41.57	58.7	38.5	0.1031
0.5	3.5	0.22	1.8040	0.0232	0.8468	0.06	1.1430	31.26	63.7	61.6	0.0685
0.7	3.7	0.36	3.0910	0.0147	0.9732	0.29	1.7440	22.32	**78.8**	74.9	0.0405

Table 4.32. EIS measurement for AA/PVL/1M NaOH

Inhibitor	R_s(Ω)	n_1	$(R_{ct})_1$ (Ωcm^2)	L ($H\ cm^2$)	R_L ($\Omega\ cm^2$)	n_2	$(R_{ct})_2$ ($\Omega\ cm^2$)	$(C_{dl})_1$ ($\mu F\ cm^{-2}$) X10^{-6}	IE(%)	IE(%)	$(C_{dl})_2$ ($\mu F\ cm^{-2}$)
Blank	2.3	0.20	0.6541	0.6177	1.7860	0.66	0.4387	84.13	-	-	6.1220
0.1	2.5	0.26	1.9980	0.4256	1.6120	0.22	0.4689	69.13	67.3	6.4	0.2113
0.3	3.2	0.36	2.7880	0.2880	2.1320	0.19	0.5441	60.21	76.5	19.4	0.1842
0.5	2.1	0.38	3.1080	0.1070	1.7740	0.14	1.339	57.98	79.0	67.2	0.0662
0.7	2.0	0.56	6.7470	0.0978	3.8470	0.50	2.3201	50.45	**90.3**	81.1	0.0421

Table 4.33. Impedance parameters for AA/SP/1M NaOH

Inhibitor	$R_s(\Omega)$	n_1	$(R_{ct})_1$ (Ωcm^2)	L ($H\ cm^2$)	R_L ($\Omega\ cm^2$)	n_2	$(R_{ct})_2$ ($\Omega\ cm^2$)	$(C_{dl})_1$ ($\mu F\ cm^{-2}$) $X10^{-6}$	IE(%)	IE(%)	$(C_{dl})_2$ ($\mu F\ cm^{-2}$)
Blank	2.3	0.20	0.6541	0.6177	1.7860	0.66	0.4387	84.13	-	-	6.1220
0.1	2.4	0.15	0.7314	0.5960	1.8570	0.00	0.4401	56.35	10.6	0.32	1.0090
0.3	2.6	0.06	0.8758	0.2003	2.1980	0.21	0.5303	39.82	25.3	17.3	0.1076
0.5	2.0	0.27	2.1170	0.1987	1.6490	0.23	1.5590	31.96	69.1	71.9	0.0652
0.7	2.7	0.41	4.2680	0.0635	0.8599	4.22	9.6230	15.18	84.7	**95.4**	0.0522

Table 4.34. Electrochemical impedance parameters for AA/PB/1M NaOH

Inhibitor	$R_s(\Omega)$	n_1	$(R_{ct})_1$ (Ωcm^2)	L ($H\ cm^2$)	R_L ($\Omega\ cm^2$)	n_2	$(R_{ct})_2$ ($\Omega\ cm^2$)	$(C_{dl})_1$ ($\mu F\ cm^{-2}$) $X10^{-6}$	IE(%)	IE(%)	$(C_{dl})_2$
Blank	2.3	0.20	0.6541	0.6177	1.7860	0.66	0.4387	84.13	-	-	6.1220
0.1	2.5	0.10	0.7979	0.3516	1.6630	0.25	0.4673	81.52	18.0	6.1	0.1115
0.3	2.6	0.09	1.2530	0.1654	1.3670	0.20	0.5544	67.96	47.8	20.9	0.1107
0.5	2.4	0.19	1.6700	0.0349	1.0120	0.14	0.6911	30.45	60.8	36.5	0.0976
0.7	2.3	0.40	3.7690	0.0258	0.6114	0.06	1.152	20.14	**82.7**	61.9	0.0723

2.6.1 Reason for electrochemical Impedance measurements for AA/PAVL/PVL/SP/PB/1M NaOH

Corrosion inhibition study on AA metal in 1M NaOH was investigated by EIS technique using PAVL, PVL, SP and PB inhibitors and given in Figures 4.22 (a), (b) 4.23 (c), (d). As can be seen from Figures 4.22 (a), (b) 4.23 (c), (d), the impedance diagram elucidated by semicircles, suggested that the corrosion reaction take place via charge transfer process **(Prabhu and Rao *et al,* 2014)**. When the concentration of the inhibitor rise, impedance diameter also increased but there was no change in corrosion mechanism. The shape of impedance modulus was a similar inhibited and uninhibited solution. Three loops were observed as shown in the Figures 4.22 (a), (b) 4.23 (c), (d): a large capacitive loop appeared at higher frequency region; a second capacitive loop appeared at lower frequency region and separated by an inductive loop of intermediate frequencies. An equivalent circuit depicted in Figure 4.24 was used to calculate the impedance parameters. This equivalent circuit was found to have solution resistance (R_s), charge transfer resistance (R_{ct}) and inductive elements (R_L and L). The appearance of L in the presence of inhibitor solution was explained by the fact that aluminium alloys still going to dissolve via charge transfer process on the adsorbed inhibitor on AA surface. In this circuit, another constant phase element (CPE_2) was present which was placed in parallel to charge transfer resistance element Rct_2. The measurement of charge-transfer resistance corresponded to the Al^{+}–Al^{3+} reaction was defined by Rct_2. To compensate for non-homogeneity in the system, the CPE was used in this model which was defined by two values, Q and n. The impedance of CPE is represented by:

$$Z_{CPE} = (1/Q(j\omega)^{n}) \quad (4.5)$$

where Q denotes the proportionality constant comparable to capacitance, j is the imaginary unit and x is the angular frequency (x= 2pf, f is the frequency at maximum in Hz), n is the phase shift which is related to the degree of surface nonhomogeneity. The double layer capacitance (Cdl) is deduced from the following equation.

$$C_{dl} = Q \times (2\pi f_{max})^{n-1} \quad (4.6)$$

From the Table 4.31-4.34, it was found that the value of double layer capacitance (C_{dl}) decreased in the presence of PAVL, PVL, SP and PB inhibitors, due to adsorption of inhibitor molecules over the AA surface. Analysis of Table 4.31-4.34, revealed that R_{ct} value increased in presence of inhibitor than the blank solution. The increased in R_{ct}

values for the inhibited system was related to the decrease in the active surface essential for the corrosion process and as a result slower corrosion rate. The inhibition efficiency associated with charge transfer resistance value is calculated by the following equation:

$$\%IE = R_{CT(i)}\text{-}R_{CT(o)}/R_{CT(i)} \quad (4.7)$$

where $R_{ct(i)}$ and $R_{ct(o)}$ are the charge transfer resistance values in the absence and presence of the inhibitor solution, respectively. Bode impedance and phase angle plots are shown in Table 4.31-4.34. A maximum %IE obtained at 0.7% concentration of the investigated inhibitors. The R_{ct} values increased and C_{dl} value decreased with increase in PAVL, PVL, SP and PB extract concentration. This may be due to the adsorption of the investigated inhibitors over the AA surface.

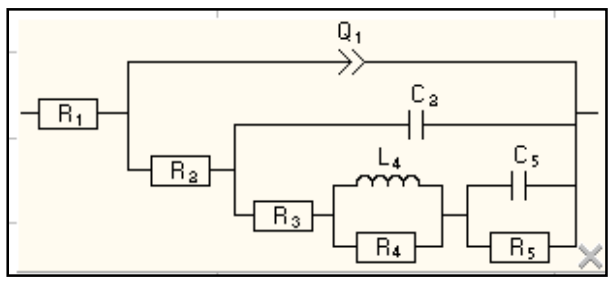

Figure 4.24. Equivalent circuit model for AA/Inhibitors/1M NaOH

Bode plots for AA in alkaline medium indicated that the addition of an increasing amount of the investigated inhibitors led to an increase in the electrode impedance. However, the absence of linear log Z relations with a slope of -1 and the departure of phase angle at intermediate frequencies from 90^o indicated that the circuit tends to the resistive behaviour **(Noor, 2009a)**

4.3 Mass Loss Method

The simple method for measuring corrosion process in boiler plants and industrial equipments is the mass loss method. Due to its reliability and simple application, this method of observing corrosion rate is useful. Although there are many experimental techniques used to evaluate the percentage inhibition efficiency of the investigated inhibitors, mass loss method is most widely and frequency used method **(Ekpe *et al,* 1995)**. In the current study experiments were performed by changing the concentration of the inhibitior for different immersion period and at different temperatures.

4.3.1 Mass loss measurements for MS/PAVL/PVL/SP/PB/1M HCl

Gravimetric measurements are used to find the corrosion rate and % IE for all the investigated inhibitors. Different concentrations of the investigated inhibitors (0.1% to 0.7%) were added to 1M HCl solution and the MS samples were exposed in the solution for various immersion periods (1/2h, 1h, 3h, 6h, 12h and 24h). The observed results are summarised in Table 4.35-4.38. The Inhibition efficiency increased and the corrosion rate decreased with the increase of concentration of the investigated inhibitors.

In the case of PAVL extract, the IE of the PAVL increased from 92.3 percentage at ½ h to 97.1 percentage at 12h of 0.7% concentration of the inhibitor solution. And thereafter a slight decline was observed and the efficiency stabilised to 95.4% at 24h of immersion time. It can be seen from Table 4.35 and Figure 4.25 (a) the highest (%IE) 97.1% was achieved at 12h and further increased in the concentration of PAVL extract did not cause any appreciable change in the performance of the inhibition efficiency. The reason was that the total surface coverage was accomplished by the said concentration and beyond that, any further addition did not yield increased in the inhibition efficiency **(Ashok Kumar *et al,* 2012)**.

In the case of PVL extract, it could be seen that a maximum IE (%) of 97% was maintained till 6hr and thereafter a slight decline was observed Table 4.36 and Figure 4.25 (b). But the inhibition efficiency was found to stabilise at 24h to afford an efficiency of 94.3% demonstrating the effectiveness of the inhibitor at longer periods of immersion. Further increased in concentration did not cause any appreciable change in the inhibition efficacy. The corrosion inhibition may be attributed to the adsorption of the inhibitor at the steel/hydrochloric acid solution interface **(Wang, 2006)**.

In the case of SP extract, the greater inhibition efficiency (%IE) of 94.9% was achieved at 0.7% concentration of the SP extract for 12hr immersion time. Thereafter a slight decline was noticed, but the efficiency stabilised to 91% at 24hr of immersion period. Table 4.37 and Figure 4.25 (c) shows the plot of inhibition efficiency versus inhibitor concentration of seaweed extract of SP on MS in 1M HCl. The inhibitor molecules were adsorbed on the mild steel surface and prevented the surface from further corrosion **(Bhuvaneswari *et al*, 2018)**.

In the case of PB extract, the highest corrosion rate was observed in the free acid solution. Hence, in the presence of PB extract the corrosion rate reduced, implying that PB extracts retarded the mild steel corrosion. A similar trend has also been reported in literature **(Fouda *et al*, 2013).** From the Table 4.38 and Figure 4.25 (d), it can be seen

that the maximum IE of 97.7% for PB was attained at 3h and thereafter a slight decline was noticed. However, the efficiency stabilised to 92.4% at 24h and after 24h there was no further increase in IE with increasing the concentration of the inhibitor.

Table 4.35. Inhibition efficiency as a function of immersion time and concentration for MS/PAVL/1M HCl

Conc (%v/v)	1/2 h		1h		3h		6h		12h		24h	
	CR (mpy)	IE (%)	CR (mpy)	IE (%)	CR (mpy)	IE (%)	CR (mpy)	IE (%)	CR (mpy)	IE (%)	CR (mpy)	IE (%)
Blank	2167	-	2307	-	2706	-	2965	-	2461	-	1707	-
0.1	296	86.3	226	90.2	269	90.1	219	92.6	172	93.0	157	90.8
0.2	255	88.2	168	92.7	191	93.0	160	94.6	110	95.5	108	93.7
0.3	223	89.7	159	93.1	159	94.1	142	95.2	91	96.3	103	94.0
0.4	195	91.0	147	93.6	137	95.0	121	95.9	83	96.6	92	94.6
0.5	184	91.5	133	94.2	131	95.2	106	96.4	73	97.0	91	94.7
0.6	179	91.7	131	94.3	117	95.7	103	96.5	73	97.0	82	95.2
0.7	166	92.3	122	94.7	112	95.8	91	96.9	71	97.1	79	95.4

Table-4.36. Inhibition efficiency as a function of immersion time and concentration for MS/PVL/1M HCl

Conc (%v/v)	1/2 h		1h		3h		6h		12h		24h	
	CR (mpy)	IE (%)	CR (mpy)	IE (%)	CR (mpy)	IE (%)	CR (mpy)	IE (%)	CR (mpy)	IE (%)	CR (mpy)	IE (%)
Blank	2167	-	2307	-	2706	-	2965	-	2461	-	1707	-
0.1	268	87.6	343	85.1	216	92.0	203	93.2	300	87.8	170	90.0
0.2	188	91.3	262	88.6	173	93.6	146	95.1	196	92.0	162	90.5
0.3	175	91.9	228	90.1	152	94.4	127	95.7	184	92.5	143	91.6
0.4	151	93.0	212	90.8	127	95.3	110	96.3	174	92.9	117	93.1
0.5	140	93.5	191	91.7	116	95.7	97	96.7	155	93.7	112	93.4
0.6	125	94.2	166	92.8	105	96.1	96	96.8	147	94.0	110	93.6
0.7	106	95.1	131	94.3	102	96.2	92	97.0	118	95.2	97	94.3

Table-4.37 Inhibition efficiency as a function of immersion time and concentration for MS/SP/1M HCl

Conc (%v/v)	1/2 h		1h		3h		6h		12h		24h	
	CR (mpy)	IE (%)	CR (mpy)	IE (%)	CR (mpy)	IE (%)	CR (mpy)	IE (%)	CR (mpy)	IE (%)	CR (mpy)	IE (%)
Blank	2167	-	2307	-	2706	-	2965	-	2461	-	1707	-
0.1	597	72.5	401	82.6	270	90.0	352	88.1	231	90.6	269	84.2
0.2	495	77.2	367	84.1	216	92.0	275	90.7	189	92.3	218	87.2
0.3	375	82.7	328	85.8	211	92.2	257	91.3	162	93.4	199	88.3
0.4	333	84.6	277	88.0	202	92.5	222	92.5	159	93.5	165	90.3
0.5	307	85.8	243	89.5	181	93.3	207	93.0	147	94.0	165	90.3
0.6	299	86.2	218	90.6	175	93.5	180	93.9	140	94.3	163	90.5
0.7	282	87.0	205	91.1	162	94.0	177	94.0	125	94.9	153	91.0

Table 4.38 Inhibition efficiency as a function of immersion time and concentration for MS/PB/1M HCl

Conc (%v/v)	1/2 h		1h		3h		6h		12h		24h	
	CR (mpy)	IE (%)	CR (mpy)	IE (%)	CR (mpy)	IE (%)	CR (mpy)	IE (%)	CR (mpy)	IE (%)	CR (mpy)	IE (%)
Blank	2167	-	2307	-	2706	-	2965	-	2461	-	1707	-
0.1	270	87.5	253	89.0	162	94.0	216	92.7	185	92.5	211	87.6
0.2	212	90.2	198	91.4	121	95.5	174	94.1	116	95.3	155	90.9
0.3	179	91.7	154	93.3	97	96.4	136	95.4	102	95.8	160	90.6
0.4	175	91.9	145	93.7	86	96.8	109	96.3	96	96.1	141	91.7
0.5	149	93.1	126	94.5	75	97.2	97	96.7	80	96.7	136	92.0
0.6	143	93.4	124	94.6	70	97.4	88	97.0	75	97.0	134	92.1
0.7	134	93.8	92	96.0	62	97.7	83	97.2	69	97.2	129	92.4

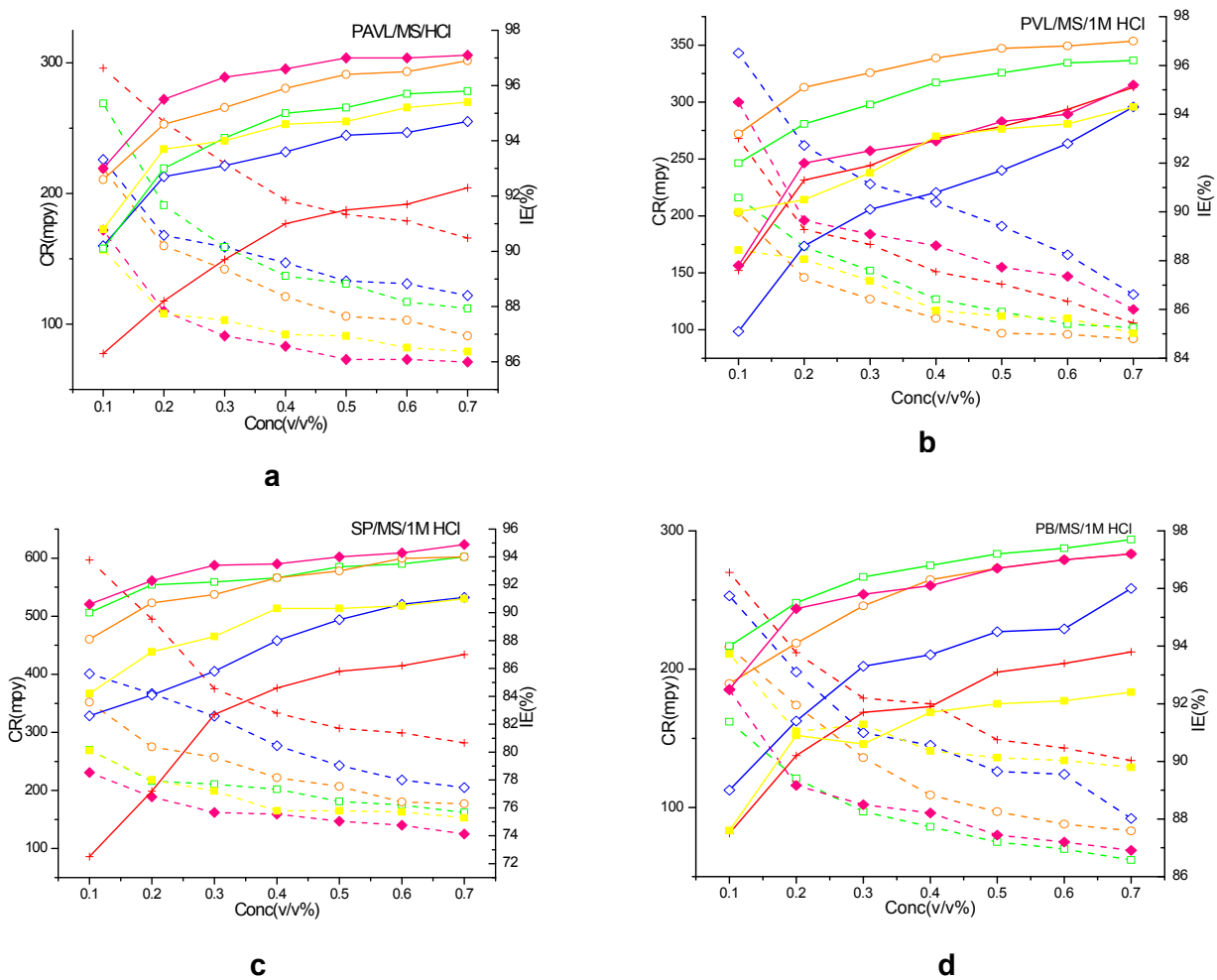

Figure 4.25. IE as a function of concentration and time of immersion for MS in 1M HCl in the absence and presence of (a) PAVL (b) PVL (c) SP (d) PB

4.3.2 Role of temperature on MS/PAVL/PVL/SP/PB/1M HCl

The impact of temperature on the corrosion inhibition behavior of the investigated inhibitors was evaluated by mass loss method in the temperature range of 303 to 353 K. The results are presented in Tables 4.39-4.42 and Figures 4.26 (a-d). Tables 4.39-4.42 and Figures 4.26 (a-d) represented the variation of the inhibition efficiency of PAVL with temperature in 1M HCl. Corrosion rate increased with an increase in temperature because at higher temperature reacting molecules gain more kinetic energy and speed up the corrosion reaction. In general, the corrosion rate of MS decreased at any given temperature with increase in the inhibitor concentration, whereas at constant inhibitor concentration, the corrosion rate increases with the rise in temperature.

i. MS/PAVL/1M HCl

Inspection of the temperature effect of PAVL, the IE increased with increased in temperature up to 333K giving rise to 94.0 percentage for PAVL then a slight decrease was noticed at 343K to 353K and then stabilized to 90.8 percentage at 353K (Table 4.39 and Figure 4.26 (a)). The decrease in the inhibition efficiency of the inhibitor as the temperature increased may be attributed to the desorption of the adsorbed molecular species of the PAVL extracts **(Ogwo *et al*, 2017)**.

ii. MS/PVL/1M HCl

Examine the temperature effect of PVL, the IE increased with increase in temperature up to 323K giving rise to 94.6 percentage for PVL due to adsorption process on MS surface and then a slight decrease was noticed at 333 to 353K which then stabilized to 90.5 percentage for PVL at 353K (Table 4.40 and Figure 4.26 (b)). These results were noticed due to decrease of the strength of the adsorption process at high temperature, indicating that increase of temperature caused the rise of the dissolution of mild steel, which can slow down adsorption of PVL molecules on the metal surface **(Bourazmi *et al*, 2018)**.

iii. MS/SP/1M HCl

In order to study the effect of temperature of SP extract on MS in 1M HCl solution, mass loss measurements were done in the temperature range 303K-353K. Table 4.41 and Figure 4.26(c) reflected that IE decreased with increasing temperature. It can be observed from Table 4.41 that the maximum IE obtained was 91.4 percentage for SP extract in 1M HCl .The results of the study revealed that the IE increased up to 313K afforded an efficiency of 91.4 percentage (for SP) and then a slight decrease was

observed 323K to 353K. The reason was that the inhibition efficiency reduced at high temperature due to increase rate of desorption of SP extract on the MS surface **(Prabakaran *et al,* 2015)**. It was found to stabilize at 353K (80.8 %).

iv. MS/PB/1M HCl

To find out the effect of temperature on the %IE and CR, mass loss experiments were carried out by varying temperature from 303K to 353K in the absence and presence of varying concentrations of the extract of PB and the results obtained were given in Table 4.42. It can be observed from Table 4.42 and Figure 4.26(d) that the obtained highest %IE was 93.8 percentage for PB extract in 1M HCl at 303K. As the temperature increased from 313K to 353K, the corrosion rate increased and the %IE of the inhibitor decreased. The reason was that increase of temperature affect the rate of adsorption/desorption ratio and the rate of desorption was faster than the rate of adsorption, leading to decrease in the IE with temperature **(Zacchini *et al,* 1971)**. The decreased in IE with an increase in temperature generally increased the activation energy of the corrosion process in the presence of the inhibitor **(Khamis*,* 1990, El-Etre *et al,* 2007)**. The effect of temperature on the studied systems is pictorially presented in Figure 4.26 (d).

Table 4.39. Relationship between Inhibition efficiency and concentration at various temperatures for MS/PAVL/1M HCl

Conc (%v/v)	303K		313K		323K		333K		343K		353K	
	CR (mpy)	IE (%)	CR (mpy)	IE (%)	CR (mpy)	IE (%)	CR (mpy)	IE (%)	CR (mpy)	IE (%)	CR (mpy)	IE (%)
Blank	2167	-	5775	-	9229	-	14406	-	20991	-	30723	-
0.1	296	86.3	791	86.3	1365	85.2	2837	80.3	3967	81.1	7250	76.4
0.2	255	88.2	675	88.3	1107	88.0	1627	88.7	2833	86.5	5007	83.7
0.3	223	89.7	554	90.4	969	89.5	1483	89.7	2434	88.4	4116	86.6
0.4	195	91.0	479	91.7	867	90.6	1440	90.0	2057	90.2	3809	87.6
0.5	184	91.5	479	91.7	802	91.3	1195	91.7	1805	91.4	3410	88.9
0.6	179	91.7	421	92.7	701	92.4	1152	92.0	1679	92.0	3195	89.6
0.7	166	92.3	404	93.0	655	92.9	864	94.0	1616	92.3	2826	90.8

Table 4.40. Inhibition efficiency as a function of immersion time and concentration at various temperatures for MS/PVL/1M HCl

Conc (%v/v)	303K		313K		323K		333K		343K		353K	
	CR (mpy)	IE (%)	CR (mpy)	IE (%)	CR (mpy)	IE (%)	CR (mpy)	IE (%)	CR (mpy)	IE (%)	CR (mpy)	IE (%)
Blank	2167	-	5775	-	9229	-	14406	-	20991	-	30723	-
0.1	268	87.6	906	84.3	1172	87.3	1858	87.1	3421	83.7	6236	79.7
0.2	188	91.3	710	87.7	932	89.9	1411	90.2	2560	87.8	4700	84.7
0.3	175	91.9	612	89.4	849	90.8	1152	92.0	2183	89.6	4024	86.9
0.4	151	93.0	525	90.9	738	92.0	1080	92.5	2036	90.3	3778	87.7
0.5	140	93.5	513	91.1	701	92.4	979	93.2	1763	91.6	3287	89.3
0.6	125	94.2	496	91.4	590	93.6	907	93.7	1595	92.4	2980	90.3
0.7	106	95.1	467	91.9	498	**94.6**	835	94.2	1553	92.6	2918	90.5

Table 4.41. Inhibition efficiency as a function of immersion time and concentration at various temperatures for MS/SP/1MHCl

Conc (%v/v)	303K		313K		323K		333K		343K		353K	
	CR (mpy)	IE (%)	CR (mpy)	IE (%)	CR (mpy)	IE (%)	CR (mpy)	IE (%)	CR (mpy)	IE (%)	CR (mpy)	IE (%)
Blank	2167	-	5775	-	9229	-	14406	-	20991	-	30723	-
0.1	597	72.5	1083	81.2	1996	78.4	3497	75.7	6082	71.0	11105	63.9
0.2	495	77.2	827	85.7	1544	83.3	3088	78.6	4768	77.3	10995	64.2
0.3	375	82.7	691	88.0	1365	85.2	2729	81.1	4333	79.4	7668	75.0
0.4	333	84.6	674	88.3	1211	86.9	2508	82.6	4077	80.6	6917	77.5
0.5	307	85.8	631	89.1	1177	87.2	2346	83.7	3830	81.8	6397	79.2
0.6	299	86.2	529	90.8	1058	88.5	2243	84.4	3685	82.4	6192	79.8
0.7	282	87.0	495	**91.4**	938	89.8	1962	86.4	3301	84.3	5885	80.8

Table 4.42. Inhibition efficiency as a function of immersion time and concentration at various temperatures for MS/PB/1MHCl

Conc (%v/v)	303K		313K		323K		333K		343K		353K	
	CR (mpy)	IE (%)	CR (mpy)	IE (%)	CR (mpy)	IE (%)	CR (mpy)	IE (%)	CR (mpy)	IE (%)	CR (mpy)	IE (%)
Blank	2167	-	5775	-	9229	-	14406	-	20991	-	30723	-
0.1	270	87.5	941	83.7	1541	83.3	2722	81.1	4890	76.7	9677	68.5
0.2	212	90.2	762	86.8	1116	87.9	1930	86.6	3568	83.0	6943	77.4
0.3	179	91.7	623	89.2	1061	88.5	1599	88.9	3337	84.1	5714	81.4
0.4	175	91.9	519	91.0	784	91.5	1339	90.7	2497	88.1	4946	83.9
0.5	149	93.1	502	91.3	766	91.7	1210	91.6	2183	89.6	4331	85.9
0.6	143	93.4	421	92.7	710	92.3	1066	92.6	1973	90.6	4055	86.8
0.7	134	**93.8**	404	93.0	581	93.7	907	93.7	1763	91.6	3717	87.9

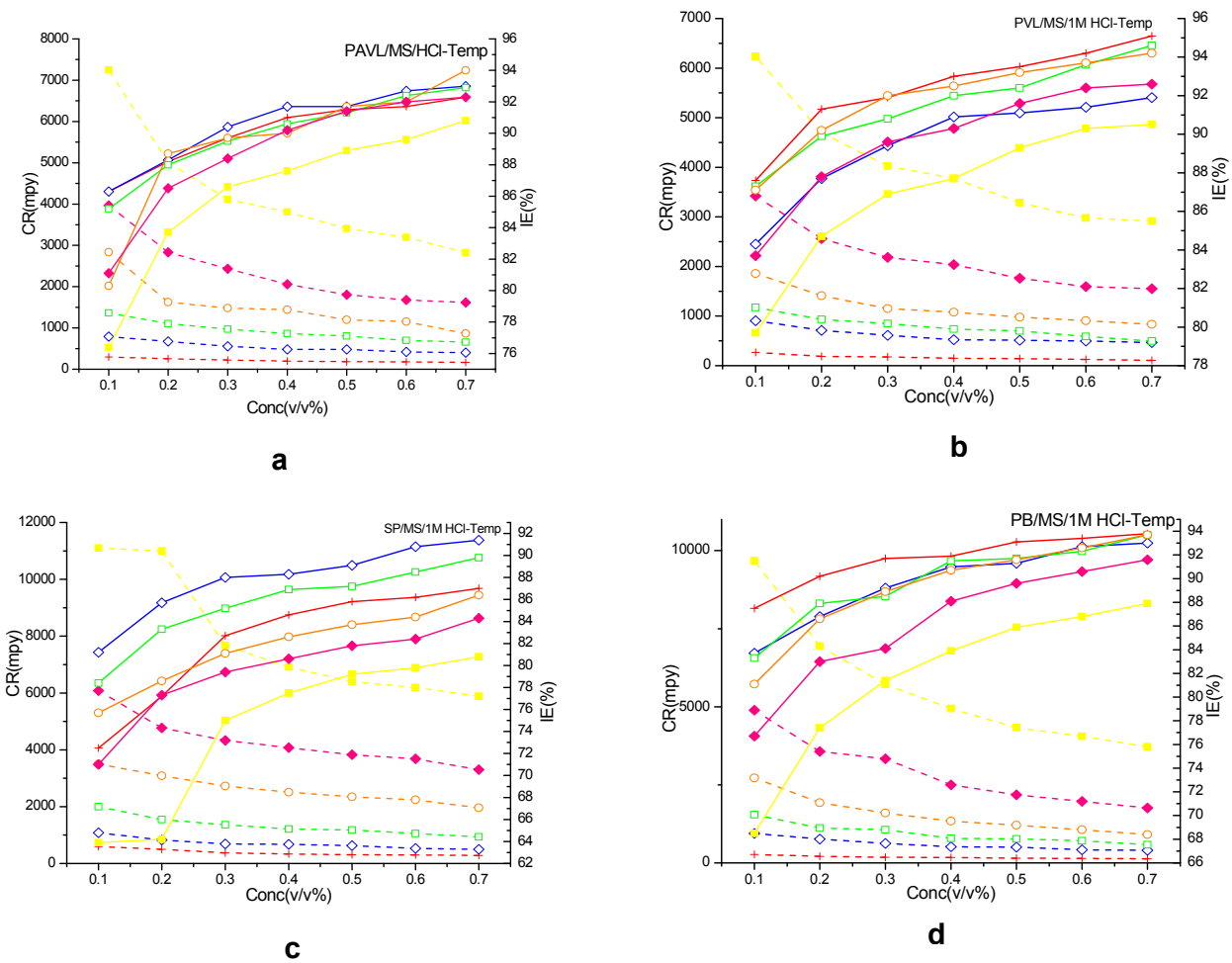

Figure. 4.26. Effect of temperature on CR and IE on MS in 1M HCl in the absence and presence of (a) PAVL (b) PVL (c) SP (d) PB

4.3.3 Inhibition efficiency as a function of immersion time and concentration for AA/PAVL/PVL/SP/PB/1M HCl

i. AA/PAVL/1M HCl

Mass loss measurements were performed for AA in 1M HCl in the absence and presence of different doses of PAVL are shown in Figure 4.27(a). The inhibition efficiency (%IE) values were calculated and listed in Table 4.43. From the table, it was clear that the %IE increased steadily with increasing the dose of inhibitor. The observed inhibitive action of PAVL could be attributed to the adsorption of its components on AA surface. The inhibition efficiency increased with increase in the concentration of PAVL extract from 1/2h to 1h (92.8% to 97.1%). The highest IE (%) obtained for PAVL is 97.1% for 0.7%

concentration of the extract at 1h of immersion time. The increase in%IE was due to increase the degree of surface coverage by increased adsorption of inhibitor molecules on the metal. The increased coverage can prevent AA from corrosion process as it was created the separation of the AA surface from an acidic solution. The IE(%) decreased after 3h for a longer immersion period of the system. The main reason was due to desorption of the inhibitor from the metal surface **(Gusti *et al,* 2015)**.

ii. AA/PVL/1M HCl

A maximum IE (%) was observed 96% at 1h immersion time. Further increasing the immersion time from 3h to 24h decreased the IE of the PVL extract. This may be due to desorption of PVL extract on AA surface due to prolonged immersion period. The results also infer that increase in concentration of inhibitor increased in the adsorption of PVL at the metal/electrolyte boundary (Table 4.44 and Figure 4.27(b)).

iii. AA/SP/1M HCl

Table 4.45 showed the CR and (%) IE for SP extract in 1M HCl at room temperature. From the table, it was found that the concentration of the inhibitor increased the corrosion rate decreased and the IE increased. The results revealed that the %IE of SP was greatly enhanced by the addition of inhibitor from 0.1% to 0.7%. This was indicated that the inhibitor molecules get adsorbed on the AA surface and prevented further corrosion. The immersion time was another important parameter which ascertained the inhibitive effect of SP extract. From the table, it was clear that as the immersion time and concentration of SP extract increased from 1/2h to 1h, the IE increased due to adsorption of SP molecules on AA surface. The maximum %IE 97.4% was obtained at 1h immersion period. Similarly, the increased immersion period from 3h to 24h with increasing concentration of SP resulted in decreasing IE. It might be due to desorption occurred by longer immersion period (Table 4.45 and Figure 4.27(c)).

v. AA/PB/1M HCl

The mass loss method was done for AA in 1M HCl with various concentrations of PB extract from 0.1% to 0.7% and corresponding values of %IE and corrosion rate are given in Table 4.46(Figure 4.27(d). It was observed from the table that corrosion rate decreased and thus inhibition efficiency increased with increasing concentration of PB extract. The maximum inhibition efficiency of about 96.5% was achieved at 0.7% concentration of PB extract for 3h immersion time. The results revealed that the IE increased from 1/2h to 3h with increasing concentration of PB extract which can increase

in surface coverage on AA surface. Further increasing the immersion time with a concentration of PB extract can decrease the IE. The reason was that desorption occurred on AA surface with enhanced immersion time.

Table 4.43 Inhibition efficiency as a function of immersion time and concentration for AA/PAVL/1MHCl

Conc (%v/v)	1/2h		1hr		3h		6h		12h		24h	
	CR (mpy)	IE (%)	CR (mpy)	IE (%)	CR (mpy)	IE (%)	CR (mpy)	IE (%)	CR (mpy)	IE (%)	CR (mpy)	IE (%)
Blank	2362	-	4103	-	9519	-	10580	-	4767	-	2660	-
0.1	366	84.5	336	91.8	675	92.9	1481	86.0	1020	78.6	1021	61.6
0.2	318	86.5	242	94.1	656	93.1	1248	88.2	896	81.2	901	66.1
0.3	250	89.4	213	94.8	647	93.2	1237	88.3	791	83.4	840	68.4
0.4	217	90.8	180	95.6	523	94.5	1142	89.2	781	83.6	766	71.2
0.5	193	91.8	151	96.3	418	95.6	1121	89.4	729	84.7	750	71.8
0.6	181	92.3	131	96.8	333	96.5	1068	89.9	667	86.0	688	74.1
0.7	170	92.8	118	97.1	285	97.0	1005	90.5	643	86.5	678	74.5

Table 4.44. Inhibition efficiency as a function of immersion time and concentration for AA/PVL/1MHCl

Conc (%v/v)	1/2h		1hr		3h		6h		12h		24h	
	CR (mpy)	IE (%)	CR (mpy)	IE (%)	CR (mpy)	IE (%)	CR (mpy)	IE (%)	CR (mpy)	IE (%)	CR (mpy)	IE (%)
Blank	2362	-	4103	-	9519	-	10580	-	4767	-	2660	-
0.1	335	85.8	303	92.6	713	92.5	1946	81.6	3017	36.7	2223	16.4
0.2	297	87.4	283	93.1	609	93.6	1756	83.4	2571	46.1	2045	23.1
0.3	281	88.1	258	93.7	590	93.8	1692	84.0	2552	46.5	2034	23.5
0.4	262	88.9	225	94.5	571	94.0	1639	84.5	2510	47.3	2002	24.7
0.5	236	90.0	188	95.4	514	94.6	1597	84.9	2455	48.5	2000	24.8
0.6	226	90.4	180	95.6	447	95.3	1555	85.3	2452	48.6	1960	26.3
0.7	207	91.2	164	96.0	399	95.8	1512	85.7	2321	51.3	1909	28.2

Table 4.45. Inhibition efficiency as a function of immersion time and concentration for AA/SP/1MHCl

Conc (%v/v)	1/2h		1hr		3h		6h		12h		24h	
	CR (mpy)	IE (%)	CR (mpy)	IE (%)	CR (mpy)	IE (%)	CR (mpy)	IE (%)	CR (mpy)	IE (%)	CR (mpy)	IE (%)
Blank	2362	-	4103	-	9519	-	10580	-	4767	-	2660	-
0.1	229	90.3	311	92.4	1066	88.8	2719	74.3	2370	50.3	1784	32.9
0.2	172	92.7	213	94.8	904	90.5	2708	74.4	2141	55.1	1532	42.4
0.3	162	93.1	184	95.5	847	91.1	2592	75.5	2135	55.2	1508	43.3
0.4	141	94.0	180	95.6	799	91.6	2570	75.7	2098	56.0	1502	43.5
0.5	118	95.0	151	96.3	790	91.7	2264	78.6	2000	58.1	1488	44.1
0.6	89	96.2	123	97.0	713	92.5	2220	79.2	1704	64.3	1430	46.2
0.7	70	97.0	106	97.4	628	93.4	2041	80.7	1530	67.9	1424	46.5

Table 4.46. Inhibition efficiency as a function of immersion time and concentration for AA/PB/1MHCl

Conc (%v/v)	1/2h		1hr		3h		6h		12h		24h	
	CR (mpy)	IE (%)	CR (mpy)	IE (%)	CR (mpy)	IE (%)	CR (mpy)	IE (%)	CR (mpy)	IE (%)	CR (mpy)	IE (%)
Blank	2362	-	4103	-	9519	-	10580	-	4767	-	2660	-
0.1	572	75.8	721	82.4	475	95.0	1132	89.3	1720	63.9	2261	15.0
0.2	472	80.0	709	82.7	447	95.3	1005	90.5	1239	74.0	1782	33.0
0.3	448	81.1	485	88.2	437	95.4	931	91.2	1225	74.3	1566	41.1
0.4	423	82.1	460	88.8	409	95.7	920	91.3	1063	77.7	1439	45.9
0.5	373	84.2	423	89.7	390	95.9	793	92.5	1015	78.7	1399	47.4
0.6	348	85.3	410	90.0	380	96.0	761	92.8	977	79.5	1345	49.4
0.7	323	86.3	398	90.3	333	96.5	687	93.5	962	79.8	1337	49.7

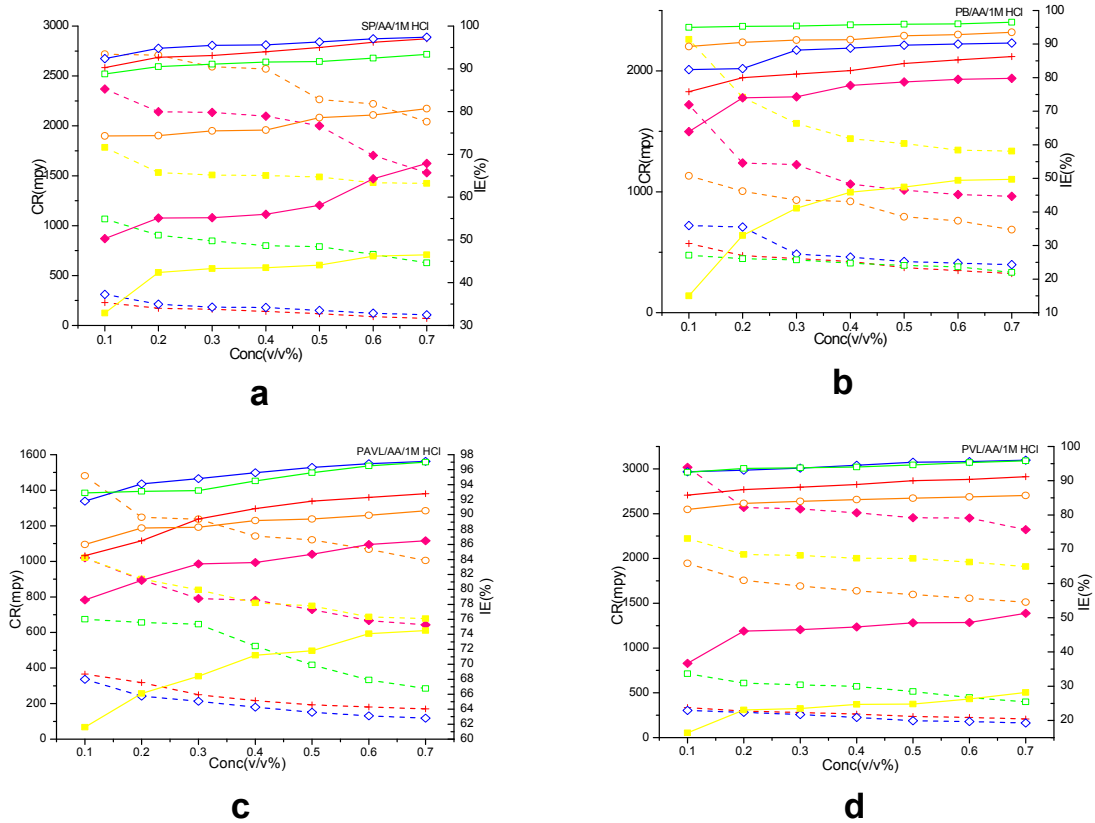

Figure 4.27. Variation of CR and IE with concentration on AA in 1M HCl in the absence and presence of (a) PAVL (b) PVL (c) SP (d) PB

4.3.4 Effect of Temperature on AA/PAVL/PVL/SP/PB1MHCl

i. AA/PAVL/1M HCl

Mass loss studies were performed with and without the addition of the investigated extracts by varying the temperature from 303K to 353K. IE(%) increased with increasing inhibitor concentration for a given temperature. This behaviour explained from the formation of the shielding layer separated AA from the corrosive medium. The evolution of inhibition efficiency versus temperature is showed in Figure 4.28 (a) and the results are summarized in Table 4.47. As shown in Figure 4.28 (a) the %IE decreased with rising in temperature for the studied concentration range (0.1% to 0.7%). The maximum IE found for PAVL extract was 92.8% (303K) and then there was decreased IE with the rise of temperature. At 323K it showed 89.9% of %IE. Further increasing temperature from 333K to 353K, corrosion rate increased with decrease in IE(%) by desorption reaction of PAVL on AA surface.

According to the literature **(Santhini *et al,* 2012)**, the lesser inhibition efficiency with the increase in temperature suggested that adsorption reaction on the PAVL on the corroding metal surface was physisorption. This effect was related to the reaction products precipitated on the metal surface and increased in the solubility of protective film hence, increased the metal surface exposure to corrosive attack by raising the temperature.

ii. AA/PVL/1M HCl

The mass loss values for temperature study of the PVL extract is presented in Table 4.48 (Figure 4.28 (b)). The increased in the CR in the absence of PVL extract was higher at all the temperatures, suggested the aggressive nature of the hydrochloric acid solution. The highest %IE of PVL extract was 91.2% with respect to 303K. Further rising temperature from 313K to 353K the inhibition efficiency decreased due to desorption of the PVL molecules from AA surface. Due to the decrease in the strength of adsorption and roughening of the electrode surface, enhancing the corrosion rate with an increase in temperature which enhanced the corrosion process **(Singh *et al*, 2012b)**.

iii. AA/SP/1M HCl

The IE of the SP extract increased by raising the temperature from 303K-353K. The greater IE(%) 97% was obtained at 303K and then IE decreased with further increasing of temperature (Table 4.49 and Figure 4.28 (c)). The reason was that an

increase in temperature increased the corrosion reaction of metal dissolution rate and hydrogen gas evolution by reduced adsorption and increased desorption process. When rising the temperature the thermal motion of SP extract molecules increased at elevated temperatures. It proved that inhibitor adsorption on AA surface was through physical adsorption which was related to Vander Waals force of attraction **(Raghavendra *et al,* 2018b)**.

iv. AA/PB/1M HCl

Figure 4.28 (d) (Table 4.50) show that the %IE reduced by enhancing temperature. A maximum IE of 86.3% was achieved at 303K. The enhanced efficiency with concentration was due to the absorption of PB molecules on AA surface. The metal surface was covered by a protecting layer, which separated it from its environment. Similar observations **(Obot *et at*, 2011, Manamela *et al*, 2014)** were reported in the literature. IE decreased with increasing the temperature from 313K to 353K. The reason was that the reaction took place between inhibited acid-metal was a somewhat complex reaction **(Bentiss *et al*, 2005)**. The increased rate of desorption of the inhibitor can cause decrease in %IE with a rise in temperature.

Table 4.47. Inhibition efficiency as a function of immersion time and concentration at various temperatures for AA/PAVL/1MHCl

Conc (%v/v)	303K		313K		323K		333K		343K		353K	
	CR (mpy)	IE (%)	CR (mpy)	IE (%)	CR (mpy)	IE (%)	CR (mpy)	IE (%)	CR (mpy)	IE (%)	CR (mpy)	IE (%)
Blank	2362	-	25636	-	64748	-	98241	-	103587	-	110773	-
0.1	366	84.5	6690	73.9	20913	67.7	51674	47.4	73961	28.6	95264	14.0
0.2	318	86.5	5896	77.0	15086	76.7	48334	50.8	70439	32.0	95154	14.1
0.3	250	89.4	5486	78.6	14762	77.2	46173	53.0	69610	32.8	90944	17.9
0.4	217	90.8	5281	79.4	10618	83.6	40770	58.5	69299	33.1	90390	18.4
0.5	193	91.8	5178	79.8	8805	86.4	38706	60.6	69092	33.3	88064	20.5
0.6	181	92.3	4178	83.7	7122	89.0	36349	63.0	66088	36.2	84298	23.9
0.7	170	**92.8**	3794	85.2	6539	89.9	26328	73.2	60805	41.3	81085	26.8

Table 4.48. Inhibition efficiency as a function of immersion time and concentration at various temperatures for AA/PVL/1MHCl

Conc (%v/v)	303K		313K		323K		333K		343K		353K	
	CR (mpy)	IE (%)	CR (mpy)	IE (%)	CR (mpy)	IE (%)	CR (mpy)	IE (%)	CR (mpy)	IE (%)	CR (mpy)	IE (%)
Blank	2362	-	25636	-	64748	-	98241	-	103587	-	110773	-
0.1	335	85.8	6075	76.3	24798	61.7	61695	37.2	87323	15.7	107450	3.0
0.2	297	87.4	5383	79.0	19359	70.1	51773	47.3	81005	21.8	101579	8.3
0.3	281	88.1	4127	83.9	19035	70.6	51674	47.4	79140	23.6	100250	9.5
0.4	262	88.9	3768	85.3	18557	71.4	50299	48.8	76550	26.1	100028	9.7
0.5	236	90.0	3383	86.8	17999	72.2	47941	51.2	76240	26.4	99363	10.3
0.6	226	90.4	3127	87.8	16899	73.9	46075	53.1	75929	26.7	96926	12.5
0.7	207	**91.2**	2768	89.2	14374	77.8	31338	68.1	69921	32.5.	95486	13.8

Table 4.49. Inhibition efficiency as a function of immersion time and concentration at various temperatures for AA/SP/1MHCl

Conc (%v/v)	303K		313K		323K		333K		343K		353K	
	CR (mpy)	IE (%)	CR (mpy)	IE (%)	CR (mpy)	IE (%)	CR (mpy)	IE (%)	CR (mpy)	IE (%)	CR (mpy)	IE (%)
Blank	2362	-	25636	-	64748	-	98241	-	103587	-	110773	-
0.1	229	90.3	7665	70.1	16251	74.9	55702	43.3	77379	25.3	101357	8.5
0.2	172	92.7	6050	76.4	14438	77.7	50004	49.1	71785	30.7	100139	9.6
0.3	162	93.1	5614	78.1	13820	78.5	47450	51.7	71578	30.9	99806	9.9
0.4	141	94.0	5434	78.8	12949	80.0	47155	52.0	69714	32.7	97701	11.8
0.5	118	95.0	4640	81.9	12172	81.2	44896	54.3	68574	33.8	96926	12.5
0.6	89	96.2	4101	84.0	11913	81.6	44110	55.1	67331	35.0	92827	16.2
0.7	70	**97.0**	3922	84.7	9776	84.9	37724	61.6	63498	38.7	87953	20.6

Table 4.50. Inhibition efficiency as a function of immersion time and concentration at various temperatures for AA/PB/1MHCl

Conc (%v/v)	303K		313K		323K		333K		343K		353K	
	CR (mpy)	IE (%)	CR (mpy)	IE (%)	CR (mpy)	IE (%)	CR (mpy)	IE (%)	CR (mpy)	IE (%)	CR (mpy)	IE (%)
Blank	2362	-	25636	-	64748	-	98241	-	103587	-	110773	-
0.1	572	75.8	13004	49.3	35358	45.4	66340	32.5	89091	14.0	100028	9.7
0.2	472	80.0	8380	67.3	34935	46.0	64897	33.9	88270	14.8	98813	10.8
0.3	448	81.1	8280	67.7	26730	58.7	59576	39.4	83049	19.8	96849	12.6
0.4	423	82.1	6614	74.2	25114	61.2	59104	39.8	75540	27.1	96725	12.7
0.5	373	84.2	6564	74.4	24989	61.4	57388	41.6	75167	27.4	96526	12.9
0.6	348	85.3	5644	78.0	16983	73.8	55598	43.4	72407	30.1	93840	15.3
0.7	323	**86.3**	4575	82.2	12532	80.6	53360	45.7	70293	32.1	93045	16.0

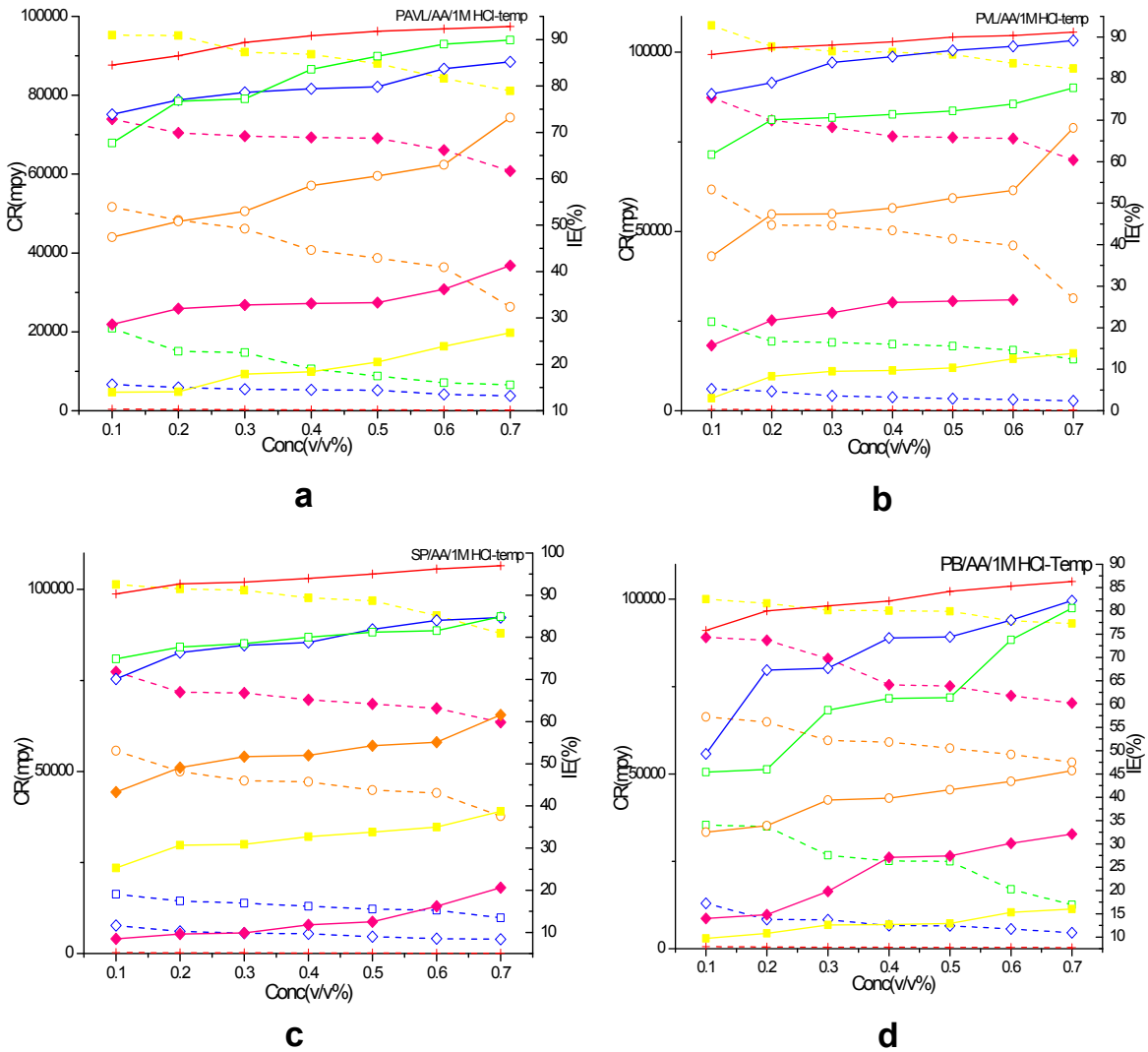

Figure 4.28. Temperature as a function of IE and concentration on AA in 1M HCl in the absence and presence of (a) PAVL (b) PVL (c) SP (d) PB

4.3.5 Effect of concentration/Immersion time-AA/PAVL/PVL/SP/PB/1M NaOH

i. AA/PAVL/1M NaOH

Mass loss measurements performed with and without using various concentrations of the PAVL inhibitor (0.1% to 0.7%) (Table 4.51). The influence of immersion time from 1/2h to 24h was also studied. The impact of exposure time on %IE of AA in 1M sodium hydroxide at room temperature with and without using of PAVL extract is shown in Figure 4.29 (a). The results revealed that with a rise in the concentration of PAVL, CR decrease and inhibition performance increased from 59.0% to 81.1% in 0.7% concentration of PAVL extract. The main reason was that on enhancing

the surface coverage on the metal surface, AA surface was protected from corrosion. A maximum IE of 81.1% was achieved at 24hr of immersion time. According to the results in Table 4.51 and Figure 4.29 (a) CR (mpy) decreased with rising immersion time. The increase in inhibition of AA extract with immersion time reflected strong adsorption on AA surface resulting in a more protective layer.

ii. AA/PVL/1M NaOH

The ability of PVL extract on minimising AA corrosion in 1M NaOH medium was measured using mass loss method from 1/2h to 24h of immersion time (Table 4.52 and Figure 4.29 (b)). The values of CR (mpy) and IE (%) were presented in Table 18. It showed that maximum IE of 67% was obtained at 1hr immersion time for 0.7% concentration of PVL extract. The %IE increased from 1/2h to 1h of immersion time (62.6% to 67.0%) due to absorption of PVL molecules in the AA/solution interface. The %IE decreased from 1h to 24h of immersion time (58.9% to 58.3%). The reason was that a longer immersion period can cause desorption of PVL extract from the surface of aluminium alloy **(Pradeep kumar *et al,* 2013)**.

iii. AA/SP/1M NaOH

In the case of AA/SP/1M NaOH, the IE increased from 67.2% to 83.7%, due to increase in concentration of SP extract from 0.1% to 0.7%. This may enhance the adsorption by raising the concentration of SP extract (Table 4.53 and Figure 4.29 (c)). Consequently, more extract molecules were adsorbed on the AA surface which can decrease the surface area available for the attack of the aggressive alkali OH- ions from alkaline solution. It was suggested that 0.7% is the optimum concentration to obtain high corrosion prevention for aluminium alloy corrosion. The slight decrease in IE (%) at longer immersion period (76.9% to 76%) might be due to decrease the strength of adsorption and an increase in hydrogen evolution reaction **(Namrata Chaubey *et al,* 2015b)**.

iv. AA/PB/1M NaOH

In the case of PB extract, the inhibition performance increased from 84.2% to 86.9% for 1/2h to 6h. The reason was that the increase in inhibitor efficiency occurred due to greater surface coverage with enhancing PB concentration (Table 4.54 and Figure 4.29 (d)). Thus, the aluminium surface was separated from the alkaline medium and this decreased the dissolution of aluminium alloy by enhancing the PB extract concentration **(Umoren *et al*, 2008)**. The slight decrease in IE from 12h to 24h (85.4% to 83.8%) observed was due to occurance of desorption by increasing immersion period.

Table 4.51. Inhibition efficiency as a function of immersion time and concentration for AA/PAVL/1M NaOH

Conc (%v/v)	1/2h		1hr		3h		6h		12h		24h	
	CR (mpy)	IE (%)	CR (mpy)	IE (%)	CR (mpy)	IE (%)	CR (mpy)	IE (%)	CR (mpy)	IE (%)	CR (mpy)	IE (%)
Blank	10095	-	13937	-	16017	-	17457	-	10396	-	12610	-
0.1	4845	52.0	8153	41.5	5483	65.8	5037	71.1	5097	51.0	3332	73.6
0.2	4815	52.3	7442	46.6	5122	68.0	4784	72.6	4937	52.5	2913	76.9
0.3	4704	53.4	7191	48.4	4915	69.3	4612	73.6	4882	53.0	2795	77.8
0.4	4391	56.5	7024	49.6	4675	70.8	4459	74.5	4805	53.8	2605	79.3
0.5	4260	57.8	6968	50.0	4666	70.9	4384	74.9	4770	54.1	2474	80.4
0.6	4239	58.0	6926	50.3	4658	70.9	4389	74.9	4709	54.7	2395	81.0
0.7	4138	59.0	6912	50.4	4571	71.5	4368	75.0	4650	55.3	2377	**81.1**

Table 4.52. Inhibition efficiency as a function of immersion time and concentration for AA/PVL/1M NaOH

Conc (%v/v)	1/2h		1hr		3h		6h		12h		24h	
	CR (mpy)	IE (%)	CR (mpy)	IE (%)	CR (mpy)	IE (%)	CR (mpy)	IE (%)	CR (mpy)	IE (%)	CR (mpy)	IE (%)
Blank	10095	-	13937	-	16017	-	17457	-	10396	-	12610	-
0.1	6178	38.8	7331	47.4	7624	52.4	6825	60.9	7173	31.0	5510	56.3
0.2	5461	45.9	6870	50.7	7319	54.3	6598	62.2	7090	31.8	5460	56.7
0.3	4835	52.1	6188	55.6	7111	55.6	6389	63.4	7069	32.0	5434	56.9
0.4	4653	53.9	5728	58.9	6935	56.7	6336	63.7	7048	32.2	5409	57.1
0.5	4381	56.6	5170	62.9	6887	57.0	6301	63.9	6871	33.9	5359	57.5
0.6	3977	60.6	4808	65.5	6775	57.7	6162	64.7	6819	34.4	5308	57.9
0.7	3775	62.6	4599	**67.0**	6582	58.9	6127	64.9	6705	35.5	5258	58.3

Table 4.53. Inhibition efficiency as a function of immersion time and concentration for AA/SP/1M NaOH

Conc (%v/v)	1/2h		1hr		3h		6h		12h		24h	
	CR (mpy)	IE (%)	CR (mpy)	IE (%)	CR (mpy)	IE (%)	CR (mpy)	IE (%)	CR (mpy)	IE (%)	CR (mpy)	IE (%)
Blank	10095	-	13937	-	16017	-	17457	-	10396	-	12610	-
0.1	4501	55.4	4933	64.6	4837	69.8	3857	77.9	2973	71.4	3404	73.0
0.2	3780	62.6	4055	70.9	4244	73.5	3526	79.8	2838	72.7	3127	75.2
0.3	3730	63.1	3832	72.5	3924	75.5	3386	80.6	2806	73.0	3127	75.2
0.4	3680	63.5	3665	73.7	3667	77.1	3229	81.5	2765	73.4	3102	75.4
0.5	3556	64.8	3637	73.9	3523	78.0	2967	83.0	2619	74.8	3064	75.7
0.6	3382	66.5	3567	74.4	3443	78.5	2915	83.3	2547	75.5	3051	75.8
0.7	3307	67.2	3498	74.9	3395	78.8	2845	**83.7**	2401	76.9	3026	76.0

Table 4.54. Inhibition efficiency as a function of immersion time and concentration for AA/PB/1M NaOH

Conc (%v/v)	1/2h		1hr		3h		6h		12h		24h	
	CR (mpy)	IE (%)	CR (mpy)	IE (%)	CR (mpy)	IE (%)	CR (mpy)	IE (%)	CR (mpy)	IE (%)	CR (mpy)	IE (%)
Blank	10095	-	13937	-	16017	-	17457	-	10396	-	12610	-
0.1	3371	66.6	4933	64.6	6166	61.5	4695	73.1	2525	75.8	3216	74.5
0.2	2877	71.5	4306	69.1	4580	71.4	3439	80.3	2245	78.4	2850	77.4
0.3	2604	74.2	4292	69.2	4340	72.9	3002	82.8	2120	79.6	2585	79.5
0.4	2251	77.7	3762	73.0	3379	78.9	2828	83.8	1933	81.4	2383	81.1
0.5	2180	78.4	2884	79.3	3299	79.4	2618	85.0	1798	82.7	2295	81.8
0.6	2150	78.7	2731	80.4	2786	82.6	2374	86.4	1652	84.1	2119	83.2
0.7	1595	84.2	2397	82.8	2562	84.0	2286	**86.9**	1517	85.4	2043	83.8

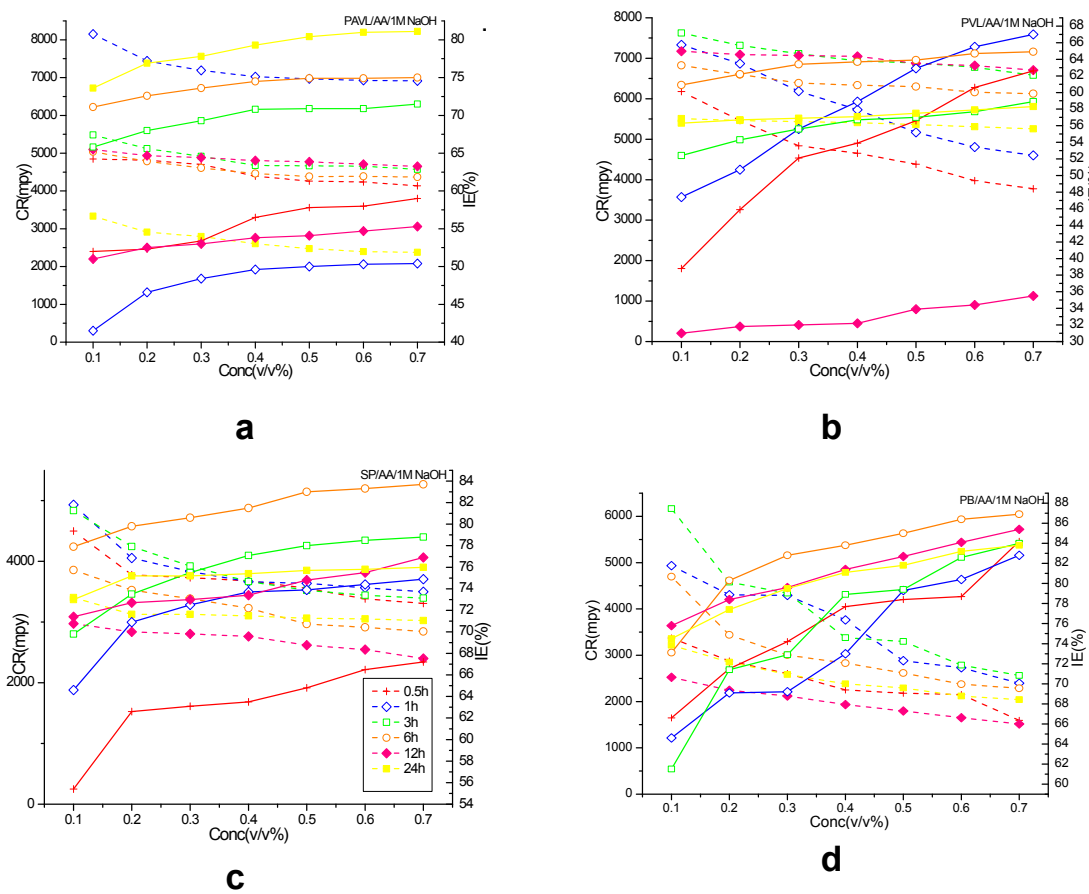

Figure 4.29. IE as a function of concentration and time of immersion for AA in 1M NaOH in the absence and presence of (a) PAVL (b) PVL (c) SP (d) PB

4.3.6 Impact of Temperature on AA/PAVL/PVL/SP/PB/1M NaOH

i. AA/PAVL/1M NaOH

The influence of the temperature on corrosion of AA in 1M NaOH solution with and without using PAVL inhibitor solution was performed through mass loss measurement and is depicted in Figure 4.30 (a) and the results were listed in Table 4.55. The results revealed that IE increased from 303K to 323K (59% to 82.1%). This might be due to the adsorption of the PAVL on AA surface. A maximum IE of 82.1% was achieved at 323K. As the temperature rose from 333K to 353K, IE was found to slightly decrease from 80% to 74.8%. The reason was that after 323K desorption process occurred which means that physisorption took place on AA surface.

ii. AA/PVL/1M NaOH

Analysis of temperature dependence of IE (%) and CR (mpy) with and without the addition of PVL extract reflected the adsorption mechanism of the inhibitor. Mass loss measurements were performed in temperatures (303K to 353K) and the concentration ranges from 0.1% to 0.7%. A greater IE of 62.6% was obtained at 303K (Table 4.56 and Figure 4.30 (b)). The inhibition efficiency decreased further on increasing temperature from 313K to 353K (55.9% to 34.7%). The main reasons were that when the temperature increased, the desorption of PVL extract also increased as a result increased rate of hydrogen gas evolution, which retarded the inhibition performance of the inhibitor on AA surface. This behaviour reflected the physical nature of adsorption on AA surface **(Abdallah, 2004)**.

iii. AA/SP/1M NaOH

To gain knowledge about the adsorption behaviour, temperature study (303K-353K) was conducted through mass loss method. IE with respect to temperature of the SP extract was plotted in Figure 4.30 (c) and (Table 4.57). The CR (mpy) and IE values were presented in Table 4.57. IE increased from 303K to 323K (67.2% to 78.9%) which may be due to adsorption reaction of SP extract on the surface of AA. The highest IE (%) 78.9% was observed at 323K. Further on increasing the temperature (after 333K), there was a slight decrease in IE (%). This may be due to slight desorption that occurred while increasing the temperature **(Obot *et al,* 2009, Nawafleh *et al*, 2013)**.

iv. AA/PB/1M NaOH

Mass loss study was performed to analyze the impact of temperature on PB using AA in 1M NaOH solution. CR (mpy) and %IE values are presented in Table 4.58. Figure 4.30 (d) reflected that IE decreased with rising in temperature (313K to 353K), reflected

an increase in CR. It observed maximum IE (%) 84.2% at 303K. IE decreased slightly from 313K to 353K (54% to 74.6%) due to the desorption process of PB extract molecules at high temperatures **(Chakravarthy *et al,* 2014)**.

Table 4.55. Impact of Temperature on AA/PAVL/1M NaOH

Conc (%v/v)	303K		313K		323K		333K		343K		353K	
	CR (mpy)	IE (%)	CR (mpy)	IE (%)	CR (mpy)	IE (%)	CR (mpy)	IE (%)	CR (mpy)	IE (%)	CR (mpy)	IE (%)
Blank	11164	-	22553	-	41674	-	88444	-	163959	-	229080	-
0.1	5358	52.0	9562	57.6	14127	66.1	40684	54.0	64435	60.7	111561	51.3
0.2	5325	52.3	7870	65.1	11460	72.5	29186	67.0	52466	68.0	90944	60.3
0.3	5202	53.4	6698	70.3	10043	75.9	25206	71.5	45416	72.3	76970	66.4
0.4	4856	56.5	5931	73.7	9585	77.0	23349	73.6	42957	73.8	74909	67.3
0.5	4711	57.8	5412	76.0	8626	79.3	20076	77.3	37710	77.0	71702	68.7
0.6	4688	58.0	5074	77.5	7793	81.3	18750	78.8	35251	78.5	63455	72.3
0.7	4577	59.0	4894	78.3	7459	**82.1**	17688	80.0	33283	79.7	57728	74.8

Table 4.56. Impact of Temperature on AA/PVL/1M NaOH

Conc (%v/v)	303K		313K		323K		333K		343K		353K	
	CR (mpy)	IE (%)	CR (mpy)	IE (%)	CR (mpy)	IE (%)	CR (mpy)	IE (%)	CR (mpy)	IE (%)	CR (mpy)	IE (%)
Blank	11164	-	22553	-	41674	-	88444	-	163959	-	229080	-
0.1	6838	38.8	13377	40.7	29067	30.3	66837	24.4	107168	34.6	185368	19.1
0.2	6042	45.9	12109	46.3	26208	37.1	60695	31.4	105527	35.6	174005	24.0
0.3	5346	52.1	11587	48.6	24417	41.4	57537	34.9	101822	37.9	166844	27.2
0.4	5147	53.9	10990	51.3	23895	42.7	56294	36.4	101374	38.2	166421	27.4
0.5	4849	56.6	10468	53.6	22627	45.7	55921	36.8	99037	39.6	163313	28.7
0.6	4401	60.6	10244	54.6	22080	47.0	54031	38.9	96799	41.0	151999	33.6
0.7	4177	**62.6**	9946	55.9	20563	50.7	53261	39.8	95929	41.5	149587	34.7

Table 4.57. Impact of Temperature on AA/SP/1M NaOH

Conc (%v/v)	303K		313K		323K		333K		343K		353K	
	CR (mpy)	IE (%)	CR (mpy)	IE (%)	CR (mpy)	IE (%)	CR (mpy)	IE (%)	CR (mpy)	IE (%)	CR (mpy)	IE (%)
Blank	11164	-	22553	-	41674	-	88444	-	163959	-	229080	-
0.1	4956	55.4	8367	62.9	15044	63.9	33785	61.8	64107	60.9	92319	59.7
0.2	4175	62.6	7668	66.0	12668	69.6	26798	69.7	52302	68.1	73992	67.7
0.3	4119	63.1	6585	70.8	11085	73.4	23614	73.3	45908	72.0	63226	72.4
0.4	4074	63.5	6427	71.5	10293	75.3	23172	73.8	43285	73.6	59560	74.0
0.5	3929	64.8	6089	73.0	9793	76.5	21315	75.9	41317	74.8	56811	75.2
0.6	3739	66.5	5908	73.8	9043	78.3	20076	77.3	37874	76.9	52230	77.2
0.7	3661	67.2	5593	75.2	8793	**78.9**	19280	78.2	36890	77.5	49023	78.6

Table 4.58. Impact of Temperature on AA/PB/1M NaOH

Conc (%v/v)	303K		313K		323K		333K		343K		353K	
	CR (mpy)	IE (%)	CR (mpy)	IE (%)	CR (mpy)	IE (%)	CR (mpy)	IE (%)	CR (mpy)	IE (%)	CR (mpy)	IE (%)
Blank	11164	-	22553	-	41674	-	88444	-	163959	-	229080	-
0.1	3728	66.6	14163	37.2	16461	60.5	46167	47.8	97719	40.4	135157	41.0
0.2	3181	71.5	13419	40.5	15836	62.0	36350	58.9	61976	62.2	105376	54.0
0.3	2880	74.2	12742	43.5	13085	68.6	29894	66.2	52138	68.2	83156	63.7
0.4	2489	77.7	11953	47.0	12543	69.9	25029	71.7	49187	70.0	79032	65.5
0.5	2411	78.4	11366	49.6	12293	70.5	24056	72.8	48203	70.6	76054	66.8
0.6	2377	78.7	10802	52.1	11168	73.2	21757	75.4	42465	74.1	69640	69.6
0.7	1763	**84.2**	10374	54.0	9334	77.6	18927	78.6	37546	77.1	58186	74.6

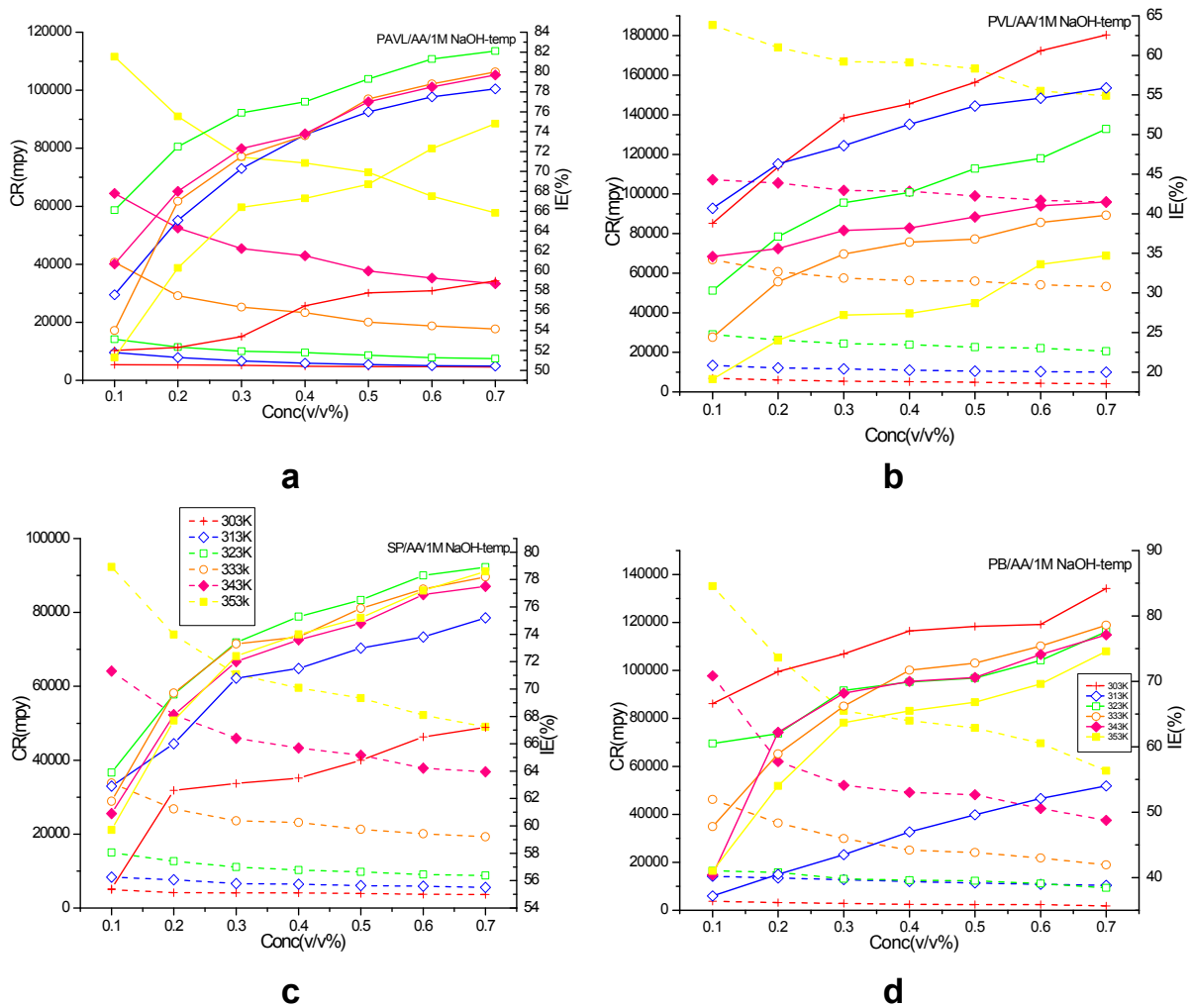

Figure 4.30. Effect of temperature on IE and Concentration on AA in1M NaOH.in the absence and presence of (a) PAVL (b) PVL (c) SP (d) PB

4.3.6.1 Comparison for effect of temperature on AA/Inhibitor/1M HCl and AA/Inhibitor/1M NaOH

The mass loss study in terms of temperature show better performance in case of AA/Inhibtors/1M HCl than AA/inhibitors/1M NaOH (Figure 4.31(a, b)).

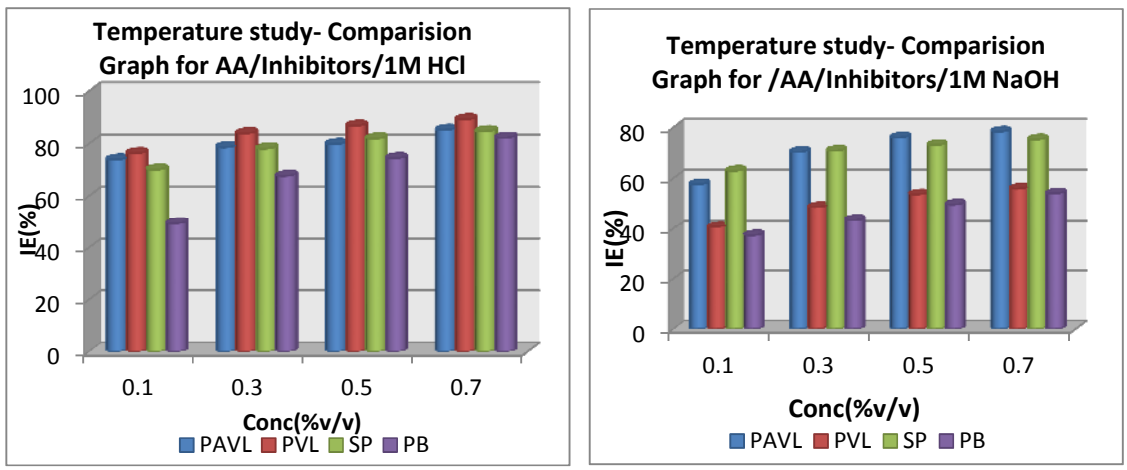

a **b**

Figure 4.31. Impact of temperature on IE and Concentration on (a) AA/Inhibitors/1M HCl (b) AA/Inhibitors/1M NaOH- comparison graph

4.3.6.2 Assessment of IE of investigated inhibitors by mass loss and EIS methods on MS/AA/Inhibitors/1M HCl and AA/Inhibitors/1M NaOH systems

IE (%) obtained from mass loss and electrochemical techniques was compared and it was noticed that the average corrosion rate observed from mass loss method was higher than that of electrochemical method. This was due to instantaneous corrosion rate obtained in the case of electrochemical measurement (Figure 4.32(a-c)). This was due to the difference in time needed to form a protective layer over the metal surface by the organic compounds present in the studied inhibitors which can reduce the corrosion reaction **(Muralidharan *et al,* 1995)**. Significant corrosion inhibition results were observed for the PAVL/PVL/SP/PB/MS/AA/1M HCl system. The obtained results by EIS techniques were parallel and comparable with those achieved in mass loss method. The investigated inhibitors were showed good performance in MS/AA/1M HCl system than AA/1M NaOH system. Good agreement results were obtained from all the studied techniques.

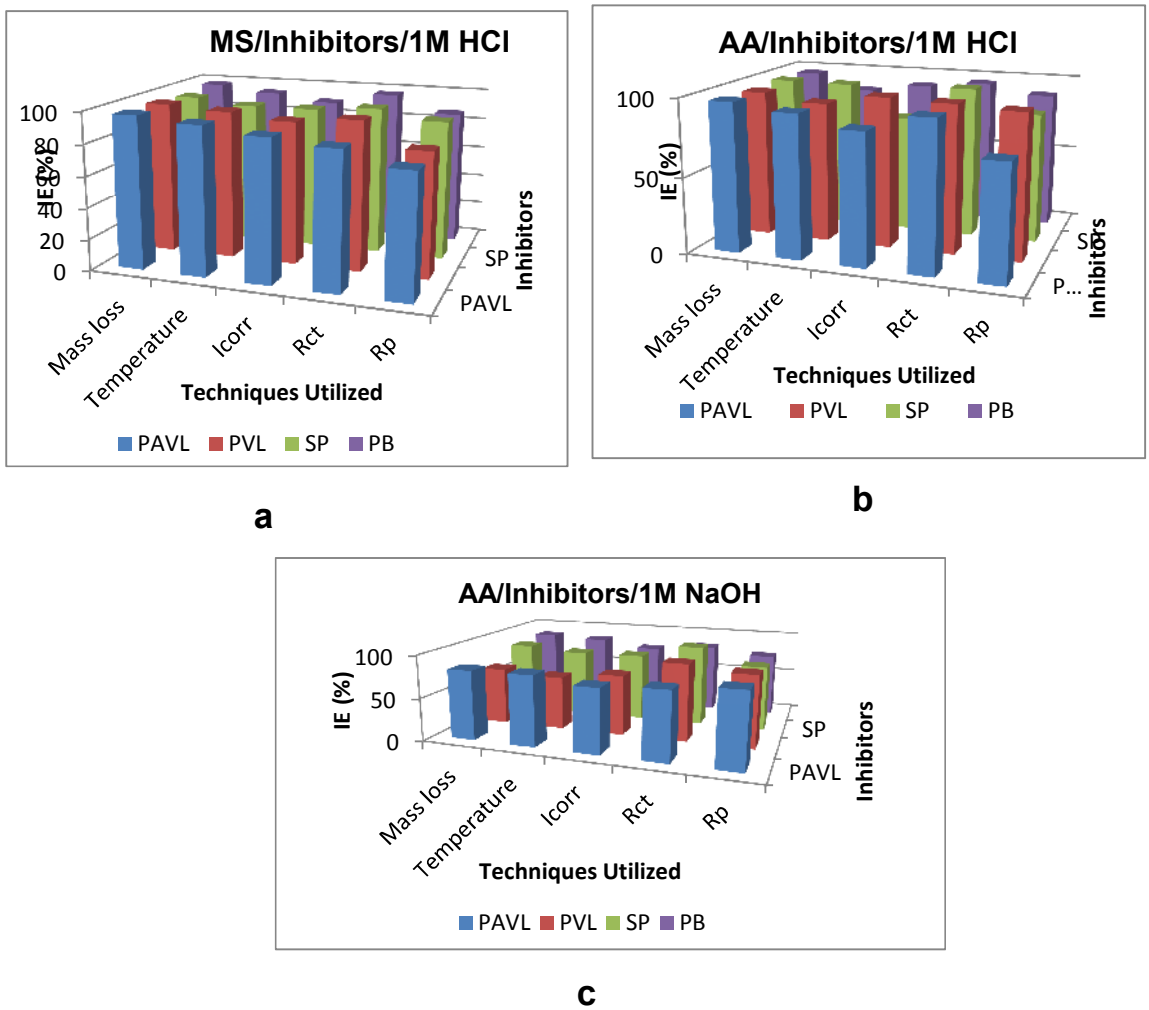

Figure 4.32. Assessment of IE of investigated inhibitors by mass loss and EIS methods on MS/Inhibitors/1M HCl (b) AA/Inhibitors/1M HCl (c) AA/Inhibitors/1M NaOH

4.3.6.2 Shelf life performance of studied inhibitors at room temperature

In industries, a huge volume of extracts is utilized and kept storing it for 3 years for various industrialization activities. This can help to reduce the burden for manpower in industries. Considering the necessary action was taken to prepare the more volume of inhibitors and kept for a store in room temperature. For analysing these extract, weight loss is a suitable method. Experiments were performed at 0.7% concentration of the investigated inhibitors through mass loss methods and the obtained values were summarized in picture form (Figure 4.33 (a-c)). The results revealed that %IE is quite comparable for all studied inhibitors during the 3 years study period. Long lasting ability and appreciable inhibitive performance of the inhibitors kept back at room temperature for

the 3 years period of the studied inhibitors are confirmed by mass loss method. It is the industries choice for using these inhibitors at room temperature **(Das *et al*, 2004)**. It was free from fungal and bacterial attack during the storage period and no unpleasant smell occurred **(El-Etre *et al*, 2005)**. There was some change in the viscosity induce antioxidant behaviour by phytochemicals present in the studied inhibitors. Hence, these extracts were confirmed as good inhibitors for years and they have an appreciable shelf life.

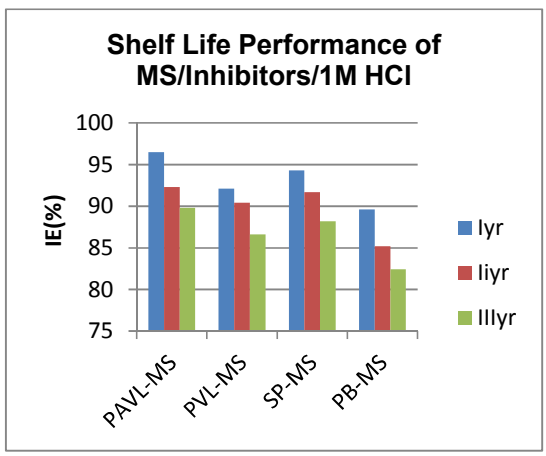

a

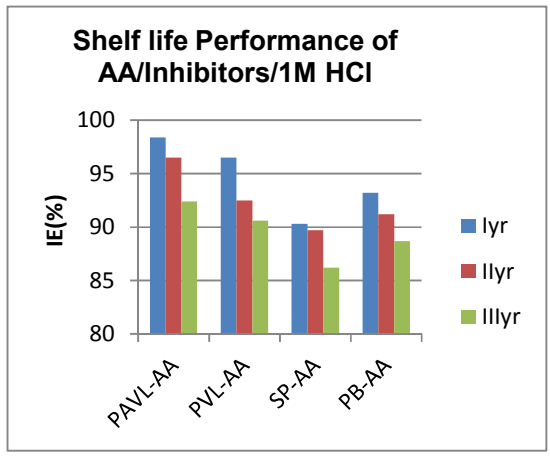

b

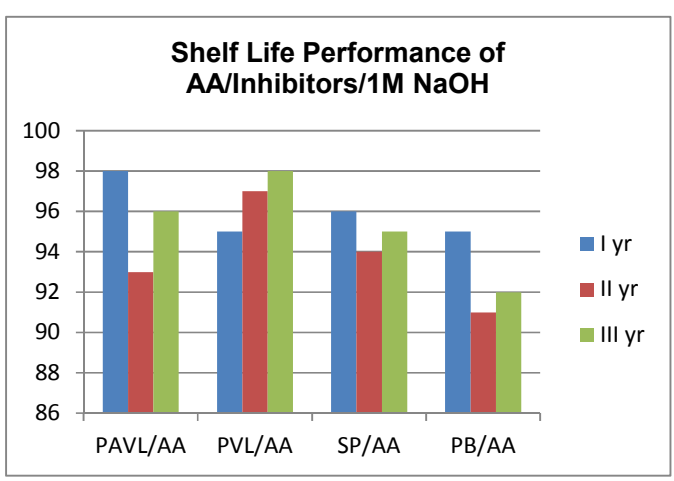

c

Figure 4.33. Shelf life performance of (a) MS/Inhibitors/1M HCl (b) AA/Inhibitors/1M HCl (c) AA/Inhibitors/1M NaOH

4.3.7 Adsorption Isotherm

Adsorption isotherm describe the interactions of the investigated inhibitors molecules with the metal surface which is contained active sites. The adsorption isotherm reflected the metal-inhibitor interaction of the investigated inhibitors. The efficiency of the adsorbent type of studied inhibitors can be finding out by using one of the well-known adsorption isotherm models by fitting the experimental values.

Corrosion inhibition study was performed by the adsorption process of the inhibitors molecules over the metal surface and separation process of the metal and corrosive medium by the distribution of some compounds between two phases. There are two types of adsorption process one is physical adsorption and another one is chemical adsorption. Physisorption means absorbed molecules are bonded by weak Vander Waals forces of attraction, not stable at high temperature whereas chemical adsorption means adsorbed molecules are bonded by charge sharing/transfer of electrons. It is stronger than physical adsorption. Chemical bonds are more stable even at a higher temperature.

Adsorption isotherm provided the coordination between the inhibitor and the metal surface. The linear relation between the degree of surface coverage (θ) values (θ = %I/100) and concentration of the studied inhibitor (C) are used to find out the isotherm. The θ values were fitted to various isotherm models namely “Langmuir, Temkin, Freundlich, Frumkin, Bockris-Swinkel’s, Flory-Huggins, El-Awady” kinetic thermodynamic adsorption isotherms. SPSS 17 software package has been used to find out the adsorption isotherm model for all the investigated inhibitors. A model which is having highest R^2 is the most excellent model to get information about theperformance of the adsorbent-type inhibitors- PAVL/PVL/SP/PB.

4.3.7.1 Adsorption isotherm nature for all the investigated inhibitors in various systems

Tables 4.59-4.70 recorded that the estimated coefficients of the results of the adsorption factors derived from different isotherms of the investigated inhibitors in 1M acidic and 1M alkaline solution.

Table -4.59 Adsorption parameters deduced from various adsorption isotherms –MS/PAVL/1M HCl

Adsorption isotherms	Temp	Slope	t	intercept	R^2	F
Langmuir	303K	0.965	32.096 (0.000)	0.029	1.000	3.473E5 (0.000)
	313K	1.005	4.350 (0.007)	0.004	1.000	2.700E5 (0.000)
	323K	1.009	2.728 (0.041)	0.003	1.000	1.793E5 (0.000)
	333K	0.956	3.869 (0.018)	0.005	1.000	1.99E5 (0.000)
	343K	1.377	2.240 (0.089)	0.006	1.000	2.389E4 (0.000)
	353K	0.970	3.786 (0.019)	0.004	1.000	1.109E5 (0.000)
Temkin	303K	0.032	528.762 (0.000)	0.935	0.990	50.868 (0.000)
	313K	0.878	2.764 (0.040)	0.106	0.989	431.983 (0.000)
	323K	0.800	4.135 (0.009)	0.181	0.982	271.349 (0.000)
	333K	0.460	6.961 (0.001)	0.489	0.935	34.480 (0.002)
	343K	0.537	12.277 (0.000)	0.424	0.975	191.114 (0.000)
	353K	0.432	13.935 (0.000)	0.528	0.951	96.966 (0.000)
Frumkin	303K	-20.635	17.392 (0.000)	21.905	0.978	218.033 (0.000)
	313K	-16.446	12.506 (0.000)	18.273	0.954	104.019 (0.000)
	323K	-14.760	22.570 (0.000)	16.591	0.985	326.721 (0.000)
	333K	-5.395	4.897 (0.004)	8.116	0.630	8.505 (0.033)
	343K	-7.761	16.882 (0.000)	10.102	0.964	133.010 (0.000)
	353K	-6.105	11.298 (0.000)	8.228	0.913	52.393 (0.001)
Freundlich	303K	0.035	-33.099 (0.000)	-0.066	0.990	496.044 (0.000)
	313K	0.882	-3.998 (0.010)	-0.017	0.989	452.041 (0.000)
	323K	0.798	-3.828 (0.012)	-0.020	0.982	280.225 (0.000)
	333K	0.445	-5.784 (0.002)	-0.055	0.868	32.924 (0.002)
Freundlich	343	0.521	-8.417 (0.000)	-0.042	0.972	170.928 (0.000)
	353	0.402	-6.419 (0.001)	-0.044	0.945	85.587 (0.000)
Flory-Huggins	303	3.139	20.688 (0.000)	3.605	0.985	335.157 (0.000)
	313	2.626	16.675 (0.000)	3.154	0.977	209.628 (0.000)
	323	2.512	18.874 (0.000)	2.968	0.981	264.234 (0.000)
	333	1.654	9.533 (0.000)	2.086	0.922	59.064 (0.001)
	343	1.965	41.088 (0.000)	2.332	0.996	1.156E3 (0.000)
	353	1.968	27.024 (0.000)	2.141	0.990	489.532 (0.000)
El-Awady kinetic thermodynamic	303	0.338	119.450 (0.000)	1.127	0.987	382.894 (0.000)
	313	0.842	2.726 (0.041)	0.130	0.984	312.801 (0.000)
	323	0.799	3.452 (0.018)	0.196	0.974	187.531 (0.000)
	333	0.524	5.803 (0.002)	0.466	0.889	40.209 (0.001)
	343	0.624	11.353 (0.000)	0.392	0.983	285.039 (0.000)
	353	0.610	10.725 (0.000)	0.470	0.964	133.633 (0.000)
Bockris-Swinkles	303	0.370	99.933 (0.000)	1.048	0.987	371.510 (0.000)
	313	0.841	2.594 (0.049)	0.113	0.984	310.075 (0.000)
	323	0.800	3.403 (0.019)	0.176	0.974	185.432 (0.000)
	333	0.530	5.664 (0.002)	0.416	0.890	40.652 (0.001)
	343	0.631	11.543 (0.000)	0.353	0.984	300.103 (0.000)
	353	0.631	11.236 (0.000)	0.425	0.967	147.628 (0.000)

Figure within ( ) give t values; F Figure within [ ] give F ratio.
** - 1% level of significance, * - 5% level of significance.

Table -4.60 Adsorption parameters deduced from various adsorption isotherms –MS/PB/1M HCl

Adsorption isotherms	Temp	Slope	t	intercept	R^2	F
Langmuir	303K	0.965	18.934 (0.000)	0.021	1.000	2.187E5 (0.000)
	313K	1.022	-0.278 (0.792)	0.000	1.000	7.827E4 (0.000)
	323K	1.024	0.440 (0.678)	0.001	1.000	3.272E4 (0.000)
	333K	1.039	3.050 (0.028)	0.005	1.000	9.624E4 (0.000)
	343K	1.061	-0.653 (0.542)	-0.002	1.000	2.408E4 (0.000)
	353K	1.104	-2.557 (0.051)	-0.012	1.000	1.191E4 (0.000)
Temkin	303K	0.032	416.788 (0.000)	0.951	0.984	309.243 (0.000)
	313K	0.641	7.279 (0.001)	0.342	0.968	149.568 (0.000)
	323K	0.604	6.326 (0.001)	0.374	0.933	84.421 (0.000)
	333K	0.507	20.074 (0.000)	0.464	0.987	384.043 (0.000)
	343K	0.407	17.327 (0.000)	0.565	0.959	116.364 (0.000)
	353K	0.321	55.479 (0.000)	0.654	0.990	498.691 (0.000)
Frumkin	303K	-18.595	14.759 (0.000)	20.552	0.968	149.887 (0.000)
	313K	-9.916	15.375 (0.000)	12.180	0.962	126.141 (0.000)
	323K	-8.696	8.353 (0.000)	11.125	0.873	34.456 (0.002)
	333K	-6.077	25.512 (0.000)	8.697	0.981	253.968 (0.000)
	343K	-4.786	10.263 (0.000)	7.106	0.877	35.657 (0.002)
	353K	-3.767	23.326 (0.000)	5.706	0.970	159.195 (0.000)
Freundlich	303K	0.035	-18.520 (0.000)	-0.049	0.982	276.909 (0.000)
	313K	0.625	-3.261 (0.022)	-0.019	0.969	154.856 (0.000)
	323K	0.589	-3.325 (0.021)	-0.024	0.946	87.530 (0.000)
	333K	0.487	-10.488 (0.000)	-0.032	0.987	390.124 (0.000)
Freundlich	343K	0.378	-5.637 (0.002)	-0.031	0.961	124.151 (0.000)
	353K	0.276	-10.095 (0.000)	0.031	0.988	399.717 (0.000)
Flory-Huggins	303K	2.665	22.582 (0.000)	3.339	0.987	389.400 (0.000)
	313K	2.063	18.631 (0.000)	2.495	0.980	243.003 (0.000)
	323K	1.910	12.454 (0.000)	2.361	0.955	106.155 (0.000)
	333K	1.689	28.483 (0.000)	2.108	0.991	531.071 (0.000)
	343K	1.668	14.854 (0.000)	1.886	0.965	139.611 (0.000)
	353K	1.772	96.978 (0.000)	1.728	0.999	5.891E3 (0.000)
El-Awady kinetic thermodynamic	303K	0.393	119.802 (0.000)	1.238	0.989	430.380 (0.000)
	313K	0.761	4.823 (0.005)	0.325	0.960	119.568 (0.000)
	323K	0.705	4.327 (0.008)	0.371	0.928	64.751 (0.000)
	333K	0.633	11.634 (0.000)	0.452	0.980	246.455 (0.000)
	343K	0.616	10.614 (0.000)	0.546	0.953	101.084 (0.000)
	353K	0.634	29.914 (0.000)	0.627	0.989	437.908 (0.000)
Bockris-Swinkles	303K	0.431	103.198 (0.000)	1.170	0.989	430.321 (0.000)
	313K	0.765	4.965 (0.004)	0.307	0.959	117.177 (0.000)
	323K	0.708	4.413 (0.007)	0.348	0.927	63.822 (0.000)
	333K	0.639	11.630 (0.000)	0.421	0.979	238.056 (0.000)
	343K	0.632	10.656 (0.000)	0.514	0.950	94.219 (0.000)
	353K	0.691	31.661 (0.000)	0.581	0.990	483.104 (0.000)

Figure within ( ) give t values; F Figure within [ ] give F ratio.
** - 1% level of significance, * - 5% level of significance.

Table -4.61 Adsorption parameters deduced from various adsorption isotherms –MS/PVL/1M HCl

Adsorption isotherms	Temp	Slope	t	intercept	R^2	F
Langmuir	303K	0.961	10.061 (0.000)	0.016	1.000	1.059E5 (0.000)
	313K	1.005	-6.148 (0.002)	-0.011	1.000	7.423E4 (0.000)
	323K	1.000	-2.755 (0.040)	-0.004	1.000	1.167E5 (0.000)
	333K	1.000	-1.583 (0.174)	-0.002	1.000	1.222E5 (0.000)
	343K	1.013	-4.823 (0.005)	-0.007	1.000	1.155E5 (0.000)
	353K	1.028	-8.208 (0.000)	-0.015	1.000	7.580E4 (0.000)
Temkin	303K	0.036	292.830 (0.000)	0.962	0.974	185.093 (0.000)
	313K	0.894	1.807 (0.131)	0.123	0.965	137.765 (0.000)
	323K	0.998	0.159 (0.886)	0.010	0.974	190.262 (0.000)
	333K	0.989	0.240 (0.820)	0.016	0.975	196.131 (0.000)
	343K	0.777	4.931 (0.004)	0.226	0.979	230.863 (0.000)
	353K	0.640	9.830 (0.000)	0.367	0.978	222.204 (0.000)
Frumkin	303K	-14.159	9.764 (0.000)	16.698	0.921	58.519 (0.001)
	313K	-15.052	11.308 (0.000)	16.731	0.943	83.016 (0.000)
	323K	-15.085	8.223 (0.000)	17.303	0.896	43.072 (0.001)
	333K	-15.279	16.302 (0.000)	17.573	0.971	169.561 (0.000)
	343K	-11.594	17.681 (0.000)	13.687	0.973	180.727 (0.000)
	353K	-9.560	16.996 (0.000)	11.338	0.969	155.759 (0.000)
Freundlich	303K	0.039	-9.930 (0.000)	-0.037	0.971	169.090 (0.000)
	313K	0.864	1.955 (0.108)	0.016	0.966	141.909 (0.000)
	323K	0.995	1.321 (0.244)	0.009	0.974	188.144 (0.000)
	333K	0.983	0.694 (0.519)	0.004	0.976	199.438 (0.000)
Freundlich	343K	0.752	0.417 (0.694)	0.002	0.979	237.356 (0.000)
	353K	0.597	0.673 (0.531)	0.004	0.979	230.380 (0.000)
Flory-Huggins	303K	2.141	14.599 (0.000)	2.867	0.969	154.926 (0.000)
	313K	2.744	20.840 (0.000)	3.142	0.985	328.267 (0.000)
	323K	2.224	9.795 (0.000)	2.849	0.933	69.800 (0.000)
	333K	2.373	39.408 (0.000)	3.053	0.996	1.154E3 (0.000)
	343K	2.296	30.771 (0.000)	2.727	0.993	684.112 (0.000)
	353K	2.350	29.256 (0.000)	2.527	0.992	609.365 (0.000)
El-Awady kinetic thermodynamic	303K	0.474	67.591 (0.000)	1.324	0.972	178.384 (0.000)
	313K	1.196	-0.216 (0.838)	-0.027	0.943	83.179 (0.000)
	323K	1.043	0.109 (0.917)	0.008	0.980	239.464 (0.000)
	333K	1.067	-0.401 (0.705)	-0.037	0.968	151.215 (0.000)
	343K	1.020	1.523 (0.188)	0.125	0.966	142.706 (0.000)
	353K	1.023	3.207 (0.024)	0.241	0.964	134.142 (0.000)
Bockris-Swinkles	303K	0.520	59.198 (0.000)	1.265	0.972	176.391 (0.000)
	313K	1.203	0.008 (0.994)	0.001	0.944	84.392 (0.000)
	323K	1.043	0.257 (0.807)	0.017	0.979	236.455 (0.000)
	333K	1.067	-0.330 (0.755)	-0.028	0.968	152.133 (0.000)
	343K	1.026	1.824 (0.128)	0.136	0.967	144.488 (0.000)
	353K	1.046	3.750 (0.013)	0.251	0.965	136.960 (0.000)

Figure within ( ) give t values; F Figure within [ ] give F ratio.
** - 1% level of significance, * - 5% level of significance.

Table -4.62 Adsorption parameters deduced from various adsorption isotherms –MS/SP/1M HCl

Adsorption isotherms	Temp	Slope	t	intercept	R^2	F
Langmuir	303K	0.901	8.724 (0.000)	0.039	1.000	1.199E4 (0.000)
	313K	0.957	2.443 (0.058)	0.011	1.000	1.116E4 (0.000)
	323K	0.965	0.868 (0.425)	0.004	1.000	1.156E4 (0.000)
	333K	0.965	-3.454 (0.018)	-0.016	0.999	9.750E3 (0.000)
	343K	0.981	-4.752 (0.005)	-0.021	0.999	9.661E3 (0.000)
	353K	1.045	-3.221 (0.023)	-0.030	0.999	2.229E3 (0.000)
Temkin	303K	0.079	116.726 (0.000)	0.908	0.970	160.991 (0.000)
	313K	1.536	-3.706 (0.014)	-0.526	0.948	90.482 (0.000)
	323K	1.399	-3.295 (0.022)	-0.375	0.957	111.127 (0.000)
	333K	1.456	-2.991 (0.030)	-0.368	0.949	93.625 (0.000)
	343K	1.215	-1.432 (0.212)	-0.144	0.949	92.835 (0.000)
	353K	0.729	4.628 (0.006)	0.281	0.941	80.224 (0.000)
Frumkin	303K	-5.943	10.443 (0.000)	7.543	0.902	45.992 (0.001)
	313K	-10.778	11.056 (0.000)	12.549	0.933	69.582 (0.000)
	323K	-10.122	15.719 (0.000)	11.561	0.965	139.034 (0.000)
	333K	-12.015	13.215 (0.000)	12.429	0.956	109.348 (0.000)
	343K	-9.605	12.475 (0.000)	10.100	0.947	89.290 (0.000)
	353K	-3.849	5.032 (0.004)	5.038	0.622	8.238 (0.035)
Freundlich	303K	0.098	-8.738 (0.000)	-0.090	0.966	143.147 (0.000)
	313K	1.663	0.0892 (0.413)	0.021	0.950	95.420 (0.000)
	323K	1.475	1.499 (0.194)	0.0333	0.959	115.820 (0.000)
	333K	1.480	3.274 (0.022)	0.102	0.951	96.550 (0.000)
Freundlich	343K	1.179	2.611 (0.048)	0.074	0.950	95.597 (0.000)
	353K	0.652	-0.047 (0.964)	-0.001	0.934	70.399 (0.000)
Flory-Huggins	303K	2.158	16.736 (0.000)	2.041	0.974	188.302 (0.000)
	313K	2.397	15.360 (0.000)	2.635	0.971	169.809 (0.000)
	323K	2.541	19.843 (0.000)	2.573	0.983	283.862 (0.000)
	333K	3.185	12.533 (0.000)	2.762	0.959	117.808 (0.000)
	343K	3.117	18.254 (0.000)	2.545	0.980	246.300 (0.000)
	353K	2.073	7.304 (0.001)	1.594	0.872	34.023 (0.002)
El-Awady kinetic thermodynamic	303K	0.507	50.348 (0.000)	0.920	0.979	228.777 (0.000)
	313K	1.111	-2.268 (0.057)	-0.285	0.935	71.446 (0.000)
	323K	1.159	-2.399 (0.062)	-0.230	0.949	92.483 (0.000)
	333K	1.409	-2.400 (0.062)	-0.247	0.943	82.982 (0.000)
	343K	1.332	-1.314 (0.246)	-0.113	0.946	87.301 (0.000)
	353K	0.936	5.589 (0.003)	0.238	0.952	118.929 (0.000)
Bockris-Swinkles	303K	0.518	43.473 (0.000)	0.812	0.979	229.371 (0.000)
	313K	1.051	-2.446 (0.058)	-0.239	0.933	70.179 (0.000)
	323K	1.114	-2.318 (0.068)	-0.187	0.948	90.861 (0.000)
	333K	1.393	-2.195 (0.080)	-0.188	0.942	80.806 (0.000)
	343K	1.371	-1.219 (0.277)	-0.089	0.945	85.098 (0.000)
	353K	1.053	5.368 (0.003)	0.186	0.965	137.175 (0.000)

Figure within ( ) give t values; F Figure within [ ] give F ratio.
** - 1% level of significance, * - 5% level of significance.

ble -4.63 Adsorption parameters deduced from various adsorption isotherms – AA/PAVL/1M HCl

Adsorption isotherms	Temp	Slope	t	intercept	R^2	F
Langmuir	303K	0.949	13.435(0.000)	0.023	1.000	9.062E4 (0.000)
	313K	1.016	-8.064(0.000)	-0.046	0.999	6.508E3 (0.000)
	323K	1.111	-0.168(0.873)	-0.001	0.999	4.711E3 (0.000)
	333K	1.174	-9.226(0.000)	-0.153	0.990	516.206 (0.000)
	343K	1.102	-38.141(0.000)	-0.425	0.991	544.577 (0.000)
	353K	1.374	-20.524(0.000)	-0.771	0.964	132.085 (0.000)
Temkin	303K	0.046	270.934(0.000)	0.947	0.982	267.746 (0.000)
	313K	0.751	2.569(0.050)	0.299	0.841	26.505 (0.004)
	323K	0.378	16.057(0.000)	0.589	0.935	71.348 (0.000)
	333K	0.322	16.381(0.000)	0.710	0.792	19.007 (0.007)
	343K	0.647	9.620(0.000)	0.678	0.662	9.782 (0.026)
	353K	0.595	31.093(0.000)	0.782	0.815	22.095 (0.005)
Frumkin	303K	-11.245	11.021 (0.000)	13.379	0.933	69.151 (0.000)
	313K	-10.525	4.872 (0.005)	10.849	0.740	14.206 (0.013)
	323K	-1.855	6.169 (0.002)	4.154	0.504	5.080 (0.074)
	333K	-2.873	3.379 (0.020)	3.090	0.404	3.393 (0.125)
	343K	-10.404	2.926 (0.033)	3.940	0.581	6.943 (0.046)
	353K	-6.614	1.796 (0.132)	0.916	0.571	6.646 (0.050)
Freundlich	303K	0.051	-13.573(0.000)	-0.053	0.982	270.340 (0.0000)
	313K	0.678	1.555(0.181)	0.046	0.820	28.409 (0.003)
	323K	0.336	-4.215(0.008)	-0.039	0.934	70.706 (0.000)
	333K	0.221	0.540(0.612)	0.013	0.837	25.627 (0.004)
Freundlich	343	0.262	2.107(0.089)	0.176	0.702	11.759 (1019)
	353	0.135	2.961(0.031)	0.115	0.871	33.735 (0.002)
Flory-Huggins	303	2.203	15.629 (0.000)	2.637	0.972	174.393 (0.000)
	313	2.965	5.575 (0.003)	2.443	0.812	22.622 (0.005)
	323	1.305	10.305 (0.000)	1.382	0.921	58.605 (0.001)
	333	1.960	3.854 (0.012)	0.988	0.648	9.206 (0.029)
	343	7.542	2.839 (0.036)	1.360	0.622	8.224 (0.035)
	353	6.197	1.631 (0.164)	0.331	0.639	8.836 (0.031)
El-Awady kinetic thermodynamic	303	0.470	65.445(0.000)	1.179	0.976	202.968(0.000)
	313	1.229	1.513(0.191)	0.221	0.840	26.200(0.004)
	323	0.596	11.500(0.000)	0.554	0.939	77.025(0.000)
	333	0.792	23.786(0.000)	0.841	0.814	29.932(0.005)
	343	1.584	10.704(0.000)	1.420	0.720	12.848(0.016)
	353	1.017	17.252(0.000)	1.598	0.909	49.667(001)
Bockris-Swinkles	303	0.514	55.249(000)	1.105	0.975	196.429(o.0000)
	313	1.306	1.808(0.130)	0.235	0.829	24.312(0.004)
	323	0.635	10.963(000)	0.503	0.934	70.701(0.000)
	333	1.146	16.497(0.000)	0.752	0.724	13.107(0.015)
	343	7.283	5.930(0.002)	1.565	0.592	7.250(0.043)
	353	-30.655	-2.814(0.037)	-2.712	0.734	13.774(0.014)

Figure within ( ) give t values; F Figure within [ ] give F ratio.
** - 1% level of significance, * - 5% level of significance.

Table -4.64 Adsorption parameters deduced from various adsorption isotherms –AA/PB/1M HCl

Adsorption isotherms	Temp	Slope	t	intercept	R^2	F
Langmuir	303K	0.936	26.534 (0.000)	0.056	1.000	5.912E4 (0.000)
	313K	1.216	-0.190 (0.857)	-0.003	0.992	655.559 (0.000)
	323K	1.29	-2.180 (0.081)	-0.065	0.987	189.283 (0.000)
	333K	1.135	-46.844 (0.000)	-0.312	0.997	1.614E3 (0.000)
	343K	1.669	-14.179 (0.000)	-0.679	0.928	64.565 (0.000)
	353K	1.231	-35.804 (0.000)	-0.909	0.991	527.877 (0.000)
Temkin	303K	0.052	211.9483 (0.000)	0.877	0.980	248.286 (0.000)
	313K	0.325	23.422 (0.000)	0.592	0.944	83.941 (0.000)
	323K	0.251	21.171 (0.000)	0.668	0.830	24.416 (0.004)
	333K	0.714	13.719 (0.000)	0.539	0.912	52.041 (0.001)
	343K	0.453	35.774 (0.000)	0.714	0.861	31.061 (0.003)
	353K	1.51	20.297 (0.000)	0.627	0.891	40.685 (0.001)
Frumkin	303K	-12.217	11.798 (0.000)	12.657	0.946	87.586 (0.000)
	313K	-1.562	6.801 (0.001)	3.092	0.544	5.970 (0.058)
	323K	-0.301	2.690 (0.043)	1.752	0.016	0.083 (0.785)
	333K	-9.551	6.977 (0.001)	4.423	0.877	35.812 (0.002)
	343K	-2.922	1.854 (0.123)	0.557	0.533	5.702 (0.063)
	353K	-19.648	2.863 (0.035)	1.684	0.791	18.913 (0.007)
Freundlich	303K	0.064	-26.402 (0.000)	-0.128	0.982	274.969 (0.000)
	313K	0.254	-8.477 (0.000)	-0.106	0.927	63.557 (0.001)
	323K	0.188	-5.002 (0.004)	-0.101	0.840	26.331 (0.004)
	333K	0.338	2.619 (0.047)	0.118	0.909	49.770 (0.001)
Freundlich	343K	0.120	-0.569 (0.594)	-0.019	0.857	29.880 (0.003)
	353K	0.240	4.299 (0.008)	0.297	0.912	51.617 (0.001)
Flory-Huggins	303K	3.205	12.281 (0.000)	2.804	0.958	113.458 (0.000)
	313K	1.497	9.782 (0.000)	1.139	0.914	53.213 (0.001)
	323K	1.013	4.080 (0.010)	0.687	0.604	7.625 (0.040)
	333K	6.794	6.919 (0.001)	1.554	0.900	44.904 (0.001)
	343K	3.240	1.760 (0.139)	0.208	0.700	11.655 (0.019)
	353K	18.025	2.694 (0.043)	0.654	0.803	20.366 (0.006)
El-Awady kinetic thermodynamic	303K	0.344	53.314 (0.000)	0.831	0.967	145.252 (0.000)
	313K	0.466	21.448 (0.000)	0.485	0.943	82.888 (0.000)
	323K	0.376	25.999 (0.000)	0.590	0.845	27.359 (0.003)
	333K	1.131	29.372 (0.000)	0.881	0.922	59.468 (0.001)
	343K	0.512	19.010 (0.000)	0.939	0.869	32.288 (0.002)
	353K	1.142	13.524 (0.000)	1.624	0.927	63.881 (0.000)
Bockris-Swinkles	303K	0.356	41.703(0.000)	0.720	0.962	126.685 (0.000)
	313K	0.594	18.991(0.000)	0.376	0.954	104.384(0.000)
	323K	0.496	17.875 (0.000)	0.475	0.799	19.906 (0.007)
	333K	4.202	21.588 (0.000)	0.848	0.926	62.618 (0.001)
	343K	6.815	1.340 (0.238)	1.322	0.109	0.610 (0.470)
	353K	-13.898	-5.173 (0.004)	-0.919	0.932	68.876 (0.000)

Figure within ( ) give t values; F Figure within [ ] give F ratio.
** - 1% level of significance, * - 5% level of significance.

Table - 4.65 Adsorption parameters deduced from various adsorption isotherms –AA/PVL/1M HCl

Adsorption isotherms	Temp	Slope	t	intercept	R^2	F
Langmuir	303K	0.969	31.762 (0.000)	0.037	1.000	2.054E5 (0.000)
	313K	1.057	-0.610 (0.569)	-0.002	1.000	2.184E4 (0.000)
	323K	1.073	-10.068 (0.000)	-0.074	0.999	3.528E3 (0.000)
	333K	1.238	-9.374 (0.000)	-0.212	0.978	222.043 (0.000)
	343K	1.407	-34.277 (0.000)	-0.624	0.985	338.007 (0.000)
	353K	1.829	-3.633 (0.015)	-1.489	0.585	7.057 (0.045)
Temkin	303K	0.025	366.871 (0.000)	0.918	0.974	185.280 (0.000)
	313K	0.386	16.883 (0.000)	0.564	0.950	94.523 (0.000)
	323K	0.361	15.054 (0.000)	0.632	0.883	37.587 (0.002)
	333K	0.181	38.471 (0.000)	0.797	0.800	19.990 (0.007)
	343K	0.349	69.292 (0.000)	0.802	0.920	57.436 (0.001)
	353K	0.519	114.725 (0.000)	0.839	0.911	51.485 (0.001)
Frumkin	303K	-25.952	10.193 (0.000)	26.223	0.941	80.3335 (0.000)
	313K	-7.065	10.192 (0.000)	8.718	0.906	48.312 (0.001)
	323K	-8.445	5.425 (0.003)	7.999	0.769	16.651 (0.010)
	333K	-2.151	2.461 (0.057)	2.191	0.234	1.529 (0.271)
	343K	-7.020	4.179 (0.009)	1.683	0.793	19.199 (0.007)
	353K	-3.848	-3.068 (0.28)	-0.876	0.271	1.856 (0.231)
Freundlich	303K	0.031	-31.796 (0.000)	-0.085	0.976	205.969 (0.000)
	313K	0.359	-7.964 (0.001)	-0.056	0.947	88.653 (0.000)
	323K	0.280	-1.356 (0.233)	-0.022	0.875	35.154 (0.002)
	333K	0.109	-2.873 (0.035)	-0.042	0.849	28.011 (0.003)
Freundlich	343K	0.090	0.469 (0.659)	0.008	0.912	51.559 (0.001)
	353K	0.038	-1.309 (0.250)	-0.027	0.808	21.045 (0.006)
Flory-Huggins	303K	3.868	10.412 (0.000)	4.122	0.973	87.897 (0.000)
	313K	2.154	13.389 (0.000)	2.145	0.961	121.707 (0.000)
	323K	3.479	6.223 (0.002)	2.216	0.852	28.702 (0.003)
	333K	1.782	2.751 (0.040)	0.724	0.489	4.787 (0.080)
	343K	6.260	3.924 (0.011)	0.631	0.830	24.459 (0.004)
	353K	4.582	-3.201 (0.024)	-0.383	0.389	3.184 (0.134)
El-Awady kinetic thermodynamic	303K	0.268	70.264 (0.000)	1.032	0.952	99.191 (0.000)
	313K	0.537	13.763 (0.000)	0.510	0.959	118.154 (0.000)
	323K	0.753	12.004 (0.000)	0.608	0.879	36.438 (0.002)
	333K	0.441	61.532 (0.000)	0.902	0.813	21.748 (0.006)
	343K	0.605	25.875 (0.000)	1.204	0.897	43.471 (0.001)
	353K	0.306	15.859 (0.000)	1.215	0.773	17.051 (0.009)
Bockris-Swinkles	303K	0.293	58.107 (0.000)	0.944	0.951	96.647 (0.000)
	313K	0.558	14.327 (0.000)	0.457	0.962	126.276 (0.000)
	323K	0.945	11.986 (0.000)	0.536	0.887	39.311 (0.002)
	333K	0.762	38.103 (0.000)	0.792	0.695	11.413 (0.020)
	343K	7.880	2.633 (0.046)	1.720	0.282	1.963 (0.220)
	353K	-3.709	5.831 (0.002)	0.471	0.782	17.929 (0.008)

Figure within ( ) give t values; F Figure within [ ] give F ratio.
** - 1% level of significance, * - 5% level of significance.

Table -4.66 Adsorption parameters deduced from various adsorption isotherms –AA/SP/1M HCl

Adsorption isotherms	Temp	Slope	t	intercept	R^2	F
Langmuir	303K	0.965	5.990 (0.002)	0.010	1.000	9.2345E4 (0.000)
	313K	1.065	-17.880 (0.000)	-0.052	1.000	2.699E4 (0.000)
	323K	1.023	-23.170 (0.000)	-0.063	1.000	2.925E4 (0.000)
	333K	1.135	-30.189 (0.000)	-0.230	0.998	1.998E3 (0.000)
	343K	1.184	-70.619 (0.000)	-4.697	0.997	1.610E3 (0.000)
	353K	1.441	-10.070 (0.000)	-1.083	0.891	40.717 (0.001)
Temkin	303K	0.032	248.995 (0.000)	0.976	0.956	108.334 (0.000)
	313K	0.446	25.529 (0.000)	0.587	0.979	236.431 (0.000)
	323K	0.696	7.334 (0.001)	0.385	0.957	111.994 (0.000)
	333K	0.390	29.251 (0.000)	0.736	0.930	66.664 (0.000)
	343K	0.537	52.228 (0.000)	0.776	0.966	142.823 (0.000)
	353K	0.48	27.039 (0.000)	0.879	0.828	24.001 (0.004)
Frumkin	303K	-10.962	3.750 (0.013)	14.219	0.597	7.396 (0.042)
	313K	-7.477	9.712 (0.000)	8.358	0.905	47.443 (0.001)
	323K	-14.145	5.729 (0.002)	13.762	0.816	22.124 (0.005)
	333K	-7.442	5.337 (0.003)	5.086	0.772	16.933 (0.009)
	343K	-11.112	5.871 (0.002)	3.950	0.853	29.104 (0.003)
	353K	-4.799	-0.561 (0.599)	-0.273	0.258	1.736 (0.245)
Freundlich	303K	0.035	-5.978 (0.002)	0.024	0.959	117.365 (0.000)
	313K	0.368	3.918 (0.011)	0.025	0.975	196.139 (0.000)
	323K	0.593	5.894 (0.002)	0.072	0.961	122.304 (0.000)
	333K	0.217	4.901 (0.004)	0.079	0.940	77.793 (0.000)
Freundlich	343K	0.180	8.092 (0.000)	0.142	0.965	136.375 (0.000)
	353K	0.073	3.893 (0.001)	0.093	0.895	42.828 (0.001)
Flory-Huggins	303K	1.526	6.904 (0.001)	2.358	0.865	31.919 (0.002)
	313K	2.573	11.119 (0.000)	2.147	0.945	86.386 (0.000)
	323K	3.664	6.023 (0.002)	2.938	0.848	27.889 (0.003)
	333K	4.372	5.212 (0.003)	1.611	0.812	21.640 (0.006)
	343K	8.474	5.619 (0.002)	1.428	0.869	33.180 (0.002)
	353K	4.977	-0.743 (0.491)	-0.147	0.335	2.519 (0.173)
El-Awady kinetic thermodynamic	303K	0.583	28.063 (0.000)	1.502	0.876	35.337 (0.002)
	313K	1.388	4.666 (0.006)	0.410	0.947	90.094 (0.000)
	323K	2.061	-0.112 (0.915)	0.013	0.956	108.154 (0.000)
	333K	1.799	49.159 (0.000)	1.150	0.924	60.588 (0.001)
	343K	2.120	21.723 (0.000)	1.908	0.927	63.597 (0.001)
	353K	1.157	27.753 (0.000)	2.216	0.969	157.887 (0.000)
Bockris-Swinkles	303K	0.636	25.240 (0.000)	1.457	0.879	36.178 (0.002)
	313K	1.526	6.386 (0.001)	0.438	0.959	117.678 (0.000)
	323K	2.195	0.928 (0.396)	0.098	0.954	104.062 (0.000)
	333K	3.536	39.538 (0.000)	1.061	0.920	57.618 (0.001)
	343K	14.924	17.683 (0.000)	2.667	0.953	101.646 (0.000)
	353K	-16.642	-5.504 (0.003)	-0.557	0.983	290.543 (0.000)

Figure within ( ) give t values; F Figure within [ ] give F ratio.
** - 1% level of significance, * - 5% level of significance.

Table -4.67 Adsorption parameters deduced from various adsorption isotherms –AA/PAVL/1M NaOH

Adsorption isotherms	Temp	Slope	t	intercept	R^2	F
Langmuir	303K	0.927	32.780 (0.000)	0.221	0.999	5.610E3 (0.000)
	313K	1.106	16.843 (0.000)	0.140	0.998	2.768E3 (0.000)
	323K	1.041	18.475 (0.000)	0.152	0.998	2.965E3 (0.000)
	333K	1.148	9.858 (0.000)	0.156	0.994	810.176 (0.000)
	343K	1.077	16.934 (0.000)	0.142	0.998	2.745E3 (0.000)
	353K	1.133	9.077 (0.000)	0.110	0.996	1.169E3 (0.000)
Temkin	303K	0.040	68.971 (0.000)	0.599	0.870	33.411 (0.002)
	313K	0.360	6.384 (0.001)	0.300	0.857	30.080 (0.003)
	323K	0.477	2.531 (0.052)	0.192	0.823	23.211 (0.005)
	333K	0.284	6.902 (0.001)	0.352	0.764	16.143 (0.010)
	343K	0.402	4.558 (0.006)	0.263	0.838	25.867 (0.004)
	353K	0.328	6.597 (0.001)	0.340	0.781	17.859 (0.008)
Frumkin	303K	-17.716	5.321 (0.003)	11.154	0.816	22.113 (0.005)
	313K	-4.318	29.466 (0.000)	5.088	0.985	320.259 (0.000)
	323K	-6.887	22.329 (0.000)	7.531	0.980	244.002 (0.000)
	333K	-2.793	13.880 (0.000)	4.051	0.905	47.780 (0.001)
	343K	-5.310	28.348 (0.000)	5.961	0.986	340.928 (0.000)
	353K	-4.199	12.368 (0.000)	4.523	0.921	57.915 (0.001)
Freundlich	303K	0.072	-32.846 (0.000)	-0.510	0.873	34.340 (0.002)
	313K	0.435	-14.046 (0.000)	-0.439	0.834	25.062 (0.004)
	323K	0.632	-10.701 (0.000)	-0.416	0.807	20.913 (0.006)
	333K	0.331	-14.360 (0.000)	-0.476	0.723	13.038 (0.015)
Freundlich	343K	0.502	12.112 (0.000)	-0.428	0.817	22.304 (0.005)
	353K	0.362	-10.678 (0.000)	-0.435	0.754	15.333 (0.011)
Flory-Huggins	303K	8.875	5.552 (0.003)	3.350	0.844	27.140 (0.003)
	313K	2.321	36.133 (0.000)	1.614	0.994	861.686 (0.000)
	323K	2.704	22.642 (0.000)	2.070	0.986	359.978 (0.000)
	333K	1.889	25.937 (0.000)	1.392	0.988	413.210 (0.000)
	343K	2.510	27.252 (0.000)	1.780	0.990	504.585 (0.000)
	353K	2.494	14.138 (0.000)	1.475	0.964	134.173 (0.000)
El-Awady kinetic thermodynamic	303K	0.162	11.343 (0.000)	0.174	0.869	33.236 (0.002)
	313K	0.313	-1.335 (0.239)	-0.029	0.886	38.885 (0.002)
	323K	0.367	-2.543 (0.052)	-0.092	0.852	28.869 (0.003)
	333K	0.251	-0.307 (0.771)	-0.008	0.809	21.172 (0.006)
	343K	0.337	-1.841 (0.125)	-0.050	0.866	32.364 (0.002)
	353K	0.307	0.358 (0.735)	0.008	0.798	19.802 (0.007)
Bockris-Swinkles	303K	0.098	10.653 (0.000)	0.102	0.862	31.341 (0.003)
	313K	0.225	-1.102 (0.320)	-0.011	0.909	50.020 (0.001)
	323K	0.236	-2.246 (0.075)	-0.039	0.865	31.964 (0.002)
	333K	0.186	-0.253 (0.811)	-0.003	0.853	29.037 (0.003)
	343K	0.232	-1.567 (0.178)	-0.020	0.886	38.711 (0.002)
	353K	0.249	0.440 (0.678)	0.005	0.827	23.873 (0.005)

Figure within ( ) give t values; F Figure within [ ] give F ratio.
** - 1% level of significance, * - 5% level of significance.

Table -4.68 Adsorption parameters deduced from various adsorption isotherms –AA/PB/1M NaOH

Adsorption isotherms	Temp	Slope	t	intercept	R^2	F
Langmuir	303K	0.891	12.421 (0.000)	0.070	0.999	7.540E3 (0.000)
	313K	1.108	-37.278 (0.000)	-0.203	0.998	2.762E3 (0.000)
	323K	1.015	-5.863 (0.002)	-0.038	0.999	3.831E3 (0.000)
	333K	1.189	-0.072 (0.946)	0.000	0.997	1.937E3 (0.000)
	343K	1.237	-0.001 (0.999)	-4.221E-5	0.986	171.984 (0.000)
	353K	1.243	-1.820 (0.128)	-0.030	0.992	598.885 (0.000)
Temkin	303K	0.081	77.232 (0.000)	0.847	0.945	85.984 (0.000)
	313K	0.895	7.254 (0.001)	0.345	0.939	76.989 (0.000)
	323K	0.921	1.736 (0.143)	0.124	0.941	79.411 (0.000)
	333K	0.516	11.164 (0.000)	0.412	0.948	90.573 (0.000)
	343K	0.427	8.607 (0.000)	0.477	0.842	26.714 (0.004)
	353K	0.489	12.337 (0.000)	0.455	0.933	70.101 (0.000)
Frumkin	303K	-6.162	6.304 (0.001)	6.931	0.784	18.186 (0.008)
	313K	-6.790	8.583 (0.000)	4.075	0.899	44.462 (0.001)
	323K	-6.162	5.473 (0.003)	6.139	0.743	14.421 (0.013)
	333K	-1.878	20.861 (0.000)	3.103	0.937	73.840 (0.000)
	343K	-1.042	5.544 (0.003)	2.468	0.330	2.463 (0.177)
	353K	-1.765	9.622 (0.000)	2.697	0.759	15.756 (0.011)
Freundlich	303K	0.109	-12.432 (0.000)	-0.160	0.958	112.710 (0.000)
	313K	0.543	3.192 (0.024)	0.145	0.947	89.366 (0.000)
	323K	0.838	0.981 (0.372)	0.037	0.937	74.601 (0.000)
	333K	0.425	-5.078 (0.004)	-0.105	0.942	81.554 (0.000)
Freundlich	343K	0.313	-4.471 (0.007)	-0.143	0.815	22.051 (0.005)
	353K	0.360	-3.961 (0.011)	-0.101	0.917	55.227 (0.001)
Flory-Huggins	303K	2.365	6.951 (0.001)	1.837	0.866	32.395 (0.002)
	313K	4.610	8.222 (0.000)	1.388	0.919	56.845 (0.001)
	323K	2.815	6.121 (0.002)	1.756	0.839	26.077 (0.004)
	333K	1.647	25.126 (0.000)	1.125	0.986	365.346 (0.000)
	343K	1.467	8.218 (0.000)	1.001	0.881	37.007 (0.002)
	353K	1.717	12.462 (0.000)	1.008	0.938	91.682 (0.000)
El-Awady kinetic thermodynamic	303K	0.439	20.589 (0.000)	0.714	0.905	47.569 (0.001)
	313K	1.213	32.037 (0.000)	0.588	0.927	63.366 (0.001)
	323K	1.086	2.983 (0.031)	0.127	0.947	89.226 (0.000)
	333K	0.633	10.147 (0.000)	0.300	0.930	66.112 (0.000)
	343K	0.542	8.225 (0.000)	0.344	0.820	22.778 (0.005)
	353K	0.632	14.171 (0.000)	0.366	0.912	51.894 (0.001)
Bockris-Swinkles	303K	0.418	15.690 (0.000)	0.589	0.881	36.939 (0.002)
	313K	2.804	25.158 (0.000)	0.461	0.917	55.334 (0.001)
	323K	1.224	2.656 (0.045)	0.088	0.951	96.413 (0.000)
	333K	0.797	8.015 (0.000)	0.201	0.942	80.819 (0.000)
	343K	0.805	6.008 (0.002)	0.212	0.880	36.568 (0.002)
	353K	0.945	12.029 (0.000)	0.242	0.948	91.283 (0.000)

Figure within ( ) give t values; F Figure within [ ] give F ratio.
** - 1% level of significance, * - 5% level of significance.

Table -4.69 Adsorption parameters deduced from various adsorption isotherms –AA/PVL/1M NaOH

Adsorption isotherms	Temp	Slope	t	intercept	R^2	F
Langmuir	303K	0.757	34.678 (0.000)	0.167	0.999	7.375E3 (0.000)
	313K	0.904	-9.115 (0.000)	-0.037	0.999	4.043E3 (0.000)
	323K	1.008	-29.853 (0.000)	-0.099	0.999	4.732E3 (0.000)
	333K	0.993	-31.712 (0.000)	-0.184	0.996	1.289E3 (0.000)
	343K	0.838	-53.150 (0.000)	-0.145	0.999	6.143E3 (0.000)
	353K	1.061	-42.640 (0.000)	-0.287	0.996	1.162E3 (0.000)
Temkin	303K	0.121	90.400 (0.000)	0.660	0.989	432.701 (0.000)
	313K	1.537	-4.836 (0.005)	-0.242	0.980	240.401 (0.000)
	323K	1.221	0.579 (0.588)	0.015	0.988	407.944 (0.000)
	333K	1.545	-0.127 (0.904)	-0.006	0.962	127.604 (0.000)
	343K	3.170	-7.636 (0.001)	-0.686	0.974	183.685 (0.000)
	353K	1.530	3.094 (0.027)	0.104	0.971	166.401 (0.000)
Frumkin	303K	-4.106	15.868 (0.000)	3.377	0.955	106.519 (0.000)
	313K	-8.714	31.495 (0.000)	5.460	0.992	641.625 (0.000)
	323K	-5.807	14.213 (0.000)	3.207	0.960	120.148 (0.000)
	333K	-8.136	9.844 (0.000)	3.262	0.937	73.870 (0.000)
	343K	-21.378	8.091 (0.000)	8.805	0.919	56.948 (0.001)
	353K	-7.118	5.448 (0.003)	2.116	0.845	27.356 (0.003)
Freundlich	303K	0.243	-34.662 (0.000)	-0.384	0.993	759.590 (0.000)
	313K	1.484	6.312 (0.001)	0.384	0.983	293.528 (0.000)
	323K	0.967	5.269 (0.003)	0.200	0.990	514.852 (0.000)
	333K	0.972	4.264 (0.008)	0.393	0.963	129.995 (0.000)
Freundlich	343K	2.393	7.575 (0.001)	1.651	0.937	111.724 (0.000)
	353K	0.803	5.732 (0.002)	0.407	0.978	225.272 (0.000)
Flory-Huggins	303K	2.953	14.221 (0.000)	1.173	0.967	148.254 (0.000)
	313K	5.447	26.598 (0.000)	1.827	0.992	593.735 (0.000)
	323K	4.405	12.841 (0.000)	1.148	0.967	145.124 (0.000)
	333K	6.544	11.263 (0.000)	1.223	0.963	129.209 (0.000)
	343K	14.184	7.915 (0.001)	3.037	0.924	60.826 (0.001)
	353K	6.154	5.111 (0.004)	0.785	0.872	34.030 (0.002)
El-Awady kinetic thermodynamic	303K	0.492	21.375 (0.000)	0.283	0.988	410.014 (0.000)
	313K	1.551	5.450 (0.003)	0.048	0.979	234.163 (0.000)
	323K	1.177	19.702 (0.000)	0.217	0.987	376.425 (0.000)
	333K	1.338	10.154 (0.000)	0.425	0.947	89.628 (0.000)
	343K	3.037	14.937 (0.000)	0.680	0.976	199.279 (0.000)
	353K	1.213	17.136 (0.000)	0.562	0.981	259.126 (0.000)
Bockris-Swinkles	303K	0.251	10.857 (0.000)	0.156	0.948	90.860 (0.000)
	313K	1.708	4.969 (0.004)	0.028	0.968	152.464 (0.000)
	323K	1.963	17.572 (0.000)	0.140	0.980	242.548 (0.000)
	333K	4.513	17.550 (0.000)	0.453	0.982	266.163 (0.000)
	343K	5.996	24.292 (0.000)	0.507	0.990	516.892 (0.000)
	353K	6.968	4.977 (0.004)	0.814	0.819	22.676 (0.005)

Figure within ( ) give t values; F Figure within [ ] give F ratio.
** - 1% level of significance, * - 5% level of significance.

Table - 4.70 Adsorption parameters deduced from various adsorption isotherms –AA/SP/1M NaOH

Adsorption isotherms	Temp	Slope	t	intercept	R^2	F
Langmuir	303K	0.911	23.040 (0.000)	0.157	0.999	5.294E3 (0.000)
	313K	1.004	6.640 (0.001)	0.048	0.998	3.179E3 (0.000)
	323K	1.023	13.947 (0.000)	0.073	0.999	6.571E3 (0.000)
	333K	1.031	21.622 (0.000)	0.071	1.000	1.680E4 (0.000)
	343K	1.038	16.566 (0.000)	0.068	1.000	1.072E4 (0.000)
	353K	1.055	16.759 (0.000)	0.074	0.999	9.383E3 (0.000)
Temkin	303K	0.054	76.011 (0.000)	0.692	0.919	56.375 (0.001)
	313K	0.811	0.592 (0.580)	0.062	0.858	30.322 (0.003)
	323K	0.699	1.779 (1.135)	0.118	0.924	60.555 (0.001)
	333K	0.677	3.345 (0.020)	0.139	0.966	140.778 (0.000)
	343K	0.650	3.328 (0.021)	0.165	0.947	89.698 (0.000)
	353K	0.580	4.714 (0.005)	0.215	0.944	84.810 (0.000)
Frumkin	303K	-12.652	6.815 (0.001)	9.641	0.865	32.150 (0.002)
	313K	-10.543	13.034 (0.000)	9.390	0.955	106.692 (0.000)
	323K	-7.789	31.352 (0.000)	7.870	0.991	525.354 (0.000)
	333K	-7.140	12.343 (0.000)	7.288	0.940	78.016 (0.000)
	343K	-6.919	18.555 (0.000)	7.021	0.972	174.141 (0.000)
	353K	-5.654	17.142 (0.000)	6.130	0.963	130.936 (0.000)
Freundlich	303K	0.089	-22.962 (0.000)	-0.363	0.909	50.001 (0.001)
	313K	0.915	-2.286 (0.071)	-0.137	0.856	29.615 (0.003)
	323K	0.818	-6.333 (0.001)	-0.207	0.925	62.094 (0.001)
	333K	0.775	-10.217 (0.000)	-0.211	0.968	150.958 (0.000)
Freundlich	343K	0.737	-8.307 (0.000)	-0.214	0.940	94.901 (0.000)
	353K	0.677	-10.322 (0.000)	-0.243	0.948	90.878 (0.000)
Flory-Huggins	303K	5.921	8.022 (0.000)	2.861	0.914	53.157 (0.001)
	313K	4.232	14.869 (0.000)	2.576	0.972	171.841 (0.000)
	323K	3.170	44.941 (0.000)	2.199	0.997	1.472E3 (0.000)
	333K	3.116	19.759 (0.000)	2.120	0.983	282.658 (0.000)
	343K	3.087	32.325 (0.000)	2.055	0.993	753.225 (0.000)
	353K	2.709	28.690 (0.000)	1.855	0.991	571.510 (0.000)
El-Awady kinetic thermodynamic	303K	0.231	21.350 (0.000)	0.347	0.923	60.145 (0.001)
	313K	0.729	-0.766 (0.478)	-0.040	0.858	30.331 (0.003)
	323K	0.590	-0.811 (0.455)	-0.030	0.918	55.880 (0.001)
	333K	0.591	-0.805 (0.457)	-0.019	0.962	127.899 (0.000)
	343K	0.574	-0.027 (0.980)	0.000	0.943	82.640 (0.000)
	353K	0.512	0.902 (0.408)	0.023	0.940	77.694 (0.000)
Bockris-Swinkles	303K	0.167	21.201 (0.000)	0.232	O.933	69.682 (0.000)
	313K	0.612	-0.435 (0.682)	-0.013	0.866	32.311 (0.002)
	323K	0.470	-0.296 (0.779)	-0.006	0.920	57.283 (0.001)
	333K	0.482	-0.167 (0.874)	-0.002	0.961	122.190 (0.000)
	343K	0.475	0.480 (0.651)	0.008	0.941	80.359 (0.000)
	353K	0.424	1.323 (0.243)	0.021	0.937	74.209 (0.000)

Figure within ( ) give t values; F Figure within [ ] give F ratio.
** - 1% level of significance, * - 5% level of significance.

The results of F values for the studied inhibitors were analysed and highest F values are mentioned in the Table 4.71.

Table 4.71.The results of SPSS statistical analysis on adsorption isotherms and the various models obeyed by the investigated inhibitors and their highest F values

Inhibitors	MS/1M HCl			AA/1M HCl			AA/1M NaOH		
	Adsorption models	Highest F values	R^2	Adsorption models	Highest F values	R_2	Adsorption models	Highest F values	R^2
PAVL	Langmuir	347300	1	Langmuir	90620	1	Langmuir	5610	0.999
PVL	Langmuir	116700	1	Langmuir	205400	1	Langmuir	7375	0.999
SP	Langmuir	11990	1	Langmuir	92350	1	Langmuir	6571	0.999
PB	Langmuir	218700	1	Langmuir	59120	1	Langmuir	7540	0.999

4.3.7.2 Langmuir Adsorption model for investigated inhibitors:

SPSS statistical data analysis identified that MS/AA/PAVL/PVL/SP/PB extract in acidic and alkaline media may be described by Langmuir adsorption isotherm model.

Langmuir Adsorption Isotherm:

From the various adsorption isotherms examined to find out the adsorption nature inhibitor on the metal surface in 1M HCl/1M NaOH, it was noticed that the Langmuir adsorption isotherm model ($C_{inh}/\theta = 1/K_{ads}+C_{inh}$) fitted the best.

In the above equation K_{ads} denoted equilibrium constant, C_{inh} - Inhibitor concentration and θ - fraction of surface of the metal covered by the inhibitor through the adsorption process. Straight line observed on plotting C_{inh}/θ against C_{inh} (Figures 4.34 (a-c)) with a correlation coefficient (R^2=1) reflected that Langmuir isotherm model fitted best with the observed data. The slopes of C_{inh}/θ versus C_{inh} plot were almost equal to 1 with a little deviation from unity and it further proved the validity of Langmuir adsorption isotherm **(Lebrini *et al,* 2011a, b)**.

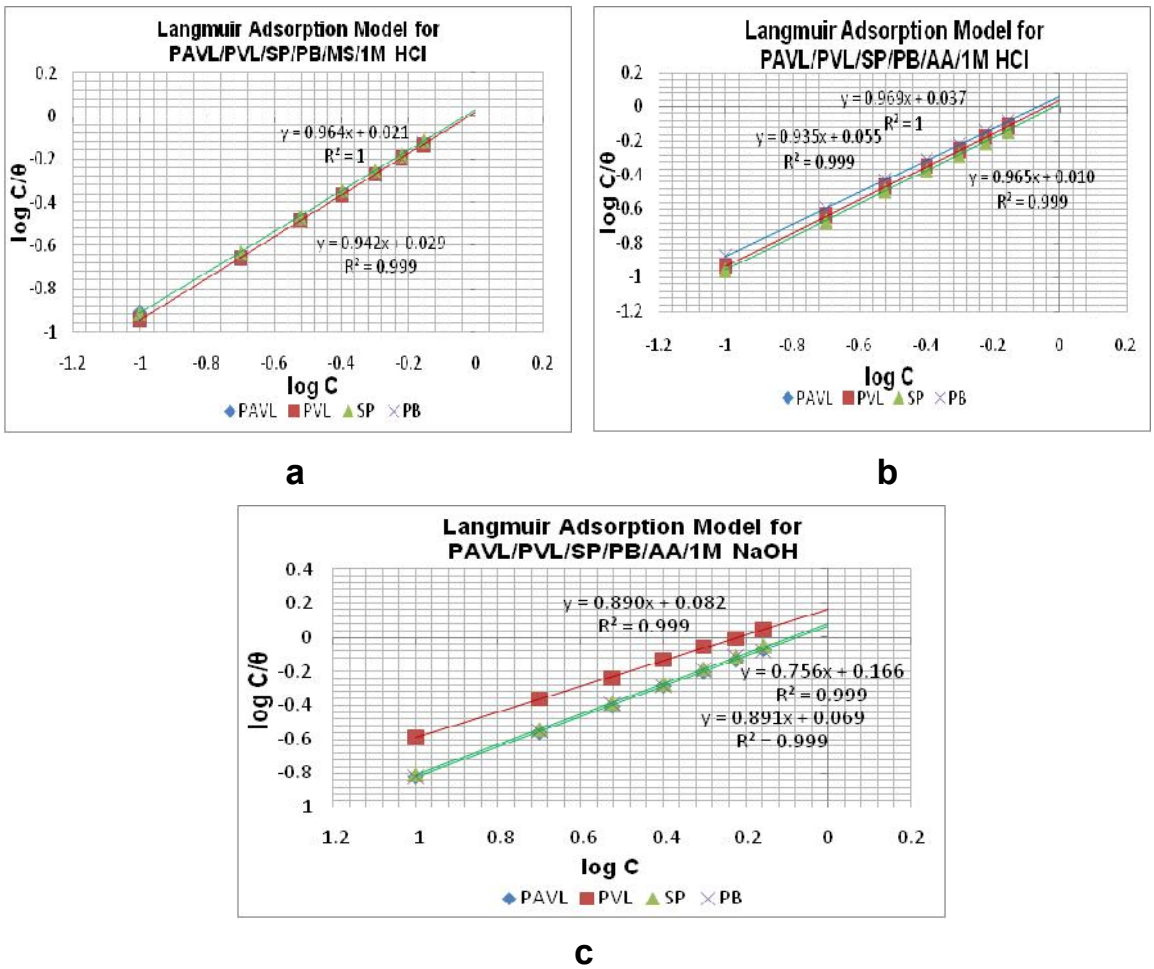

Figure 4.34. Langmuir Adsorption Isotherms for (a) MS/Inhibitors/1 M HCl (b) AA/Inhibitors/1M HCl (c) AA/Inhibitors/1M NaOH

4.3.8 Activation Parameters for the inhibition process

4.3.8.1 The energy of Activation:

. The apparent activation energy (E_a) and pre-exponential factor (A) is related to Arrhenius equation in which the logarithm of the corrosion rate ($\ln \nu$) is a linear function with 1/Tfor the acid/alkaline corrosion of metal surface

$$\ln \nu = -E_a/RT + \ln A \qquad (4.8)$$

where E_a and A represented apparent activation energy and pre-exponential factor. Arrhenius plots of $\ln \nu$ vs. 1/Tfor the corrosive medium containing investigated inhibitors are shown in Figures 4.35 (a-c) and the values are summarized in Table 4.72. The results revealed that all linear regression coefficients (r) were very close to 1 suggested that the

corrosion inhibition process followed the Arrhenius equation. Figures 4.35 (a-c) showed the relationship between E_a and inhibitor concentration in both media. It was found that the value of activation energy E_a was greater in the presence of the investigated inhibitors. The higher activation energy in the presence of the studied inhibitor was due to the formation of a protective layer on the metal surface thus preventing the metal from the corrosive attack of the acidic/alkaline medium. The higher activation energy in the presence of the inhibitor was probably considered as physical adsorption in the surface of the metal. Similar behaviour was reported in earlier studies **(Behpour *et al,* 2010, Martinez *et al*, 2002)**. Higher value of activation energy also implied that the energy barrier for the corrosion process enhanced in the presence of PAVL, PVL, SP and PB extracts. It was the evidence for the existence of electrostatic attraction between the adsorbed molecules and the surface of the metal.

Analysis of the results showed that activation energy was higher in the following order AA/HCl>AA/NaOH>MS/HCl. It was identified that the formation of a protective layer on AA/HCl/NaOH was more adsorbed than formed layer on MS/1M HCl. The results revealed that among the investigated inhibitors and their systems, PAVL/AA/1M HCl system showed much prominent increased in activation energy.

Table 4.72 Activation parameters for the investigated inhibitors for MS/AA in acidic and alkaline medium

Conc (%v/v)	E_a(kJ/mol)											
	PAVL			PVL			SP			PB		
	MS/ HCl	AA/ HCl	AA/ NaOH	MS/ HCl	AA/ HCl	AA/ NaOH	MS/ HCl	AA/ HCl	AA/ NaOH	MS/ HCl	AA/ HCl	AA/ NaOH
Blank	45	62	56	45	62	56	45	62	56	45	62	56
0.1	55	93	58	51	98	60	52	100	59	60	84	63
0.2	50	96	57	52	99	61	54	105	58	58	89	59
0.3	50	99	59	50	101	63	54	106	57	58	90	56
0.4	50	101	62	52	103	63	54	108	57	56	91	57
0.5	48	103	61	51	105	64	54	111	60	55	93	57
0.6	49	105	60	50	106	65	55	115	59	55	95	55
0.7	47	104	59	53	106	65	55	117	60	55	98	56
Average	49	95	59	51	97	62	53	103	58	55	88	57

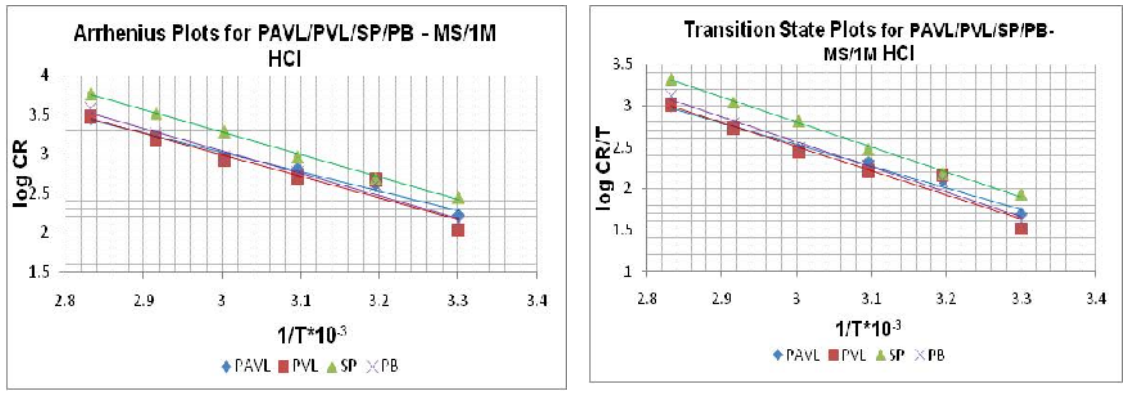

a

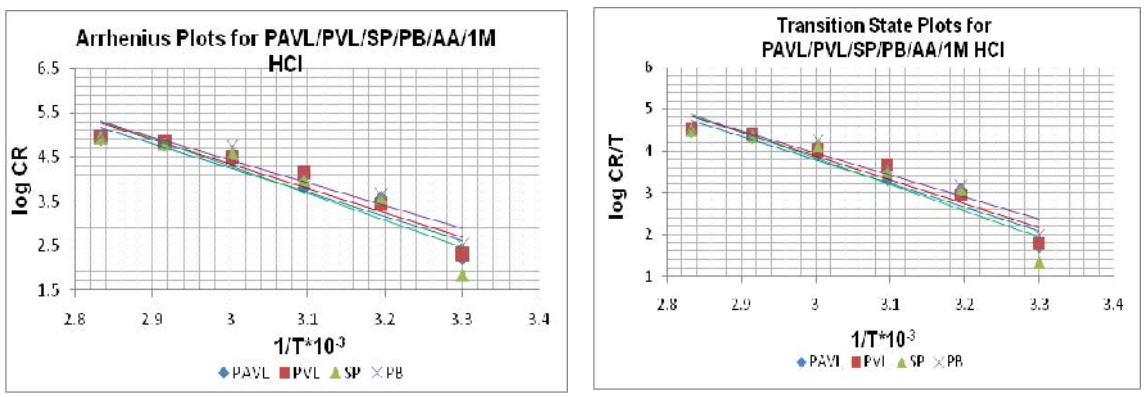

b

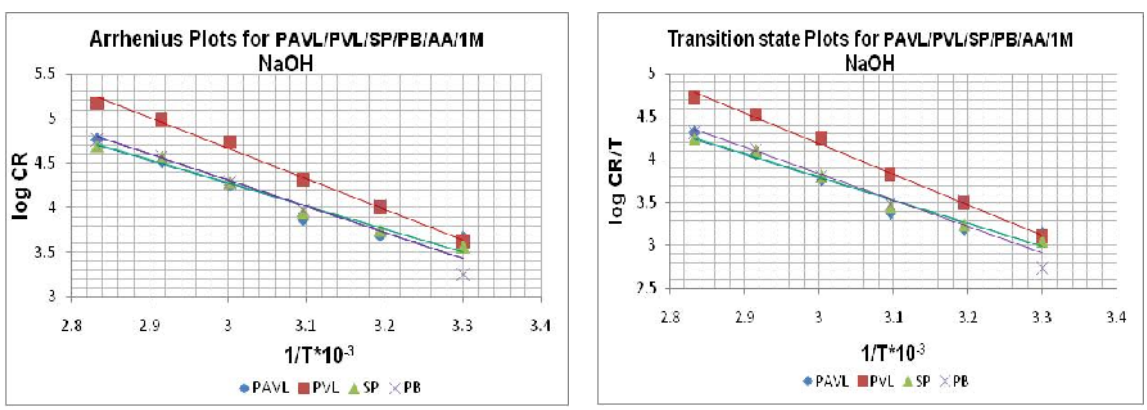

c

Figure 4.35. Arrhenius plots and Transition plots for (a) MS/Inhibitors/1M HCl (b) AA/Inhibitors/1M HCl (c) AA/Inhibitors/IM NaOH

4.3.8.2 Activation parameters – Entropy of Activation and Enthalpy of Activation

The entropy of activation ΔS_a enthalpy of activation, ΔH_a are derived from Eyring and transition state equation which relates CR/T versus 1/T. Log (CR/T) against 1/T for the corrosion of MS and AA with and without the addition of various concentrations of PAVL, PVL, SP and PB extracts were shown in Figure 4.35 (a-c). ΔH_a and ΔS_a values were derived from the slope of ($-\Delta H_a/2.303R$) and an intercept of (log R/Nh + $\Delta S_a/2.303R$) and their results are presented in Table 4.73. Analyzing the activation parameters for the MS/ AA corrosion in PAVL, PVL, SP and PB extracts listed in Table 4.73, it was suggested that all the studied inhibitors on MS/HCl and AA/HCl/NaOH systems were showed positive values of ΔH_a. The positive value of the enthalpies (ΔH_a) indicated the endothermic nature of the MS/AA dissolution process and it denoted that metal dissolution process was difficult in the presence of the inhibitors **(Belkhaouda *et al*, 2013)**. This proved that the activation energy strongly increased in the presence of the inhibitor.

Table 4.73. Average values of activation parameters on MS/AA corrosion for all the investigated inhibitors in acidic and alkaline medium

Inhibitor	E_a(KJ/mol)			ΔH_a(KJ/mol)			ΔS_a(J/Kmol)		
	MS/ HCl	AA/ HCl	AA/ NaOH	MS/ HCl	AA/ HCl	AA/ NaOH	MS/ HCl	AA/ HCl	AA/ NaOH
Blank	45	62	56	48	65	58	16	80	62
PAVL	49	95	59	52	98	55	12	172	43
PVL	51	97	62	53	100	65	16	180	79
SP	53	103	58	56	106	55	27	120	42
PB	55	88	57	58	91	60	31	152	60

The values of activation energy and enthalpy were nearer to each other with and without the addition of the studied inhibitors as expected from the transition state theory. The differences in the activation energy and enthalpy values were constant for the particular temperature**.** The entropies of the studied inhibitors in MS/1M hydrochloric acid and AA/HCl/NaOH corrosion were positive. The positive values of entropies (ΔS_a) for the studied extracts in 1 M hydrochloric acid/1M NaOH indicated that the adsorption reaction occurred by enhancing in entropy and this was confirmed that the driving force of the adsorption of inhibitor molecules present in the extract on the metal surface. Therefore

raising disorderliness took place going from reactants to the activation complex **(Elachouri *et al*, 1996)**.

4.3.9 Thermodynamic Adsorption Parameters

The equilibrium constant of the adsorption process, K in $Lmol^{-1}$, is associated with the standard free energy adsorption, ΔG^{o}_{ads} by the equation given below **(Li *et al*, 2011b)**.

$$K_{ads} = 1/55.5 \exp(-\Delta G^{o}ads /RT) \quad (4.9)$$

Where R denoted universal gas constant and T represented the absolute temperature. The ΔG^{o}_{ads} values were calculated and presented in Table. The ΔG^{o}_{ads} value also decreased with increasing temperature. In general, the values of ΔG^{o}_{ads} up to -20 $KJmol^{-1}$ are consistent with the electrostatic interaction between the charged molecules and the charged metal (physical adsorption) while those more negative than -40 $KJmol^{-1}$ involved sharing or transfer of electrons from the inhibitor molecules to the metal surface to form a coordinate type of bond (chemisorptions) **(Badawy *et al,* 1999)**. In the present study, the ΔG^{o}_{ads} values were lower than -20 $KJmol^{-1}$, which was confirmed that the adsorption of the studied plant/seaweed on the metal surface might be due to physisorption. Due to the complex nature of the inhibiting process chemisorption may not be excluded **(Ahamad *et al,* 2010)**.

4.3.9.1 ΔS^{o}_{ads} and ΔH^{o}_{ads}

Enthalpy of adsorption (ΔH^{o}_{ads}) was deduced from the integrated version of the Van't Haff equation, According to Van't Hoff equation

$$\ln K_{ads} = -\Delta H^{o}_{ads}/RT + constant \quad (4.10)$$

ΔH^{o}_{ads} can be also derived from the plot of $\ln K_{ads}$ versus 1/T giving straight lines with slopes of ($-\Delta H^{o}_{ads}$ /R). Then the adsorption entropy can be calculated via the thermodynamic function.

$$\Delta G^{o} = \Delta H^{o} - T\Delta S^{o} \quad (4.11)$$

The calculated mean values of ΔG^{o}_{ads}, ΔH^{o}_{ads}, ΔS^{o}_{ads} at all the studied temperatures (303K-353K) using different concentrations of PAVL/PVL/SP/PB extracts are represented in Table 4.74. According to the thermodynamic basic equation $\Delta G^{o}_{ads} = \Delta H^{o}_{ads} - T\Delta S^{o}_{ads}$, it was suggested that the driving force for the spontaneous adsorption of inhibitor on the metal surface was increased in entropy. The negative sign of enthalpy of adsorption reflected that the adsorption process was exothermic. An

exothermic adsorption reaction influenced either physisorption or chemisorption by taking into account the absolute value of adsorption. In the current study, the absolute values reflected the physisorption process **(Nnanna *et al,* 2013)** (Table 4.74).

The negative entropy (Figure 4.36(a-c)) reflected that the exothermic adsorption process with decreased in disorders during the adsorption process. It was clear that extract molecules liberally move in the whole of the solution and adsorb on MS/AA in the 1M HCl and AA in 1M NaOH which was orderly adsorbed onto the metal surface resulting negative entropy was observed **(Mu *et al*, 2004)**. Analysis of Table 4.74 revealed that lesser in enthalpy and entropy was the driving power of the adsorption of PAVL, PVL, SP and PB on MS/AA surface **(Umoren *et al,* 2007)**. The positive values of entropy of all the investigated inhibitors in AA/1M HCl for revealed that disorders took place between the metal and the inhibitor molecules.

Table 4.74. Thermodynamic adsorption parameters on MS/AA corrosion for all the investigated inhibitors in acidic and alkaline medium

Inhibitors	-∆G°(KJ/mol)						∆S°(J/mol)	∆H°(KJ/mol)
	303	313	323	333	343	353		
	MS/1M HCl							
PAVL	18.4	19.2	19.6	20.2	20.6	19.9	-33.8	-18.6
PVL	19.2	18.9	20.1	20.9	20.8	20.0	-30.3	-10.1
SP	16.8	18.4	18.5	18.3	18.4	17.6	-23.3	-14.3
PB	18.9	19.0	19.7	20.1	19.9	18.9	-21.1	-16.4
AA/1M HCl								
PAVL	18.4	16.8	17.9	15.0	12.6	10.4	158.7	-67.3
PVL	18.1	17.7	16.1	14.2	11.3	7.9	205.6	-81.8
SP	20.0	16.8	17.4	14.4	12.4	8.9	203.5	-81.8
PB	16.7	15.6	15.0	12.9	11.0	9.0	154.9	-64.2
AA/1M NaOH								
PAVL	13.4	15.7	16.9	17.2	17.4	16.4	-58.0	-34.0
PVL	13.1	13.2	12.8	12.3	13.2	11.8	-38.8	-29.9
SP	14.2	15.5	16.5	16.9	17.3	17.3	-59.8	-23.7
PB	15.8	12.9	15.9	16.2	16.5	16.0	-40.6	-23.9

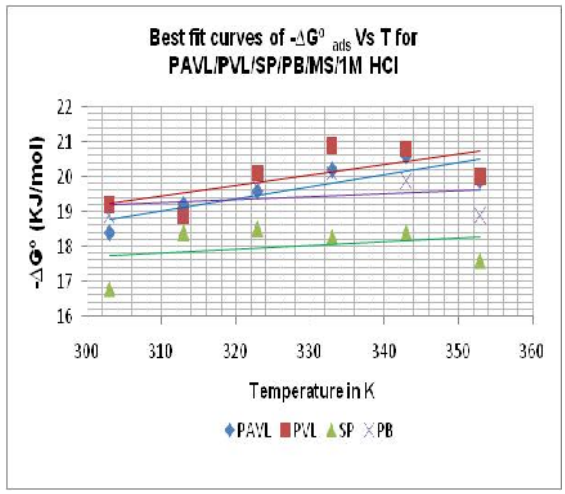

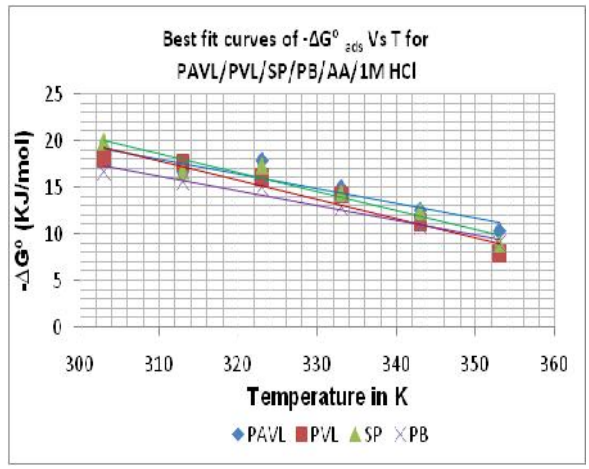

a **b**

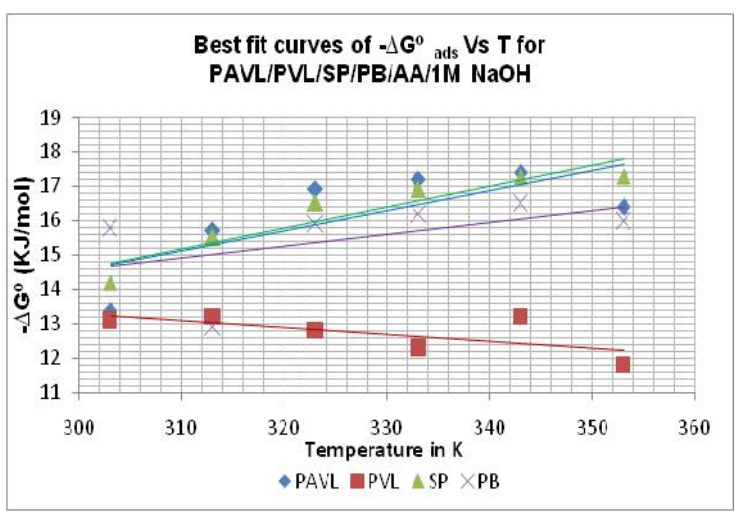

c

Figure 4.36. Best fit curves of ΔG_{ads} Vs T for (a) MS/Inhibitors/1M HCl (b) AA/Inhibitors/1M HCl (c) AA/Inhibitors/1M NaOH

4.4 SURFACE ANALYTICAL TECHNIQUES

Surface analytical techniques are used to characterize the adsorbed layer and to find out an active constituent present in the extract of plant/seaweed materials. The following surface analytical techniques were applied to study the topography of the MS/AA with and without the addition of the investigated inhibitors.

4.4.1. UV- Visible spectroscopic analysis

4.4.2. FT-IR spectral analysis

4.4.3. Scanning Electron Microscopic (SEM) analysis

4.4.4. Energy Dispersive X-ray analysis

4.4.5. X-ray diffraction analysis

4.4.6. 3D optical profilometry

4.4.1 UV Visible spectral Analysis

The plant/seaweed extracts have possessed the most important active compounds which are responsible for the inhibiting action. They form a complex with the metal surface during the inhibition process. UV-Visible spectrum is used to find out the formed metal complexes. UV-Visible spectroscopy proved the formation of a metal complex with the inhibitor molecules **(Singh *et al*., 2012c).**

i. MS/PAVL/PVL/SP/PB/1 M HCl

UV-Visible spectra obtained for the powdered plant/seaweed extract and solution of MS/AA/1 M HCl/1M NaOH at 0.7% concentration of the PAVL/PVL/SP/PB extracts after 3h immersion is shown in Figures 4.37 (a-d). The absorption bands of PAVL/PVL/SP/PB extracts are listed in Table 4.75.

Table 4.75. UV spectral results for the investigated inhibitors, corrodent solution on MS in 1 M HCl

Inhibitors	Absorption bands (nm)		
	Crude plant extract	MS/Inhibitors/1M HCl	Transitions
PAVL	322, 308, 270, 250, 232, 200	239, 335, 343	$n \rightarrow \pi^*$ $\pi \rightarrow \pi^*$
PVL	409, 380, 225, 200	237, 345,353	
SP	404, 380, 377, 340, 219, 200	240, 270,310,375,354,298,	
PB	401, 380, 379, 340, 230, 200	241, 305,365	

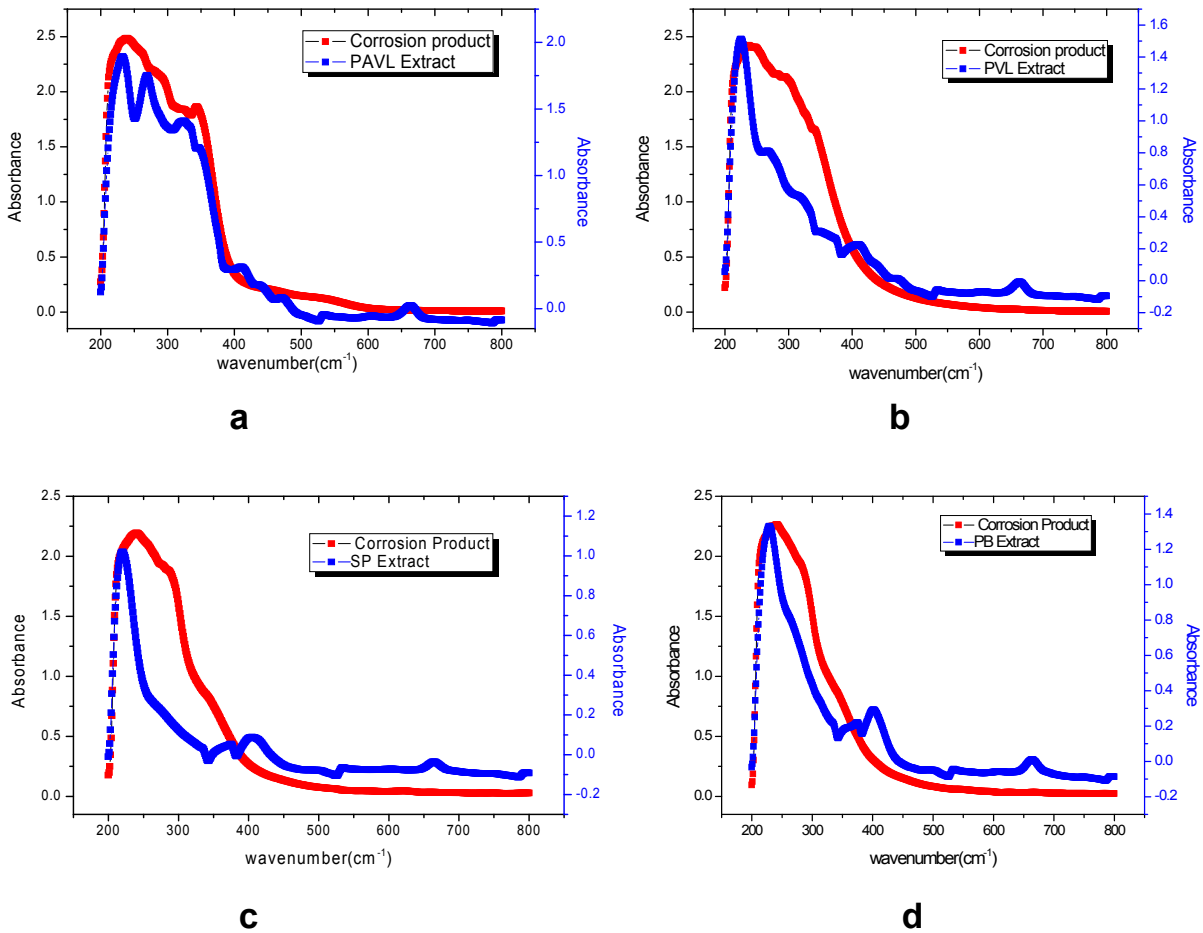

Figure 4.37 UV-Vis spectra for crude inhibitors (a) PAVL (b) PVL (c) SP (d) PB, corrodent solution on MS in 1 M HCl

The UV-Visible spectra of AA taken before and after the addition of 1M HCl contained investigated inhibitors (Figure 4.37(a-d)). The mild steel sample exposed in 1M HCl exhibited two bands in UV region which were due to π-π* and n- π* transitions. The change in the position of the absorption maximum was observed for MS exposed after addition of inhibitor solution which indicated that the complex formation reaction took place between metal/solution interfaces. Hence, there was no major change in the shape of the spectra which was the evidence of complex formation between inhibitor molecules and steel surface and formation of a protective layer on the metal surface **(Njoku *et al*, 2013, Yadav *et al*, 2012)**.

ii. **AA/PAVL/PVL/SP/PB/1 M HCl**

The UV-Vis spectroscopy of the plant extract was studied at a wavelength range of 200 nm to 800 nm. The results of the UV spectral studies indicated that one major band was recorded between 200 nm - 400 nm confirmed that the presence of heteroatoms present in the extract interacted with AA surface. These values were tabulated in Table 4.76 related Figure 4.38 (a-d) is depicted.

Table 4.76. UV spectral values for investigated inhibitors, corrodent solution on AA in 1 M HCl

Inhibitors	Absorption bands(nm)		
	Crude inhibitors	AA/Inhibitors/1M HCl	Transitions
PAVL	322, 308, 270, 250, 232, 200	238, 325,338,342	n → π* π → π*
PVL	409, 380, 225, 200	247, 266, 278, 356	
SP	404, 380, 377, 340, 219, 200	221, 246, 260,363	
PB	401, 380, 379, 340, 230, 200	224, 260, 380,423	

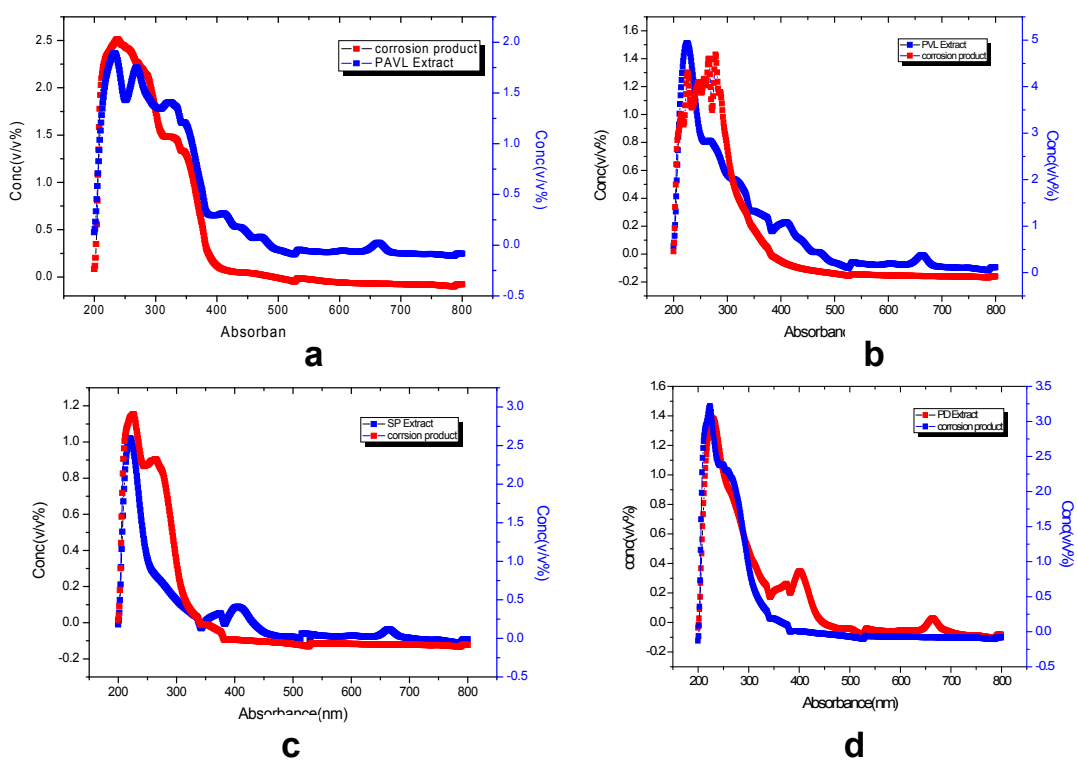

Figure 4.38. UV-Vis spectra for crude inhibitors (a) PAVL (b) PVL (c) SP (d) PB , corrodent solution on AA in 1 M HCl

iii. AA/PAVL/PVL/SP/PB/1M NaOH

The UV-Visible spectra of AA were depicted in Figure 4.39 (a-d) (before and after the addition of 1M NaOH containing studied inhibitors). The Figure 4.39 (a-d) (Table 4.77) shown that there was some deviation occurred between absorbance and their intensities. The absorbance value was increased for AA after exposed in investigated inhibitor solution which was confirmed that the complex compound formed between the aluminium ion and phyto constituents present in the studied inhibitors. The deviation of absorbance with intensity may due to the formation of the complex compound which can reflect the corrosion inhibition behaviour of the phytochemical compounds. There was no appreciable change in the shape of the spectra before and after addition of the inhibitor solution which was confirmed that weak bond (physisorption) formed between the metal and studied inhibitors.

Table 4.77 UV spectral data for the studied inhibitors, corrodent solution on AA in 1 M NaOH

Inhibitors	Absorption bands (nm)		
	Crude inhibitors	AA/Inhibitors/1M NaOH	Transitions
PAVL	333, 328, 275, 232, 200	248,338, 341, 356	$n \rightarrow \pi^*$, $\pi \rightarrow \pi^*$
PVL	407, 382, 237, 203	245, 341, 371	
SP	402, 374, 376, 344, 220, 200	245, 342, 371, 383, 393	
PB	402, 382, 378, 341, 231, 200	244, 343, 362, 380,426	

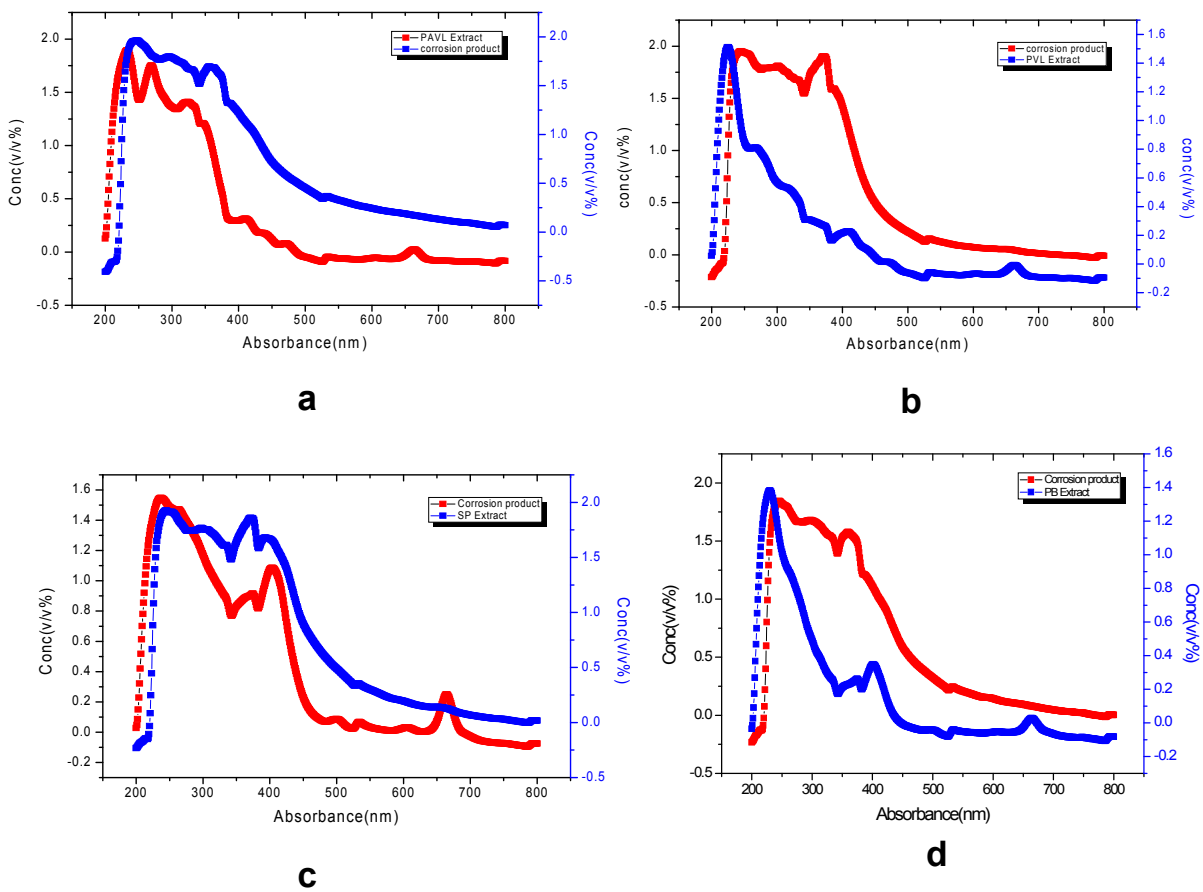

Figure 4.39. UV-Vis spectra for crude inhibitors (a) PAVL (b) PVL (c) SP (d) PB, corrodent soluion on AA in 1 M NaOH

4.4.2 FT-IR Spectral studies

FT-IR spectrometer is used to determine the type of bonding for organic inhibitor absorbed on the metal surface. FT-IR studies helped to deduce the wave number and intensities of adsorption, in terms of the height of the different peaks, the functional groups of the adsorption bands and the arrangement of the inhibitor molecules in the surface of the metal. To find new bonding in the metal surface after immersion in inhibited acid solutions FT-IR spectral is used. In the present study, FT-IR spectra obtained for crude plant/seaweed extract on mild steel in 1M HCl and AA/1 M HCl/1M NaOH at 0.7% concentration of the PAVL/PVL/SP/PB extracts after 3h of immersion are shown in Figures 4.40(a-d), 4.41(a-d), 4.42(a-d).

4.4.2.1 FT-IR spectral details for MS/PAVL/PVL/SP/PB/1M HCl

4.78. FT-IR spectral details for crude inhibitors and corrosion product on MS in 1M HCl

PAVL		PVL		SP		PB		Frequency Assignment
Crude Extract	CP	Crude Extract	CP	Crude Extract	CP	Crude Extract	CP	
3699	3599	3459	3475	3981	3849	3861	3947	O-H stretching
3317	3718	3360	3336	3344	3718	3788	3849	N-H / O-H stretching
1489	1523	1446	1520	1408	1519	1435	1439	C-H bending
1396	1388	1381	1388	1302	1388	1308	1388	C-O-C stretching
1604	1670	1627	1674	1627	1685	1643	1689	C=O stretching
1045	1053	1222	-	1226	1288	1234	1288	C-O stretching
-	-	2322	2307	-	-	2318	2368	C≡ N
2924	2978	-	-	2924	2985	-	-	C-H stretching
-	-	1049	1053	-	-	1060	1022	Aromatics
-	-	717	-	744	-	779	823	OH bending
632	-	-	-	1084	1072	617	-	C=C bending
-	671	-	667	-	667	-	671	γ- Fe_2O_3

CP -corrosion product

i) MS/PAVL/1M HCl

The FT-IR spectrum of PAVL extract (Figure 4.40 (a) and Table 4.78) identified a strong band obtained at 3699 cm^{-1} and 3317 cm^{-1} (N-H/O-H), 2924 cm^{-1} (CH_2), 1604 cm^{-1} (C=O) stretching. These peaks were shifted to higher frequency regions on adsorption over the mild steel surface after exposure of the specimens to the extract. It showed two peaks at 3599 cm^{-1} and 3718 cm^{-1} for mild steel exposed in PAVL extract. The peak obtained at 3699 cm^{-1} and 3317 cm^{-1} was shifted to 3599 cm^{-1} and 3718 cm^{-1}. The $–CH_2$ asymmetric band at 2924 cm^{-1} was shifted to 2978 cm^{-1}. The absorption band at 1604cm^{-1} (C=O stretching) shifted to 1670 cm^{-1}. The shift in the adsorption frequencies of MS surface indicated the adsorption of the phytochemical constituents present in the extract on the surface **(Bothi Raja, *et al,* 2011)**.

ii) MS/PVL/1 M HCl

The FT-IR spectrum of PVL extract reflected a strong band at 3459 cm^{-1} and 3360 cm^{-1} (N-H/OH), 2322 ($–CH_2$), and a intense band at 1627 cm^{-1} related to C=O stretching. The peak obtained at 3459 cm^{-1} and 3360 cm^{-1} was shifted to 3475 cm^{-1} and 3336 cm^{-1}. A band at 2322 cm^{-1} ascribed to C ≡ N stretching obtained in the PVL spectra shifted to 2307 cm^{-1} in the PVL extract on MS surface. The band at 1627 cm^{-1} (C=O stretching) shifted to 1674 cm^{-1}. The absorption band at 1049 cm^{-1} (Aromatics) shifted to 1053 cm^{-1}. The interaction between the inhibitor and the metal surface was indicated by the shift in the frequencies of vibration **(Karthik *et al,* 2015)** (Table 4.78 and Figure 4.40 (b)).

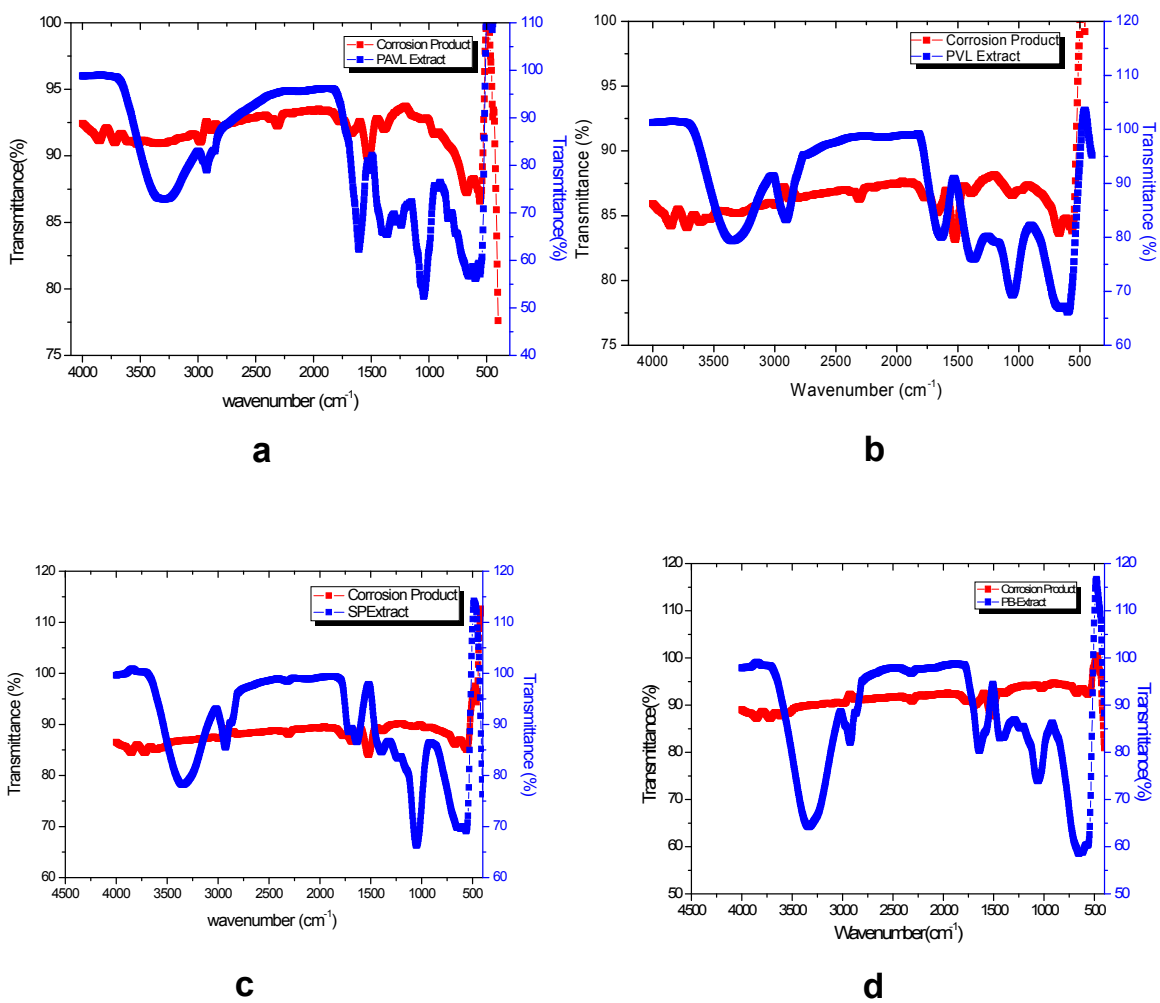

Figure 4.40. FT-IR Spectrum of the investigated inhibitors and their corrosion product on MS in 1M HCl for (a) PAVL (b) PVL (c) SP (d) PB

iii) MS/SP/1 M HCl

FT-IR of Figure 4.40 (c) and (Table 4.78) highlighted the FT IR spectrum of MS/SP/1M HCl inhibited metal surface indicated two peaks at 3848 cm^{-1} and 3718 cm^{-1}. The band at 3981 cm^{-1} observed for O-H stretching of SP spectra shifted to 3849 cm^{-1} in the corrosion product. The band obtained at 3344 cm^{-1} was shifted to 3718 cm^{-1}. The absorption band at 1627 cm^{-1} (C=O stretching) diminished and shifted to 1685 cm^{-1}. These spectral analyses strongly supported the coordination between the metal-inhibitor. The peak at 667 cm^{-1} obviously originates mainly from γ -Fe_2O_3. The spectral results revealed that functional groups were supported for adsorbing the inhibitor to the metal surface **(Helen *et al*, 2014).**

iv) MS/PB/1M HCl

From the FT-IR spectra of MS/PB/1M HCl the following points may be noticed. The observed band at 3861 cm^{-1} and 3788 cm^{-1} shifted to 3947 cm^{-1} and 3849 cm^{-1}. The $–CH_2$ asymmetric band at 2318 cm^{-1} was shifted to 2368 cm^{-1}. The absorption band at 1643 cm^{-1} (C=O stretching) shifted to 1689 cm^{-1}. It was confirmed that there was an interaction between Fe-PB extract **(Al-Moghrabi *et al,* 2018, Flores-De los Rios *et al,* 2015)**. (Figure 4.40 (d) and Table 4.78).

4.4.2.2 FT-IR spectral details for AA/PAVL/PVL/SP/PB/1M HCl

4.79. FT-IR spectral details of crude inhibitors and corrosion product on AA in 1M HCl

PAVL		PVL		SP		PB		Frequency Assignment
Crude Extract	CP	Crude Extract	CP	Crude Extract	CP	Crude Extract	CP	
3977	3911	3459	3911	3988	3923	3861	3934	O-H stretching
3317	3263	3360	3537	3344	3406	3788	3838	N-H / O-H stretching
2924	2985	-	-	2924	2978	-	-	C-H stretching
-	-	2322	2345	-	-	2318	2310	C≡ N
1604	-	1627	1658	1627	1724	1643	1689	C=O stretching
1489	1585	1446	-	1408	1446	1435	1512	C-H bending
1396	-	1381	1396	1392	1381	1308	1381	C-O-C stretching
1045	1049	1049	1072	1226	1249	1234	1249	C-O stretching
-	-	-	-	-	-	1060	1075	Aromatics
767	806	717	823	784	-	779	817	OH bending
632	-	-	-	644	682	655	644	C=C bending

CR-corrosion product

i) AA/PAVL/1M HCl

The infrared spectrum of the corrosion product showed two peaks at 3911 cm^{-1} and 3263 cm^{-1}. The peaks at 3977 cm^{-1} and 3317 cm^{-1} shifted to 3911 cm^{-1} and 3263 cm^{-1}. The $-CH_2$ asymmetric band at 2924 cm^{-1} shifted to 2985 cm^{-1}. A signal corresponding to C-O stretching at 1045 cm^{-1} shifted to 1049 cm^{-1}. The peak obtained for C-H bend at 1489 cm^{-1} shifted to 1585 cm^{-1}. Some authors have stated and agreed with the fact that corrosion inhibition took place and occurred as a result of the interaction between the metal and the inhibitor (Figure 4.41 (a) and Table 4.79).

ii) AA/PVL/1 M HCl

The infrared spectrum of the MS after immersion in 1M HCl containing PVL extract is shown in Figure 4.41(b) (Table 4.79). Two bands observed at 3459 cm^{-1} and 3360 cm^{-1} shifted to 3911 cm^{-1} and 3537 cm^{-1} and these signals were assigned for O-H and N-H functional groups. The $-CH_2$ asymmetric stretching frequency at 2322 cm^{-1} was shifted to 2345 cm^{-1}. The band related to C-O stretching at 1049 cm^{-1} shifted to 1072 cm^{-1}. It proved the formation of Al^{3+}-PVLcomplex in the anodic sites of the metal surface.

iii) AA/SP/1M HCl

The FT IR spectrum of the corrosion reflected that peaks at 3923 cm^{-1} and 3406 cm^{-1} (Figure 4.41 (c) and Table 4.79). The band observed at 3988 cm^{-1} and 3344 cm^{-1} was shifted from 3923 cm^{-1} and 3406 cm^{-1}. A band at 2924 cm^{-1} ascribed to C-H stretching frequency detected for the SP spectra has shifted to 2978 cm^{-1} in the corrosion product. The band at 1627 cm^{-1} (C=O stretching) diminished and shifted to 1724 cm^{-1}. FTIR spectra proved that complex formed between the active principle of the SP extract and Al^{3+} ion. It was confirmed the protective film formed in the metal surface.

iv) AA /PB/1 M HCl

Fourier Transform Infra-Red tests were carried out to gain some information about the possibility of interactions between the absorbed PB molecules and AA surface (Figure 4.41 (d) and Table 4.79. The FTIR spectrum of the corrosion product reflected two bands at 3934 cm^{-1} and 3838 cm^{-1}. The peaks observed at 3861 cm^{-1} and 3788 cm^{-1} have shifted to 3934 cm^{-1} and 3838 cm^{-1}. The band at 2318 cm^{-1} was attributed to C≡ N in PB extract was shifted to 2310 cm^{-1} in the corrosion product. The band at 1643 cm^{-1} (C=O stretching) diminished and shifted to 1689 cm^{-1}. These variations and shifts in the

wavelength of adsorption reflected the coordination took place between PB extract and AA metal surface. Few missing bonds for the corrosion product may involve in bond formation.

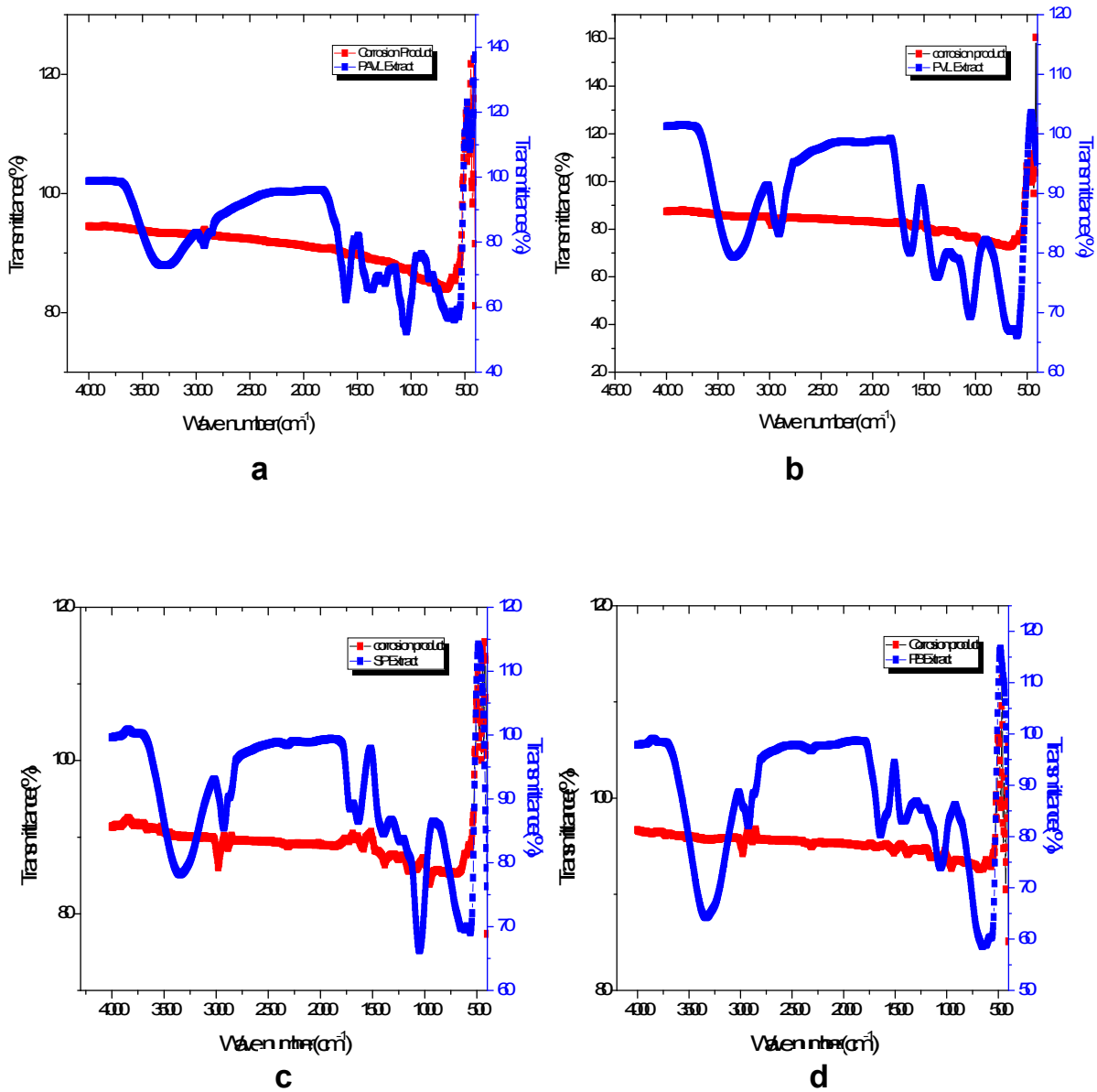

Figure 4.41. FT-IR Spectrum of the investigated inhibitors and their corrosion products on AA in 1M HCl for (a) PAVL (b) PVL (c) SP (d) PB

4.4.2.3 FT-IR spectral details for AA/PAVL/PVL/SP/PB/1M NaOH

4.80. FT-IR spectral details for the crude inhibitors and corrosion products on AA in 1M NaOH

PAVL		PVL		SP		PB		Frequency Assignment
Crude Extract	CP	Crude Extract	CP	Crude Extract	CP	Crude Extract	CP	
3977	3954	3459	3861	3988	3861	3861	3915	O-H stretching
3317	3332	3360	3310	3344	3363	3788	3726	N-H / O-H stretching
2924	2956	-	-	2924	2936	-	-	C-H stretching
-	-	2322	2314	-	-	2318	2376	C≡ N
1604	1643	1627	1639	1627	1639	1643	1681	C=O stretching
1489	1492	1446	1427	1408	1427	1435	1477	C-H bending
1396	1377	1381	1373	1392	1323	1308	1388	C-O-C stretching
1045	1033	1049	1014	1226	1288	1234	1288	C-O stretching
-	-	-	-	-	-	1060	1014	Aromatics
767	752	717	763	784	-	779	794	OH bending
632	675	-	-	644	648	655	691	C=C bending

CP-corrosion product

i) AA/PAVL/1M NaOH

The FT IR spectrum of the inhibited metal sample indicated two major peaks at 3954 cm^{-1} and 3332 cm^{-1}. The signal obtained at 3977 cm^{-1} and 3317 cm^{-1} shifted to 3954 cm^{-1} and 3332 cm^{-1} in the corrosion product. The $–CH_2$ asymmetric frequency at 2924 cm^{-1} shifted to 2956 cm^{-1}. A peak assigned for C-O stretching frequency shifted from 1045 cm^{-1} to 1033 cm^{-1}. One peak for C-H bending frequency at 1489 cm^{-1} shifted to 1492 cm^{-1}. Hence, the FTIR spectra studies revealed that there was an interaction of the inhibitor on the AA surface for the adsorption in corrosion protection (Table 4.80 and Figure 4.42 (a))

ii) AA/PVL/1M NaOH

The FTIR spectra of the corrosion product are displayed in Figure 4.42 (b) (Table 4.80). The two signals were obtained at 3459 cm^{-1} and 3360 cm^{-1} and they were shifted to 3861 cm^{-1} and 3310 cm^{-1}. The $–CH_2$ asymmetric band at 2322 cm^{-1} was shifted to 2314 cm^{-1}. A peak showed for C-O stretching at 1049 cm^{-1} shifted to 1014 cm^{-1}. The peaks corresponding to O-H bend at 717 cm^{-1} shifted to 763 cm^{-1}. The presence and shift in the stretching frequency of the functional groups confirmed the formation of an active compound $–Al^{3+}$ complex on the metal surface. This proved the interaction took place between the inhibitor and the metal surface.

iii) AA/SP/1M NaOH

The FT IR spectrum of SP/AA/1M NaOH reflected two peaks at 3861 cm^{-1} and 3363 cm^{-1}. A band observed at 3988 cm^{-1} and 3344 cm^{-1} was shifted to 3861 cm^{-1} and 3363 cm^{-1}. A band at 2924 cm^{-1} ascribed to C-H stretching shifted to 2936 cm^{-1} in the corrosion product (Table 4.80 and Figure 4.42 (c)). The absorption band at 1627 cm^{-1} (C=O stretching) diminished and shifted to 1639 cm^{-1}. These results indicated that there has been interaction and bonding between metal and extracts on the metal surface.

iV) AA/PB/1M NaOH

The Figure 4.42 (d) and (Table 4.80) showed the FTIR spectrum of the protective material that adhered on the surface of the metal coupon owing to the addition of the PB in 1M NaOH solution. Corrosion product reflected two FTIR spectra one at 3915 cm^{-1} frequency and another at 3726 cm^{-1} frequency. The observed absorption peak at 3861cm^{-1} and 3788 cm^{-1} were shifted to 3915 cm^{-1} and 3726 cm^{-1}. A band at 2318 cm^{-1} assigned to C≡ N obtained for PB spectra shifted to 2376 cm^{-1} related to corrosion product. The band at 1643 cm^{-1} (C=O stretching) disappeared and shifted to 1681 cm^{-1}. This spectral evidence confirmed that there was an interaction between PB extract and AA surface.

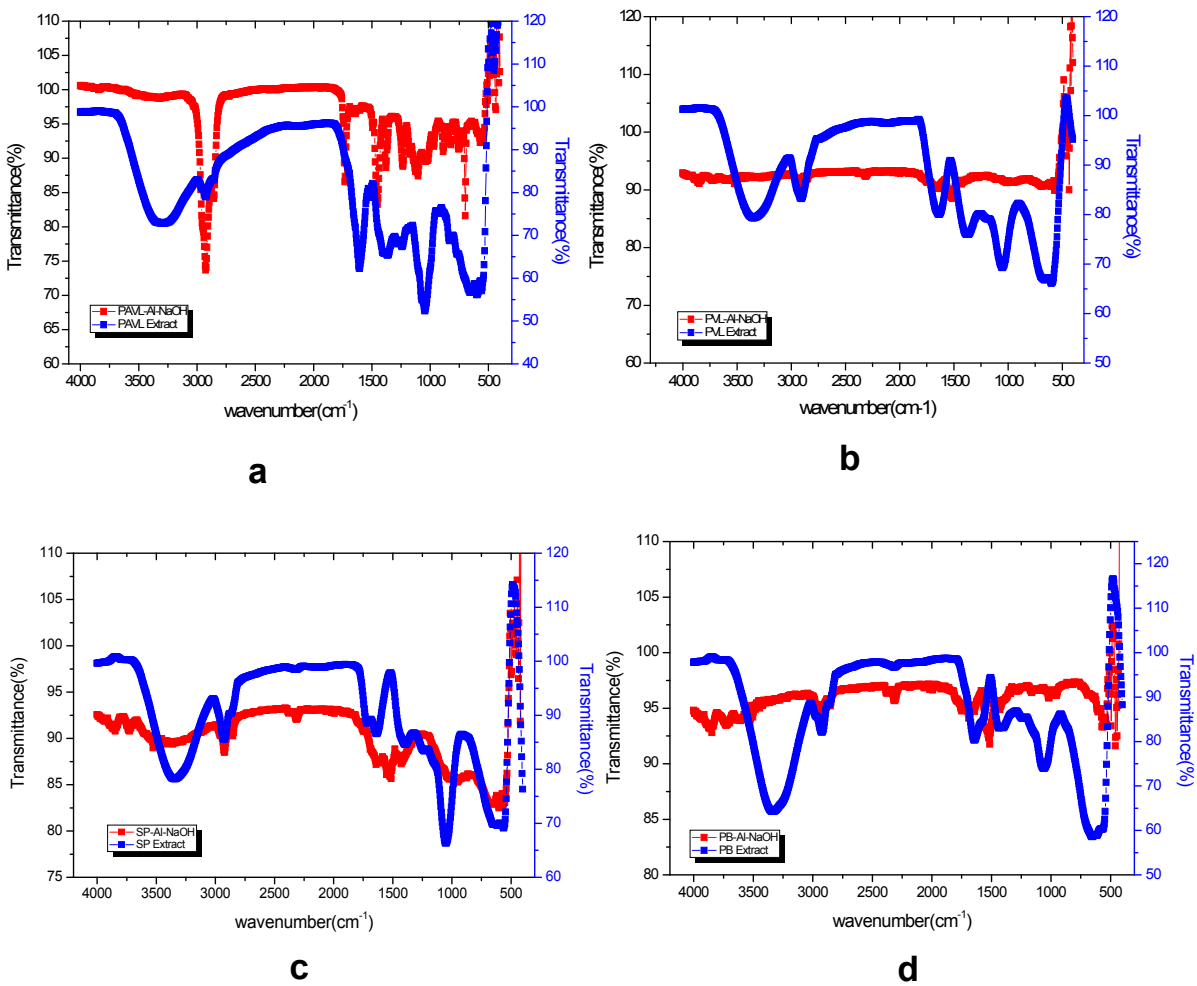

Figure. 4.42. FT-IR spectrum of the investigated inhibitors and their corrosion products on AA in 1M NaOH for (a) PAVL (b) PVL (c) SP (d) PB

4.4.3 Scanning Electron Microscopic studies (SEM)

The surface topography studies of MS/1M HCl and AA/1M HCl/1M NaOH in the surface have been investigated by scanning electron microscope. In the present investigation, SEM micrograph images were taken before and after the addition of investigated inhibitors in 1M HCl/1M NaOH solution

4.4.3.1 Scanning electron micrograph of MS/1M HCl, AA/1M HCl and AA/1M NaOH in the presence and absence of PAVL/PVL/SP/PB Extract

The surface topography of plain samples of MS/AA shown in Figures 4.43 (a), 4.44 (a), 4.45 (a) was studied by scanning electron microscope technique. The surface topography of treated MS/AA in 1M HCl/1M NaOH was examined by an electron microscope is shown in Figures 4.43 (b), 4.44 (b), 4.45 (b). The SEM images of Figures 4.43(c-f) were the MS/1M HCl system, Figures 4.44(c-f) were the AA/1M HCl system and SEM Figures of 4.45(c-f) were the AA/1M NaOH system The scanning electron micrograph of plain samples of MS/AA show analogous grooves with moderately light areas, which were recognized as a clean surface. The SEM images in the absence of the inhibitor solution show micro cracks and porous, shown non-protective nature of them (Figures 4.43 (b), 4.44 (b), 4.45 (b)). In every Figures 4.43(c-f), Figures 4.44(c-f), Figures 4.45(c-f), we can clearly see that the finer surface images protect the metal surface which were treated with an investigated inhibitors as compared to without inhibitor solution **(Verma *et al,* 2016)**.

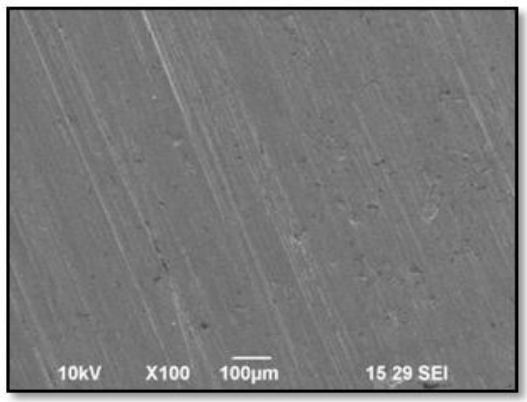

a. Plain Mild Steel

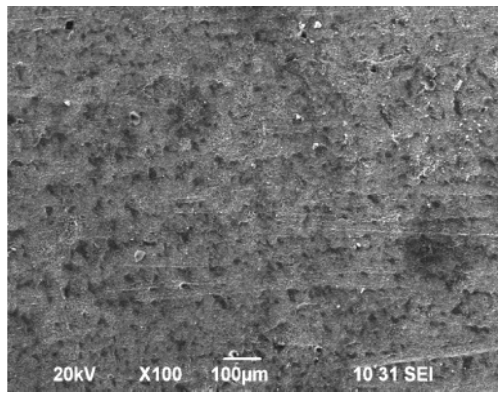

b. MS in 1M HCl

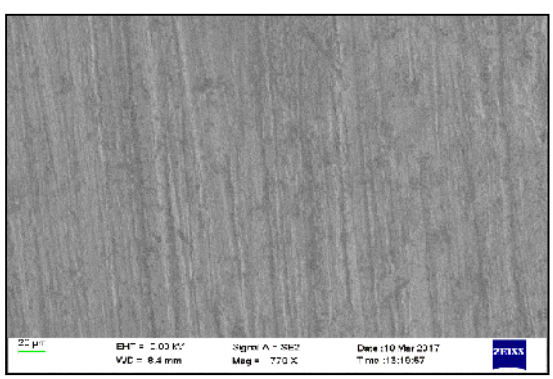

c. PAVL/MS/1M HCl

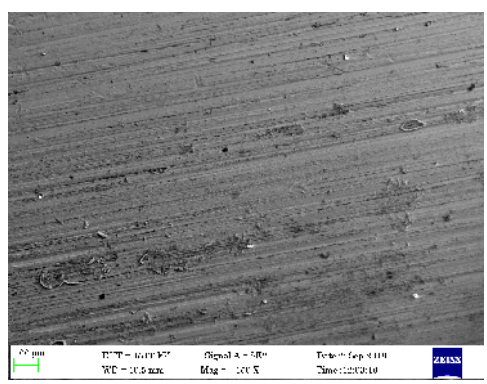

d. PVL/MS/1M HCl

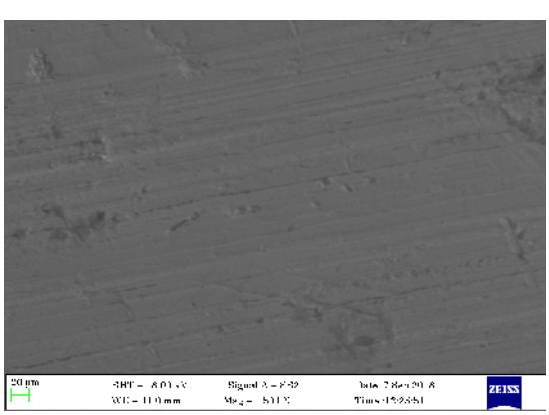

e. SP/MS/1M HCl

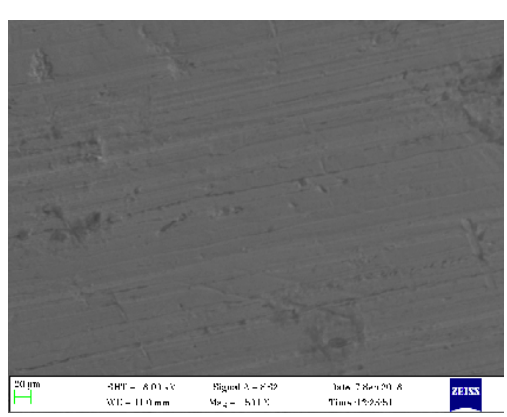

f. PB/MS/1M HCl

Figure 4.43. SEM pictures for MS corrosion without/with addition of (c) PAVL (d) PVL (e) SP (f) PB extracts in 1 M HCl, (a) Plain MS, (b) MS in 1M HCl

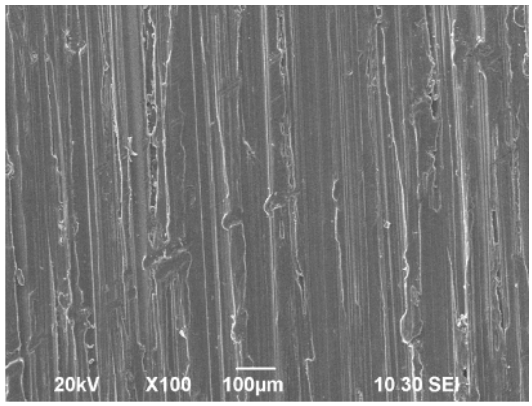

a. Plain Aluminium

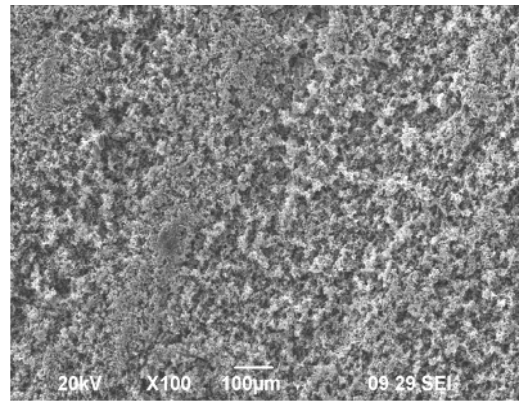

b. Aluminium in 1M HCl

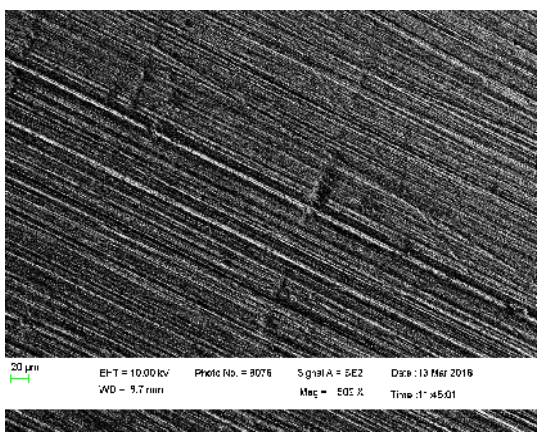

c. PAVL/AA/1M HCl

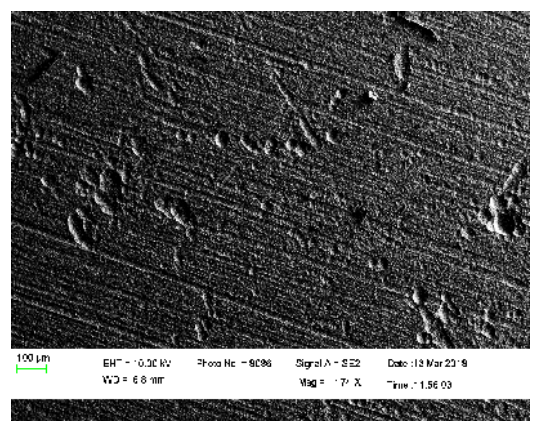

d. PVL/AA/1M HCl

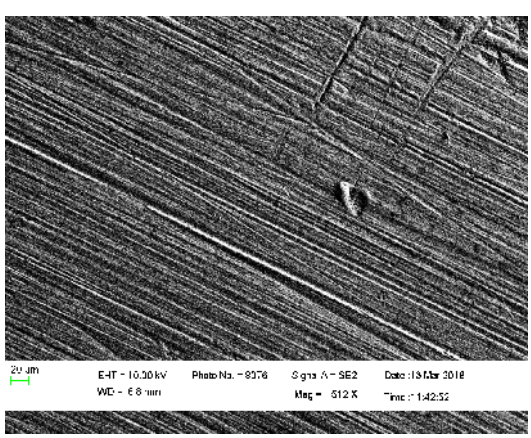

e.SP/AA/1M HCl

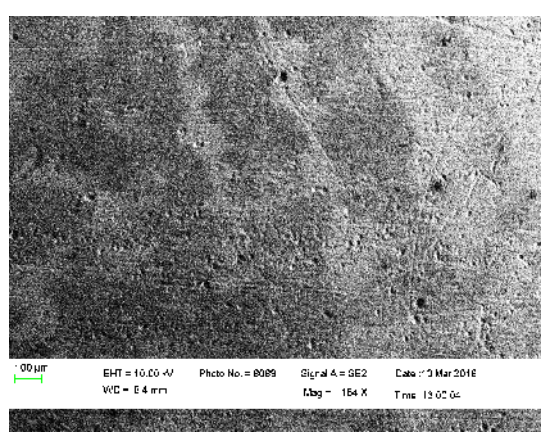

f. PB/AA/1M HCl

Figure 4.44. SEM pictures for AA corrosion without/with addition of (c) PAVL (d) PVL (e) SP (f) PB extract in 1 M HCl (a) Plain AA, (b) AA in 1M HCl

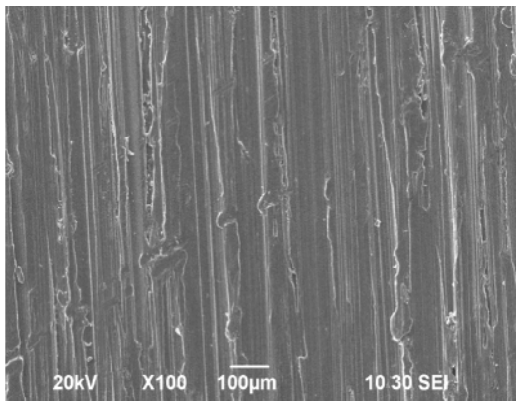

a. Plain Aluminium

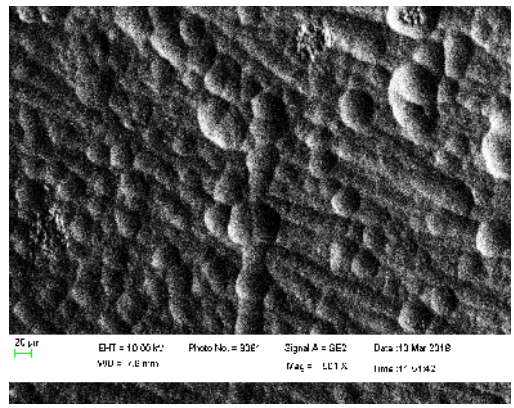

b. Aluminium in 1M NaOH

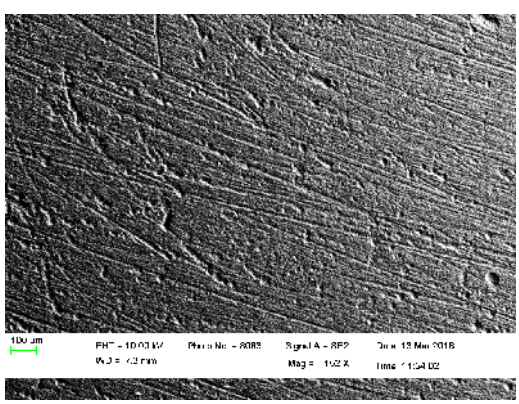

c.PAVL/AA/1M NaOH

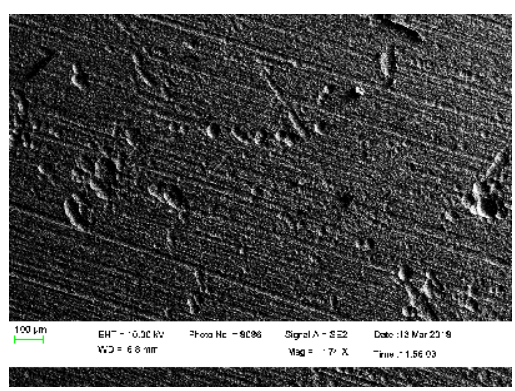

d. PVL/AA/1M NaOH

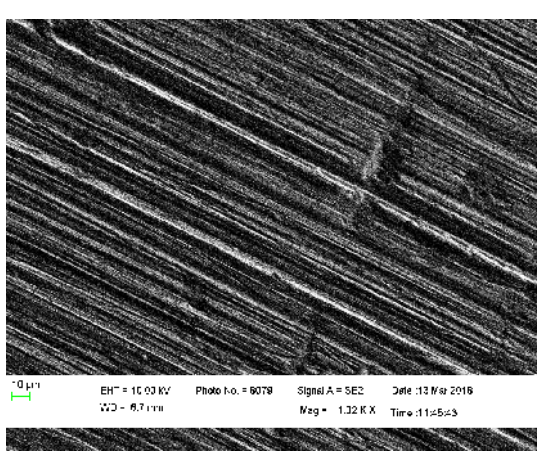

e. SP/AA/1M NaOH

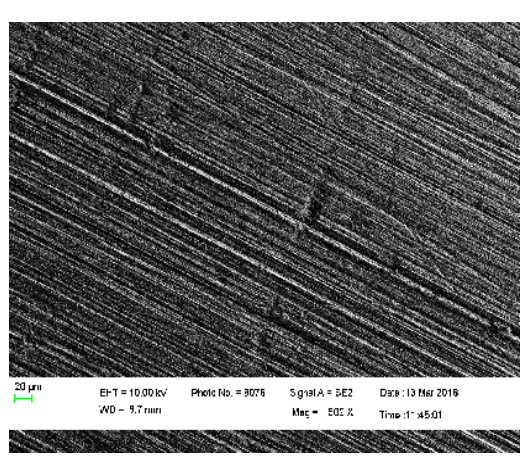

f. PB/AA/1M NaOH

Figure 4.45. SEM pictures for AA corrosion without/with addition of (c) PAVL (d) PVL (e) SP (f) PB extract in 1 M NaOH, (a) Plain AA, (b) AA in 1M NaOH

4.4.4 Energy dispersive X-ray analysis (EDX)

EDX technique was performed to acquire information about elements present before and after the addition of investigated inhibitors through which identified the nature of the protective film formed on the metal surface.

4.4.4.1 EDX spectra for MS/ PAVL/PVL/SP/PB/1M HCl

The EDX spectrum of the metal specimen and their percentage of atomic content in MS samples in 1 M HCl solution with and without the addition of 0.7% optimum concentration of PAVL/PVL/SP/PB extracts are depicted in Figures 4.46, 4.47, 4.48. The analysis EDX spectra of MS samples showed Fe, Mn, Si & P peaks of elements as minimum compounds. Due to the mechanical abrasion prior to experiment Si peak was obtained for MS surface.

EDX analysis of MS in 1 M HCl reported 81% Fe &19% Oxygen (in weight %). The small peak of oxygen was identified due to the formation of iron oxide layer of MS in 1M hydrochloric acid. The lesser Fe content in the blank while compared to the iron content in the plain sample (98.24%), the nonexistence of manganese and the existence of higher oxygen percentage identified that the mild steel sample was totally sheltered with a protective film of corrosion product. Fe peaks are significantly increased after MS exposed in 1 M HCl containing 0.7% concentration of PAVL/PVL/SP/PB extracts and the samples exposed in 1 M hydrochloric acid solution (blank) and also the oxygen peak was also suppressed. The increased in Fe content corroborated the formation of iron – inhibitor complex on the MS surface **(Nazeer *et al*, 2014)** (Figure 4.46 (c-f)).

4.4.4.2 EDX spectra of AA/PAVL/PVL/SP/PB/1M HCl and 1M NaOH

The analysis of EDX spectra of AA/1 M HCl and AA/1M NaOH without and with addition of 0.7% of PAVL/PVL/SP/PB extracts are shown in Figures 4.47(c-f) and 4.48(c-f). When AA was exposed in uninhibited solution (blank) some peaks were observed for aluminium and oxygen identified for the formation of oxides of aluminium in the surface. For inhibited solution, the spectra reflected that the AA peaks were appreciably increased when compared to the samples exposed in 1 M HCl and 1M NaOH solution (blank) **(Al-Haj-Ali *et al*, 2014)**.

a.Plain MS

Element	Wt %	At %
Si	0.34	0.68
P	0.11	0.19
Mn	1.34	2.40
Fe	98.24	97.63

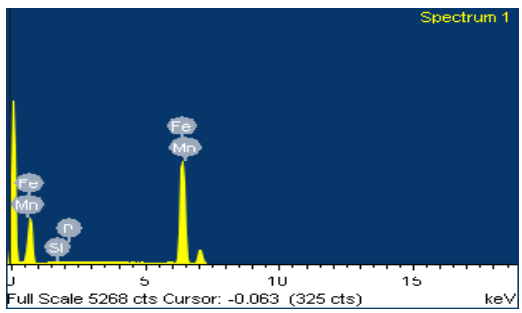

b.Blank HCl

Element	Wt %	At %
O	19.00	45.59
Fe	81.00	54.41

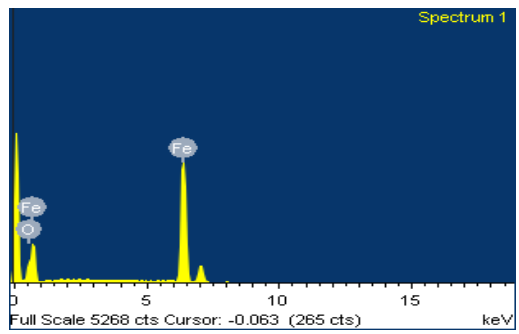

c. Mild Steel /PAVL extract / 1 M HCl

Element	Wt %	At %
C	7.39	26.69
Na	0.62	1.17
Al	0.29	0.47
Si	0.62	0.96
Fe	91.08	70.72

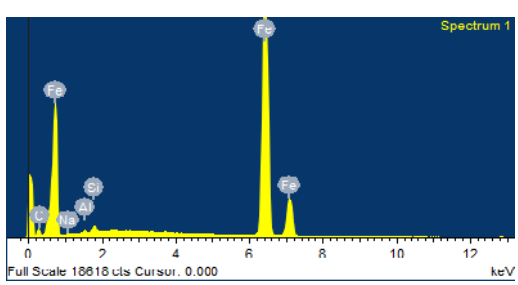

d. Mild Steel /PVL extract / 1 M HCl

Element	Wt %	At %
C	1.04	19.88
O	2.33	15.07
Al	0.23	0.27
Si	0.50	0.57
Fe	95.91	64.20

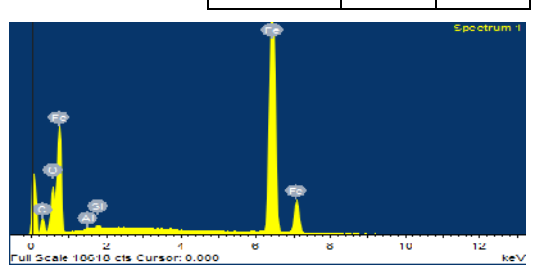

e. Mild Steel /SP extract / 1 M HCl

Element	Wt %	At %
C	7.75	24.77
O	6.76	16.22
Si	0.36	0.49
Fe	85.13	58.52

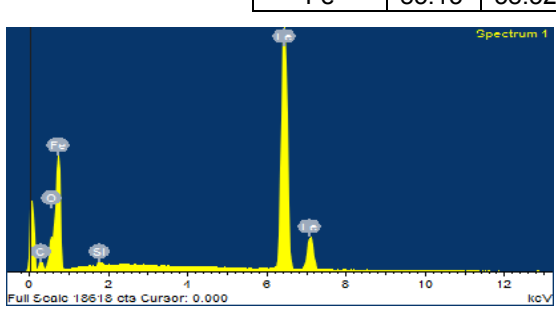

f. Mild Steel /PB extract / 1 M HCl

Element	Wt %	At %
C	4.80	27.56
O	1.53	11.98
Si	0.44	0.48
Fe	93.23	59.98

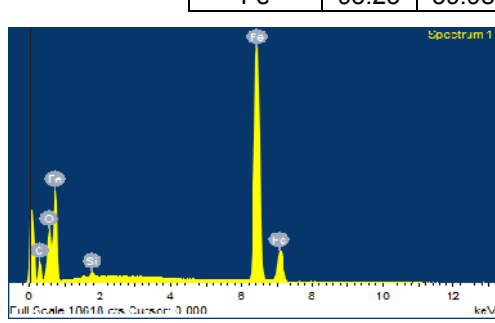

Figure 4.46 EDX images of Mild steel corrosion in the absence and presence of (c) PAVL (d) PVL (e) SP (f) PB extract in 1M HCl, (a) Plain MS, (b) MS in 1M HCl

a. Plain AA

Element	Wt %	At %
C	3.66	6.47
Ag	0.42	0.09
Al	97.25	93.28

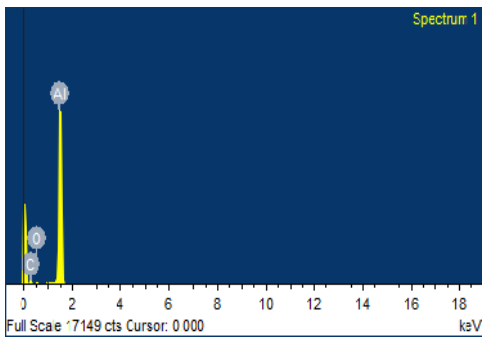

b.Blank HCl

Element	Wt %	At %
C	9.61	14.99
O	9.27	10.74
Ag	80.47	74.03
Cu	0.65	0.24

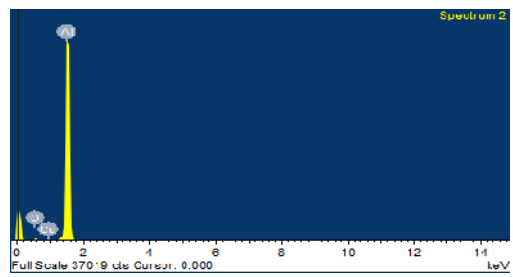

c. AA /PAVL extract / 1 M HCl

Element	Wt %	At %
C	10.24	20.01
Ag	1.00	0.22
O	4.69	6.88
Al	83.55	72.67
Fe	0.52	0.22

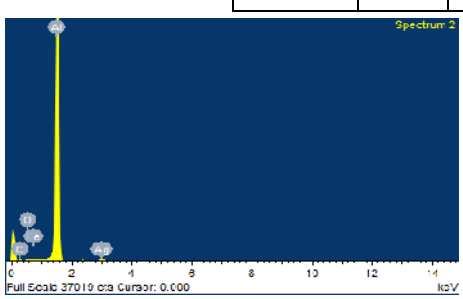

d. AA/PVL extract / HCl

Element	Wt %	At %
C	10.64	20.49
O	6.12	8.85
Ag	1.04	0.22
Al	81.66	66.99
Si	0.54	0.45

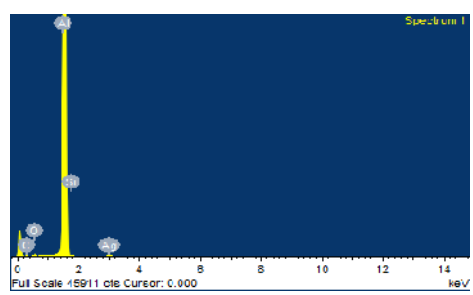

e. AA /SP extract / HCl

Element	Wt %	At %
C	11.02	20.87
O	7.54	10.71
Fe	0.49	0.20
Al	80.95	68.22

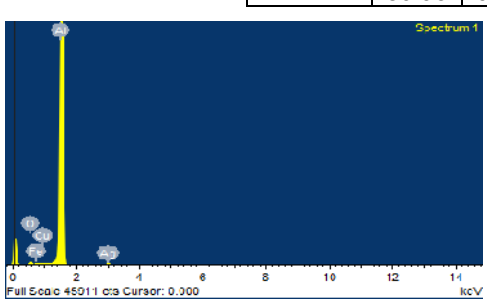

f. AA/PB extract / 1 M HCl

Element	Wt %	At %
C	13.58	30.11
O	4.47	6.09
Al	82.95	63.80

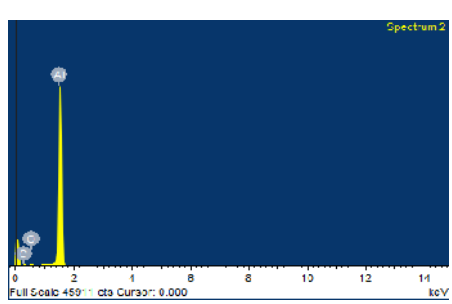

Figure 4.47 EDX images of AA corrosion in the absence and presence of (c) PAVL (d) PVL (e) SP (f) PB extract in 1M HCl, (a) Plain MS, (b) MS in 1M HCl

a. Plain AA

Element	Wt %	At %
C	3.66	6.47
Ag	0.42	0.09
Al	97.25	93.28

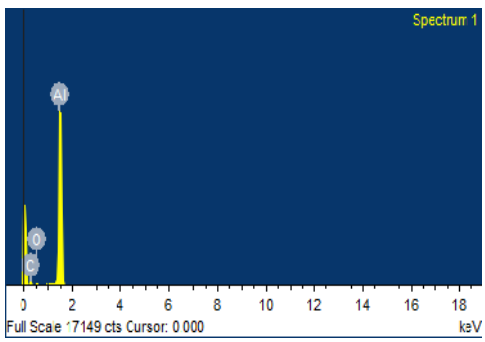

b.Blank NaOH

Element	Wt %	At %
C	0.47	0.81
Fe	0.17	0.06
Ag	1.79	0.34
O	16.69	18.01
Al	80.89	80.78

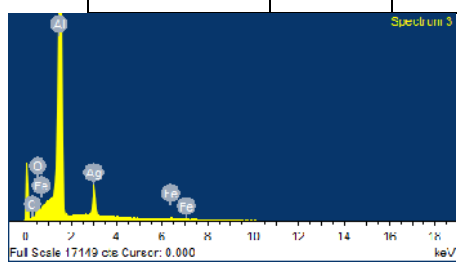

c. AA /PAVL extract / 1 M NaOH

Element	Wt %	At %
C	1.31	1.46
Si	0.19	0.13
O	10.50	10.61
Al	83.99	80.79

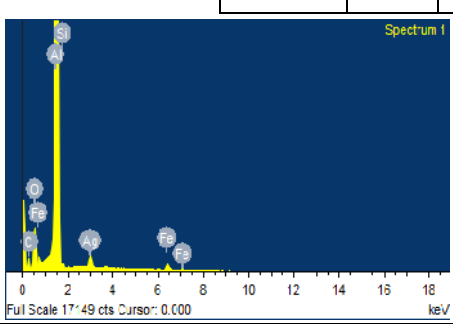

d. AA/PVL extract / NaOH

Element	Wt %	At %
O	5.96	6.40
Si	0.66	0.48
Ag	0.47	0.09
Al	90.91	88.23

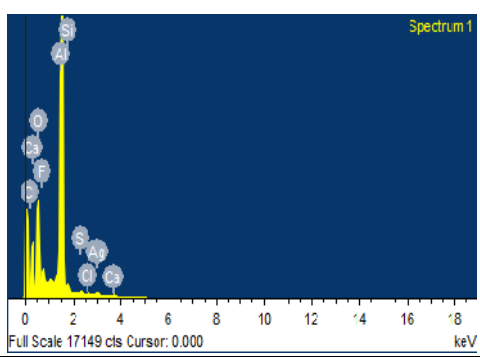

e. AA /SP extract / NaOH

Element	Wt %	At %
Si	0.33	0.21
Ag	0.90	0.15
O	6.33	7.03
Al	92.04	89.77

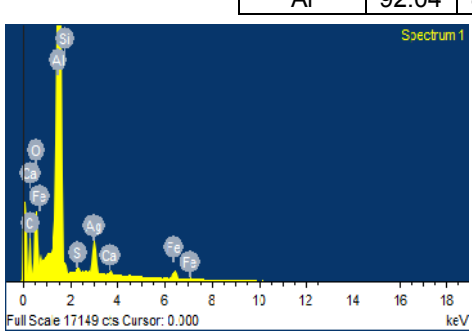

f. AA/PB extract / 1 M NaOH

Element	Wt %	At %
Si	0.34	0.25
Ag	1.35	0.26
O	4.32	5.56
Al	87.62	86.30

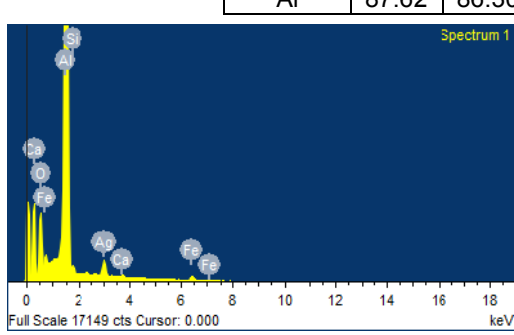

Figure 4.48 EDX images of AA corrosion in the absence and presence of (c) PAVL (d) PVL (e) SP (f) PB extract in 1M NaOH, (a) Plain MS, (b) MS in 1M HCl

4. 4.5 X-ray diffraction Analysis (XRD)

Quantitative phase analysis was carried out by XRD technique. It is used to measure the intensity of the diffraction units in the pattern for corrosion product.

4.4.5.1 . XRD spectrum of MS / PAVL / PVL / SP / PB/1M HCl

The figure reflected the XRD spectrum of MS with and without the addition of the investigated inhibitor. XRD peaks at 45.5, 45.6 for MS exposed in 1M HCl indicated that the metal contained iron. Oxides of iron corresponded to peak at 65.7 because the metal was immersed in 1M HCl contained Fe_3O_4 and FeOOH. The obtained important corrosion product peak at 45.5 identified from the peak at 2θ of 45.5. This line indicated the fingerprint of Fe with maximum relative intensity. XRD spectrum was combined with a grazing angle of the MS exposed with the studied inhibitors are presented in Figure 4.49 (a). It was indicated that the amorphous nature of the metal surface film was due to the adsorption of Fe^- complex in the MS surface. The smooth and very small peaks of iron oxide of XRD pattern indicated that the metal surface was immersed in the inhibited solution.

4.4.5.2. XRD spectrum of AA / PAVL/PVL/SP/PB/1M HCl and 1M NaOH

The Figures 4.49 (b-c) showed the XRD pattern of AA without and with addition of the studied extracts. XRD pattern of AA exposed to 1M hydrochloric acid and 1M NaOH indicated that a number of peaks related with Al and Al_2O_3. The XRD spectrum suggested 2θ values of 36.01° and 39.22° related to the oxides of aluminium **(Qiang *et al,* 2014)**. In the current study, the XRD spectrum of AA with and without the addition of the studied inhibitors observed that the 2θ values of two diffraction peaks were observed at 38.2. **Khan *et al*, 2013** reported. XRD spectrum of alumina confirmed that the 2θ values of two diffraction peaks were observed at 38.82° and 45.2° corresponding to Al_2O_3 H_2O and $Al(OH)_3$ phases The XRD spectrum observed for the studied inhibitors were confirmed by the literature study. Even and small peaks of aluminium oxide pattern of XRD spectrum obtained for inhibited solutions compared with the spectral values for AA exposed in 1M acidic and 1M alkaline solution.

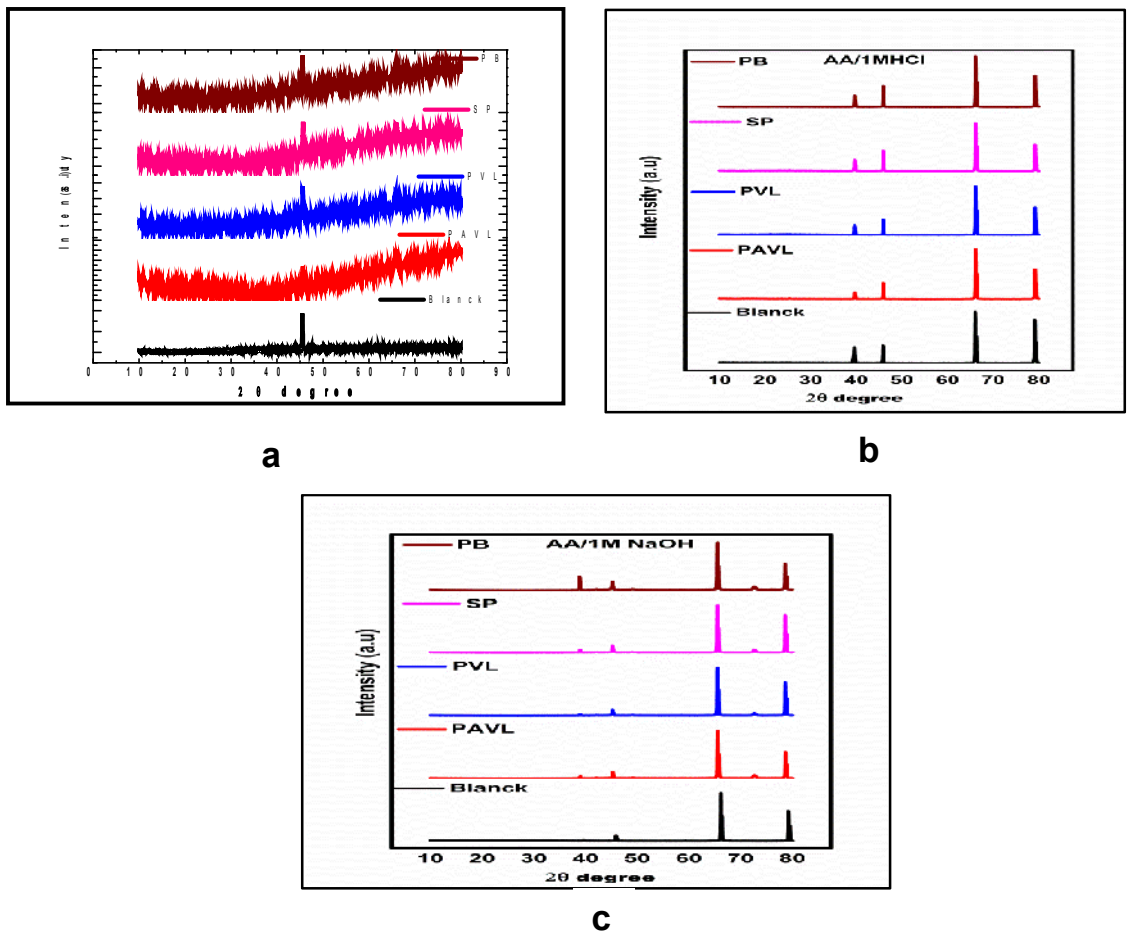

Figure 4.49. XRD spectrum of (a) MS/Inhibitors/1M HCl (b) AA/Inhibitors/1M HCl (c) AA/Inhibitors/1M NaOH

4.4.6 3D Optical profilometer

3D Optical profilometer study was used to find out the topography of various samples and test the influence of corrosion inhibitors on MS/AA surface in the nano-micro scale. The performance of the inhibitor can be recognized by the roughness profile values under the study. The roughness and uniformity of the surface may be analysed from this study.

4.4.6.1 Optical Profilometry analysis of MS/Inhibitors/1M HCl, AA/Inhibitors/1M HCl, AA/Inhibitors/1M NaOH

The R_a values play an important role and it is used to find the nature of the formed protective layer in the metal surface. Figures 4.50 (a), 4.51 (a), 4.52 (a) show

the 3D images of polished MS/AA. Figures 4.50 (b), 4.51 (b), 4.52 (b) show that the 3D images MS/1M HCl and AA/1M HCl and AA/1M NaOH without inhibitor solution. Figures 4.50 (c-f), 4.51 (c-f), 4.52 (c-f) show that the 3D images MS/1M HCl and AA/1M HCl and AA/1M NaOH with inhibitor solutions.

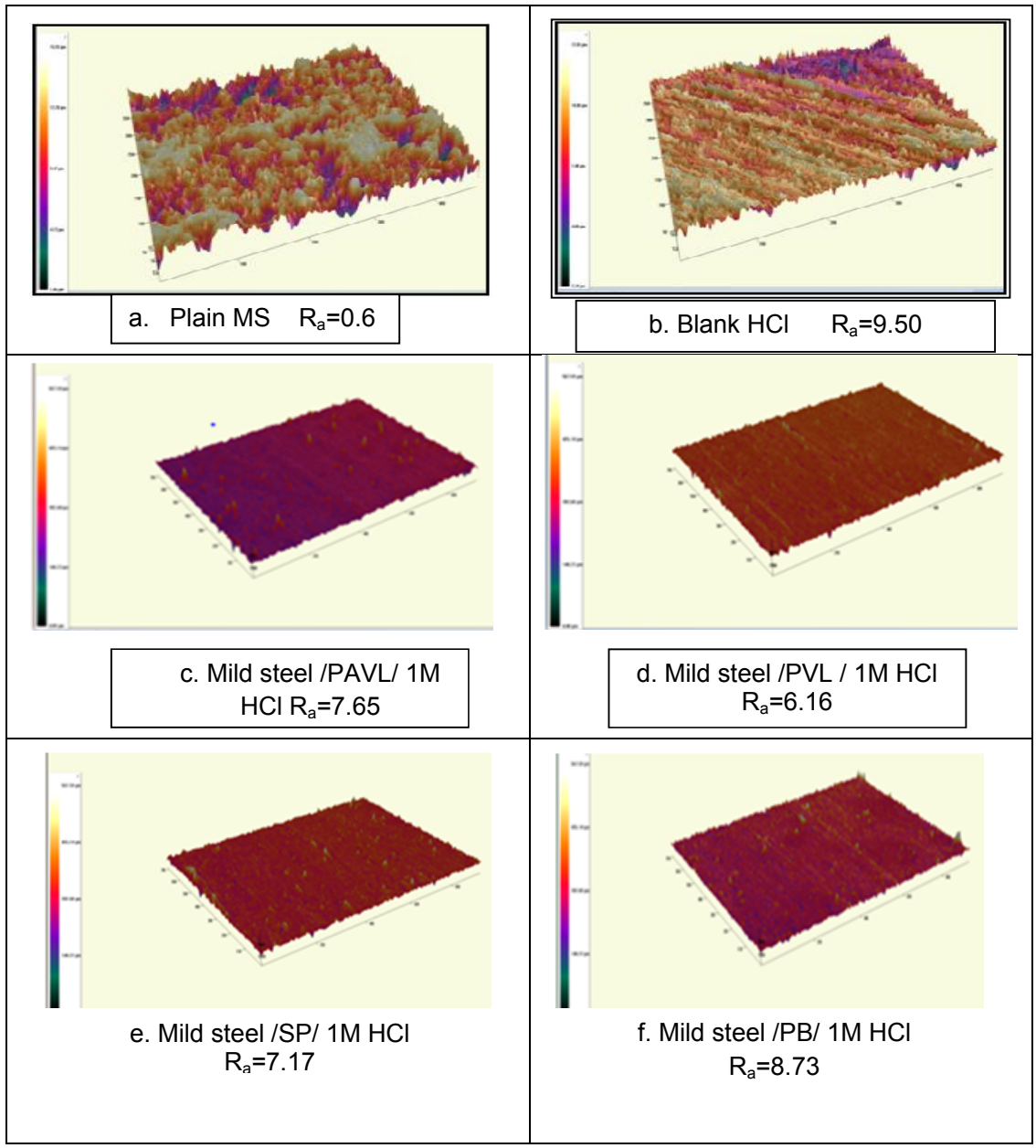

Figure 4.50. 3D Optical Profilometry pictures for MS corrosion in the absence and presence of (c) PAVL (d) PVL (e) SP (d) PB extract in 1M HCl , (a) Plain MS, (b) MS in 1M HCl

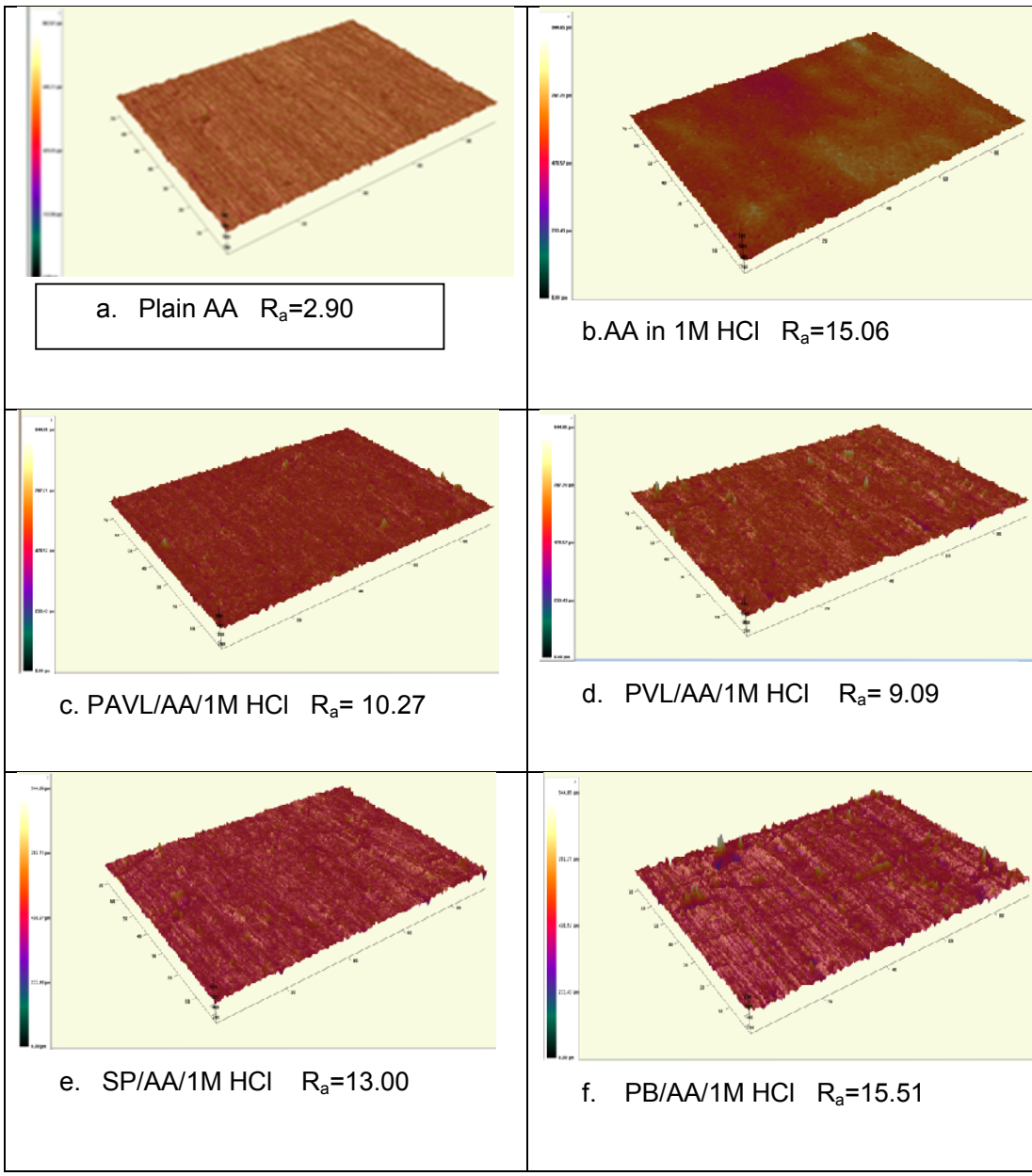

Figure 4.51. 3D Optical Profilometry pictures for AA corrosion in the absence and presence of (c) PAVL (d) PVL (e) SP (d) PB extract in 1M HCl, (a) Plain AA, (b) AA in 1M HCl

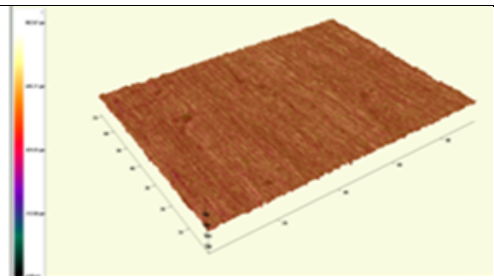

a. Plain AA R_a=2.90

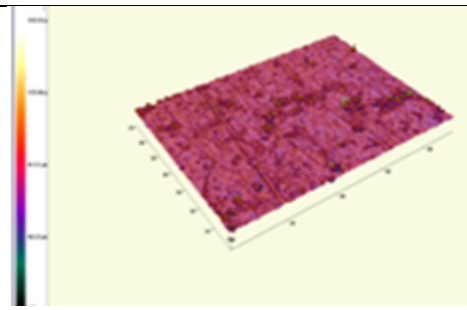

b. AA in 1M NaOH

R_a=21.53

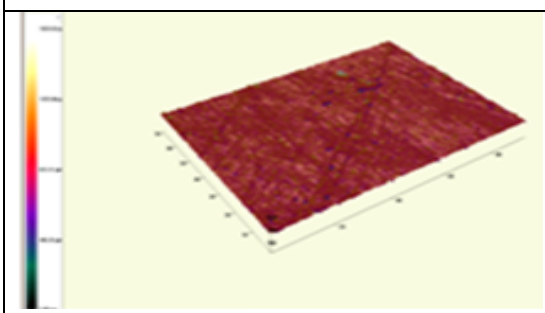

c. PAVL/AA/1M NaOH

R_a=10.86

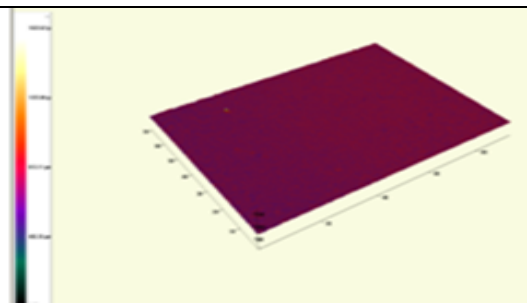

d. PVL/AA/1M NaOH

R_a=4.58

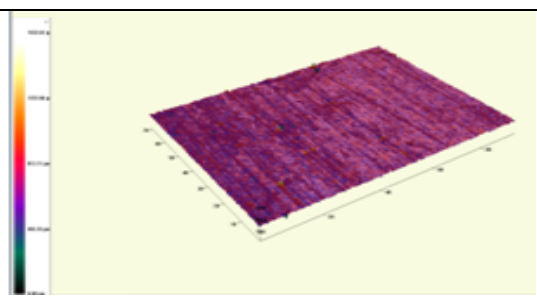

e. SP/AA/1M NaOH

R_a=13.37

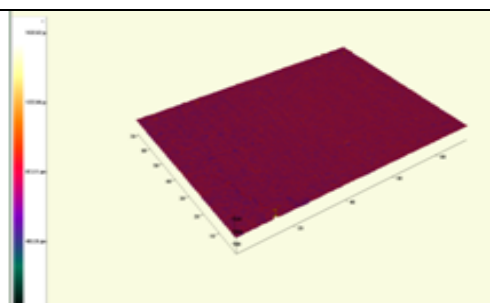

f. PB/AA/1M NaOH

R_a=4.82

Figure 4.52. 3D Optical Profilometry pictures for AA corrosion in the absence and presence of (c) PAVL (d) PVL (e) SP (d) PB extract in 1M NaOH, (a) Plain AA, (b) AA in 1M NaOH

From Figures 4.50 (b), 4.51 (b), 4.52 (b), the surface of MS/AA electrode immersed in 1M HCl/1M NaOH solution have a significantly porous structure with large and deep pores. Figures 4.50 (c-f), 4.51 (c-f), 4.52 (c-f) revealed that protective film was formed on MS/AA metal surface. It was clearly seen that film formed on the metal surface prevented the mild steel/aluminium alloy from corrosion reaction. The microstructure of the surface only can be examine by this method. It can compare the MS/AA surface corrosion with and without the addition of the inhibitor solutions. This method does not give information about the chemical composition of the formed protective film.

The results revealed that higher the distance related to the high roughness value. The average roughness R_a is 9.50 for the uninhibited solution (Figures 4.50 (b)). From the Figure 4.50(c-f) reflected that the R_a of MS exposed in 1M hydrochloric acid with 0.7% of studied inhibitors differs from 7.65, 6.16, 7.17, 8.73 for PAVL, PVL, SP and PB as compared to blank solution. Likewise, the observed value of 15.06 was denoted for AA exposed in acid solution and AA in 1M NaOH showed 21.53. R_a value was lesser in the presence of inhibitors than the blank solution. The reduced R_a values reflected that the adsorption of the studied inhibitor molecules on MS/AA surface and hence decreased the corrosion rate.

The MS/AA in 1M HCl and AA in 1M NaOH with the studied inhibitor solution, PVL has the superior performance in corrosion mitigating reaction and it was found to reduce corrosion of AA as well as MS more efficiently than the other studied inhibitors. The excellent corrosion inhibition behaviour of PVL was identified from the R_a values (6.16 for MS/1M HCl and 9.09 for AA/1M HCl). The R_a value for AA in PVL contained 1M NaOH was 4.58. This confirmed that the PVL extract showed the highest efficiency among the investigated inhibitors.

4.5 QUANTUM CHEMICAL CALCULATION (THEORETICAL STUDY)

Corrosion inhibition mechanism of the inhibitor was examined by quantum chemical calculation method and it was used to identify the high inhibition performance of the inhibitors by the quantitative structure-activity relationship method.

The experimental results reflected that PAVL/PVL/SP/PB extracts acted as adsorption type corrosion inhibitors. The metal-inhibitor interactions associated with complex formation process was theoretically inspected by the molecular level using computer simulations of suitable models in the framework. The efficiency of the inhibitor was associated with their frontier molecular orbitals of HOMO and LUMO. The significant

differences between E_{HOMO} and E_{LUMO} can be appreciated referring to the inhibitory efficiency of phytochemical constituents. The present study was focused on the adsorption mechanism of the studied inhibitors depend on relationship between structures of the inhibitor and their adsorption behaviour. The adsorption of the investigated inhibitor influenced the structural/electronic properties of the studied inhibitor molecule **(Bhawsar *et al*, 2018)**.

In the current study, PAVL/PVL/SP/PB extracts were characterised by FT-IR, UV and GC-MS and HPTLC techniques. Based on these results and phytochemical screening, the major components present in PAVL/PVL/SP/PB extracts were flavonoids, alkaloids, steroids, tannins, carbohydrates, cumarins, sterol, saponins and polyphenols which were confirmed by characterization of PAVL/PVL/SP/PB extracts by HPTLC, GC-MS, FT-IR,UV techniques. Based on these study, to confirm a suitable mechanism for inhibitive behaviour of PAVL/PVL/SP/PB extracts on metal surface, to perform theoretical calculations for few phytochemicals - Flavone(C1),Desycarpidan-1-methanol, acetate(ester)(C2), Palmitic acid(C3), (-)Spanthulenol(C4), Oleic acid(C5), 9-Octadecenoic acid[Z] methyl ester(C6), Cis-9-Hexadecennal(C7), E-2-Tetradecen-1-ol(C8) and these have been fully optimized using Mopac software using the PM3 semi empirical parameterization.

The quantum chemical parameters which are given below are used to indicate the structural characteristics of these common phytochemical constituents present in the investigated inhibitors. The values of some quantum chemical parameters such as E_{HOMO}, E_{LUMO}, (E_{LUMO}-E_{HOMO}) and dipole moment (μ) for selected major components in the investigated PAVL/PVL/SP/PB extracts are presented in Table 4.81 and calculated quantum chemical parameters namely ionisation potential, electron affinity, hardness, softness, electronegativity and electrophilic index are presented in Table 4.82.

Phytochemical constituents of the optimized geometry and frontier molecular orbital density distributions were analysed by this method. It was found that the phenyl ring, C=O and –OH, N-H groups present in the phytochemical constituents interacted with the surface of the metal. The ground state geometry of the studied inhibitor and the performance of its molecular orbitals namely HOMO and LUMO were included in the inhibition action performance of the studied inhibitors. The HOMO was localized over the oxygen, phenyl ring, -OH and C=O and it was the most suitable region for the molecular coordination with the surface of the metal. C=O and –OH groups present in the studied inhibitors can interact with the metal surface.

Discussion

The observed quantum chemical parameters of the corrosion inhibition reaction described as follows:

Figure 4.53-4.60 represented the optimized structures and the HOMO and LUMO pictures of phytochemicals of PAVL/PVL/SP/PB extract. The spatial distribution of the HOMO and the LUMO were essential for the adsorption properties of the inhibitors. Considering that the inhibitors would be electron donors with respect to the metal surface, the HOMO distribution would be of particular importance. The HOMO distribution maps presented in Figure 4.53-4.60 are very similar and the HOMO was localized on the phenyl ring suggesting strong docking to the phenyl ring and lone pair of electrons. From the Table 4.81, it is clear that the phytochemical constituents furnished high values of E_{HOMO}, low values of E_{LUMO} and large energy gap. These results favoured the greater affinity of the phytochemical constituents to offer electrons to the metal atoms.

The adsorption performance of the phytochemical constituents in the metal surface reflected the lesser μ value and also the hydrophobic nature of the molecule. Values of μ ranging from 3 to 5 were reported in the literature **(Khaled *et al*, 2003)**. The inhibitor molecules were found to be softer molecules which are giving the same values of global softness (σ). IP and EA values were calculated and presented in the Table 4.82. IP values were directly corresponding to E_{HOMO} and EA is corresponding to E_{LUMO}.

In the current study, the studied extracts and the metal samples acted as Lewis base/ Lewis acid. Thus, frontier molecular orbital theory applied to infer probable interaction methods between the investigated inhibitors and metal **(Sastri, 1998)**. When metal specimen and investigated extract molecules are coming closer, the movement of the electrons took place by the molecules had lesser electronegativity value to the metal possessed greater electron affinity values till the chemical potential values were equal. The stability of the adsorption bonds associated with Pearson's HSAB principle **(Pearson, 1989)**. The soft base inhibitors were more competent for the metals oxidizing in acid medium and the bulk metals were acted as a soft acid **(Klopman, 1968)**. The soft-soft and hard-hard bond behaviour was related to covalent and electrostatic reactions. In the soft-soft character of the metal-inhibitor coordination, the bond was mainly covalent in nature due to the favourable overlap of the frontier molecular orbitals, i.e., HOMO/LUMO. The results revealed that (Table.4.82) in soft-soft interaction, the metal functioned as a soft acid/inhibitor worked as a soft base **(Martinez and Stagljar, 2003)**.

Table 4.81: Quantum chemical parameters for the selected phytochemical constituents

Selected phytoconstituents	Studied Inhibitors	Total energy (Kcal/ mol)	E_{Homo} (eV)	E_{Lumo} (eV)	Change in Energy ∆E (eV)	Dipole moment- μ (Debye)
Flavone (C1)	PAVL	-1973	-9.092	-1.423	7.7	5.26
Dasycarpidan-1-methanol, acetate (ester)(C2)	PAVL,PVL	-3177	-7.867	0.413	8.2	3.73
Palmitic acid (C3)	PVL, SP, PB	-2396	-8.783	0.555	9.3	4.11
(-) Spanthulenol (C4)	PVL	-2072	-9.075	1.471	10.5	3.80
Oleic acid (C5)	PVL, SP, PB	-2668	-8.785	0.548	9.3	4.12
9-Octadecenoic acid [z]-methyl ester (C6)	SP,PB	-2819	-8.598	0.987	9.6	3.81
Cis-9-Hexadecennal (C7)	SP, PB	-2245	-8.811	0.539	9.4	4.14
E-2-Tetradecen-1-ol (C8)	SP, PB	-2099	-9.585	1.261	10.8	4.16

Table 4.82. Derived Quantum chemical parameters for the selected phytoconstituents

Selected phytoConstituents	IP(eV)	EA(eV)	η(eV)	σ(eV)	χ (eV)	ω
Flavone (C1)	9.1	1.423	3.8	0.26	5.3	3.6
Dasycarpidan-1-methanol, acetate (ester)(C2)	7.9	-0.413	4.1	0.24	3.7	1.7
Palmitic acid (C3)	8.8	-0.555	4.7	0.21	4.1	1.8
(-) Spanthulenol (C4)	9.1	-1.471	5.3	0.19	3.8	1.4
Oleic acid (C5)	8.8	-0.548	4.7	0.21	4.1	1.8
9-Octadecenoic acid [z]-methyl ester (C6)	8.6	-0.987	4.8	0.21	3.8	1.5
Cis-9-Hexadecennal (C7)	8.8	-0.539	4.7	0.21	4.1	1.8
E-2-Tetradecen-1-ol (C8)	9.6	-1.261	5.4	0.18	4.2	1.6

Figure No	Optimised Structure	Frontier Molecular Orbital distribution - HOMO	Frontier Molecular Orbital distribution - LOMO
4.53	Flavone (C1) 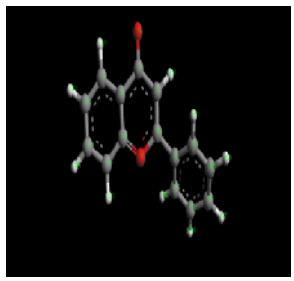	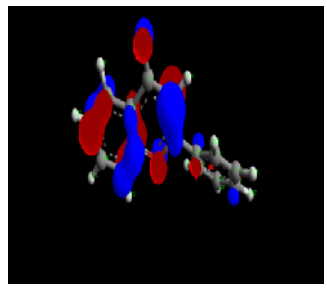	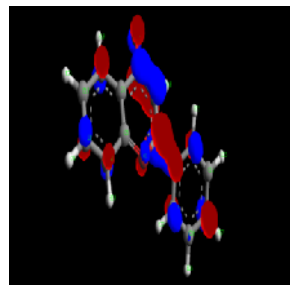
4.54	Dasycarpidan-1-methanol, acetate (ester)(C2) 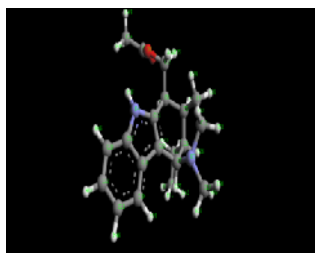	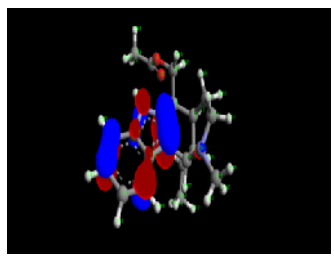	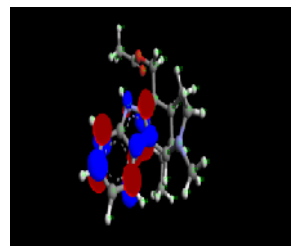
4.55	Palmitic acid (C3) 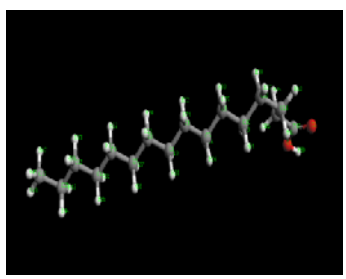	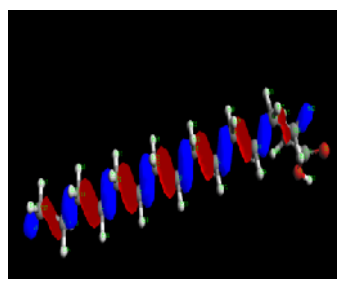	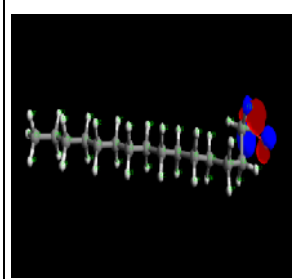
4.56	(-) Spanthulenol (C4) 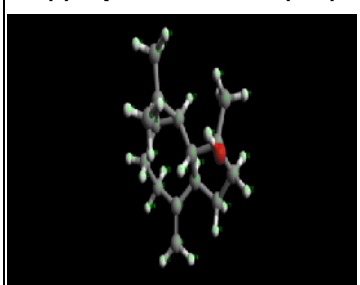	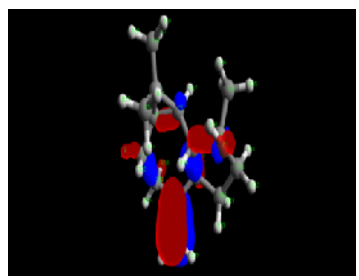	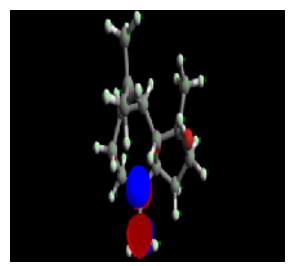

Figure No	Optimised Structure	Frontier Molecular Orbital distribution - HOMO	Frontier Molecular Orbital distribution - LOMO
4.57	Oleic acid (C5) 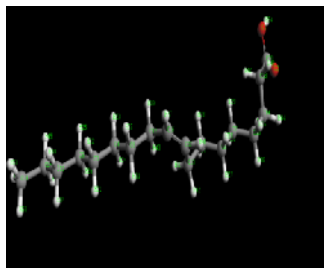	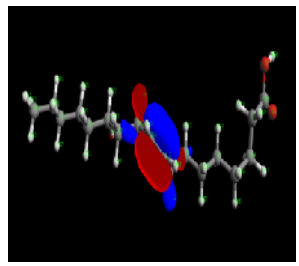	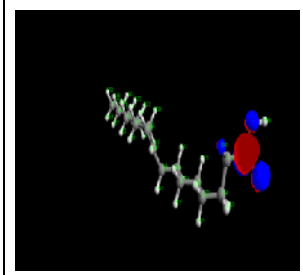
4.58	9-Octadecenoic acid [z]-methyl ester (C6) 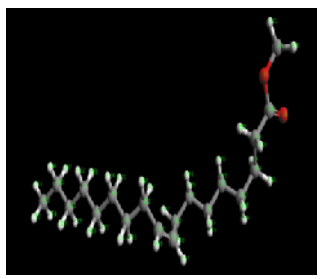	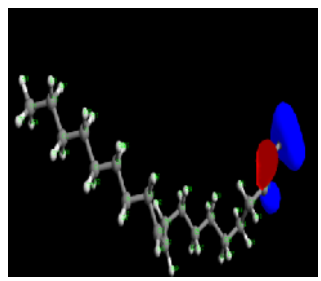	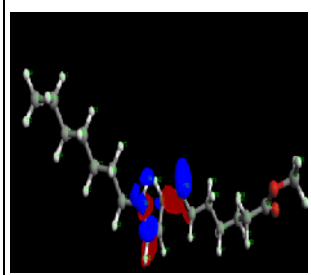
4.59	Cis-9-Hexadecennal (C7) 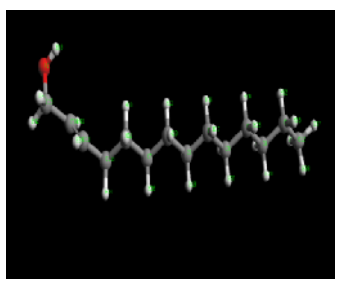	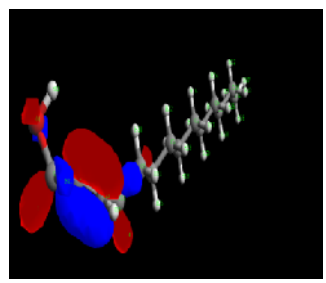	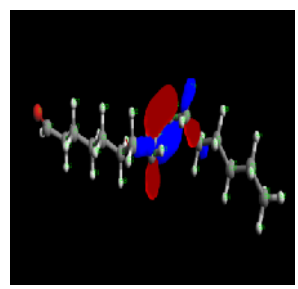
4.60	E-2-Tetradecen-1-ol (C8) 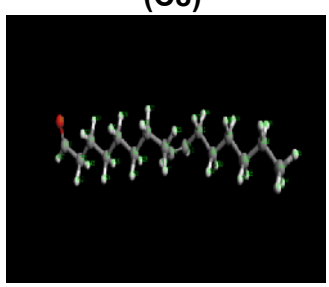	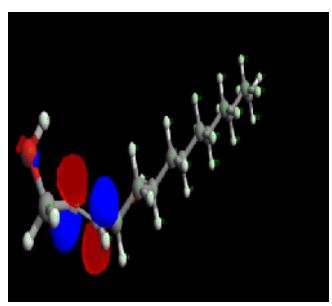	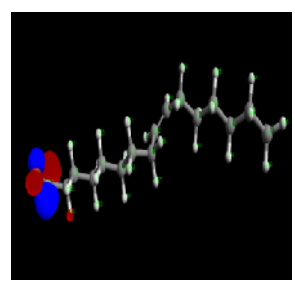

4.6 Mechanism of Inhibition Process

(i) MS/Inhibitors/1M HCl

The inhibitive mechanism can be attributed to the mechanical properties of the metal, chemical property of the electrolyte and structure of the inhibitor. Adsorption process on the metal surface took place in two ways one is chemisorption and another one is physisorption. Chemisorptions involved by the sharing of electrons between the metal and the medium and neutral molecule can adsorb on the metal surface. Another way of adsorption on the metal surface is donor-acceptor interaction between the π electron of the aromatic ring and vacant d orbital of the surface iron atom. The MS in HCl medium, there was coordination between the adsorbed Cl^- ions and protonated inhibitors. Corrosion inhibition reaction performed by active phytochemicals present in the aqueous solution. These phytochemical constituents of the inhibitors existed as neutral molecules or protonated molecules in the aqueous acidic solution.

"In the current study two types of adsorption may occur:

i. Removal of H_2O molecule from the metal surface by the studied neutral PAVL / PVL / SP / PB using chemisorptions process and electrons were shared between O atom and Fe. The investigated inhibitors with their phytochemical constituents were adsorbed on the metal surface by the vacant d-orbitals offend donor-acceptor interactions between π-electrons of the aromatic ring.

$$Fe \longrightarrow Fe^{2+} + 2e^- \quad (4.12)$$

$$[PAVL/PVL/SP/PB] + Fe^{2+} \leftrightarrow [PAVL/PVL/SP/PB\text{-}Fe]^{2+} \quad (4.13)$$

ii. The protonated PAVL / PVL / SP / PB inhibitors can be adsorbed by electrostatic interactions between the positively charged molecules and the negatively charged metal surface. Hence, there may be co-ordination between Cl^- and PAVL / PVL / SP / PB extract and develop the inhibitive performance of the studied inhibitors.

$$[PAVL / PVL / SP / PB\ H\mathit{x}]^{x+} + Fe^{2+} \leftrightarrow [PAVL / PVL / SP / PB\text{-}Fe]^{(2+x)+} \quad (4.14)$$

$$[PAVL / PVL / SP / PB] + Fe^{2+} \leftrightarrow [PAVL / PVL / SP / PB\text{-}Fe]^{2+} \quad (4.15)$$

The coordination bond formed by the partial transference of electrons from polar atoms (O atoms) to the metal surface with the protonated PAVL / PVL / SP / PB extract was adsorbed on the metal surface. In addition, metal-inhibitor complexes by lone-pair electrons of O atoms present in PAVL / PVL / SP / PB extract or protonated inhibitor

coordinates with newly produced Fe^{2+} ions on steel surface **(Li *et al,* 2010)**. The formed complexes can adsorb on the metal surface through Vander Waals force and prevent MS surface from corrosion.

The important phytochemical constituents of the PAVL/PVL/SP/PB extracts were flavonoids, alkaloids, steroids etc. The potential of the inhibitors were due to the large size of the phytochemical compounds present in the plant/seaweed extracts shielding the metal surface and control the corrosion reaction. The performance of the inhibition efficiency was due to electron rich O and N atoms contained phytoconstituents present in the inhibitors. Unshared electron pair of heter O - atoms and p - electrons of the aromatic ring were the feasible reaction centres. Due to donor-acceptor interactions between π (pi) electrons of the O and aromatic ring and vacant d orbitals of the surface iron, the phytoconstituents present in the studied inhibitors adsorbed on the MS surface **(Noor, 2007 and Oguzie, 2008)"**.

(ii) AA/Inhibitors/1M HCl

"**Brett, 1990** suggested a suitable mechanism for Aluminium in acidic solution; the inhibitors might be protonated due to the interaction between the oxygen atom and H^+ ion. The aluminium surface is positively charged due to the accumulation of $Al\text{-}OH_2^+$ species in acidic solution. In HCl solution, Cl^- ions can accumulate slowly to the aluminium/solution interface, being specifically adsorbed and they formed an excess negative charge towards the solution and favour more adsorption of the cations.

i) **Li *et al,* 2012b** suggested that due to electrostatic interactions between the positively charged molecules, the protonated investigated inhibitor molecules may adsorb on the negatively charged metal surface. Hence, there was an interaction between Cl^- and protonated inhibitor.

$$Al_{(s)} + H_2O \longleftrightarrow AlOH_{ads} + H^+ + e^- \quad (4.16)$$

$$AlOH_{ads} + 5\,H_2O + H^+ \longleftrightarrow Al^{3+}.6\,H_2O + 2\,e^- \quad (4.17)$$

$$Al^{3+} + H_2O \longleftrightarrow [AlOH]^{2+} + H^+ \quad (4.18)$$

$$[AlOH]^{2+} + X^- \longleftrightarrow [AlOHX]^+ \quad (4.19)$$

The complexation reaction took place between the hydrated cation and the anion. The corrosion reaction was controlled in equation 4.18. Corrosion reaction in the presence of the Cl^- ions are as follows

$$[AlOH]^{2+} + Cl^- \longleftrightarrow [AlOHCl]^+ \quad (4.20)$$

ii) The metal dissolution rate increased due to the formation of soluble complexion and it was depended on the concentration of the chloride ion. To find out the adsorption mechanism of protonated inhibitors to positively charged AA surface, corrosion mechanism of AA in HCl must be known. When considering this mechanism, anodic dissolution reaction of aluminium is as follows:

$$Al + Cl^- \longleftrightarrow AlCl^-_{ads} \quad (4.21)$$

$$AlCl^-_{ads} + Cl^- \longleftrightarrow AlCl^-_2 + 3e^- \quad (4.22)$$

The cathodic hydrogen evolution reaction is given below:

$$H^+ + e^- \longrightarrow Hads \quad (4.23)$$

$$H^+ + H_{ads} \longrightarrow H_2 \quad (4.24)$$

The protonated inhibitor molecules electrostatically adsorbed onto the anion covered AA surface by their protonated form. Hence the oxidation process given in equation 4.21 can be prohibited. Due to electrostatic interaction of the studied inhibitor molecules, stabilisation occurred on the adsorbed halide ions as a result increased the surface coverage. The protonated molecules present in the studied inhibitors also adsorb on the cathodic sites in competition with H^+ ions. In addition, the inhibitors can adsorb from the negatively charged O atoms and the pi bonds of the aromatic ring systems to positively charged AA surface".

(iii) AA/Inhibitors/1M NaOH

"The affinity of Al towards ambient oxygen will result in the formation of the oxide layer which is responsible for the protection of the Al surface.

$$2Al_{(metal)} + 3/2O_2 \leftrightarrow Al_2O_3 \quad (4.25)$$

Zhang *et al* (2009) explained that the oxide film acted as a state barrier and isolated Al from the bulk solution.

$$Al + 3H_2O+OH^- \rightarrow 3/2H_2 + [Al(OH)_4]^- \quad (4.26)$$

The Aluminium dissolved in alkaline solution to form a soluble complex. **Prabhu and Rao (2013b)** clearly described that the adsorption of the studied inhibitor molecules results in the elimination of adsorbed H_2O molecules from the aluminium surface.

$$Inhibitor_{(soln)} + nH_2O_{(ads)} + Inhibitor_{(ads)} + nH_2O_{(soln)} \quad (4.27)$$

Phytochemicals of the studied plant/seaweed extract are mainly playing a role in the inhibition process. Due to the adsorption of phytochemicals present in the studied inhibitors, the protective film formed on the Aluminium surface. This prevented the anodic reaction of the corrosion process. The performance of inhibition mainly depended on the various organic components present in the plant/seaweed extract. The formed protective film can stop the diffusion of ions from the metal surface which can delay the corrosion reaction. The interactions of the adsorbed inhibitor molecules with the metal surface can protect the metal surface from corrosion reaction by the anodic reaction. It was clear that the simple blocking effect can reduce the number of metal atoms involved in the corrosion reactions decreasing the corrosion rate".